

FINAL REPORT

DEVELOPMENT OF ADVANCED

FUEL CELL SYSTEM

(Phase II)

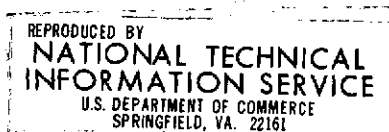
by

L. M. Handley
A. P. Meyer
W. F. Bell

PRATT & WHITNEY AIRCRAFT
South Windsor Engineering Facility
Box 109, Governors Highway
South Windsor, Connecticut 06074

prepared for

NATIONAL AERONAUTICS AND SPACE ADMINISTRATION



CONTRACT NAS3-15339

NASA Lewis Research Center
Cleveland, Ohio
Dr. L. H. Thaller, Project Manager

(NASA-CR-134721) DEVELOPMENT OF ADVANCED
FUEL CELL SYSTEM, PHASE 2 Final Report, 30
Jun. 1972 - 30 Sep. 1973 (Pratt and Whitney
Aircraft) 170 p HC \$6.25

CSSL 10A

N75-16084

G3/44 Unclass
09593

NOTICE

This report was prepared as an account of Government-sponsored work. Neither the United States, nor the National Aeronautics and Space Administration (NASA), nor any person acting on behalf of NASA:

- (A) Makes any warranty or representation, expressed or implied, with respect to the accuracy, completeness, or usefulness of the information contained in this report, or that the use of any information, apparatus, method, or process disclosed in this report may not infringe privately-owned rights; or
- (B) Assumes any liabilities with respect to the use of, or for damages resulting from the use of, any information, apparatus, method or process disclosed in this report.

As used above, "person acting on behalf of NASA" includes any employees or contractor of NASA, or employee of such contractor, to the extent that such employee or contractor of NASA or employee of such contractor prepares, disseminates, or provides access to any information pursuant to his employment or contract with NASA, or his employment with such contractor.

N O T I C E

**THIS DOCUMENT HAS BEEN REPRODUCED FROM
THE BEST COPY FURNISHED US BY THE SPONSORING
AGENCY. ALTHOUGH IT IS RECOGNIZED THAT CER-
TAIN PORTIONS ARE ILLEGIBLE, IT IS BEING RE-
LEASED IN THE INTEREST OF MAKING AVAILABLE
AS MUCH INFORMATION AS POSSIBLE.**

DEVELOPMENT OF ADVANCED

FUEL CELL SYSTEM

(Phase II)

by

L. M. Handley

A. P. Meyer

W. F. Bell

PRATT & WHITNEY AIRCRAFT

prepared for

NATIONAL AERONAUTICS AND SPACE ADMINISTRATION

NASA Lewis Research Center

Contract NAS3-15339

Dr. L. H. Thaller, Project Manager

FOREWORD

This report describes the several research and development tasks performed during Phase II of an advanced fuel cell technology program.

The work was performed under a NASA Contract NAS3-15339 from 30 June 1972 through 30 September 1973. The NASA Program Manager for this contract was Dr. Lawrence H. Thaller. The contributions of Dr. Thaller and other members of the Direct Energy Conversion Laboratory staff at the NASA Lewis Research Center are gratefully acknowledged.

Principal Pratt & Whitney Aircraft personnel who directed the tasks performed in this program were:

Paul E. Grevstad
Raymond L. Gelting
James K. Stedman
William F. Bell
Myron S. Freed
Richard C. Nickols
Raymond W. Vine

CONTENTS

	Page
I SUMMARY	1
A. Cell Component Research	1
1.0 Electrodes	1
2.0 Structural Materials Compatibility	1
3.0 Lightweight Electrolyte Reservoir Plate	2
4.0 Matrix Materials	2
B. Power Section Component Development	2
1.0 Single Cell Development	2
2.0 Evaporative Cooler Development	3
3.0 Plaque and Partial Stack Development	3
II INTRODUCTION	5
III CELL COMPONENT RESEARCH	7
A. Electrodes	7
1.0 Approach	7
2.0 Cathode Catalysts	7
3.0 Post Endurance Test Evaluations of Full-Size Cathodes	14
4.0 Anode Development	17
5.0 Corrosion Studies	20
6.0 Diagnostic and Analytical Techniques	21
B. Structural Materials Compatibility	24
1.0 Materials Selection	24
2.0 Electrolyte Compatibility	25
3.0 Steam-Water Compatibility	27
4.0 Electrolyte Carbonation	29
5.0 Oxygen Compatibility Tests	30
C. Lightweight Electrolyte Reservoir Plate	32
D. Matrix Materials	36

Preceding page blank

CONTENTS (CONT'D)

	Page
IV CELL AND STACK DEVELOPMENT	40
A. Single Cell Development	40
1.0 Introduction	40
2.0 Single Cell Design	41
3.0 Cell Fabrication and Unitization Research	45
4.0 Electrolyte Carbonation	50
5.0 Single Cell Tests	54
5.1 Introduction	54
5.2 Test Facilities and Test Procedures	55
5.3 Summary of Single Cells Tested	62
5.4 Single Cell Test Results	64
B. Evaporative Cooler Development	88
1.0 Requirements and Operation	88
2.0 Design and Fabrication	91
3.0 Evaporative Cooler Assembly	92
4.0 Evaporative Cooler Test Results	93
C. Plaque and Partial Stack Development	95
1.0 Introduction	95
2.0 Plaque Fabrication	96
3.0 Test Fixture Assembly	98
4.0 Partial Stack Test Results	99
V. APPENDICES	
A. Engineering Model System	A-1
B. Improvement of Epoxy-Based Structures for Fuel Cell Unitized Electrode Assemblies (UEA)	B-1

ILLUSTRATIONS

Figure	Caption	Page
1	Endurance Evaluation of High Surface Area Au-Pt Catalyst Cathodes	9
2	Performance of High Power Density Cell Using Gold-Platinum Cathode (Air Force High Power Density Configuration)	12
3	Average Performance of Multicell Stack Using Gold-Platinum Cathodes	13
4	Endurance Evaluation of Cell No. 2390 with 90Au-10Pt Catalyst Cathode Made in Shop	13
5	Post-Test Cathode Half-Cell Performance	15
6	2-Inch x 2-Inch Cell No. 2381 Performance	18
7	2-Inch x 2-Inch Cell No. 2382 Performance	19
8	Endurance Evaluation of 3 mg/cm ² Pt-Pd Anodes	19
9	Endurance Evaluation of Rh-Ni Anode	20
10	Voltametric Sweep Comparison of Base Cell Catalysts	22
11	Corrosion Test Results	23
12	Electrolyte Compatibility Test Apparatus	25
13	Steam Compatibility Test Apparatus	27
14	Electrolyte Carbonation Test Apparatus	29
15	Electrolyte Reservoir Plate Functions	32
16	Mercury Porosimeter Data on Polysulfone ERP	35
17	Evolutionary Single Cell Development Process	41
18	Size Comparison of Cell Designs Tested	42
19	Electrolyte Reservoir Plate	43
20	Single Cell Development Plastic Frame	44
21	Single Cell Development Test Fixture	44
22	Impregnated Matrix Unitization Method	46
23	Gas Chromatography — Various Epoxy Resin - Hardener Formulations	47

ILLUSTRATIONS (CONT'D)

Figure	Caption	Page
24	Gas Chromatography Results - UARL-Formulated Epoxy Resins	48
25	Laminated Film Unitization	49
26	Carbonation Test Rig	52
27	Non-Operating Cell Test Results (Phase I Materials Group)	53
28	Carbonation Cell Test Results (Phase II Materials Group)	53
29	Single Cell Test Facility (Front)	55
30	Single Cell Test Facility (Rear)	56
31	Single Cell Test Stand Schematic	56
32	Catalytic Oxidizer and Scrubber System	57
33	ADAR Print Out	58
34	Dilute Gas Diagnostic Method	61
35	Electrolyte Carbonation Data	66
36	Performance History of Cell No. 16	67
37	Performance History of Cell No. 17	68
38	Performance Calibration Cell No. 17	70
39	Cell No. 17 Tafel Data	70
40	Performance History of Cell No. 20	72
41	Performance History of Cell No. 21	73
42	Performance History of Cell No. 22	74
43	Cell Shorting Implied from Tafel Data	75
44	Performance History of Cell No. 23	75, 76
45	Tafel Data Cell No. 23	77
46	Performance History of Cell No. 24	78
47	Dilute Oxygen Diagnostic Test Data of Cell No. 24	79
48	Comparison of 500 and 100 ASF (538 and 107.6 ma/cm ²) Operation on Cell No. 24	79

ILLUSTRATIONS (CONT'D)

Figure	Caption	Page
49	Tolerance Excursion Data from Cell No. 24	80
50	Performance History of Cell No. 25	81, 82
51	Tolerance Excursion Data Cell No. 25	82
52	Performance History of Cell No. 27	83
53	Tolerance Excursion Data Cell No. 27 (Polysulfone ERP)	84
54	Tolerance Excursion Data Cell No. 27 (Polysulfone ERP)	84
55	Effect of Carbonates on PPF Anode Polarization	85
56	Effect of Carbonates on Au-Pt Cathode Performance	85
57	Performance History of Cell No. 28	86
58	Performance History of Cell No. 30	87
59	Dilute Oxygen Data - Cell No. 30	88
60	Evaporative Cooler Schematic	89
61	Ideal Evaporative Cooler Performance	90
62	Details of Phase II Oxygen/Water Separator Plate	92
63	Evaporative Cooler Assembly and Test Fixture	93
64	Typical Fuel Cell Load Profile	94
65	Evaporative Cooler Verification Test	94
66	Plaque Concept Showing Intercell Seal	95
67	Plaque Impregnated Unitization Method	97
68	Plaque Cross Section Showing Electrolyte Reservoir Plate and Hydrogen Field	97
69	Six-Cell Plaque - Anode Side	98
70	Six-Cell Plaque - Cathode Side	98
71	Partial Stack Assembly	99
72	Partial Stack No. 1 Performance	100
73	Partial Stack No. 1 Individual Cell Voltages and Internal Resistances (IR)	101

ILLUSTRATIONS (CONT'D)

Figure	Caption	Page
74	Partial Stack No. 1 Tolerance Excursion	101
75	Port Modifications	102
76	Partial Stack No. 2 Individual Cell Data	103
77	Performance History - Four End Cells in Partial Stack No. 2	104
78	Partial Stack No. 3 Performance Data	105
79	Partial Stack No. 3 Performance Calibration	106
80	Partial Stack No. 4 Performance Data	107
81	Partial Stack No. 4 Endurance Data	107
82	Performance of Cell Nos. 1 and 7 in Partial Stack No. 4	110
83	Porous TFE between PWR and Hydrogen Field Screen	110
84	Impressed Voltage vs. Current for Partial Stack No. 4	111
85	Plaque Cross Section	112
86	Shunt Current Test Setup	113

TABLES

No.	Title	Page
I	Preparation of Gold-Platinum Catalysts	7
II	Cell Nos. 17, 23, and 24 Decay Analysis	16
III	Phase II Candidate Materials	25
IV	Change in Weight	26
V	Change in Compressive Strength	26
VI	Change in Compressive Modulus	27
VII	Change in Weight	28
VIII	Change in Compressive Strength	28
IX	Change in Compressive Modulus	28
X	Phase I Candidate Material Oxidation Test Results	30
XI	Phase II Candidate Material Oxidation Test Results	31
XII	Lightweight ERP Requirements	33
XIII	Effect of Sintering Time on ERP Pore Characteristics	33
XIV	ERP Compressive Strength	34
XV	Fybex-Asbestos Composite Characteristics	36
XVI	Fybex-Asbestos Composite Pore Spectra Data	37
XVII	Corrosion Test Results - Change in Weight	38
XVIII	Carbonation in Alkaline Electrolyte Cells	50
XIX	Full Size Single Cell Operation	63
XX	Full Size Single Cell Test Categories	64
XXI	Cell Test History	65
XXII	Performance Losses of Cell No. 17	71

ABSTRACT

A multiple task research and development program was performed to improve the weight, life and performance characteristics of hydrogen-oxygen alkaline fuel cells for advanced power systems. Development and characterization of a very stable gold alloy catalyst was continued from Phase I of the program. A polymer material for fabrication of cell structural components was identified and its long term compatibility with the fuel cell environment was demonstrated in cell tests. Full scale partial cell stacks, with advanced design closed cycle evaporative coolers, were tested. The characteristics demonstrated in these tests verified the feasibility of developing the Engineering Model System (EMS) concept into an advanced lightweight long life powerplant.

Preceding page blank

I. SUMMARY

This document reports the activity and results of Phase II of a long range research program to improve the life, weight, and performance of alkaline fuel cells. The specific tasks are focused on meeting technology goals defined by the Engineering Model System (EMS), an advanced, long life, lightweight, powerplant concept. The program is evolutionary in nature, work is being carried out at the laboratory level, in subscale cells and in full scale cell assemblies. As fundamental improvements are defined in the laboratory, e.g. better catalysts and materials, they are committed to evaluation in the working environment of subscale fuel cells. If their merit is demonstrated at this level, they are committed to the full scale cell tests for a final evaluation. The work completed during this phase of the program built on the accomplishments of the Phase I effort. Each of the tasks and the results achieved are summarized below and are reported in detail in the sections which follow.

A. Cell Component Research

1.0 Electrodes

Task Description - This task focused on investigation and evaluation of gold based cathode catalysts. The overall task objective was to attain higher performance/lower catalyst loading and improved long term stability. Gold was chosen as a base material because of its superior stability compared to platinum in the fuel cell environment.

Results - Improved methods for preparing 90% gold-10% platinum (90Au-10Pt) catalysts were developed: chloroplatinic acid (H_2PtCl_6) was used as a source material for platinum rather than platinum diamino dinitrite [$\text{Pt}(\text{NH}_3)_2(\text{NO}_2)_2$] and processing steps were modified. These resulted in a 70 percent increase in the catalyst surface area. The higher surface area allowed a 50 percent reduction in cathode catalyst loading without a performance penalty. This catalyst also had a higher degree of alloying between the gold and platinum. A batch of 80Au-20Pt catalyst was also prepared to further investigate the effect of alloying. X-ray diffraction tests showed this catalyst had smaller crystallite sizes than the 90 Au-10Pt catalyst and has the potential for better performance.

2.0 Structural Materials Compatibility

Task Description - The long term compatibility (up to 6000 hours) of polymer materials with the fuel cell environment was evaluated by tests in potassium hydroxide electrolyte and steam. The tendency for a material to contribute to carbonate formation in the electrolyte was also determined.

Results - Exposure of the five candidate materials to 42 weight percent KOH at 250°F (121°C) showed 30 percent asbestos/70 percent H-resin composite to be the only material which met the criterion of acceptability, less than 0.5 percent weight change.

Exposure of the five candidate materials to water vapor at 250°F (121°C) and 45 psia (31.0 n/cm²) showed only the 30 percent asbestos/70 percent polysulfone composite to be suitable in the steam-water environment.

Oxygen compatibility tests, in an atmosphere of 30 percent oxygen - 70 percent helium at 250°F (121.1°C) and 50 psia (34.5 n/cm²), showed that H-resin composites produce an unacceptably high quantity of carbon bearing oxides.

3.0 Lightweight Electrolyte Reservoir Plate

Task Description - The heaviest single component in the EMS cell is the nickel electrolyte reservoir plate. Substituting a nonmetallic material for this porous structure would result in sizeable system weight saving. The effort begun in Phase I to produce a structure with high porosity made of low density materials was continued.

Results - Full-size ERP's were fabricated of porous polysulfone and were plated internally with nickel. One such ERP was successfully tested in Cell No. 25. Compressive strength tests showed the ERP's mechanical strength exceeds the loading anticipated in fuel cell assemblies.

4.0 Matrix Materials

Task Description - Potassium titanate has demonstrated superior compatibility with electrolyte compared to the asbestos presently used in the cell's matrix. Availability of a new source for supplying potassium titanate fibers (Fybex® produced by DuPont) allowed a matrix development activity to begin near the end of Phase I. This activity was continued into Phase II.

Results - Fabrication of matrices of potassium titanate during Phase II did not repeat the achievement of the high bubble pressures attained during Phase I. This was traced to differences in the Zeta potential of the several batches of Fybex fibers supplied by DuPont. The early supply of Fybex had Zeta potentials near zero, later samples had much lower potentials. To reproduce the early high bubble pressure matrices a method to raise the Zeta potential of the Fybex must be developed.

B. Power Section Component Development

1.0 Single Cell Development

Task Description - Several single cell tasks provide the means for evaluating the performance and endurance characteristics of evolutionary EMS cell designs. The investigations performed in this area are: evaluation of alternate cell designs, testing to measure the compatibility of alternative cell frame materials and construction techniques in the actual cell environment, and development

of cell fabrication procedures to translate the most compatible materials available into practical cell configurations. Single cell hardware was also fabricated and delivered to the NASA LeRC.

Results - A total of 14 full-size cells were tested and more than 22,000 hours of test experience were accumulated during Phase II. These cells included four new designs which were Verification Tested. One cell run at 200 ASF (215.2 ma/cm²) accumulated more than 6600 hours of operation.

Cells were fabricated using the matrix-impregnation technique and the laminated film method. Two cells, Nos. 28 and 30, fabricated of polysulfone film, showed carbonation levels as low as that achieved with cells of Teflon construction. Because of their low carbonation rate both of these cells have the potential for 10,000 hours of operation without refurbishment.

Non-operating cell tests to evaluate carbonate formation were continued into Phase II. Polysulfone was shown to be the most promising material for fabrication of cells with low carbonation rates.

A diagnostic technique which permits separation of anode and cathode diffusion losses was developed. This method requires operating the cell on pure oxygen and then on an oxygen-inert gas mixture.

2.0 Evaporative Cooler Development

Task Description - The EMS concept includes removal of cell waste heat by evaporation of water. In the evaporative cooler task, effort was concentrated on developing a lightweight cooler design using a thin, porous, hydrophobic membrane to separate the steam and water.

Results - An evaporative cooler was fabricated and tested. The evaluation consisted of a one-week test using electrical heaters to simulate fuel cell operation to current densities as high as 460 ASF (495 ma/cm²). On successful completion of this test, the unit was released for incorporation into partial stacks.

3.0 Plaque and Partial Stack Development

Task Description - Development of a lightweight method for packaging groups of cells into a planar multi-cell assembly (termed a plaque) was performed under this task. The plaque integrates six EMS cells and a passive water removal water transport plate into a single assembly. Development of fabrication procedures and performance evaluation testing were included in this task.

Results - Three six-cell plaques were fabricated by the matrix-impregnation method. These plaques were assembled with evaporative coolers into partial stacks. Each partial stack consisted of two plaques and an evaporative cooler. Four partial stacks were tested and a total of 296 test hours were accumulated. Performance measurements of individual cells indicated significant degradation of the most positive cell in each plaque after about 50 hours of operation. Further evaluation and analysis indicate the degradation was caused by transfer of electrolyte from cell to cell across the surfaces of the intercell seals or through the passive water removal matrix. The transfer is caused by ionic shunt currents. The result is a loss in electrolyte from the most positive cell and a gain in the most negative cell. Modifications to the plaque design to block electrolyte transfer were identified.

II. INTRODUCTION

The Lewis Research Center of the National Aeronautics and Space Administration is conducting a fuel cell system technology advancement program oriented toward advanced space applications. The emphasis in this program is on applied fuel cell research and development to build a new technology base from which advanced fuel cell systems can be developed. The work is being guided by an advanced fuel cell system, the specifications for which require a factor of three reduction in system weight and a factor of five improvement in life.

The technology being developed has broad applicability for space and undersea power systems touching as it does on the fundamentals of fuel cell science and art (electrode catalysts and structures, matrix materials, compatibility of structural materials, lightweight cell components, and fabrication techniques).

The several work areas of the program and the emphasis in each were planned to meet the objectives stated by NASA LeRC; the key elements of these objectives are:

"Goals — The NASA Lewis Research Center is embarking on an advanced fuel cell program. . . The overall goal is to advance the technology to provide a low cost, long life fuel cell system to meet Shuttle requirements. . .

Phasing - A multi-phase development program is anticipated. The first phases cover two aspects of the total program.

- 1) The initiation of an on-going technology program to achieve necessary improvements in the fuel cells and ancillary components.
- 2) A preliminary design for an Engineering Model System that will incorporate the best current ideas for meeting the program goals."

The program consists of contractor performed work and complementary work performed at the Lewis Research Center. Phase I and II of the program have been completed. In each phase several interrelated program tasks have been performed aimed at meeting requirements of the next generation of fuel cell systems, as well as, providing supporting technology for on-going, mission-oriented fuel cell system programs. In programs that are specifically mission-oriented, very often scheduling constraints require that technology shortcomings be circumvented by design rather than being addressed directly. Advanced technology programs on the other hand permit more effort to be applied for solving basic problems. The potential benefits of such a program are two-fold. First a superior system can emerge at a technology level where a potential user can compare it to an existing inventory system. Second, and of equal importance, technology generated during such a program can be utilized by on-going mission-oriented programs.

This report describes the several research and development tasks performed by P&WA during the second phase of this advanced fuel cell program. The program tasks performed during Phase II were organized into two areas:

- A) Cell Component Research
 - Electrodes
 - Structural Materials
 - Lightweight Electrolyte Reservoir Plate
 - Matrices
- B) Power Section Component Development
 - Single Cells
 - Evaporative Cooler
 - Plaques and Partial Stacks

The goals for each task area were defined by the NASA LeRC. The Engineering Model System, the advanced powerplant concept, was defined during Phase I. This system, its characteristics, and the technology goals it defines are reviewed in Appendix A.

A summary of the results achieved during Phase II relative to these goals is presented in Section I Summary. The following sections present detailed discussions of the work performed in individual task areas.

III. CELL COMPONENT RESEARCH

A. Electrodes

1.0 Approach

The original objective of the Phase I electrode technology advancement effort was to improve the performance and stability of the alkaline electrolyte fuel cell, principally by the development of new cathode catalysts. As the work progressed, data were generated which indicated that structural development of both electrodes would improve stability of cells operating at EMS conditions. Several catalysts showed potential for improving performance and stability in both anodes and cathodes. These alloys were further evaluated and developed during the Phase II effort.

2.0 Cathode Catalysts

The cathode catalysts studied in Phase II were gold-platinum (Au-Pt) and gold-nickel (Au-Ni). Variations on the composition and fabrication methods of both catalyst materials were evaluated. The Au-Pt catalyst made at the end of Phase I contained approximately 10 percent platinum and was made by a process which produced a catalyst surface area of 10 to 12 square meters per gram (m^2/g). This catalyst was the standard of comparison for cathode catalysts in this program. Table I summarizes the surface areas of the catalyst preparations made during Phase II. Electrodes made from this catalyst have been fabricated and used as cathodes for full-size single cell tests in the NASA-LeRC program as well as for other government sponsored and P&WA sponsored programs. The development of vendor sources for this catalyst is being pursued under other government-sponsored programs.

TABLE I
PREPARATIONS OF GOLD-PLATINUM CATALYSTS

<u>PERIOD</u>		<u>SURFACE AREA, m^2/g</u>
Sept.-Dec. 1972	No. of Batches 17 Surface Area (m^2/g)	
	Range	10 to 15
	Avg. Value	11.9
Jan.-Apr. 1973	No. of Batches 10 Surface Area (m^2/g)	
	Range	11 to 15
	Avg. Value	12.8

During this program, 90Au-10Pt catalyst was also prepared by an alternative method previously developed in our laboratory which produced catalyst with surface areas on the order of $20 \text{ m}^2/\text{g}$. This method was also used to prepare catalyst in which the platinum content is more completely alloyed in solid solution with the gold and also to prepare catalyst in which the total platinum content was increased to 20 percent. In this modified method chloroplatinic acid (H_2PtCl_6) is used as the source material for platinum rather than platinum diamino dinitrite [$\text{Pt}(\text{NH}_3)_2(\text{NO}_2)_2$] as in earlier procedures. Gold chloride (HAuCl_4) is used as the source material for gold in both procedures. Increased surface area is achieved by neutralization of the acid associated with dissolution of the chlorides before reduction. Reduction to the metallic alloy and increased degree of alloying are achieved using formaldehyde in sodium hydroxide solution (NaOH) with heating to complete the reduction reaction. These catalysts were made into 2-inch x 2-inch electrodes and were compared with similar-sized electrodes of the standard 90Au-10Pt variety in endurance tests at 200 amperes per square foot (ASF) ($215.2 \text{ ma}/\text{cm}^2$). Test conditions were 35 percent KOH at 190°F (85°C), and one atmosphere reactant gas pressure. Standard platinum-palladium (PPF) electrodes were used as anodes.

As reported in the Phase I Final Report, PWA-4542, the endurance potential of Au-Pt cathodes was demonstrated by Cell Nos. 2097 and 2221, each of which was operated continuously for 5000 hours at 190°F (85°C), one atmosphere hydrogen and oxygen and a current density of 200 ASF ($215.2 \text{ ma}/\text{cm}^2$). During Phase II, additional endurance testing was performed to evaluate modifications to the catalyst which were intended to improve the decay resistance of gold catalyst cathode cells.

One of the performance decay modes of fuel cell cathodes is the gradual loss of active surface area of the catalyst by an electrochemical process resulting in coarsening and growth of the catalyst crystallites. The exact mechanism of this recrystallization phenomenon is not known but is generally attributed to either: 1) dissolution of high energy site material under the influence of the electrochemical potential and precipitation at lower energy sites; or 2) diffusional processes such as those occurring in thermal sintering of metals, but in this case activated by the high surface area form of the catalyst and the electrochemical environment. For both cases, it has been suggested that recrystallization resistance for the catalyst might be enhanced by more completely alloying the component constituents. It is also of interest to determine if recrystallization depends upon the surface area of the catalyst in the ranges of activity of interest. Electrodes were fabricated with gold-platinum catalyst prepared by a process which produced a catalyst surface area of approximately 20 square meters per gram (m^2/g) as compared with the standard catalyst of surface area 10 to 12 m^2/g . X-ray diffraction analysis indicated that approximately 55 percent of the Pt was alloyed in solid solution. This high surface area catalyst allowed the loading of catalyst to be reduced from approximately 20 milligrams per square centimeter of electrode planar area (mg/cm^2) to approximately 10 mg/cm^2 , thus maintaining the total surface area of the catalyst approximately equal. Initial performance tests performed in the floating electrode half-cell rig indicated that the activity of this cathode was indeed equivalent to that of cathodes made with the standard surface area catalyst, but that electrode diffusional losses occurred to a greater extent at higher current densities than for the standard catalyst electrodes. The higher diffusional losses indicated that the microstructure of the catalyst-Teflon layer was less than optimum. An endurance test was also performed with this cathode in

Cell No. M-0168 at standard laboratory endurance test conditions: 200 ASF (215.2 ma/cm²), 190°F (85°C) one atmosphere hydrogen and oxygen reactants, and 35 percent KOH electrolyte. Cell performance versus time is shown in Figure 1. This cell was operated for 2920 hours with an overall decay rate at 200 ASF (215.2 ma/cm²) of 36.7 μ v/hour. Correcting for the performance loss due to electrolyte carbonation (27 percent conversion or an estimated 23 mv loss) results in a carbonate-free decay rate of 28.8 μ v/hour. Comparison of cathode activity data with that for the standard surface area Au-Pt catalyst tests showed a comparable rate of activity decrease. The higher surface area material therefore maintains its advantage throughout its operating life.

In a related test, an electrode was fabricated from catalyst which had both high surface area (about 20 m²/g) and for which X-ray diffraction analysis indicated that 100 percent of the platinum (10 percent of the total composition) was alloyed in solid solution with the gold. This electrode was also tested as a cathode at standard endurance conditions in Cell No. M-0180. Cell performance vs. time is also shown in Figure 1. This cell was operated for 1335 hours at 200 ASF (215.2 ma/cm²) with an overall decay rate of 64.3 μ v/hour. Correcting for the performance loss because of electrolyte carbonation (24.8 percent conversion or an estimated 16.8 mv loss) results in a carbonate-free decay rate of 41.8 μ v/hour. The periodic diagnostic data taken during the test indicated that activity of the cathode catalyst decreased from 17 ma/mg to 6.8 ma/mg, or at a rate higher than that for both the standard surface area Au-Pt catalyst and that of the higher surface area catalyst of Cell No. M-0168.

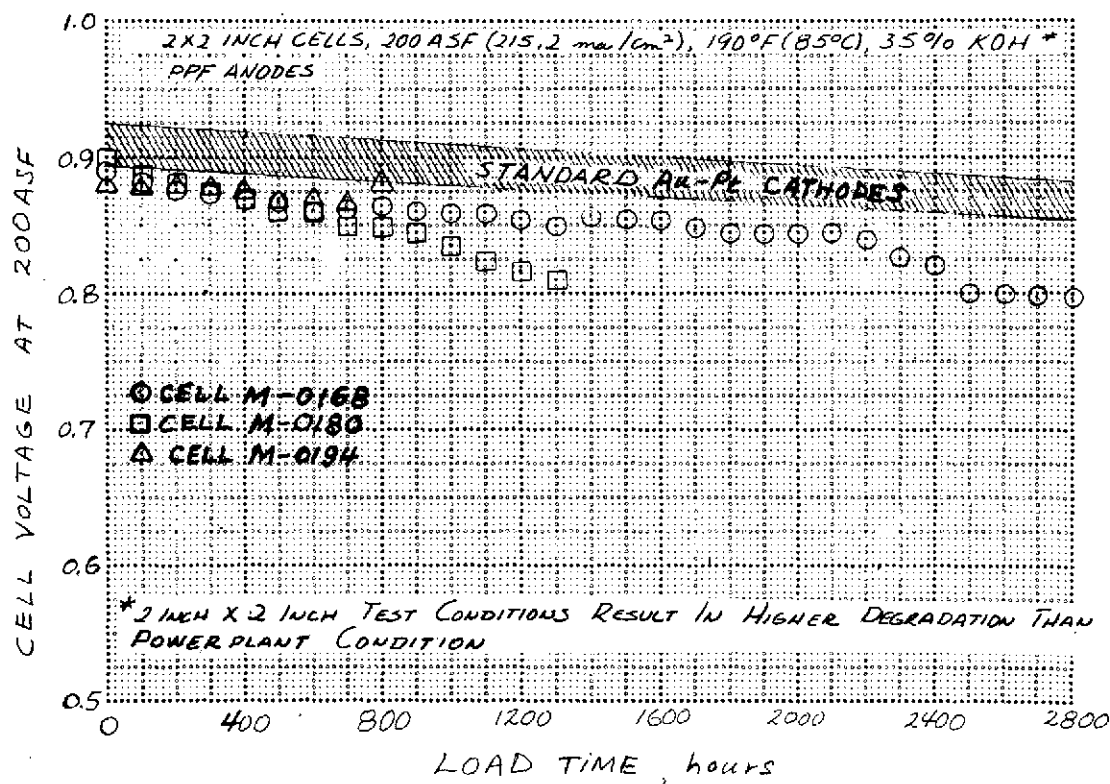


Figure 1 — Endurance Evaluation of High Surface Area Au-Pt Catalyst Cathodes

It is not clear why the increased alloying of the catalyst did not restrict or retard decay compared with the lesser alloyed catalyst. One possibility is that the higher surface area catalyst might decay because of recrystallization at a greater rate than the standard surface area catalyst. It was also predicted that the higher surface area catalyst which was also highly alloyed might decay due to recrystallization, but at a slower rate than the lesser-alloyed catalyst. Since the decay rates observed in the tests of Cells Nos. M-0168 and M-0180 do not support these predictions, it was concluded that recrystallization is not the overriding decay mechanism and that another mechanism is interfering with the investigation of recrystallization.

For example, both the performance and decay rate measured by the laboratory test could be influenced by the degree to which the catalyst in the electrode participates in the reaction. If only a portion of the catalyst is wetted with electrolyte or if a portion is flooded to the extent that it does not get enough reactant, the remainder will be operating at an effective current density higher than planned: Thus performance will be lowered and the catalyst participating will probably be recrystallizing at a rate greater than at a lower current density. Also, that portion of the catalyst which is not participating will also not be recrystallizing. Activity measurements which determine catalytic properties can be influenced by the electrode structural properties to the extent that all of the catalyst in the electrode is not participating in the reaction. It is also apparent that if the degree to which catalyst is wetted or flooded changes with time, the influence on recrystallization will be affected.

As a further test of the alloying effect, a batch of 80Au-20Pt catalyst was prepared using the high surface area procedure; about 85 percent of the platinum (17 percent of the total composition) was alloyed in solid solution with the gold. Electrodes fabricated from this catalyst, but with only about half the catalyst loading, were tested both in the floating electrode half-cell and as a cathode at standard endurance conditions in Cell No. M-0194. The half-cell tests showed that initial performance of the 10 mg/cm² 80Au-20Pt catalyst electrode was equivalent to that of the standard 20 mg/cm² 90Au-10Pt catalyst. Cell performance vs. time for Cell No. M-0194 is shown in Figure 1. This cell was operated for 1115 hours with an overall decay rate at 200 ASF (215.2 ma/cm²) of 16 μ v/hour. Correcting for the performance loss because of electrolyte carbonation (6% conversion or an estimated 3 mv loss) results in a carbonate-free decay rate of 15 μ v/hour. When the endurance test began, catalyst activity (as indicated by initial performance) was lower than predicted from the half-cell test. During the endurance test, performance increased when the electrode was temporarily starved of reactant. The lower initial performance may be attributed to incomplete filling of all of the catalyst particles with electrolyte and the increase in performance may be attributed to additional filling when the potential of the electrode cycled during reactant starvation. Additional cells containing 80Au-20Pt catalyst cathodes began endurance testing but results indicated that these electrodes were more difficult to fill properly with electrolyte. Additional work will be performed to develop this catalyst composition during the next phase of the program.

Endurance test evaluation of the various Au-Pt catalyst cathodes discussed also included measurement of the average crystallite size of the Au-Pt catalyst before and after testing. This measurement made by X-ray line broadening is a measure of recrystallization and loss of surface area because of test conditions. The data from eleven tests of various 90Au-10Pt

catalyst cathodes and for two tests of 80Au-20Pt show that the crystallite size for the 80Au-20Pt catalyst is smaller than that for the 90Au-10Pt catalyst, both initially and after about 1000 hours of test. This smaller crystallite size and attendant higher surface area is the basis for the assumption that better performance is possible from the 80Au-20Pt catalyst at equivalent loading, and equal or improved stability if the wetting characteristics can be improved.

Gold-nickel alloy was also investigated for use as a cathode catalyst. Catalyst batches were prepared with 2.5 percent nickel by the techniques used to prepare high surface area gold-platinum catalyst. However, only a small percentage of the nickel was alloyed in solid solution with the gold. Early electrochemical testing of electrode structures made from this catalyst showed transfer of electrolyte through the electrode thickness from matrix (electrolyte) side to reactant side. This electrolyte pumping phenomenon was attributed to an imbalance in electrolyte pressure across the electrode because of its microstructural characteristics. This resulted in poor performance since the electrolyte which was transferred to the gas side of the electrode inhibits diffusion of reactant to the active catalyst sites. Although this electrolyte pumping phenomenon appeared associated with the catalyst composition, the prime cause of the phenomenon seems to be a lack of properly-sized and distributed porosity in the catalyst-plus-Teflon mixture. However, this porosity distribution is influenced by properties of the catalyst such as those determined by colloidal and/or surface chemistry and the interaction of these properties with those of the Teflon particles used. For example, electron microscopic examinations showed that dry Au-Ni catalyst particles were more jagged and irregular in shape than dry Au-Pt catalyst particles. Also, Coulter Counter particle size analyses showed that Au-Ni has slightly more particles in the 1 to 3 micron diameter size range and slightly less in the 0.4 to 1.0 micron range than Au-Pt.

Laboratory testing and structural development of specimen electrodes, performed to overcome the electrolyte pumping problem, included variations in Teflon content, and variations in density of the catalyst plus Teflon layer. The electrodes which had denser than normal catalyst layers did not exhibit electrolyte pumping but did display a tendency to slowly flood with electrolyte. Attempts were made to increase the hydrophobic characteristic of the catalyst-plus-Teflon layer to reduce flooding without returning to electrolyte pumping. An electrode made by modifying electrode fabrication parameters and by modifying the catalyst particle size by ultrasonic blending did not indicate gross pumping or flooding characteristics when tested in a floating electrode half-cell test. Laboratory testing confirmed that this structure had reduced pore size. However, when this electrode was endurance tested (Cell No. M-0193), rapid decay was experienced. Diagnostic tests indicated loss of catalytic activity because of recrystallization.

Concurrent with the development of Au-Ni catalyst electrodes which were not prone to electrolyte pumping, catalyst preparation development was undertaken to provide Au-Ni catalyst which was thoroughly alloyed and therefore resistant to decay by recrystallization. Typically, the Au-2.5 Ni material was alloyed only to the extent of half the nickel content; i.e., 1.2 atomic percent nickel (which corresponds to about 0.6 volume percent) was found to be in the gold solid solution alloy as determined by the X-ray diffraction technique.

Efforts were made to increase the amount of the nickel in the alloyed phase but no significant success was achieved. Methods tried included modifications to the preparation procedure including variations in temperature at which co-precipitation of the gold and nickel was performed, variation of the reducing agent used for co-precipitation, and addition of slight amounts of platinum to stabilize the electrochemical potential at which co-precipitation takes place. In view of this lack of success and the poor endurance characteristics of the non-pumping electrode structure previously discussed, the development of Au-Ni catalyst cathodes was suspended.

A significant effort was expended, as previously discussed, to develop and improve the gold-platinum catalyst cathode. These electrode research efforts were also supplemented and amplified by the work of other programs which built on the base provided by past P&WA work and the NASA-LeRC supported work. Because of the interest in obtaining a higher performance, more corrosion resistant cathode than the present state-of-the-art platinum-palladium cathode, other programs are using the gold-platinum cathode. For example, the Air Force High Power Density Program sponsored by the Aero Propulsion Laboratory is using the gold-platinum cathode as standard in cells being developed for operation at current densities of thousands of amps/ft². Figure 2 shows the performance achieved by a cell using a 90Au-10Pt cathode. The high activity of the catalyst and low diffusion loss electrode structures make possible operation at 3500 amps/ft² (3766 ma/cm²), resulting in a power density of 2500 watts/ft² (2.69 w/cm²). Another example comes from the P&WA supported project which developed shop procedures for fabricating gold-platinum cathodes, which has resulted in the construction and testing of several multicell stacks using the gold-platinum cathode. The performance of one of these stacks is shown in Figure 3. This stack, which contains the number of cells required for a complete powerplant, has shown the excellent reproducibility of the gold-platinum cathode; the cell-to-cell performance variation was within 10 mv at 500 ASF (538 ma/cm²).

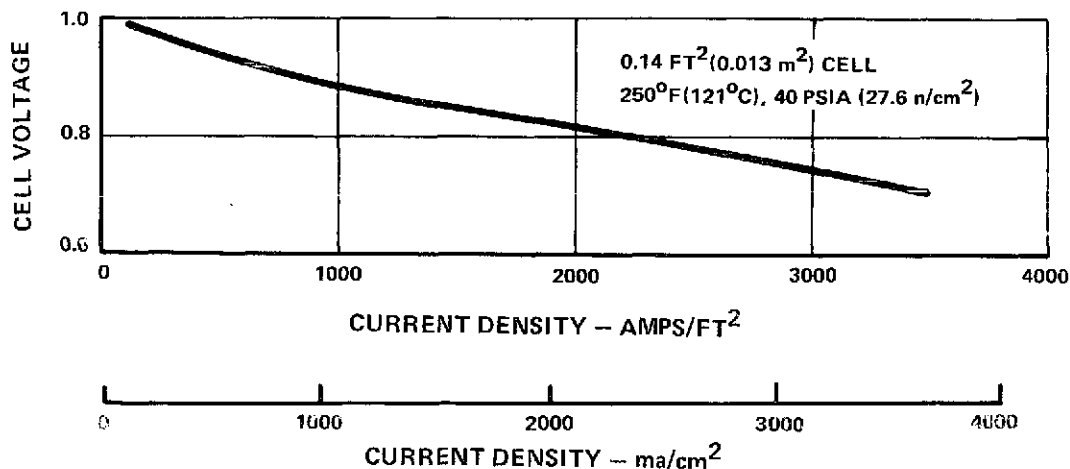


Figure 2 — Performance of High Power Density Cell Using Gold-Platinum Cathode (Air Force High Power Density Configuration)

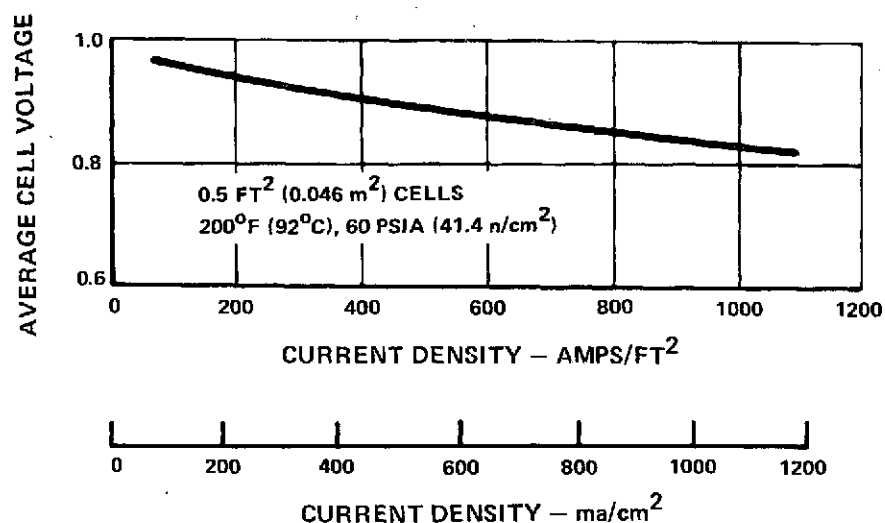


Figure 3 — Average Performance of Multicell Stack Using Gold-Platinum Cathodes

A task in a NASA-JSC sponsored program was instituted to develop vendor sources for 90Au-10Pt catalyst. Specifications were established and one vendor has delivered suitable batches of catalyst in lots of 1 kg each. Cathodes made from this catalyst have shown performance and endurance characteristics comparable to those made from P&WA produced catalyst. A laboratory endurance cell test (Cell No. 2390) was performed which demonstrated that shop-fabricated electrodes were equivalent to those prepared in the laboratory. Results are shown in Figure 4.

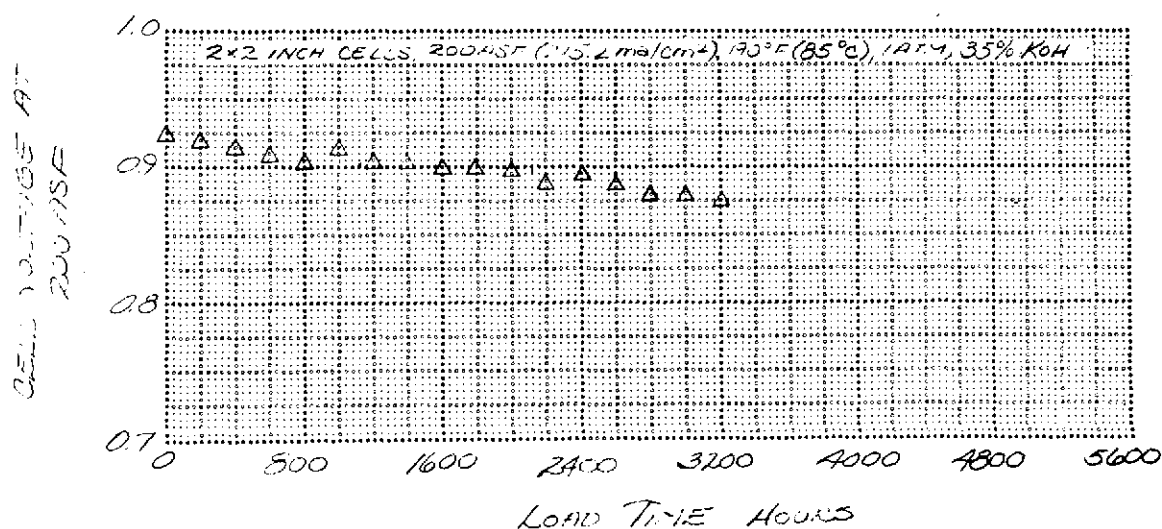


Figure 4 — Endurance Evaluation of Cell No. 2390 with 90Au-10Pt Catalyst Cathode Made in Shop

3.0 Post Endurance Test Evaluations of Full-Size Cathodes

As part of the Phase II program, three full-scale 0.114 ft^2 (0.011 m^2) cells, were endurance tested to compare degradation characteristics and losses of platinum-palladium cathodes and gold-platinum cathodes. The endurance tests are described in Section IV of this report. The post-test analyses are described in this section. The evaluations included half-cell testing of electrode sections and chemical and microstructural analyses including X-ray examination techniques to determine crystallite size. Cell No. 17, a 90Pt-10Pd cathode (PPF type) was endurance tested with a PPF anode and was the standard for these tests. Cells Nos. 23 and 24 each consisted of 90Au-10Pt cathodes tested with PPF anodes. Cell No. 24 was tested at a higher current density 500 ASF (538 ma/cm^2) than the usual 100 ASF (107.6 ma/cm^2) or 200 ASF (215.2 ma/cm^2) used for endurance tests.

All three cells were 12×1.375 inches ($30.5 \times 3.49 \text{ cm}$) with Passive Water Removal (PWR) assemblies, 22-mil ($55.9 \times 10^{-5} \text{ m}$) thick Electrolyte Reservoir Plates (ERP's) and a 10-mil ($25.4 \times 10^{-5} \text{ m}$) thick reconstituted asbestos matrix. These cells were tested at 180°F (82.2°C) with 34 weight percent KOH electrolyte and 16 psia (11.0 n/cm^2) pressure reactants. All three of these tests were eventually terminated because of low performance. Cell No. 17 was tested at 200 ASF (215.2 ma/cm^2) for 6680 hours. The cell was refurbished at 352, 4006, and 6130 hours. Cell No. 23 was tested for 4690 hours at 100 ASF (107.6 ma/cm^2) and was refurbished at 330 and 4680 hours. Cell No. 24 was tested at 100 ASF (107.6 ma/cm^2) for 350 hours followed by 500 ASF (538 ma/cm^2) for 1100 hours, 100 ASF (107.6 ma/cm^2) for 200 hours, and 500 ASF (538 ma/cm^2) for 670 hours. The cell had 1770 hours at 500 ASF (538 ma/cm^2) and 570 hours at 100 ASF (107.6 ma/cm^2) for a total time of 2340 hours. A 20 percent oxygen diagnostic was performed on the cell at 2320 hours and the cell was refurbished at 290, 1650 and 2340 hours.

Results of post-test half-cell tests for cathodes from Cell Nos. 17, 23 and 24 are presented in Figure 5. The maximum predicted performance based on half-cell tests is also shown in Figure 5. Table II shows the modes of decay for each cell at various current densities. The predicted loss is based on the results of post-test evaluations. Cell No. 17, with both a PPF anode and cathode, decayed because of cathode catalyst loss and cathode recrystallization. The results of chemical analysis show that the cathode lost 7.7 mg Pt/cm^2 of electrode, which is equivalent to 34 mv predicted decay. The results of X-ray analysis show that the average crystallite size increased 250 percent, which is equivalent to 27 mv predicted decay. The anode gained the 7.7 mg Pt/cm^2 lost from this cathode. The half-cell results in Figure 5 show that the cathode lost 61 mv in the activation-controlled region and 12 mv in the diffusion-controlled region. The activation loss from the half-cell test, 61 mv, is in excellent agreement with the sum of losses attributed to catalyst loss and recrystallization loss. The anode half-cell test showed 26 mv polarization at 200 ASF (215.2 ma/cm^2).

Cell No. 23, with a 90Au-10Pt cathode and a PPF anode, was endurance tested at 100 ASF (107.6 ma/cm^2). Anode flooding was a primary cause of performance degradation. The post-test half-cell evaluation of the anode showed 71 mv polarization at 200 ma/cm^2 . Resintering the anode at a temperature of 590°F (310°C), resulted in restoration of normal level of polarization, 30 mv at 1000 ma/cm^2 on hydrogen. A diagnostic test with 20 percent oxy-

gen, which was performed near the end of test, also indicated that decay was primarily a result of anode flooding. The Au-Pt cathode losses accounted for 25 mv decay because of recrystallization as determined from X-ray analysis. The half-cell post-test results, shown in Figure 5, indicate a 40 mv loss in the activation region. The half-cell results also show 4 mv loss at 100 ASF (107.6 ma/cm^2) due to increased diffusional resistance.

Cell No. 24, with a 90Au-10Pt cathode and a PPF anode, was endurance tested at the higher current density of 500 ASF (538 ma/cm^2). It decayed because of cathode recrystallization and increased anode polarization. The results of X-ray crystallite size determinations versus time of test for Au-Pt cathodes tested in the laboratory subscale size endurance rigs were compared with results for similar cathodes from Cell Nos. 23 and 24. The crystallite size for Cell No. 23's cathode is equivalent to those from previous low current density tests. That from Cell No. 24's cathode shows a higher growth rate in crystallite size. The crystallite size change accounts for 23 mv decay which agrees well with the half-cell test result. The anode from Cell No. 24 showed increasing polarization comparable to that from Cell No. 23 for the same time period or a loss of 8 mv at 100 ASF (107.6 ma/cm^2) and 57 mv at 500 ASF (538.0 ma/cm^2).

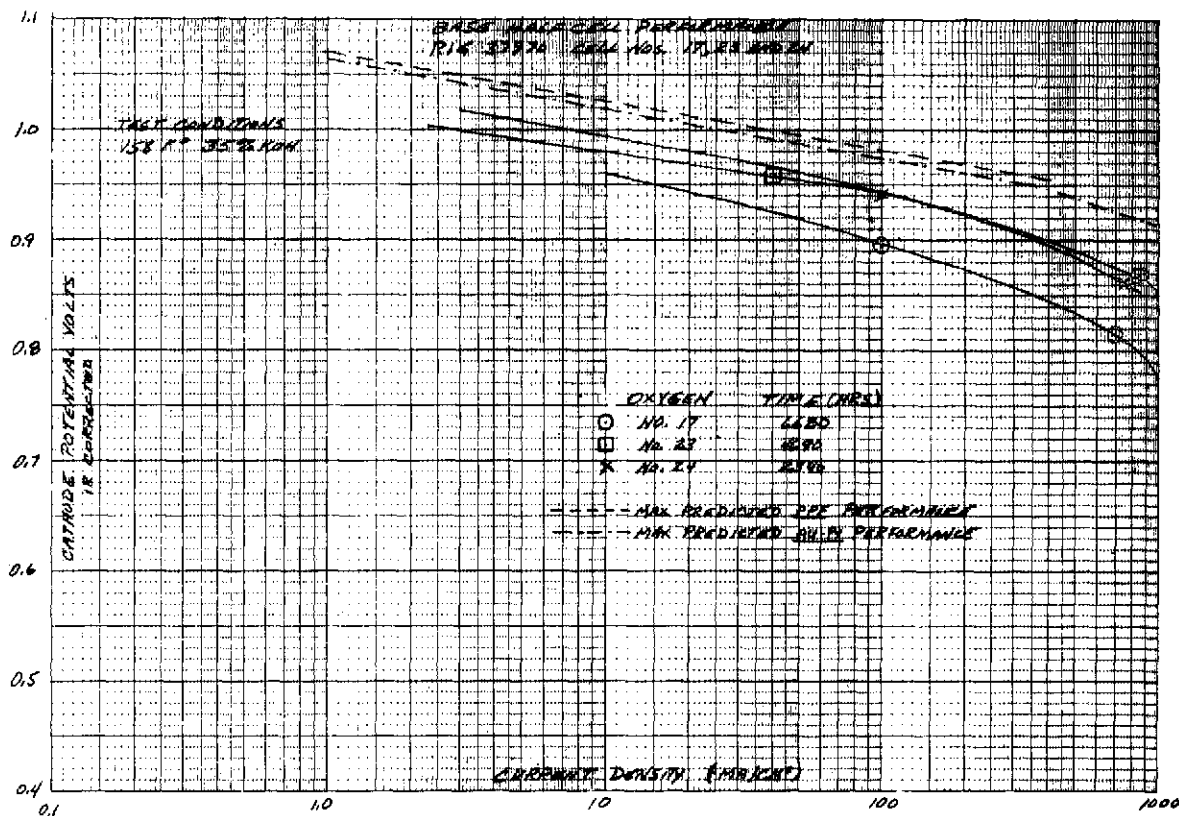


Figure 5 — Post-Test Cathode Half-Cell Performance

TABLE II
CELL NOS. 17, 23 AND 24 DECAY ANALYSES

<u>Item</u>	<u>Cell No. 17</u>	<u>Cell No. 23</u>	<u>Cell No. 24</u>		
Endurance Time - Hours	6680	4690	2320		
Current Density - ASF (ma/cm ²)	200 (215.2)	100 (107.6)	200 (215.2)	100 (107.6)	500 (538)
IR at Current Density (mv) - Initial	14	14	28	12	60
Cell Voltage (mv):					
Initial	874	908	870	918	785
Initial (IR Free)	888	922	898	930	845
Final	806	865	738	900	700
Final (IR Free)	822	882	772	918	803
Cell loss (IR Free)	66	40	126	12	42
Calculated losses from ideal performance - (mv)					
Carbonate	28	46	75	3	25
Recrystallization	27	25	25	23	23
Catalyst Loss	34	—	—	—	—
Cathode Diffusion	12	0	4	12	27
Anode Polarization	26	7	71	8	57
TOTAL (mv)	127	78	175	46	132

Based on these evaluations, it is concluded that:

- The decay of Cell No. 17 was mainly a result of PPF cathode catalyst loss and recrystallization. Analysis showed a significant platinum loss from the cathode with migration to the anode. In addition, the platinum crystallite size increase represents a considerable loss in catalyst surface area.
- The Au-Pt recrystallization is related to the operating current density. The crystallite sizes determined for the cathodes of Cell Nos. 23 and 24 were of the same

order of magnitude despite the fact that the load time on Cell No. 24 was about half that of Cell No. 23. Cell No. 24 accumulated 1770 hours at 500 ASF (538.0 ma/cm²) while Cell No. 23 operated continuously at 100 ASF (107.6 ma/cm²).

- Half-cell testing indicated that anode decay because of flooding was prevalent in Cell Nos. 23 and 24. Though this result indicates the need to improve flooding resistance of anodes, this effect may be magnified in these tests because of the relatively low reactant pressures used and the possible influence of the lack of catalyst transfer from the cathode to the anode in these Au-Pt cathode cells.
- The activation loss for Cell No. 17 is a result of platinum catalyst loss and recrystallization. For Cell Nos. 23 and 24, activation losses are due primarily to recrystallization.
- Performance losses because of recrystallization with Au-Pt catalyst cathodes are approximately the same as those observed with Pt-Pd catalyst cathodes at comparable current densities.

4.0 Anode Development

During the Phase I program, platinum-palladium (Pt-Pd) catalyst anodes were improved by: 1) more completely removing wetting agents by leaching with isopropanol; and 2) increasing sintering temperatures to increase the hydrophobicity of the electrode structure to prevent increased wetting (flooding) with time. Other modifications aimed at improved anode structures were instructive but none resulted in an unqualified success. (Ref. PWA-4542). During this program phase, anode development activities consisted of investigations of lower catalyst loadings for the Pt-Pd catalyst anode and of a rhodium-nickel (Rh-Ni) anode made by standard fabrication techniques.

The performance histories of two laboratory subscale size cells incorporating low loaded 3 mg/cm² Pt-Pd anodes are shown in Figures 6 and 7. Standard Pt-Pd anodes have 10 mg/cm² catalyst loading. Initially, Cell No. 2381 was filled with electrochemically purified electrolyte; while Cell No. 2382 was filled with standard electrolyte. This was done to investigate the relative effect that trace contaminants in electrolyte may have on the performance of low-loaded anodes. The cathodes in both cells used Au-Pt catalyst. Both cells exhibited approximately the same decay rate; and both cells exhibited a greater overall rate of performance decay than that of cells containing 10 mg/cm² anodes and Au-Pt catalyst cathodes. At about 800 hours, both test cells appeared to decay at a slightly increased rate and diagnostic tests were conducted at 1100 hours. During these diagnostic tests, the anode potential was increased to about 950 mv and impurities absorbed on the anode catalyst were oxidized (or at least desorbed) from the catalyst surface. Although the exact nature of these impurities is unknown, it is concluded that enough impurities remain, even in the initially electrochemically purified electrolyte, or that impurities in small amounts are available from cell materials or reactant gases to partially poison the anode catalyst. In cells with standard levels of catalyst loadings, the level of impurities is not sufficient to degrade performance but in cells such as these with lower catalyst loading, the percentage of active

area poisoned becomes significant. Following impurity removal by the diagnostic technique, the limiting currents of the anodes were in the same ratio as the catalyst loading which differed slightly from the nominal 3 mg/cm^2 . Decay rates following diagnostics were higher than before diagnostics until the temporary effects of anode impurity removal were dissipated. A second set of diagnostics was performed at approximately 1400 hours with similar results. Cell Nos. 2381 and 2382 were tested for 2282 and 2238 hours respectively. After shutdown, the carbonate content of both cells was determined and found to be 21.25 percent (18.1 percent conversion of KOH) for Cell No. 2381 and 31.25 percent (27.0 percent conversion of KOH) for Cell No. 2382. This amount of carbonate corresponds to a performance loss of 13 and 23 mv respectively at end of the test. The change in performance as a function of time, in which the performance has been corrected for the accumulation of carbonates, is shown in Figure 8. There is clearly no difference in the rate of performance decay between the two cells up to the time that Cell No. 2382 developed a crossover at about 2200 hours. The reaction of the cells to the diagnostic tests indicates that anode poisoning was a significant decay mechanism in both cells but was not the only mechanism later in the test. The performance of both cells up to 500 hours and immediately following the diagnostics was as good as several of the best cells operated in this program, but the overall decay rate was unsatisfactory even in the final 1000 hours is not considered. There was no significant difference with the cleaned electrolyte.

The other anode development area was the test in a laboratory 2- x 2-inch ($5 \times 5 \text{ cm}$) cell of a rhodium-nickel (90Rh-10Ni) catalyst anode (13 mg/cm^2 loading) and a standard Au-Pt catalyst cathode. This cell, No. 2391, was tested for 1200 hours with initial cell performance of 912 mv at 200 ASF (215.2 ma/cm^2) and final cell performance of 895 mv at 200 ASF (215.2 ma/cm^2). The test was terminated by cross leakage of reactants. The performance history of this cell, shown in Figure 9, indicates that this catalyst may be worth further evaluation.

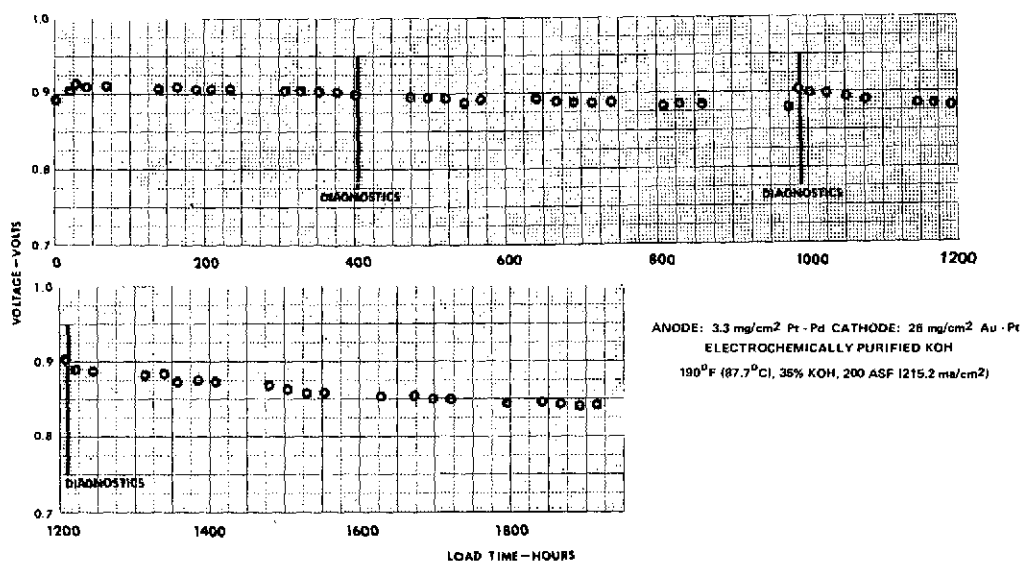


Figure 6 — 2-Inch x 2-Inch Cell No. 2381 Performance

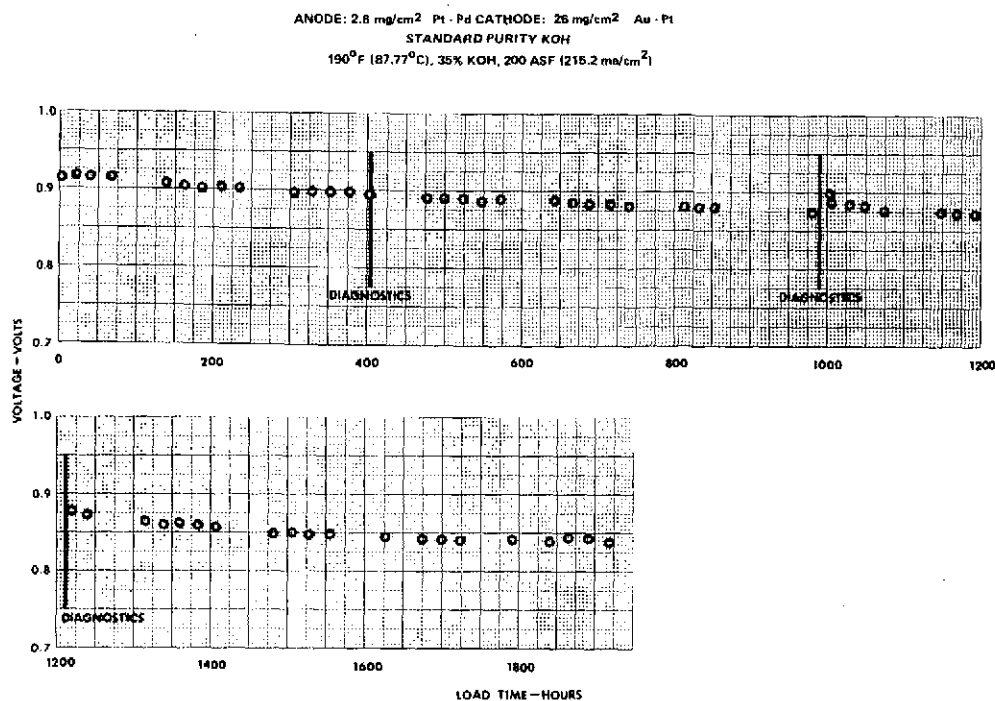
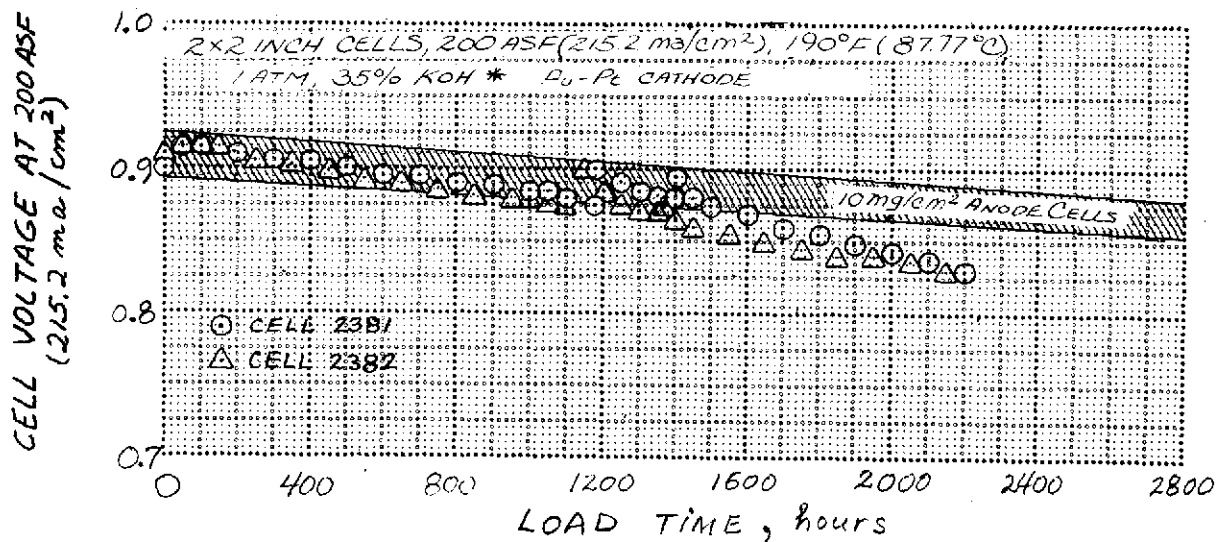
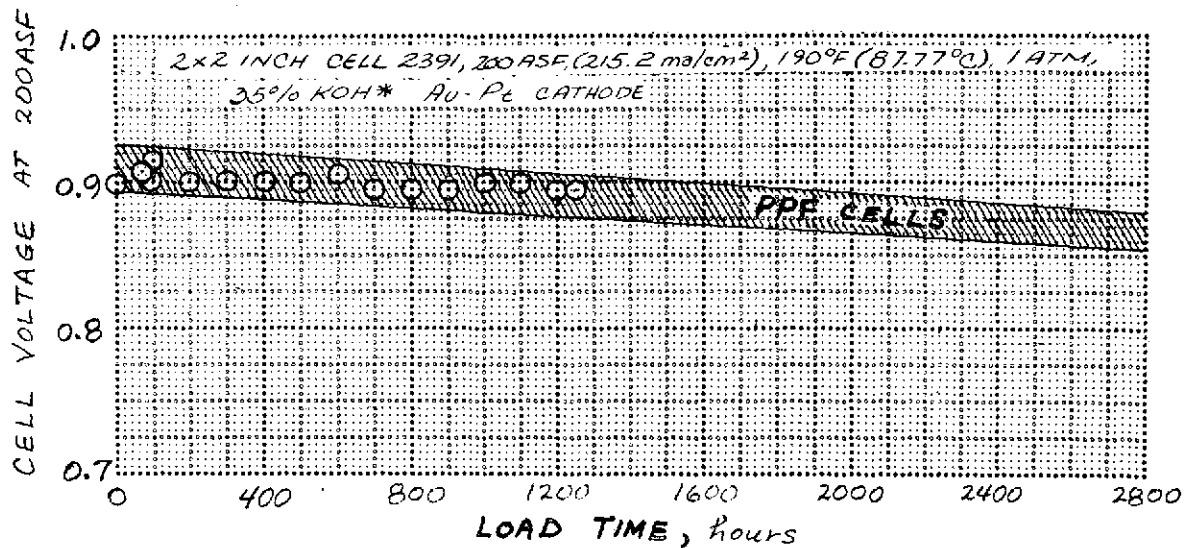


Figure 7 - 2-Inch x 2-Inch Cell No. 2382 Performance



* 2" x 2" TEST CONDITIONS RESULT IN HIGHER LOSSES
THAN POWERPLANT CONDITIONS

Figure 8 - Endurance Evaluation of 3 mg/cm² Pt-Pd Anodes



**2"x2" TEST CONDITIONS RESULT IN HIGHER LOSSES THAN POWERPLANT CONDITIONS*

Figure 9 — Endurance Evaluation of Rh-Ni Anode

5.0 Corrosion Studies

As discussed in the Phase I final report (PWA-4542), there were three factors which set the initial direction of the program. The first was the large body of data derived from previous programs which demonstrated that the dissolution of platinum (and palladium when present) from the cathode and its subsequent re-deposition in the matrix represented a life limiting mechanism. The second factor was thermodynamic data which predicted that gold would not be oxidized at cathode potential and thus would not be dissolved and transported from the cathode. Thirdly, work at P&WA over a period of several years had demonstrated that gold is an excellent catalyst for the reduction of oxygen, at least the equal of platinum.

During Phase II, a review was made of the capability of gold-platinum, platinum-palladium and gold-nickel systems from the standpoint of corrosion resistance. This review consisted of re-evaluation of the available thermodynamic information, confirmation of its validity by voltametric sweep curve testing and by correlation with corrosion tests of actual electrodes made in P&WA shop facilities under test conditions of potential and temperature more severe than those expected in a cell.

When voltametric sweep curves are generated on representative electrodes and properly interpreted, semi-quantitative or comparative measurements of the degree of corrosion are evident. Tests of this type compared 90Au-10Pt, 97.5Au-2.5Ni, 90Pt-10Pd electrodes and also a gold-wire screen. The results, shown in Figure 10, indicate that both of the gold-base electrodes are superior to the standard 90Pt-10Pd electrode, and also that gold does not show any significant corrosion at any potential up to, and including, open circuit potential.

Corrosion testing was also completed for the shop-made 90Au-10Pt and 90Pt-10Pd electrodes and a laboratory prepared 97.5Au-2.5Ni electrode. In these tests, duplicate specimens of each electrode were suspended in a 42 weight percent solution of KOH maintained at a temperature of 250°F (121°C). The electrode is maintained at a potential of 1100 mv relative to a reference electrode. These high potential and temperature conditions were selected to accelerate corrosion which might have occurred. Results are shown in Figure 11. These data indicate low weight losses for the Au-Pt and Au-Ni electrodes, with slightly larger weight losses for the Pt-Pd electrode. These results are consistent with voltametric data presented in Figure 10, and confirm the superior stability of the gold-base catalysts under these severe conditions, simulating open circuit at an elevated temperature.

There was sufficient scatter in the crystallite size determinations made before and after corrosion tests to prevent meaningful conclusions about catalyst recrystallization. However, the results suggest no significant change for either type electrode. Chemical analyses of these electrodes for constituent elements were also performed. Within the accuracy of these determinations, it could only be concluded that Pd is preferentially lost from the Pt-Pd electrode, and to a lesser extent, Pt was preferentially lost from the Au-Pt electrode.

6.0 Diagnostic and Analytical Techniques

During the time period of Phase II, certain diagnostic electrochemical techniques and chemical and physical analyses developed in P&WA sponsored fuel cell programs began to be used in this and other government-sponsored programs.

One of the techniques instituted during this period is separation of anode and cathode polarization by the dilute oxygen diagnostic test. In this procedure, the cell is operated on pure oxygen, then on 20 percent oxygen-80 percent inert gas and the individual electrode polarizations are calculated graphically. Using this procedure, the individual polarization losses can be correlated with results of half-cell tests, chemical and structural analyses determined for these electrodes, and postulated decay mechanisms or electrode structural deficiencies can be identified and corrected. This procedure makes the following assumptions:

Assumption Number 1 — Anode polarization is insignificant in the region of current density below approximately 10 ma/cm². This assumption is justified by the facts that: 1) at low current densities, concentration and ohmic polarizations are negligible; and 2) the exchange current for hydrogen oxidation on platinum catalyst is in the order of one ma/cm² of real surface area, and is therefore high enough that activation polarization is also negligible. The real surface area of platinum black in PPF-type anodes is approximately 3.0×10^3 real cm² geometric cm²; i.e. the exchange current is approximately 15 to 30 times the operating current density (100 to 200 ASF) (107.6 to 215.2 ma/cm²).

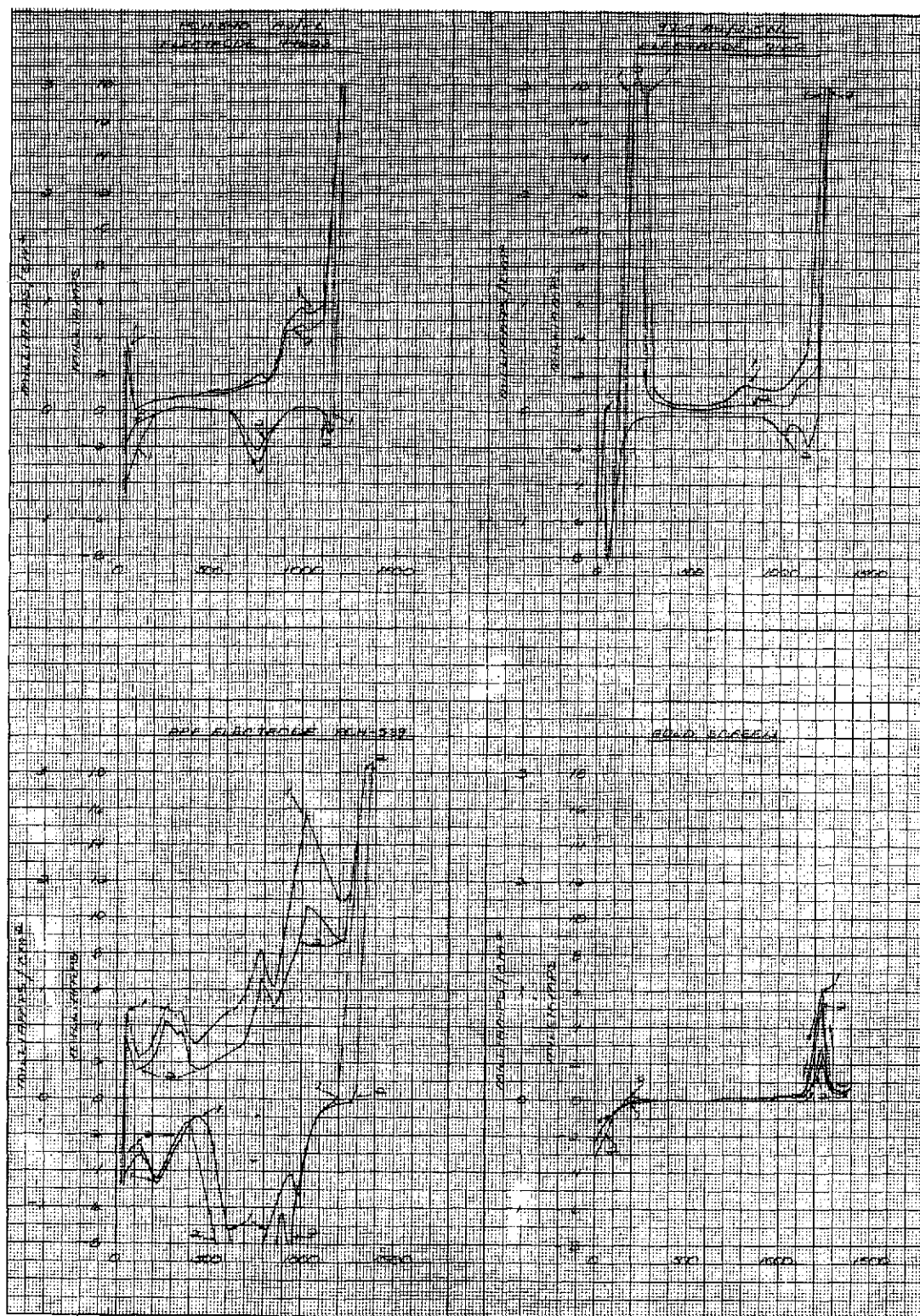


Figure 10 – Voltametric Sweep Comparison of Base Cell Catalysts

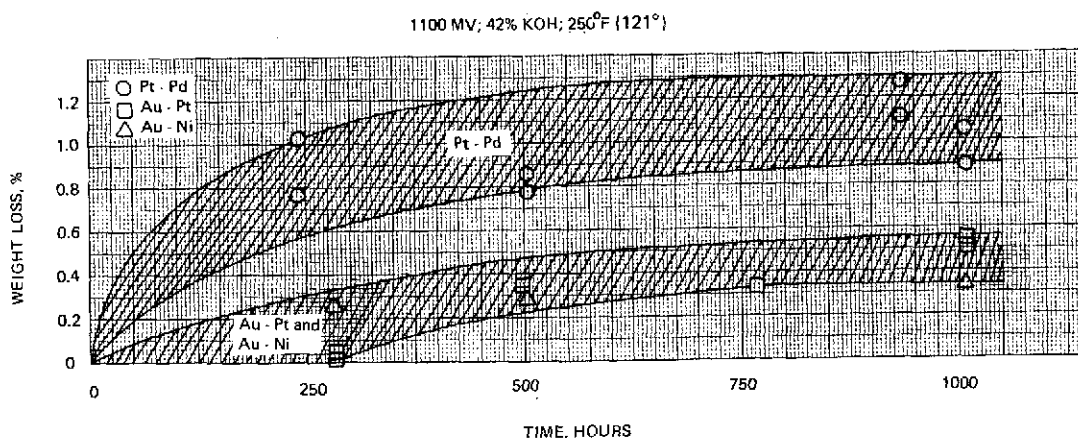


Figure 11 — Corrosion Test Results

Assumption Number 2 — The relationship between cathode current density at any constant potential on oxygen and that on air will be the same as that of the partial pressure of oxygen in the two gases, i.e., five to one. Or, at all potentials, the current is proportional to the partial pressure of oxygen in the reactant gas. This assumption is justified by the fact that not only is the electrode potential proportional to the logarithm of oxygen partial pressure under equilibrium conditions (the Nernst equation); but also, under current generating conditions in which kinetic considerations are overriding, the current is proportional to the concentration of the reacting substance (in this case oxygen); i.e., current is linear (first order) with oxygen concentration. Vetter¹ states "The cathodic current density corresponding to this reaction rate (the charge-transfer reaction associated with the cathodic partial current) is proportional to the concentration (of the oxidized substance), to the tendency of the metal to donate electrons and also to the given electron concentration near the surface".

Assumption Number 3 — There are no identified ohmic losses (either ionic or electronic) within the cathode catalyst layer structure. Assumption Number 3 is warranted, although there are ionic and electronic losses in the cathode catalyst layer structure, since in the base electrolyte electrodes in question these losses are very small and their inclusion in what the whole cell diagnostic technique terms anode polarization will not cause a gross error. These electrodes contain relatively large amounts of highly conductive Pt or Au black with relatively low percentages of non-conductive Teflon, and therefore have very small electronic losses. Since reaction in these electrodes occurs close to the electrode-matrix interface, ionic losses are also small.

The procedure is discussed further in Section IV A 5.2, Test Facilities and Test Procedures.

¹K.J. Vetter "Electrochemical Kinetics" Academic Press 1967, p. 116

Another of the diagnostic and chemical analysis techniques used in evaluation of KOH electrolyte cells is that of correction for losses due to carbonation. A body of data exists at P&WA which has quantitatively identified losses in cells because of contamination of the electrolyte by carbon dioxide and conversion of KOH to K_2CO_3 . Following test, the electrolyte is analyzed for conversion by acid-base titration technique and the loss due to carbonates can be isolated.

Several techniques used to characterize catalysts in the gold-platinum alloy system are based on X-ray diffraction analysis. Crystallite size of these powders as well as other catalyst powders down to crystallite sizes of approximately 20 to 50Å as a lower limit can be determined by the X-ray diffraction line broadening technique. In this technique, the powder is examined by X-radiation at a known diffraction angle characteristic of the alloy under study. If diffraction is from a crystal of a size large enough such that the diffracted beam is perfectly in register, then a single line peak will be observed. As the crystallites become smaller, this "line" will be broadened into a diffuse peak because of overlap of adjacent crystals in the diffracted beam until finally exceedingly small crystallites will have such a broad peak that its intensity will not be discernible from the background. The width of such broadened peaks are therefore a measure of the crystallite size.

X-ray diffraction analysis also allows determination of the degree to which the constituents of catalysts are alloyed together. For example, the gold-platinum system is one in which continuous solid solutions exist. The lattice parameters', i.e., the space between atoms in the space lattice characteristic of the metal, are known for gold and for platinum and data exists for lattice parameter as a function of platinum content in the gold-rich end of the phase diagram.² Using such data and X-ray measurements from which lattice parameters can be calculated, the extent of alloying can be determined.

B. Structural Materials Compatibility

1.0 Materials Selection

In consultation with the NASA Program Manager, several candidate fuel cell structural materials were selected for characterization during the Phase II program. The effects of the fuel cell environment on these materials were determined for up to 6000 hours of exposure. The materials were evaluated in laboratory tests which simulated cell operating conditions to determine their resistance to the potassium hydroxide electrolyte and steam-water environments typical of the Engineering Model System (EMS) Power Section. Measurements were made periodically to determine changes in mechanical properties and to determine tendencies to contaminate the electrolyte and form potassium carbonate. Test temperatures and electrolyte concentrations during Phase II were higher than during Phase I. Studies during Phase I indicated EMS operating conditions could approach 250°F (121°C) and 42 weight percent KOH. These levels of temperature and electrolyte concentration were imposed on material samples during Phase II. The materials characterized in Phase II are listed in Table III.

²E. Raub and G. Falkenburg "The System Gold-Platinum-Rhodium and the Binary Boundary Systems" Z. Metallkde, Bd. 55 (1964) H.7.p. 392-395 (In German)

TABLE III
PHASE II CANDIDATE MATERIALS

<u>Material</u>	<u>Supplier(s)</u>
50% Asbestos/50% Polyphenylene Sulfide	Johns-Manville/Phillips Petroleum
30% Fybex/70% Polysulfone	DuPont/Union Carbide
30% Asbestos/70% Polysulfone	Johns-Manville/Union Carbide
30% Fybex/70% TFE	Liquid Nitrogen Products
30% Asbestos/70% "H" — Resin	Johns-Manville/Hercules

2.0 Electrolyte Compatibility

The relative resistance of candidate materials to electrolyte was determined by immersing specimens of the materials in 42 weight percent KOH at 250°F (121°C). The electrolyte was contained in Teflon beaker in a sealed glass reaction kettle; see Figure 12. At 1000-hour intervals of testing, duplicate specimens were removed, rinsed for 48 hours in cold running water, dried for 24 hours at 150°F (65.6°C) and changes in appearance, weight, compressive strength and compressive modulus determined.

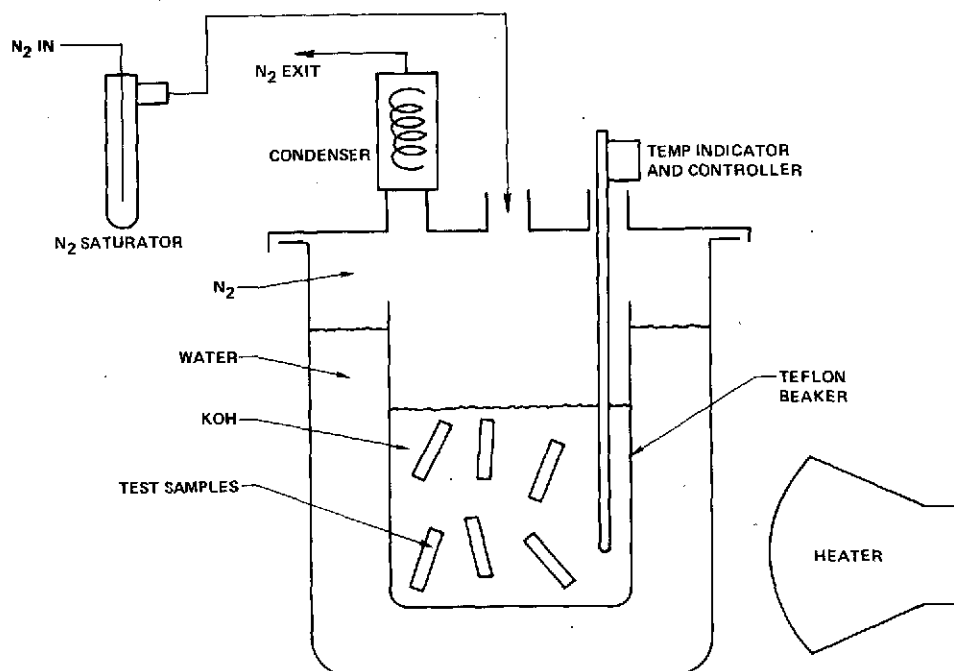


Figure 12 — Electrolyte Compatibility Test Apparatus

The changes in weight, compressive yield and compressive modulus of the materials characterized by exposure to hot KOH for 6000 hours are presented in Tables IV through VI. Only the asbestos "H" resin sample met the criterion of acceptability, less than a 0.5 percent weight change, established during the Phase I program. The 30 percent Fybex/polysulfone specimens structurally disintegrated and exhibited gross weight losses. Duplicate specimens were prepared to determine if this result could be due to faulty processing of the material used in the specimens. However, the second set of samples exhibited the same deterioration as the first set.

The changes in mechanical strength of all the materials, with the exception of asbestos - "H" - resin material, was greater than desirable for advanced fuel cell applications.

TABLE IV
CHANGE IN WEIGHT
42 w% KOH, 250°F (121°C)

Time-Hours	50 Asbestos 50 PPS	30 Fybex 70 TFE	30 Asbestos 70 H-3	30 Asbestos 70 Polysulfone	30 Fybex 70 Polysulfone
1000	+ 0.1	+ 0.3	+ 0.1	- 1.8	- 5.0 (-12.0)*
2000	- 0.9	+ 0.3	- 0.2	- 3.2	- 48.0
3000	- 1.3	- 0.4	- 0.2	- 3.7	
4000	- 1.4	- 0.9	- 0.2	- 4.0	
5000	- 1.5	- 1.8	- 0.2	- 4.8	
6000	- 2.5	- 2.5	- 0.2	- 7.1	

* Repeat test of second sample indicates similar trend.

TABLE V
CHANGE IN COMPRESSIVE STRENGTH
42 w% KOH, 250°F (121°C)

Time-Hours	50 Asbestos 50 PPS	30 Fybex 70 TFE	30 Asbestos 70 H-3	30 Asbestos 70 Polysulfone
0	5900 psi	660 psi	6,500 psi	4,650 psi
1000	- 1.8%	- 1.0%	- 11%	- 3.2%
2000	- 10%	+ 9.0%	- 7.7%	+ 7.5%
3000	- 15%	+ 21%	+ 3.0%	- 7.5%
4000	- 15%	+ 6.0%	- 6.2%	- 9.7%
5000	- 19%	- 9.0%	- 4.6%	- 13.0%
6000	- 20%	- 16%	- 1.5%	- 14.0%

TABLE VI
CHANGE IN COMPRESSIVE MODULUS
42 w% KOH, 250°F (121°C)

Time-Hours	50 Asbestos 50 PPS	30 Fybex 70 TFE	30 Asbestos 70 H-3	30 Asbestos 70 Polysulfone
0	7.3×10^3	1.6×10^5	8.1×10^5	4.6×10^5
1000	- 1.4%	+ 3.1%	- 9.8%	- 3.2%
2000	- 5.5%	+ 12%	- 7.4%	+ 7.5%
3000	- 15%	+ 25%	+ 2.5%	- 7.5%
4000	- 15%	+ 9.3%	- 6.2%	- 9.7%
5000	- 18%	- 6%	- 3.7%	- 12.9%
6000	- 20.3%	- 28%	- 1.2%	- 14.4%

3.0 Steam-Water Compatibility

Specimens of materials were exposed to a steam-water environment at 250°F (121°C) and 45 psia (31.0 n/cm²) in an autoclave; see Figure 13. Duplicate samples were removed at 2000-hour test intervals, rinsed for 48 hours in cold running water, dried for 24 hours at 150°F (65.6°C) and changes in appearance, weight, compressive strength and compressive modulus determined.

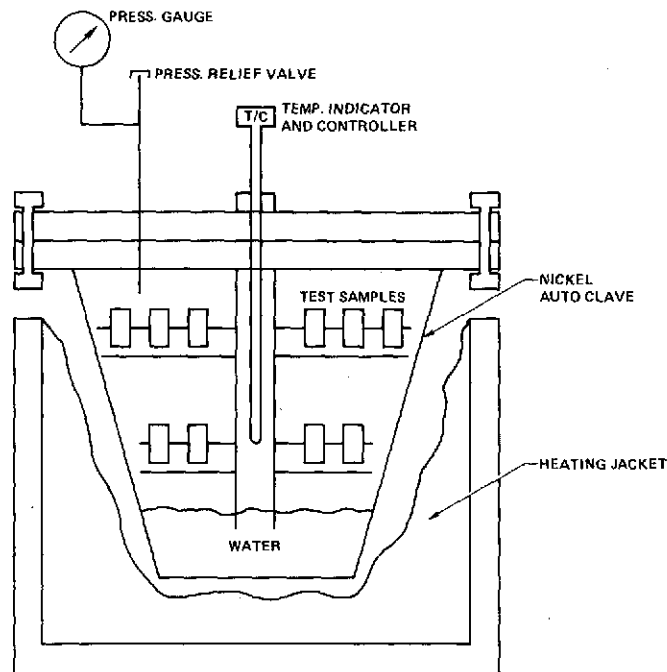


Figure 13 – Steam Compatibility Test Apparatus

Specimen size and shape for both tests were dictated by mechanical testing requirements and conformed to ASTM specification D695-63 for polymer samples.

The changes in weight, compressive yield and compressive modulus of the candidate materials upon exposure to a steam-water environment for 6000 hours are presented in Tables VII through IX. Although the weight change of all these materials is within desirable limits, the changes in mechanical strength exceeds desirable limits. Only the asbestos-polysulfone sample has potential for use in a steam-water environment. Fybex-polysulfone characterization was terminated after 2000 hours because of its gross incompatibility with KOH.

TABLE VII
CHANGE IN WEIGHT
Water-Steam, 250° F (121° C), 45 psia (31.0 n/cm²)

Time-Hours	50 Asbestos 50 PPS	30 Fybex 70 TFE	30 Asbestos 70 H-3	30 Asbestos 70 Polysulfone	30 Fybex 70 Polysulfone
2000	+ 1.3	- 0.5	- 0.05	- 0.1	+ 0.9
4000	+ 0.6	- 1.2	0	- 0.03	
6000	+ 0.6	- 1.2	0	0	

TABLE VIII
CHANGE IN COMPRESSIVE STRENGTH
Water-Steam, 250° F (121° C), 45 psia (31.0 n/cm²)

Time-Hours	50 Asbestos 50 PPS	30 Fybex 70 TFE	30 Asbestos 70 H-3	30 Asbestos 70 Polysulfone
0	5900 psi	660 psi	6,500 psi	4,650 psi
2000	- 13%	- 21%	- 7.7%	- 7.5%
4000	- 19%	- 32%	- 6.1%	- 7.5%
6000	- 18%	- 45%	- 20%	- 9.7%

TABLE IX
CHANGE IN COMPRESSIVE MODULUS
Water-Steam, 250° F (121° C), 45 psia (31.0 n/cm²)

Time-Hours	50 Asbestos 50 PPS	30 Fybex 70 TFE	30 Asbestos 70 H-3	30 Asbestos 70 Polysulfone
0	7.3×10^5	1.6×10^5	8.1×10^5	4.6×10^5
2000	- 14%	- 18%	- 7.4%	- 7.5%
4000	- 18%	- 31%	- 6.2%	- 7.5%
6000	- 18%	- 39%	- 19.0%	- 9.7%

4.0 Electrolyte Carbonation

During Phase I, the relative tendencies of materials to form carbonate in the electrolyte were determined by immersing specimens similar to those used in the compatibility tests in 30 weight percent KOH at 200°F (93.3°C). This test was found to lack the sensitivity necessary to evaluate the suitability of materials for 10,000 hours of operation. Consequently, gas chromatograph tests of samples exposed to oxygen were conducted as described in the following paragraphs. Another test developed to provide improved screening of materials is the non-operating cell test. It is described in Section IV, A, 4.0. These improved tests were used during Phase II. The Immersion Carbonation Test is reviewed for reference.

The samples are placed in a sealed Teflon bottle which in turn is contained in a sealed glass reaction kettle; see Figure 14. A sample of electrode was placed in the sealed bottle with the test specimens and an oxygen blanket covered the electrolyte to simulate cell conditions conducive to electrolyte carbonation. The test specimen surface area to electrolyte volume was standardized and remained constant throughout the test. All tests were prepared at room temperature in a glove box containing pressurized oxygen to preclude air contamination. A test set-up not containing material specimens was also prepared so that a carbonate background level for the test procedure could be established. The test procedure provided a positive oxygen pressure within the sealed bottle at the testing temperature to minimize the possibility of air contamination. The sealed glass reaction kettles also contained a carbon dioxide scrubbed nitrogen environment to further preclude contamination. Samples of electrolyte were taken at 1000-hour intervals from each test and the carbonate content determined using a double end point titration technique.

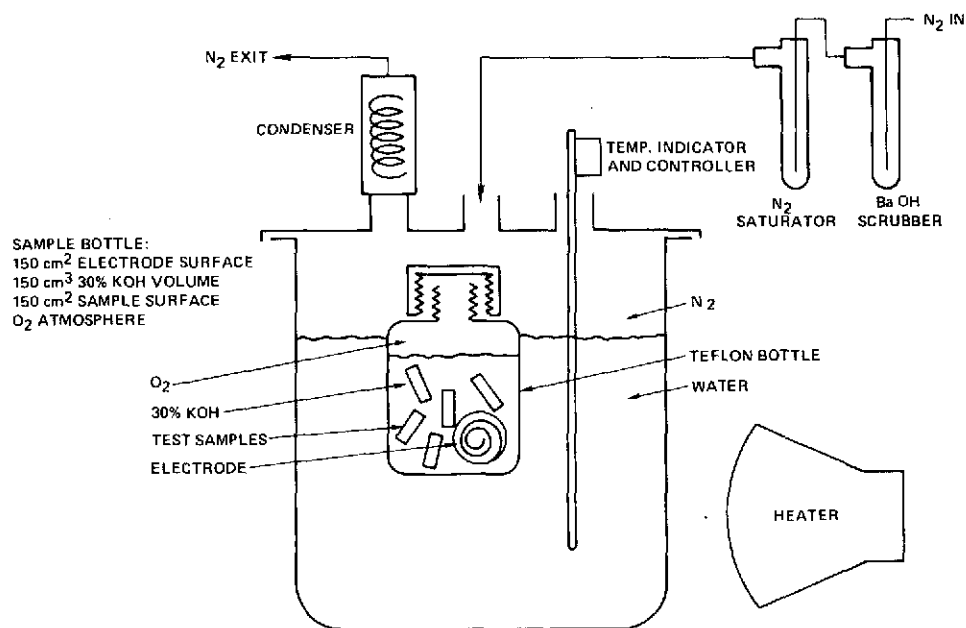


Figure 14 – Electrolyte Carbonation Test Apparatus

5.0 Oxygen Compatibility Tests

A series of tests were conducted to determine the types and amounts of gaseous reaction products that resulted from the exposure of candidate materials to an oxygen containing environment. This was accomplished by inserting material specimens having a surface area of 150 cm² into a 500 cm³ stainless steel sample bottle. The bottle was charged to 50 psia (34.5 n/cm²) with a 30 percent oxygen/70 percent helium (by volume) gas mixture. The sample bottles were then held for various periods at a temperature of 250°F (121.1°C) and the resulting gases passed through a gas chromatograph. The chromatograph indicated the relative amounts of carbon monoxide, carbon dioxide, and methane which were evolved.

Table X presents the results of oxidation resistance tests conducted early in Phase II using materials carried over from Phase I. Measurements were made at 100, 250 and 400 hours. All the materials exhibited a decreasing trend in forming reaction products with time, but none appeared to have completely stopped producing carbon dioxide. Of particular interest was the difference in the degree of stability between the polypropylene and polypropylene film samples. The film sample probably contains large quantities of processing aids which are reacting with oxygen. This illustrates the problems associated with selecting polymers without detailed specifications as to their content.

TABLE X
PHASE I CANDIDATE MATERIAL OXIDATION TEST RESULTS

Sample	Time hours	Reaction Products, PPM		
		CO ₂	CO	CH ₄
Polypropylene	100	350	140	0
	250	182	12	0
	400	290	0	0
Polysulfone	100	290	15	5
	250	210	24	5
	400	110	0	0
Asbestos Matrix	100	2000	110	5
	250	540	12	6
	400	180	0	0
30 w% Fybex Filled Polypropylene	100	1600	270	0
	400	1450	72	0
30 w% Asbestos Filled TFE	100	1260	0	5
	250	220	0	5
	400	485	0	0
30 w% Fybex Filled TFE	100	3250	165	10
	250	1100	48	0
	400	1080	0	0
FEP/Polypropylene Film Laminate	100	63000	7100	140
	250	14000	1900	15
	400	12400	840	0
Polypropylene Film	100	12600	3300	100

A sample of a pure Noryl battery case supplied by LeRC was also subjected to a gas chromatography analysis to determine the extent of oxidation. The following results were obtained:

<u>Oxidation Product</u>	<u>PPM</u>
CO	10,000
CO ₂	16,000

The results were similar to those obtained for Noryl analyzed during Phase I.

The five candidate materials selected for characterization during Phase II were oxidation tested for a longer period of time than those selected during Phase I (presented in Table X). This test consisted of 100 hours in an oxygen-helium atmosphere, followed by 2000 hours in air at 250°F (121°C) and a final oxidation period of 100 hours in the oxygen-helium atmosphere. For the five candidate materials, oxidation products were measured at the end of each 100-hour oxygen-helium environment period: The results, shown in Table XI, indicate that all of the materials passivate in an air environment at 250°F (121°C) and that their tendency to oxidize and produce carbonating reaction products is significantly reduced with time. Because of its lack of oxidation resistance, asbestos-"H"-resin is not an acceptable structural material in the oxygen environment of an alkaline fuel cell at 250°F.

TABLE XI
PHASE II CANDIDATE MATERIAL OXIDATION TEST RESULTS

<u>Sample</u>	<u>Hours Air Exposure 250°F (121°C)</u>	<u>PPM</u>		
		<u>CO₂</u>	<u>CO</u>	<u>CH₄</u>
50% Asbestos/50% PPS	0	1,536	132	21
	2,000	94	3	0
30% Fybex/70% TFE	0	1,280	90	7
	2,000	268	25	0
30% Fybex/70% Polysulfone	0	1,064	63	18
	2,000	67	1	1
30% Asbestos/70% H-Resin	0	89,600	35,712	602
	2,000	21,253	6,372	8
30% Asbestos/70% Polysulfone	0	1,770	189	17
	2,000	187	12	2

C. Lightweight Electrolyte Reservoir Plate

During Phase II, the development of lightweight electrolyte plates was continued using the basic nickel plated-porous polysulfone configuration developed during Phase I. Emphasis was placed on scaling-up the laboratory manufacturing processes, and alternative manufacturing methods were evaluated. Full-size ERP's were fabricated and were successfully tested in Cell No. 25. Figure 15 is a schematic of the Electrolyte Reservoir Plate (ERP), showing its relationship to the cell and its functions. Table XII lists required ERP characteristics.

There are four major steps involved in the fabrication of the ERP: 1) powder preparation, 2) powder sintering, 3) plating, and 4) flow field formation. Procedures were developed to make large batches of polysulfone powder using solvent spraying techniques. In this method, a solution of polysulfone resin pellets in methylene chloride (dichloro-methane) is sprayed into a large container and is allowed to settle on a liquid surface. The spray booth and liquid surface are maintained at room temperature. The resulting powder is separated by decanting and drying. Final separation and grading is effected by sieving. Both the powder shape and size can be altered by changing the percent of polysulfone dissolved in the solvent and by varying the air pressure used in the spray gun.

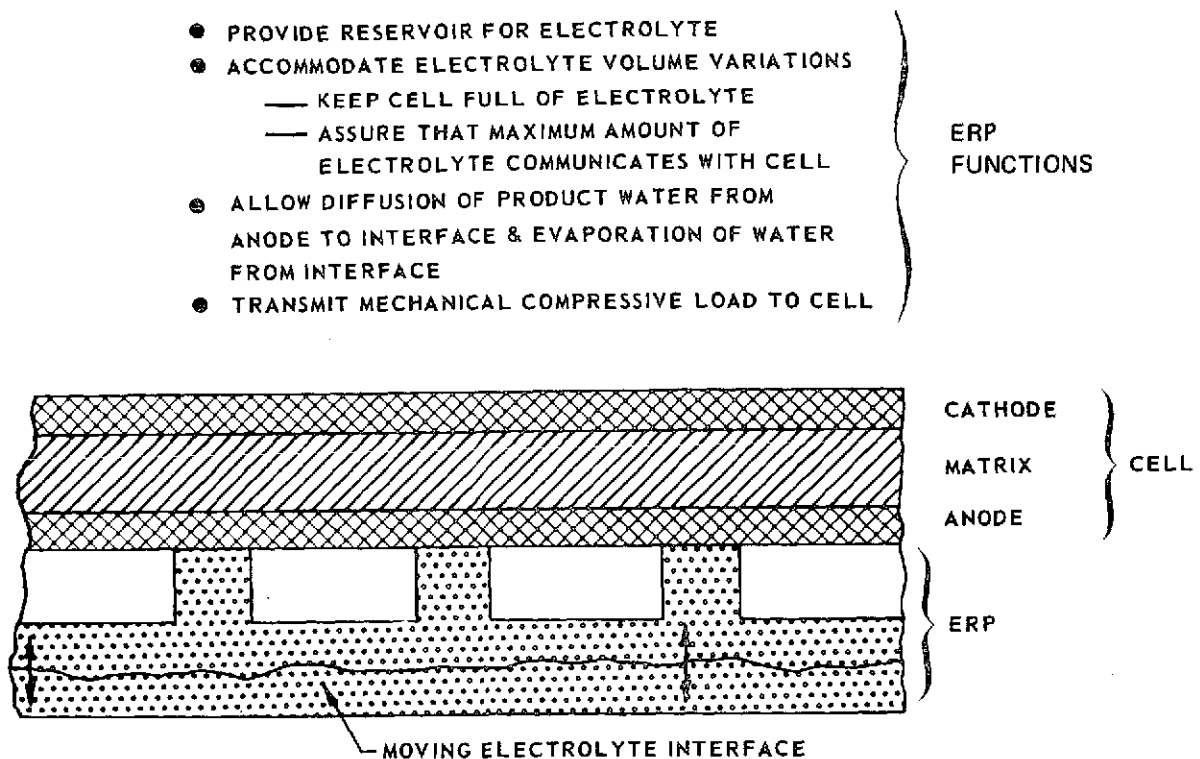


Figure 15 — Electrolyte Reservoir Plate Functions

TABLE XII
LIGHTWEIGHT ERP REQUIREMENTS

Pore size	3 to 8 microns
Porosity	As high as practical
Electrolyte flow	Readily wet by electrolyte - minimum hysteresis - ΔP vs ΔV
Compressive strength	200 psi (138 n/cm ²) minimum
Environment	200°F (93.3°C)/10,000 hrs in 25 to 45 weight percent aqueous KOH and hydrogen
Configuration	Flat plate, 10 to 30 mil (0.25 to 0.76 mm) thick, reactant flow passages in one face

The initial approach chosen to load the molding dies for sintering plates was a simple dry powder fill. Subsequent plating of these plates revealed non-uniformity of pore size related to the fill condition of the polysulfone powder prior to sintering. To achieve uniform pore size, the molds were loaded using an alcohol-powder slurry. This approach achieved uniform distribution of powder in the mold and uniformity of pore size. The effect of sintering time on ERP characteristics was also investigated.

Table XIII presents the pore spectra data obtained from these evaluations.

Additional work to increase porosity indicated porosities much greater than 60 to 65 percent resulted in an ERP too fragile to handle in a production fabrication process.

TABLE XIII
EFFECT OF SINTERING TIME ON ERP PORE CHARACTERISTICS

Sintering Time, Mins.	Sintering Temp., °F (°C)	Percent Porosity		Mean Pore Size, μ	Pore Size Range, μ
		Geom.	Pore Spectra		
60	390 (198.88)	71.6	69.4	4.0	0.2 to 5.9
90	390 (198.88)	68.6	65.5	9.3	1.4 to 12.7
120	390 (198.88)	69.4	66.1	10.9	2.7 to 16.7

Following the sintering operation, the ERP's are electroless-nickel plated to enhance their wetting characteristics. Commercial plating solutions were obtained from the Enthone Corporation and were evaluated. A process using a P&WA sensitizer and an Enthone activator produced the best uniformity and penetration of plating into the ERP. Examination of the ERP showed homogeneous distribution of the nickel throughout the ERP with a plating thickness of 0.2 mil (5.08×10^{-6} m).

Samples of ERP's prior to and following plating were tested to define their compressive strength. The results are presented in Table XIV.

TABLE XIV

ERP COMPRESSIVE STRENGTH

Sample	Proportional Limit - psi (n/cm ²)	Modulus - psi (n/cm ²)
Unplated PWA 56-4	210 (144.8)	2.5×10^5 (1.72×10^5)
Unplated PWA 56-5	230 (158.6)	2.0×10^5 (1.38×10^5)
Ni Plated PWA 57-9	1500 (1,034.2)	8.8×10^5 (6.07×10^5)

The results indicate the compressive strength of the ERP's is adequate since the compressive load they experience in a cell or stack assembly is approximately 100 psi (68.9 n/cm^2).

A large sintering mold and three plating rigs were fabricated and were used to manufacture and electroless-plate prototype ERPs. These ERPs are 3 inches (7.62 cm) wide, 14.1 inches (35.8 cm) long and have a nominal thickness of 29 mils (73.66×10^{-5} m). The thickness tolerance on the parts produced to date is ± 3 mils ($\pm 7.62 \times 10^{-5}$ m). Following plating, the blanks had a specific gravity of 1.46 gm/cc and an average porosity of 57 percent. Ten plate blanks were fabricated for use in full-scale strip cells. These blanks are oversize, flat sheets which were trimmed in size and processed to form the required hydrogen flow passages. Hydrogen flow passages are formed by pressing a screen pattern into one surface. Single Cell No. 25 was fabricated with one of these ERPs to evaluate performance characteristics. This test is described in Section IV, A, 5.3. The test results verified this approach was satisfactory for producing ERP's for full-scale cells.

Gas-phase metallization was considered as an alternative method to electroless-nickel plating for the application of nickel to the ERPs. Unplated blanks were supplied to Intertech Associates (Rochester, N.Y.) to determine if their gas-phase metallization techniques could be used to apply nickel to the blanks. Wetting tests of the processed blanks showed a slow rate of water absorption. Microscopic examination showed the reason; the outer surfaces had good coverage of nickel, but the interior surfaces had very little nickel. Consequently, this approach for application of nickel was discontinued.

Another manufacturing process was evaluated under the Air Force HPD program (Contract No. F33615-72-C-1371). Trials were initiated to prepare polysulfone powder by grinding. The resulting particle size was an order of magnitude too large and the method was not considered further.

Another complementary effort conducted under the Air Force program was development of fabrication methods for ERP's at the shop level. Powder samples were prepared in a spray booth by a solvent flash-off method as had been previously utilized in the laboratory development. These samples were measured for particle diameter and found to be in the correct range. This powder was then used to fabricate trial ERP's. The method utilized for ERP fabrication was slightly different from the laboratory process in that a dry powder casting process was used rather than slip casting with a liquid slurry. This change resulted in more rugged parts than had been previously fabricated, with improved thickness control, ± 1.5 mils vs ± 4.5 mils ($\pm 3.81 \times 10^{-5}$ m vs. $\pm 11.43 \times 10^{-5}$ m), and improved surface finish. The pore size of one of these parts was measured by mercury intrusion and found to be in the 1.5 to 6.7 micron range as shown in Figure 16. The measured porosity of 59 percent is close to the porosity of our baseline nickel ERP's which range from 65 to 70 percent. Previously, the hydrogen flow fields were pressed into the ERP's following casting and sintering. A trial piece was made with the flow fields molded into the part during the casting process. Initial visual inspection indicated that a satisfactory flow field can be obtained with this process, resulting in a higher porosity and a lighter weight than in the previous method.

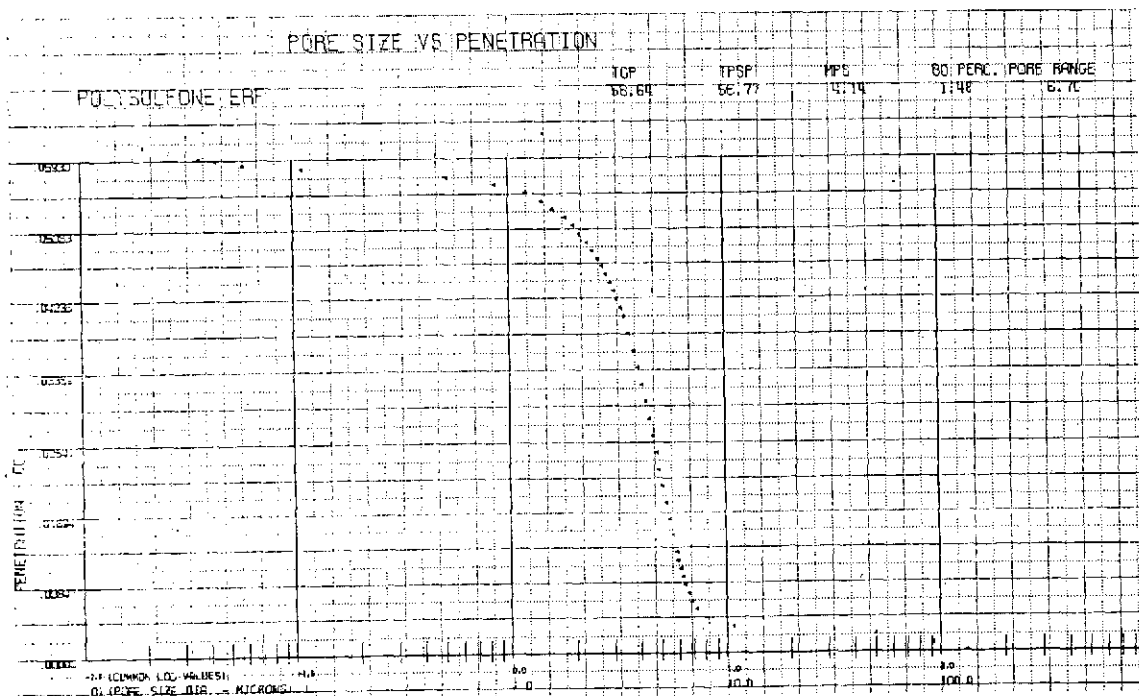


Figure 16 — Mercury Porosimeter Data on Polysulfone ERP

D. Matrix Materials

During the Phase I program, NASA-LeRC and P&WA began evaluation of potassium titanate (PKT) as a base fuel cell matrix material. The material evaluated was manufactured by E.I. DuPont de Nemours & Company under the trade name Fybex. Early tests at the LeRC and P&WA showed PKT to be compatible with KOH and to exhibit good bubble pressures, up to 20 psid (13.8 n/cm²). However, the PKT was fragile and required considerable care in handling. The strength of the matrix was improved significantly by the addition of asbestos, in quantities of up to 15 percent by weight. Characterization of this composite was begun at the end of Phase I. The results of this work are reported in Table XV for reference.

TABLE XV
FYBEX-ASBESTOS COMPOSITE CHARACTERISTICS

Fybex Weight Percent	100	95	90	85
Asbestos Weight Percent	0	5	10	15
Avg. Thickness, mils (mm)	20 (0.51)	27 (0.69)	23 (0.58)	23 (0.58)
Thickness Range, mils (mm)	19 to 22 (0.48 to 0.56)	21 to 32 (0.53 to 0.81)	20 to 25 (0.52 to 0.64)	17 to 29 (0.43 to 0.74)
Porosity at 10 mils (0.25 mm)	71%	71%	72%	68%
Bubble Pressure, psi (n/cm ²) of 4 samples from a single sheet	{ 33 (22.8) 10 (6.9) 20 (13.8) 40 (27.6)	19 (13.11) 28 (19.32) 20 (13.8) 6 (4.14)	30 (20.7) 36 (24.84) 30 (20.7) 30 (20.7)	43 (29.67) 30 (20.7) 42 (28.98) 40 (27.6)

Matrix development during Phase II began with the completion of the composite characterization and work to improve the strength of 100 percent Fybex matrices by heat treating and silk-screen printing. The last characterization tests, pore spectra determinations, are reported in Table XVI.

TABLE XVI
FYBEX-ASBESTOS COMPOSITE PORE SPECTRA DATA

Fybex - weight-percent	100	95	90	85
Asbestos - weight percent	0	5	10	15
Mean Pore Size - microns	0.7	1.9	1.6	1.3
80% pore size range - microns	0.3 - 19	0.3 - 32	0.3 - 32	0.3 - 31

The effect of heat treatment of Fybex was evaluated by sintering the material at temperatures between 750 and 1300°F (399 and 704°C). The resulting matrices, formed by the vacuum filter method, were less fragile and had better strength, but had reduced bubble pressure capability. Matrices were also fabricated using silk screen printing as a forming method rather than the vacuum filter approach. FEP Teflon was used to assist in bonding the structures. Matrices made with 6 percent FEP produced bubble pressures between 18 and 26 psid (12.4 and 17.9 n/cm²). Using Fybex from the same lots to produce matrices by the conventional vacuum filter method resulted in bubble pressures of approximately 2 psid (1.3 n/cm²).

The reduced bubble pressure of the matrices formed by the vacuum filter method was suspected to be a result of changed properties of the Fybex supplied by DuPont in later lots. Initial investigation showed no change in fiber sizes. Additional investigation, scanning electron microscope, wet chemical, emission spectrographic, and pH measurements, disclosed no significant differences in lots of Fybex fibers.

Consequently, samples of various lots of Fybex from various stages of processing were procured from DuPont. Examination of these samples and the original material revealed two differences which could impact on bubble pressure: 1) different surface roughness characteristics of the fibers; and 2) different Zeta potentials among lots of fibers.

Transmission microscopy photomicrographs show the fibers that produce low bubble pressures have a greater surface roughness. The Fybex used to produce matrices with bubble pressures greater than 20 psid (13.7 n/cm²) showed smooth surfaces.

The low bubble pressure Fybex also showed more negative values of Zeta potential: The original Fybex material (designated TTD by DuPont) had a near zero Zeta potential. (The literature indicates that the best filter papers are produced using materials which have Zeta potentials near zero.) The Zeta potential of several Fybex lots is shown below:

<u>Designation</u>	<u>Description</u>	<u>Zeta Potential - mv</u>
TTD	Fybex 11/71	0 to -5
C-602	Fybex 6/72	-25
2500 T 10	Fybex 9/72	-25
437-47-A	Hydrated Fybex	-40
437-47-D	Fiber from Breakage Ladder	-30
437-47-E	Fiber from Breakage Ladder	-32
437-47-F	Fiber from Breakage Ladder	-36
437-47-G	Fiber from Breakage Ladder	-31

An additional fifteen samples of current Fybex material, processed to various stages in DuPont's processing line and altered by controlling pH and leach time during acid leaching were procured. All had Zeta potentials between -26 and -49 mv and resulted in low bubble pressure matrix structures.

This consequently led to experimentation to increase the Zeta potential of the material. Attempts included the addition of aluminum salts (aluminum ions) to the Fybex suspension and the use of a number of different distilled water sources. Neither technique was successful with Fybex suspensions. The use of various distilled water sources did not result in significant changes; while the use of aluminum nitrate ($\text{Al}(\text{NO}_3)_3$) additions resulted in suspensions with unstable Zeta potentials. A technique to properly alter the Zeta potential of Fybex suspensions seems feasible, but would require significant development effort.

During this period, Fybex based materials and asbestos provided by the Illinois Institute of Technology (IIT) were corrosion tested in KOH. Test conditions were 42 percent KOH at 250°F (121.1°C). The results of this test are presented in Table XVII.

TABLE XVII
CORROSION TEST RESULTS — CHANGE IN WEIGHT

<u>Time Hours</u>	<u>Fybex/FEP</u>	<u>Mg(OH)₂ Asbestos</u>
250	-1.1%	-7.0%
500	-1.8	-8.0
1,000	0	-8.9

Scanning electron photomicrographs of the 75 percent Fybex, 25 percent FEP matrix showed no corrosion or reaction products after 500 hours of exposure to 42 percent KOH at 250°F (121.1°C).

The IIT material sample, prepared of leached asbestos, was 83 percent $\text{Mg}(\text{OH})_2$ and 17 percent asbestos. The asbestos contained 5.1 percent SiO_2 ; standard chrysotile asbestos contains approximately 40 percent SiO_2 . Scanning electron microscope photomicrographs of this material disclosed major fiber deterioration after 500 hours in 42 percent KOH at 250°F (121.1°C).

A matrix prepared of this material exhibited a bubble pressure of 13 psid (8.9 n/cm²). During processing, it was found that the fibers of this material would break up during reblend operations; they are considerably more fragile and brittle than asbestos.

Work on both of these materials was terminated before the conclusion of the Phase II program. The IIT material work was stopped because of its low strength and lack of corrosion resistance. The work on Fybex was interrupted because of the lack of reproducibility of matrix bubble pressure, and concern with its continued availability and its potential for reaction with TFE at the temperatures required to process the TFE-Fybex material.

IV. CELL AND STACK DEVELOPMENT

A. Single Cell Development

1.0 Introduction

The single cell task was a major portion of the technology advancement effort performed during Phase II of the Advanced Fuel Cell Program. This task again served as the focal point, integrating the results of system design analysis and the results of the materials development tasks. The NASA goals for operating life, weight and system operational features call for a significant advance in fuel cell power section state-of-the-art. These goals have led to the preliminary EMS design which established the following cell requirements:

- Minimum thickness component parts and flow fields for low weight
 - Plastic structural materials for low weight
 - Highly compatible materials for long life
 - Passive water removal
 - Evaporative cooling
 - Edge current collection, as a consequence of the above items.
- } Required by the system, and
their use favors long life

A single cell is the smallest building block for evaluation of these cell requirements. Although a single cell does not duplicate the intercell seal geometry of a plaque, and does not require evaporative cooling for temperature control, it does provide the most cost effective approach for investigation of all the other EMS cell features.

Specifically, the single cell evaluation program had as its objectives:

- (1) Test different cell component configurations and materials
- (2) Define performance characteristics
- (3) Evaluate methods for extending life

It has been conducted as an evolutionary program which allows results from the single cell tasks to feed back into the development process. The nature of the single cell program is depicted in Figure 17, which shows how the key development findings are fed back to improve performance and life characteristics.

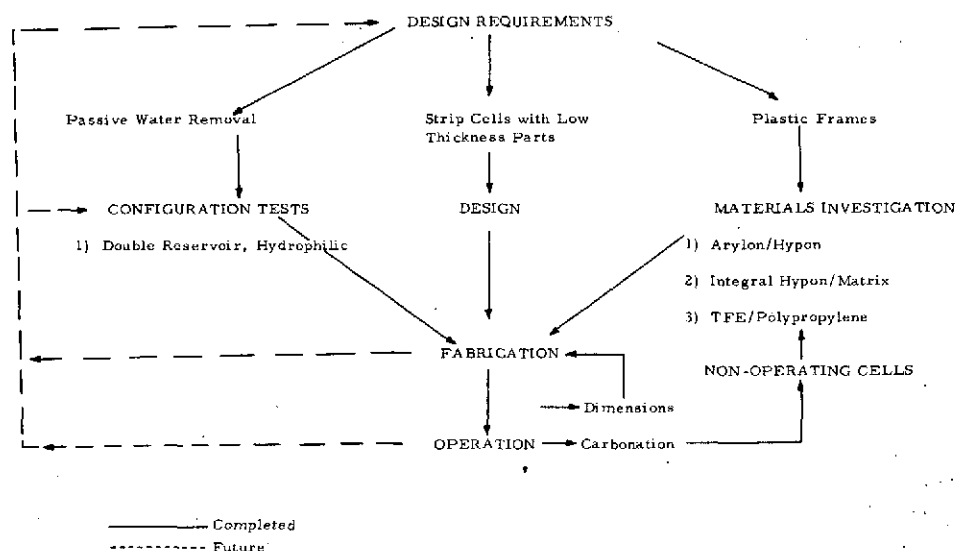


Figure 17 — Evolutionary Single Cell Development Process

The single cell program can be divided into task areas as follows:

- (1) Passive Water Removal Investigation
- (2) Single Cell Designs
- (3) Unitization Research and Cell Fabrication
- (4) Electrolyte Carbonation Investigation
- (5) Performance and Endurance Test Results

Work was carried out in each area during Phase I. During Phase II work was undertaken in only the last four areas. The passive water removal hardware developed during Phase I was used throughout Phase II. A report of the work in each task area is presented in the following sections.

2.0 Single Cell Design

This section describes the design of the single cell hardware and the successive single cell design configurations evaluated during the Phase II effort. The single cell test unit used to evaluate the results of unitization development for performance and endurance testing, and for the formal NASA Verification and Endurance category of testing was that developed in Phase I. It incorporates the novel features of the EMS design, namely:

- Strip cell - 12.0 x 1.375 inches (30.5 x 3.49 cm) cell area
- Edge current collection
- Improved compatibility frame unitization
- Passive water removal
- Minimum thickness flow fields and component parts.

Figure 18 shows the working elements of that cell and that it represents a significant improvement compared to the existing state-of-the-art as represented by the cell design used in P&WA's PC17 Space Shuttle Powerplant. The direct comparison between the PC17 and the EMS cell is not completely "fair" since the EMS requirement to remove product water by the passive method requires that an additional subassembly, the water transport plate, be added to the EMS cell. Nonetheless, the passive water removal cells tested during this program were only 60 percent as thick as PC17 cells.

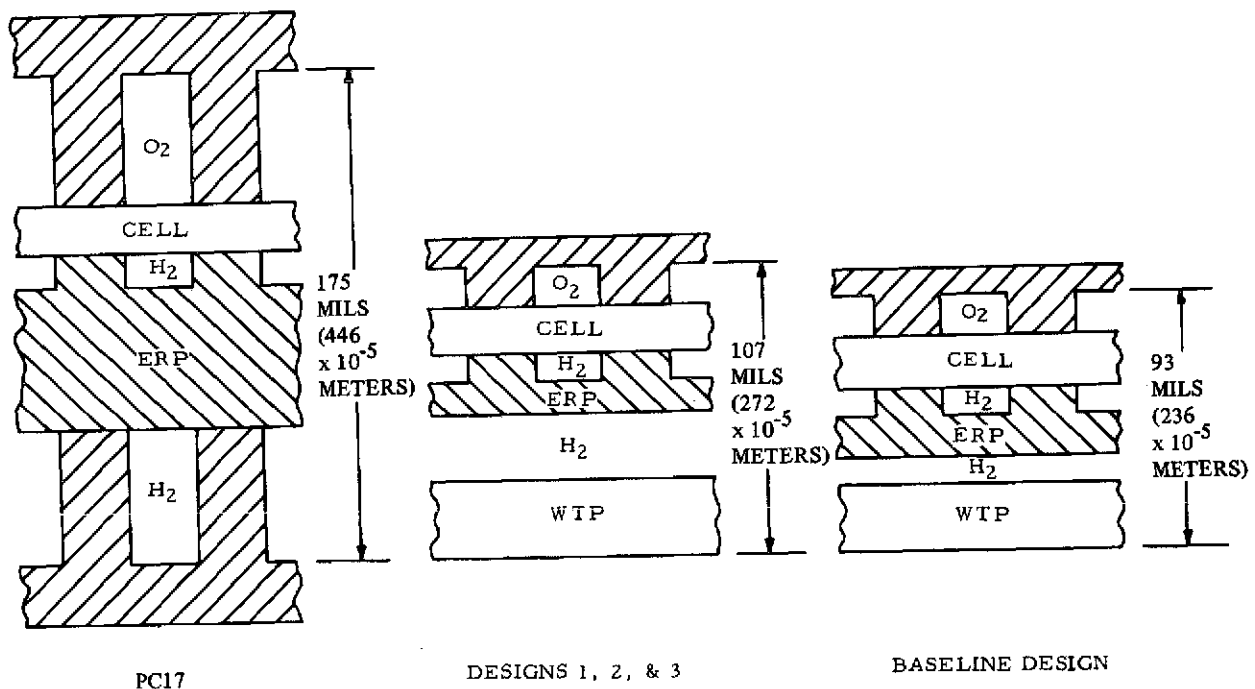


Figure 18 — Size Comparison of Cell Designs Tested

The only significant relaxation from the baseline EMS dimensions was in the hydrogen spacer, where for purposes of porting and gasketing in early cells some 15-20 mils (0.38-0.51 mm) were added. Several of the early designs also had slightly larger frame or oxygen field dimensions because of material availability problems. Baseline design values were

bettered for all the ERP thicknesses. A typical ERP used in nearly all cell designs is shown in Figure 19. It is 22 mils (0.56 mm) in total thickness. The baseline design value was 25 mils (0.64 mm). This figure shows the pin field pattern for support of the anode and the groove and hole pattern for distribution of hydrogen.

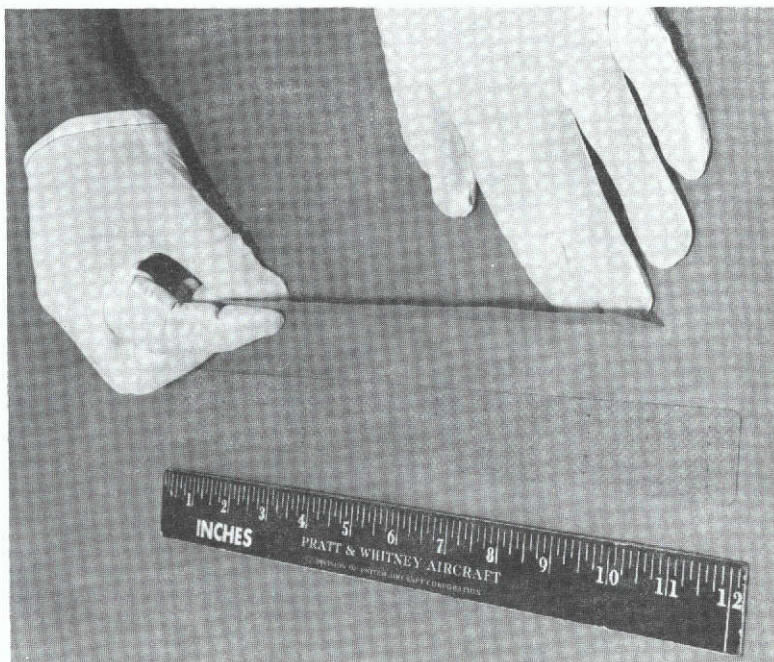


Figure 19 — Electrolyte Reservoir Plate

The cell is assembled of two sections: the unitized electrode assembly (UEA) and a unitized water transport plate, shown in Figure 20. These two components can be either bonded together or mated with an elastomer gasket between them to effect the required seal.

The cell test fixtures used during Phase II were the same as those used in Phase I. They are rigid 1/2 inch (1.27 cm) stainless steel plates with provision for sealing and fluid connections. Some of the features of the test fixtures, shown in Figure 21, are:

- Flow field inserts for interchange of field patterns
- O-ring sealing for easy assembly of unitized parts
- Isothermal operation to duplicate EMS Design
- Passive heat rejection for test simplicity
- Nickel plated to avoid corrosion

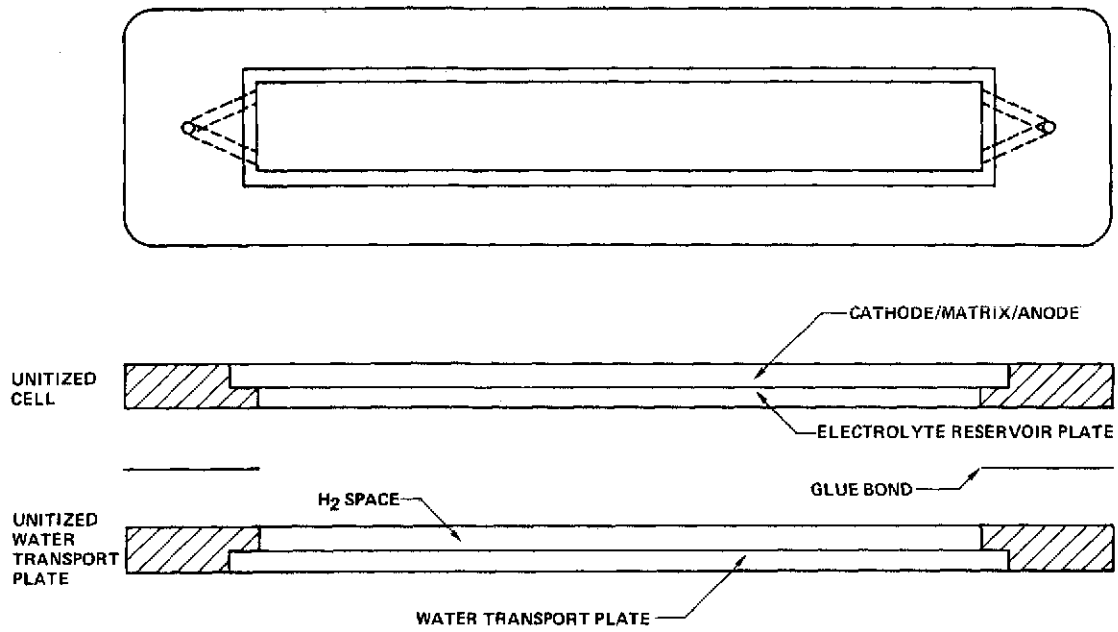


Figure 20 — Single Cell Development Plastic Frame

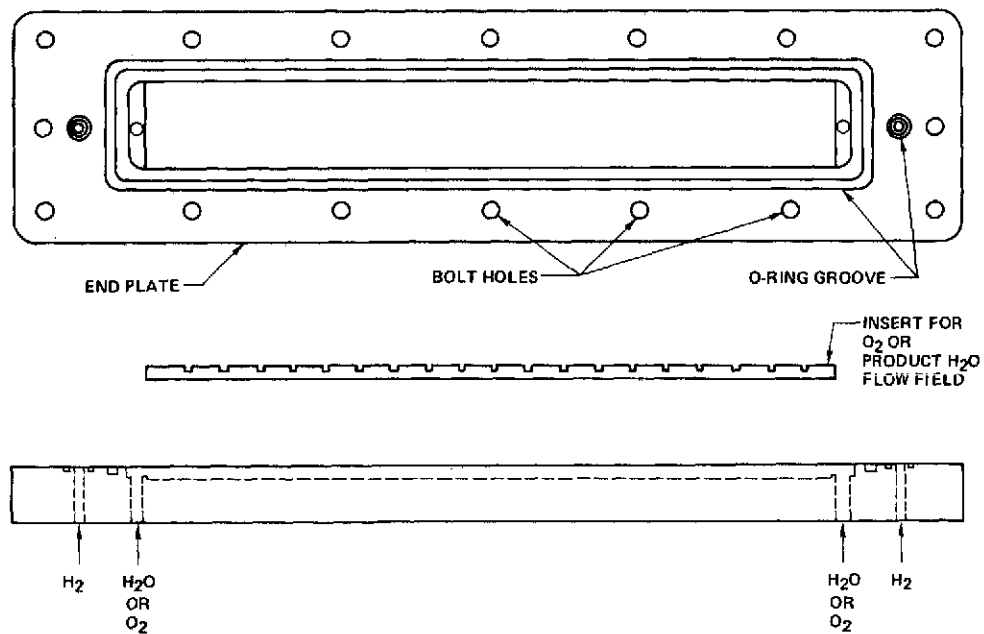


Figure 21 — Single Cell Development Test Fixture

Three thermocouples were installed in each fixture. Readings indicated uniform temperature distribution. Internal thermocouples were placed on electrodes of several cells and the temperature differed from the end plate readings by only 2 or 4°F (1.1 or 2.2°C) at the normal endurance operating conditions of 100 and 200 ASF (107.6 and 215.2 ma/cm²).

Various unitized cell assemblies were tested in the fixtures described above. The tests of two cells of Design No. 3, which had been started during Phase I, were continued into Phase II. Four additional single cell designs were submitted for Verification approval during the program, and eight cells of these new designs (4, 5, 6, and 7) were tested on Verification and/or Endurance test schedules as described in Section 5.0 (Single Cell Test Results). Two cells of Design No. 3 and two of Design No. 6 were delivered to NASA LeRC.

The configurations of the working elements of all four cell designs were the same; they differed in the construction materials used to unitize the elements and to form the cell structure. The listing below identifies the type of unitization used in the four designs. A cross sectional view of a cell showing the relative locations and dimensions of the cell elements, and the fluid flow passages appears in Section 5.0.

<u>Design No.</u>	<u>Type of Unitization</u>	<u>Cell Nos.</u>
3	Hypon Impregnated Matrix	16, 17, 18*, 19*
4	Laminated TFE/Polypropylene	21, 22
5	Hypon Impregnated Matrix	23, 24
6	Hypon Impregnated Matrix	25, 26*, 27, 29*
7	Laminated Polysulfone	28, 30

*Delivered to NASA LeRC

3.0 Cell Fabrication and Unitization Research

The EMS weight and life goals impose stringent requirements on cell fabrication technology. Thin cells are required to minimize weight and they must be fabricated to close tolerances. A cell frame thickness variation of a few thousandths of an inch which would be acceptable in conventional thicker cells would represent a significant percentage of total cell dimension for lightweight cells. This could result in degraded cell performance because of poor contact between cell components. The reactant differential pressure (bubble pressure) capability of the matrix-to-frame joint in the water transport plate and the fuel cell subassemblies must be reliable. The materials used to make this joint and to form the cell frame must be highly resistant to attack by reactants, water and electrolyte. Finally, assembly and bonding processes used must be compatible with normal manufacturing equipment and result in reasonable costs.

Phase II unitization research work consisted of two parallel efforts based on the Phase I program. The first was based on the epoxy-resin, impregnated-asbestos unitization method and the second on the laminated polymer film method of unitization.

Impregnated Matrix Unitization

The impregnated matrix unitization method was utilized as the standard fabrication process for the single cell program during Phase II. This method of cell construction resulted in frames with excellent dimensional uniformity and minimum electrode screen wrinkling. Screen wrinkling is low because of the relatively low temperature required by the fabrication process with the resulting minimal differential thermal expansion between the electrode screens and frame. In this method of fabrication, a single piece of matrix material is used and serves as the reinforcing material in the frame and also as the electrolyte retaining matrix, as shown in Figure 22. The desired frame area is impregnated with the epoxy and is allowed to air dry. Next the electrodes are laid in place with the screens extended outboard of the frame and the part is partially cured in a press. Final curing is done in an oven with the part restrained. During Phase II of this program, electrolyte reservoir plates were made an integral part of the unitized electrode assembly by bonding in place with an additional thin layer of epoxy impregnated asbestos, thus reducing the number of parts in assembly. The passive water removal units are made in a similar manner. Cell numbers 16 through 19, 23 through 27 and 29 were built in the manner described above.

All of these cells, with one exception, No. 25, were fabricated using Hypon epoxy for frame impregnation. Epon 828 was substituted for Hypon in Cell No. 25 because Hypon displayed higher corrosion rates in cell tests than had been expected based on pot corrosion tests. The Epon, however, was very brittle and no further cells were made with this material.

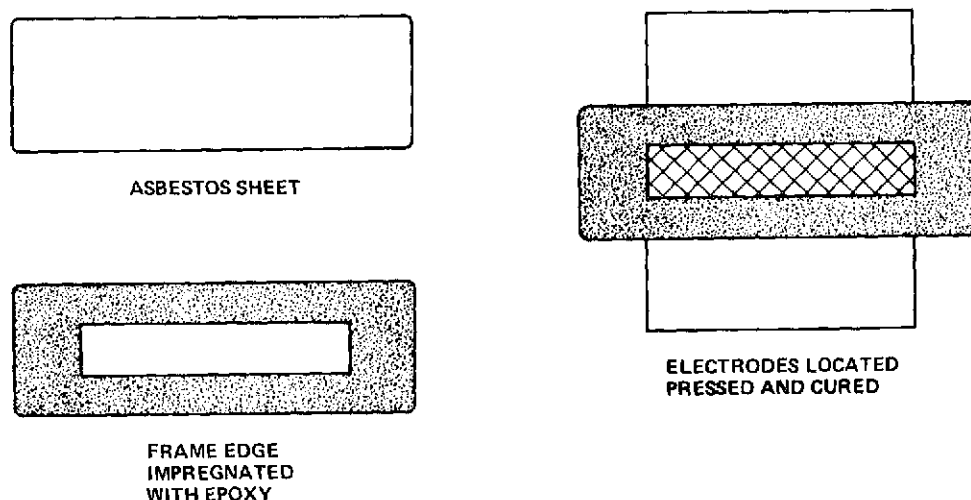


Figure 22 — Impregnated Matrix Unitization Method

Consequently, a search for a more compatible epoxy system was begun. The search was a two-pronged effort. Commercially available epoxy systems with potential for better compatibility were sought and evaluated, and a program to formulate a special epoxy system for fuel cell fabrication was begun at the United Aircraft Research Laboratories. The commercially available epoxy systems evaluated and the UARL-developed formulation are presented in Figures 23 and 24. With each listing, the result of the gas chromatography evaluation made of each material is presented. The UARL formulation E-3 demonstrated the highest corrosion resistance of all materials evaluated. This material is a resorcinol-based epoxy system, Ciba-Geigy ERE-1359, with a diaminodiphenylsulfone hardener and BF_3 accelerator. The work at UARL that led to this formulation is presented in the UARL Report M210390-1, "Improvement of Epoxy-Based Structures for Fuel Cell Unitized Electrode Assemblies", which is included in this document as Appendix B.

Based on the gas chromatography test results UARL-E3 was selected for unitization trials and corrosion testing in non-operating cell tests. The resin system, when prepared at ambient conditions, resulted in excessive flow when impregnated into the asbestos and subjected to the temperature and pressure required for unitization and dimensional control. Large void areas were also evident in the frame structure. An improvement was realized by pre-staging the liquid resin system at 250°F (121°C) for a short time before impregnating the asbestos frame. A UEA was fabricated for a non-operating cell test described in the next section; however, the void areas were not completely eliminated in this part.

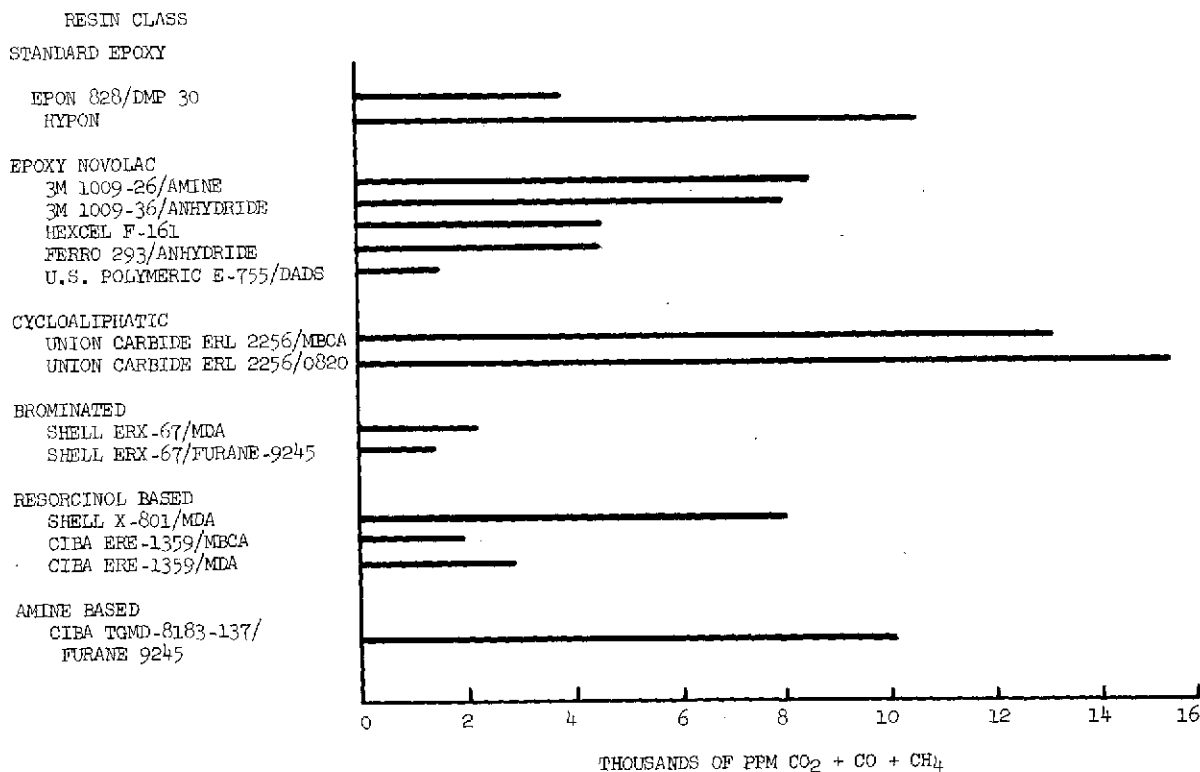


Figure 23 — Gas Chromatography — Various Epoxy Resin-Hardener Formulations

EPOXY RESIN

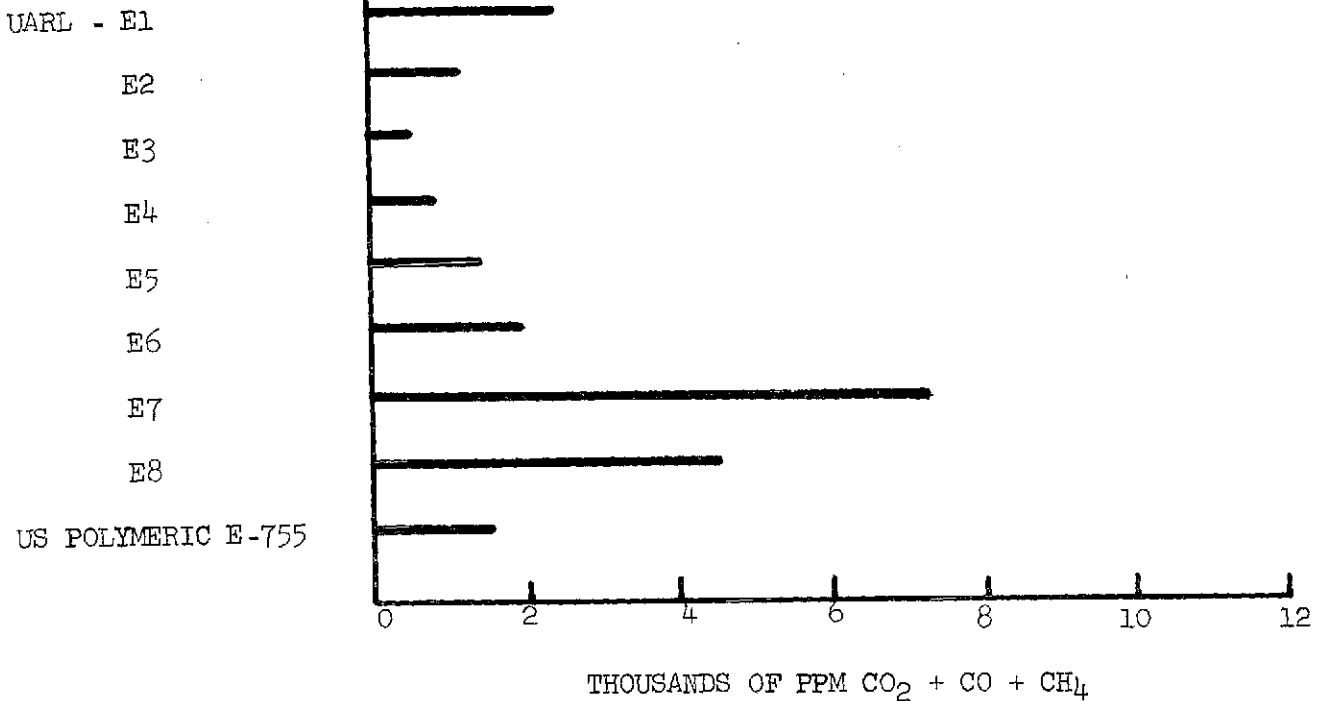


Figure 24 - Gas Chromatography Results - UARL-Formulated Epoxy Resins

Laminated Film Unitization

In the first year of this program, work was carried out on developing fabrication techniques for laminating cell frames of TFE, FEP, and polypropylene films. The basic design concept of a laminated film cell frame is shown in Figure 25. The function of the laminating film is the same as the epoxy-asbestos or epoxy-glass fiber type of unitization - to bond the several cell components together to create a unitized assembly with the required gas sealing and dimensional accuracy. The several cell components together with the film are laid-up and placed between heated platens in a press. The platen temperature is set at a level where the film material softens and flows into the cell components bonding the assembly together.

Corrosion tests in non-operating rigs demonstrated the superior corrosion resistance of these polymer materials compared with the epoxies used in impregnated matrix unitization. Two cells Nos. 21 and 22 were fabricated of these materials. They were tested as Verification Design No. 4.

Material compatibility testing revealed the excellent corrosion resistance of polysulfone films in the fuel cell environment. In addition, the somewhat lower temperatures required to unitize polysulfone assemblies made the material attractive because it was felt that electrode screen wrinkling could be minimized. Two unitized electrode assemblies were made with

adequate bubble pressure capability but efforts to make passive water removal assemblies resulted in bubble pressures short of the 12 psid (8.3 n/cm^2) requirement. Bonding of the polysulfone films was accomplished at temperatures of 400°F (204°C) in a press. Dimensional control was excellent on all parts made. Electrode screens were run through the frames for edge current collection so that in addition to testing in non-operating corrosion rigs, the assemblies could also be run as operating cells. The first of these was initially tested in a non-operating cell where it was shown that carbonate formation was minimal. These same parts were then built into an operating fuel cell with a Hypon passive water removal assembly as Cell No. 28. The cell was Verification and Endurance tested as Design No. 7. The second of these non-operating cells ran as Cell No. 30 and testing is continuing.

A more intensive development program to obtain better quality components was begun near the end of the Phase II program as part of an independent P&WA program. Though the effort to date has been concentrated on developing fabrication techniques for making polysulfone components, the program is open to the use of any material with adequate compatibility in fuel cell environment. At this time, several trial pieces using polysulfone have been fabricated with excellent dimensional control and bubble pressure in excess of 25 psid (17.2 n/cm^2). However, the degree of screen wrinkling is such that the parts are unacceptable for testing. Efforts to reduce the degree of wrinkling are under way and include use of a filled polysulfone (30% asbestos) and solvent cementing. Since screen wrinkling is due to thermal expansion differences between electrode screens and frame material, the use of a filled polysulfone, with a lower thermal expansion coefficient, should result in diminished screen wrinkling. With the use of solvent cementing, much lower temperatures can be used, again reducing the amount of wrinkling due to the smaller thermal expansion differences.

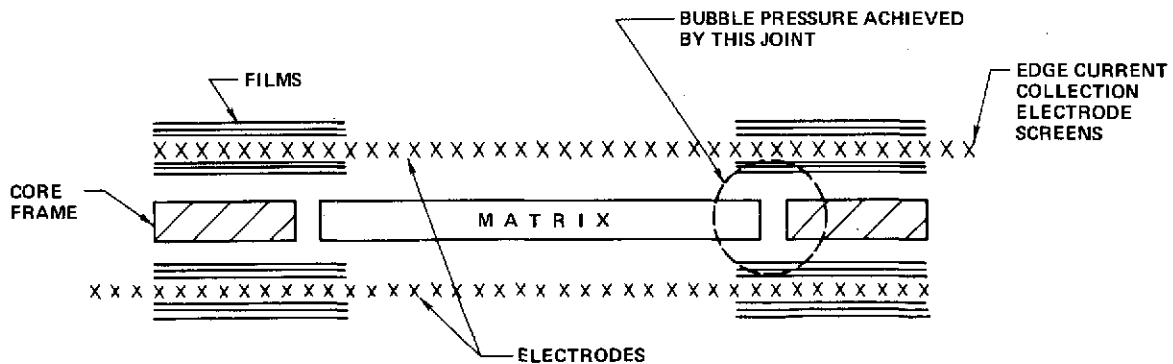


Figure 25 — Laminated Film Unitization

Hybrid Frame Unitization

Another frame concept is under consideration to overcome the corrosion or fabricating problems experienced with the previously discussed unitization methods. This is a hybrid frame fabricated of polysulfone and glass fiber-epoxy.

A narrow strip of polysulfone forms a frame around the asbestos matrix and a glass fiber-epoxy prepreg frame surrounds the polysulfone. An outer layer of polysulfone film guards against electrolyte contact with the glass fiber-epoxy. Initial samples have shown an acceptable degree of screen wrinkling. A hybrid frame structure subjected to corrosion testing in a non-operating cell, discussed in the next section, has shown this is a promising approach to overcoming corrosion.

4.0 Electrolyte Carbonation

The performance of potassium hydroxide electrolyte fuel cells can be degraded if a significant portion of the electrolyte is converted to potassium carbonate. The amount of performance loss is a function of the percentage of the electrolyte converted to carbonate and the current density. For electrolyte conversion up to approximately 25 percent, the effect is minimal at low current densities. The increasing performance losses at high current density however have an adverse effect on the voltage regulation capability of a fuel cell system. A fuel cell system whose cells contain a high percentage of carbonate would continue to operate satisfactorily but its capability to meet voltage regulation requirements would be impaired.

Two sources of contamination can cause electrolyte carbonation: (1) impurities in the reactant gases and (2) corrosion products of the cell components. This is illustrated in Table XVIII. Carbon dioxide contained in either reactant reacts with the electrolyte to form potassium carbonate. Investigations at NASA-LeRC have shown that methane contained in the oxygen may oxidize and result in electrolyte carbonation. The amount of methane converted is a function of cell design, operating conditions, and purge frequency.

TABLE XVIII
CARBONATION IN ALKALINE ELECTROLYTE CELLS

<u>Contamination Sources</u>	<u>Amount of K_2CO_3 Formation</u>
Hydrogen - CO_2	CO_2 - . PPM Contained in Reactants
Oxygen - CO_2 , CH_4	. Cell Reactant Consumption (amp-hours)
Cell Structural Materials	CH_4 - . PPM Contained in O_2
	. Stay-Time in Cell (Purge Frequency)
	. Operating Conditions
Structures	. Compatibility with KOH and O_2
	. Cure Time/Temperature of Adhesives
	. Surface Area and/or Mass of Material in Cell
	. Operating Conditions

The second potential source of electrolyte carbonation is the cell itself. The materials used in the cell can react with the fluids present, creating products which react with the electrolyte. The amount of carbonate producing substances is a function of the materials used, the surface area and mass of materials present in the cell which are exposed to electrolyte and oxygen, and the cell operating conditions.

The effect of the electrolyte carbonation on cell performance is related to the fraction of the electrolyte converted to carbonate. The cell designer has flexibility in selecting the amount of electrolyte the cell will contain. By increasing the thickness of the electrolyte reservoir plate, a larger inventory of electrolyte is made available for absorbing any carbonate producing substances, thus keeping the percentage conversion low. However, the increased weight of the reservoir plate and the electrolyte it contains results in a heavier cell. The designer can also reduce the sensitivity of the cell to any contaminants produced by the structural materials used to package the active elements of the cell by minimizing the amount of edge frame around the electrode area.

The 10,000-hour life and the tight voltage regulation goals of this program require that the performance decay due to electrolyte carbonation be extremely low. The goal for minimum cell weight dictates that large amounts of electrolyte contained in thick reservoir plates cannot be used. The system design concept requires cells with high perimeter-to-area ratios connoting stringent requirements for the compatibility of the materials used in the cell frames. These factors were the basis for planning several interrelated research tasks to develop the technology of lightweight cells capable of operating for long durations with minimum performance loss because of electrolyte carbonation.

The carbonation results from early strip cells tested in Phase I indicated a need to develop more sensitive compatibility testing techniques to allow rapid screening of candidate materials and cell unitization designs. One result was the addition of the oxidation tests using gas chromatograph techniques. Another technique developed was the use of non-operating cells to evaluate the relative carbonation characteristics of promising unitization designs. The non-operating cells provide an accelerated measurement of carbonation rates of realistic cell configurations. A cell frame represents a combination of materials not possible to simulate in simple, single fluid compatibility tests.

A non-operating cell consists of a strip cell, 1.375 x 12 inches (3.49 x 30.5 cm), without an electrolyte reservoir plate, mounted between cell end plates. A schematic drawing of this test fixture is shown in Figure 26. The cell is tested with oxygen in both reactant compartments to expose a maximum area to the oxidizing atmosphere. The cell is mounted in a 212°F (100°C) oven and the reactant passages pressurized with 16 psia (11.04 n/cm²) oxygen. During Phase II a test temperature of 212°F (100°C) was used as opposed to the 180°F (82.2°C) temperature used during Phase I. This increase in temperature reduced required exposure time for the same degree of carbonation from 200 to 100 hours. After the conclusion of the exposure period, the electrolyte is analyzed to determine the amount of carbonation present. By minimizing the amount of electrolyte in the cell only the matrix and electrodes are filled with electrolyte the non-operating cell is a sensitive indicator of carbonation produced by the cell components and structural materials.

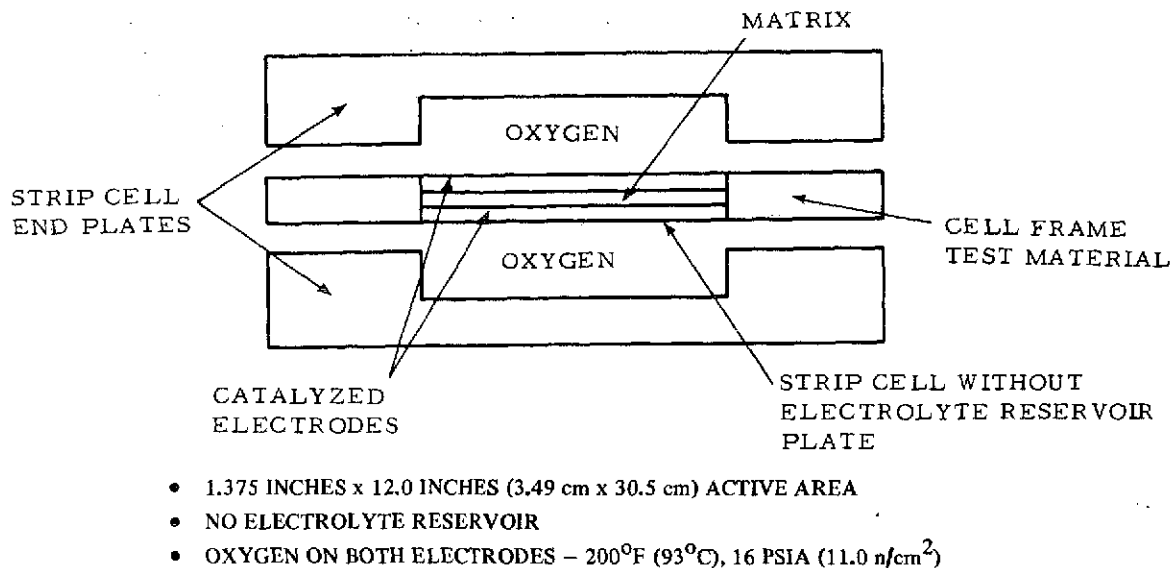


Figure 26 – Carbonation Test Rig

Non-Operating Cell Tests Results

The first task of the non-operating cell tests of Phase II was to complete the evaluations begun in Phase I. The remainder of the Phase II activity evaluated a second group of materials.

Figure 27 presents the results of the first tests of Phase II and the data from Phase I for reference.

Carbonation Cell No. 14 was tested in the full size, non-operating, oxygen-KOH corrosion rig. This cell had a unitized electrode assembly laminated from 30 percent asbestos-filled Teflon frames and polypropylene film. The cell was tested at 200°F (93°C) for 232 hours. The carbonate formation rate was very low, comparable to the all Teflon unitized electrode assembly.

Cell No. 15 was a full size cell fabricated using Epon 828 resin. Corrosion tests of Epon 828 predicted a low rate of carbonation for the cell tests.

Because of the unexpectedly high carbonation data (18 micrograms of K₂CO₃/hour-inch of perimeter), Cell No. 16 repeated the "Components Only" test of Cell No. 13. The results indicate no significant problem with the test rig. Examination of the Cell No. 15 frame suggested incomplete epoxy impregnation of the matrix, permitting exposure of more epoxy to the environment, may have produced the higher corrosion rate.

The results of the carbonation tests of the second group of materials are shown in Figure 28.

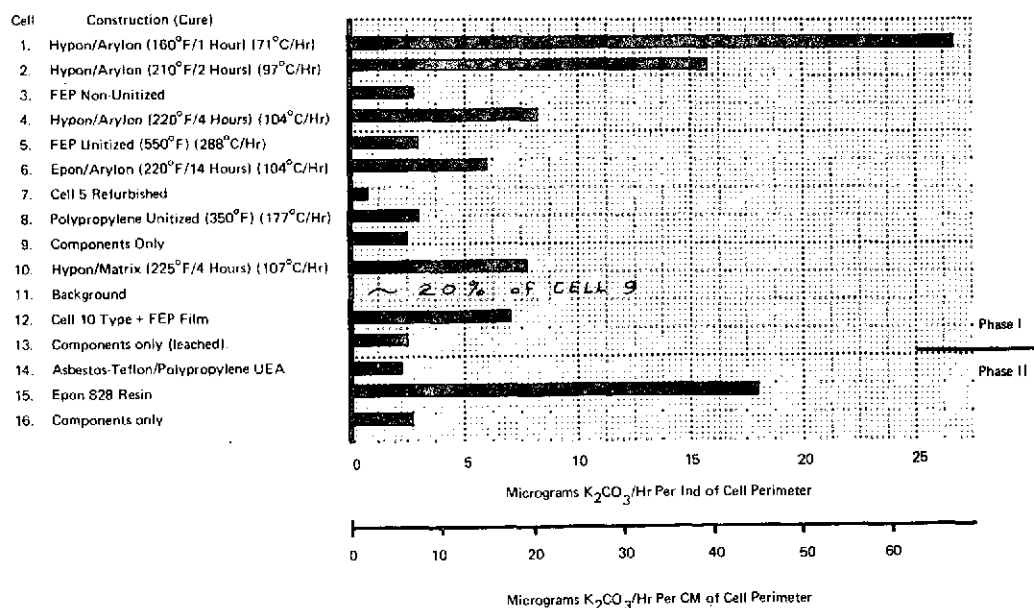


Figure 27 — Non-Operating Cell Test Results (Phase I Materials Group)

CELL CONSTRUCTION (CURE)

- 1 E-755/FIBERGLASS
- 1A E-755/FIBERGLASS
- 2 E-755/ASBESTOS (325°F)
- 3 POLYSULFONE
- 4 E-755/ASBESTOS (375°F)
- 4A E-755/ASBESTOS (375°F)
- 5 HYPON (225°F)
- 5A HYPON (225°F)
- 6 COMPONENTS
- 6A COMPONENTS
- 7 E-755/ASB IMPREG
- 7A E-755/ASB IMPREG
- 8 UARL-3 EPOXY/ASB IMPREG
- 9 PREPREG POLYSULFONE HYBRID
- 9A PREPREG POLYSULFONE HYBRID

NOTES:

STANDARD CELL

0.87 GMS KOH
16.4 IN² ACTIVE AREA
26.7 IN² PERIMETER

TEST CONDITIONS

212°F
~100 HOUR EXPOSURE TO OXYGEN

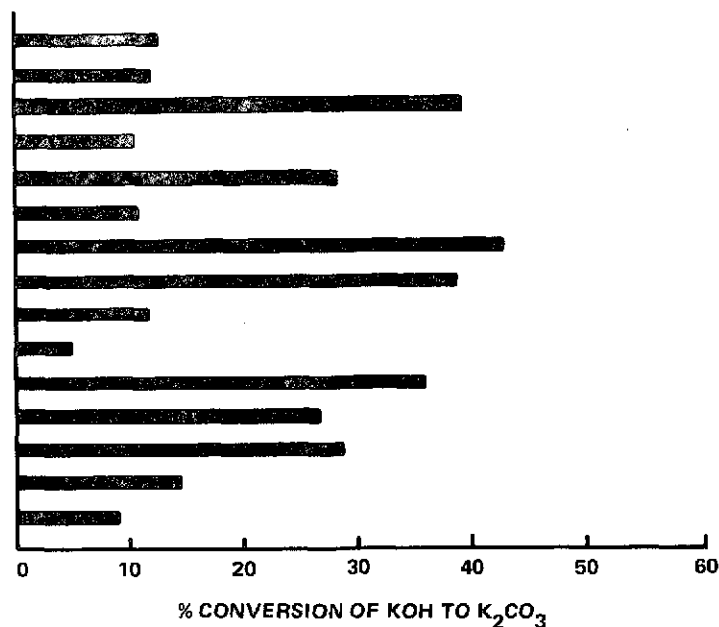


Figure 28 — Carbonation Cell Test Results (Phase II Materials Group)

As expected, Hypon appeared as the least compatible material. Carbonation data obtained from single cell test substantiate this finding. On retest, little improvement was noted. The relative ranking of polysulfone film as the best material is consistent with gas chromatography results. Results were similar to those for Teflon and polysulfone in the Phase I materials group. Retest of the polysulfone film was not carried out because the test piece was incorporated into single Cell No. 28.

The comparatively low carbonate levels from the E-755/fiberglass samples were quite surprising. This material is used in standard P&WA 0.5 ft² (0.046 m²) cells and has shown better stability since incorporating a change in matrix penetration into the frame. The E-755/asbestos prepreg and E-755/asbestos impregnated samples showed considerably higher carbonate results. Since gas chromatography results showed little difference in CO₂ levels between E-755/fiberglass and E-755/asbestos prepreg, (1930 vs. 1820 ppm) an apparent contradiction existed. A possible explanation is that KOH wicks deeper into the asbestos prepreg, thus contacting more epoxy. Also, if impregnation of epoxy in the asbestos is incomplete, more epoxy surface is exposed for attack by KOH. In-place impregnation is more susceptible to incomplete filling with epoxy, and this offers an explanation for the high carbonation results of Hypon/asbestos impregnated samples (Cell No. 7 and 7A).

As a result of the epoxy improvement program conducted at the UAC Research Laboratories, an epoxy formulation with better compatibility to oxygen, (based on gas chromatography results) was developed. This epoxy, called UARL E-3, was tested in Cell No. 8, but carbonation was disappointingly high. However, fabrication difficulties precluded making a test specimen free of void areas, and the poor results can be attributed to the high void content in the epoxy-asbestos frame. It is interesting to note that all epoxy-impregnated samples tested showed carbonate levels considerably higher than other test pieces, suggesting that fabrication techniques are not adequate to eliminate or minimize void areas in the frame.

Cells Nos. 9 and 9A were the first tests of a hybrid polysulfone-glass fiber prepreg frame. This frame concept has exhibited one of the lowest corrosion rates to date. As with previous samples, the retest result (Cell No. 9A) was considerably improved suggesting an initial level of impurities which were leached out in the first test. Because of the promise of this approach, good corrosion resistance and minimum screen wrinkling, operating cells of hybrid construction will be tested during the next phase of the program.

5.0 Single Cell Tests

5.1 Introduction - The overall goals of the single cell test program were to:

- Perform short term performance tests, with suitable diagnostics, to determine the following performance characteristics:
 - Voltage vs. current density (performance calibration)
 - Response to different operating conditions (off-design tolerance)
 - Electrolyte retention

- Define endurance limiting phenomena and develop methods for extending cell life.

This section describes the significant test results from the single cell program. In summary, over 43,200 hours of fuel cell load time were accumulated on 26 different cells. Predicted performance, off-design tolerance and electrolyte retention were demonstrated. Various cell performance deficiencies were identified by cell diagnostics and corrected. Cell endurance capability was improved markedly as a result of the unitization research program. At the conclusion of the Phase I portion of the program, cell tests were in progress at operating current densities of 100 and 200 amp/ft² (107.6 and 215.2 ma/cm²) for periods up to 6680 hours with acceptable stability.

The following sections discuss these performance and endurance results. The test facilities and procedures are first described. Next, an overview of the several cell configurations and a summary of each cell tested is presented. Then typical cell results, both good and bad, are described in sufficient depth to document the above observations.

5.2 Test Facilities and Test Procedures

The test facilities used for full size, single cell testing are shown in Figures 29 and 30. These stands were originally used for work performed under contract NAS3-13229 and were adapted for passive water removal cell testing during the present contract. A schematic of the test stands is shown in Figure 31

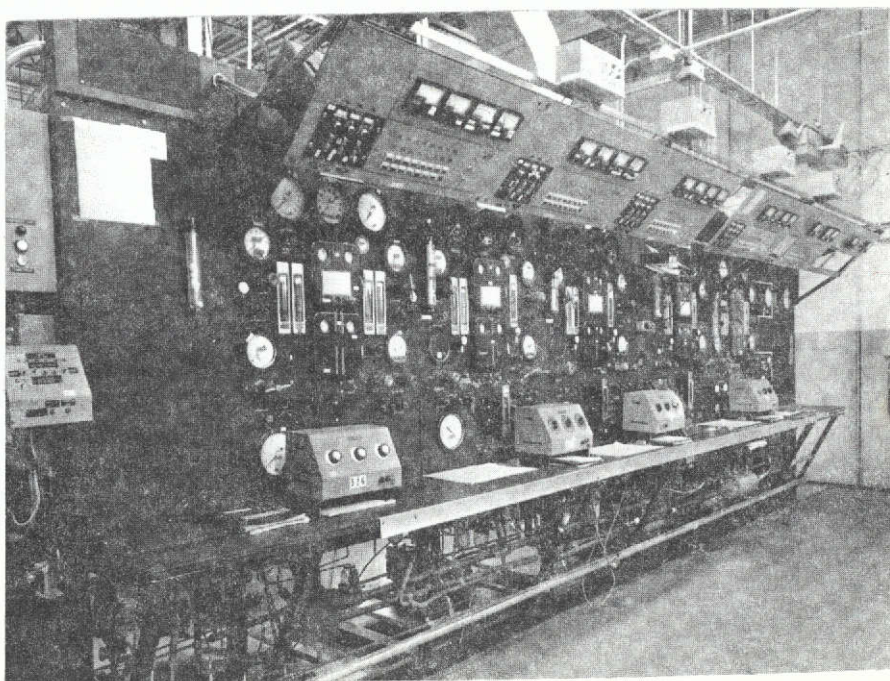


Figure 29 — Single Cell Test Facility (Front)

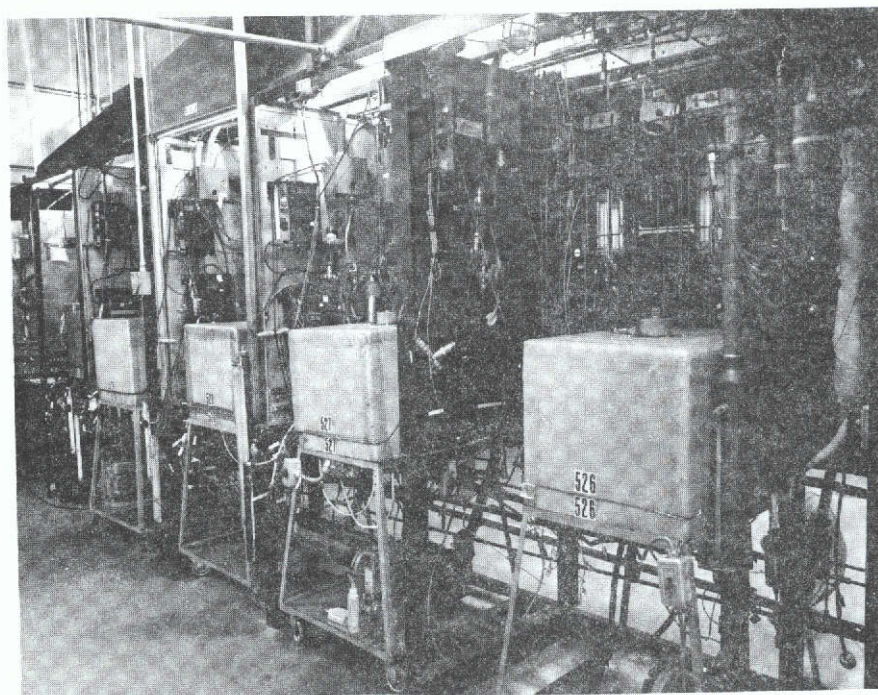


Figure 30 — Single Cell Test Facility (Rear)

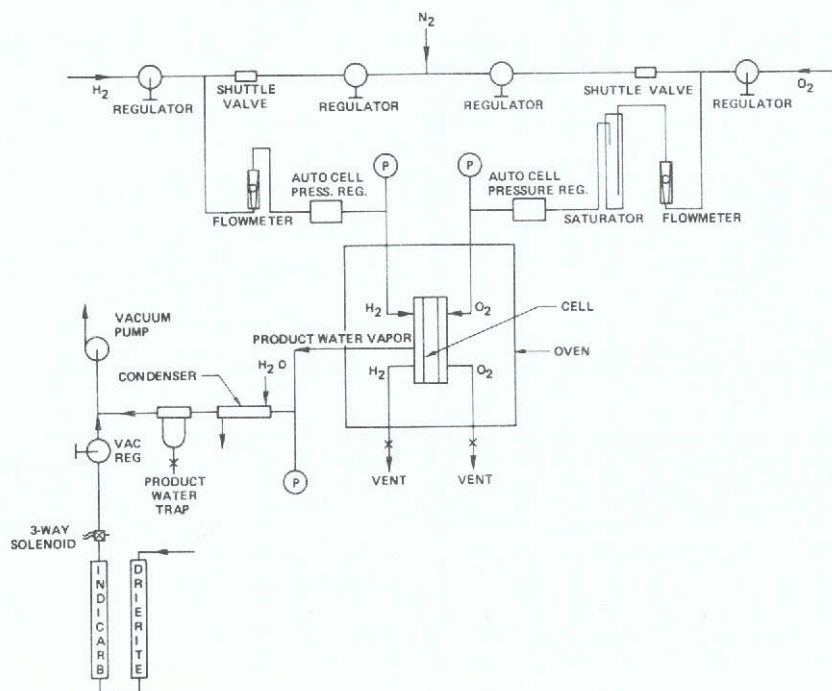


Figure 31 – Single Cell Test Stand Schematic

Reactants of fuel cell grade or better are supplied to the test stands. To eliminate test variables associated with reactant impurities, the hydrogen is further purified in a palladium-silver separator bank which reduces any contamination below detectable limits. Oxygen is purified using a Mine Safety Appliance catalytic oxidizer. This system is shown in Figure 32. Any hydrocarbons in the oxygen stream are oxidized to carbon dioxide and are removed by the sodium-hydroxide scrubber columns. The carbon dioxide level downstream of the scrubber is continuously monitored by a LIRA gas analyzer. These readings indicate that the oxidizer is removing 8 to 12 ppm (equivalent) methane from the oxygen stream and that the carbon dioxide level entering the fuel cells is less than 0.5 ppm.

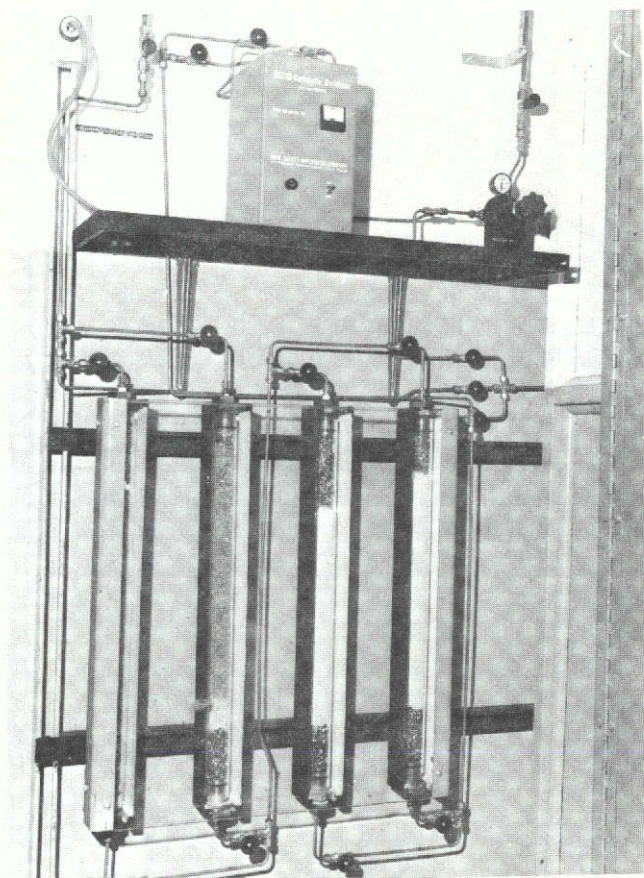


Figure 32 — Catalytic Oxidizer and Scrubber System

Temperature control of the cells is provided by an insulated oven which is maintained within $\pm 2^{\circ}\text{F}$ (1.1°C) by a thermoelectric solid-state temperature controller. The relatively massive single cell end plates, in combination with the isothermal oven, maintain a uniform cell temperature. Since metallic inserts are used to form the cell's oxygen flow field, and plastic inserts for the product water field, cell waste heat is rejected primarily on the cathode side.

Thus, the test rig approach realistically simulates system conditions. Cell temperature instrumentation showed that the simple oven temperature control method is effective in maintaining cell temperatures uniform within $\pm 1.5^\circ\text{F}$ (0.83°C) over a range of current densities to 300 ASF (322.8 ma/cm^2).

The product water removal system also duplicates the system design. A conventional Duo-Seal[®] vacuum pump is used to provide the sub-atmospheric pressure sink for product water vapor. The pH of the product water is regularly monitored. Trap water samples are checked 3 times a day, using a Beckman Zeromatic[®] pH Meter.

Single cell performance data is measured and recorded by P&WA's Automatic Data Acquisition and Recording (ADAR) System. The following parameters are recorded once every hour:

<u>Parameter</u>	<u>Accuracy</u>
Cell Voltage	$\pm 0.002\text{ v}$
Cell current	$\pm 0.02\text{ a}$
Oven Temperature	$\pm 3^\circ\text{F}$ (1.7°C)
Oxygen End Plate Temperature	$\pm 3^\circ\text{F}$ (1.7°C)
Water End Plate Temperature	$\pm 3^\circ\text{F}$ (1.7°C)

The ADAR system was designed to minimize experimental error and to reduce the amount of manual data handling. In addition to providing periodic scanning of the above parameters and transcribing them to engineering units, the ADAR system keeps an accurate log of total load hours. A sample ADAR print out for the NASA-LeRC Advanced Development Fuel Cells is shown in Figure 33.

```

STAND: X-528      LERC CELL-30

RIG: 37970-30    DATE: 6/21/73    TIME: 1 2    LHRS: 16

LOAD      TOTAL
11.281    .933

TEMPERATURES
O2 SAT EXIT ** 124.

PLUS END PLATE: 1= 174.  2= 175.  3= 175.
NEG. END PLATE: 1= 176.  2= 176.  3= 176.  4= 174.
OVEN WALL:      1= 174.

```

Figure 33 — ADAR Print Out

The heart of the ADAR system is a Hewlett-Packard Model 2114A digital computer. Other major components in the system are also from Hewlett-Packard; a Model 2911 Guarded Cross-bar Scanner and Model 2402 Digital Voltmeter to scan and measure the test signals, and a Model 2752 Teleprinter to print out the data.

All of the above data can also be read out directly at each station on conventional stand instrumentation. Pressure and flows are controlled and monitored by appropriate regulator, gages, flowmeters and valves, as shown in Figure 29.

The ADAR system has been used only for automatic data acquisition. Automatic control is provided by appropriate test stand instrumentation, with provisions for automatic shutdown of any cell when certain pre-established conditions are encountered. For the NASA-LeRC single cells, these protective controls are:

<u>Parameter</u>	<u>Limit</u>
Voltage	Low adjustable
Current	High or Low Adjustable
Temperature	High or Low Adjustable
Vacuum Pressure	High or Low

These automated control and protective features have resulted in very reliable single cell operation. Over 43,200 hours of fuel cell load were attained on 26 different fuel cells with only one stand-related failure. This occurred during a test of Cell No. 10, which was flooded because of an oxygen saturator overtemperature. Some automatic shutdowns occurred because cell conditions exceeded the protective limits described above. In all of these cases, the cells were not damaged and normal testing could continue.

Single cell testing was primarily devoted to endurance testing. However, various diagnostic procedures were performed on all of the cells to document any decay mechanisms and to determine design and off-design performance characteristics of the various cell configurations.

Typical test conditions for the programs were:

Cell Current Density	100 or 200 ASF (107.6 or 215.2 ma/cm ²)
Cell Temperature	180°F (82.2°C)
Product Water Vacuum	22 inch Hg (7.4 n/cm ²)
Hydrogen Pressure	16 psia (11.04 n/cm ²)
Hydrogen Flow	Consumption, plus 2 minute purge every 8 hours.
Hydrogen Inlet Dewpoint	Dry
Oxygen Pressure	16 psia (11.04 n/cm ²)
Oxygen Flow	2 x consumption
Oxygen Inlet Dewpoint	130°F (54.4°C)
Average Electrolyte Concentration	34 percent KOH

Diagnostic techniques which were regularly employed included the following:

Performance Calibrations: Voltage-current characteristics were generated to 500 ASF (538 ma/cm²), which is somewhat above the EMS peak power operating conditions. Taken periodically, the performance calibration changes with time are valuable tools in determining the type and extent of any decay mechanisms. This is especially true of the semi-log representation of the performance data on an IR free basis which are commonly described as Tafel plots.

Tafel Plots: The Tafel region refers to the low current density portion of a performance calibration. In this region, anode and ohmic polarizations are minimal or correctable so the cell voltage is essentially cathode activation limited performance. The Tafel region extends from approximately 1 ASF (1 ma/cm²) to a level where diffusion losses become significant, 10 to 100 ASF (10.8 to 107.6 ma/cm²), which is a function of operating temperature and pressure. In the Tafel region, the semi-log voltage-current curve should be a straight line, with a slope characteristic of the catalyst/reactant combination and a level proportional to the activation capability of the cathode.

Departures from this slope are an indication of parasitic loads, either internal cell shorting or gas crossover. Thus, the Tafel slope is a useful diagnostic tool in assessing the life expectancy of an operating cell. Changes in the levels of Tafel data are also a useful tool, since they indicate changes in the activity of the catalyst, either through changes in the number of active catalytic sites or structural modifications (e.g., recrystallization), changing the effect catalyst active area.

The so-called Tafel plot is also a useful diagnostic tool at current densities above the Tafel region. At these current densities, typical of operating cells, internal resistance (IR) corrections are required. When the cell performance is thus corrected, changes in the shape of the curves can be interpreted as changes in the diffusion characteristics of the electrodes. In this region, transport limitations are encountered if the electrode structure is not adequate for delivery of reactants or removal of product water. For example, diffusion problems can be related to microscopic flooding of the Teflon pores in a wet proofed electrode, or to increased concentration gradients in a heavily carbonated cell. While the semi-log performance plots alone do not distinguish such possible causes or even anode from cathode losses, they are valuable tools, in conjunction with previous experience and post-test analysis, in evaluating any performance decay trends.

Internal Resistance (IR): Internal resistance or ohmic polarization losses are unavoidable in any cell. However, they can be minimized by matrices with high porosity and correct assembly to insure proper cell compression. In the strip cell with edge current collection, there are also resistance losses in the electrode substrates and edge frames which are measured together with the conventional ohmic loss. IR measurements are taken periodically to insure that the initial assembly is correct and that the correct cell compression is being maintained.

IR measurements are taken by the current interruption technique. Typically, a 100 ASF (107.6 ma/cm^2) load is interrupted and the resulting step change in voltage is measured on a Tektronic Type 545 oscilloscope. Since other polarizations have a long response time, the step change is a direct measure of internal cell resistance.

Dilute Oxygen Diagnostic Test: Although the Tafel and IR tests give good indication of relative cathode-matrix-anode losses at low current densities, they cannot be used to distinguish cathode and anode losses in the diffusion regime, the area of operational interest. This technique permits identification of anode and cathode losses in the diffusion regime by running performance sweeps on 20% oxygen/80% nitrogen and pure oxygen. The assumptions implicit in this procedure are explained in Section III, A, 6.0, Diagnostic and Analytical Techniques. The method is based on the fact the cathode performance is proportional to the partial pressure of oxygen. A graphical procedure based on this relationship, illustrated in Figure 34, allows determination of individual electrode performance.

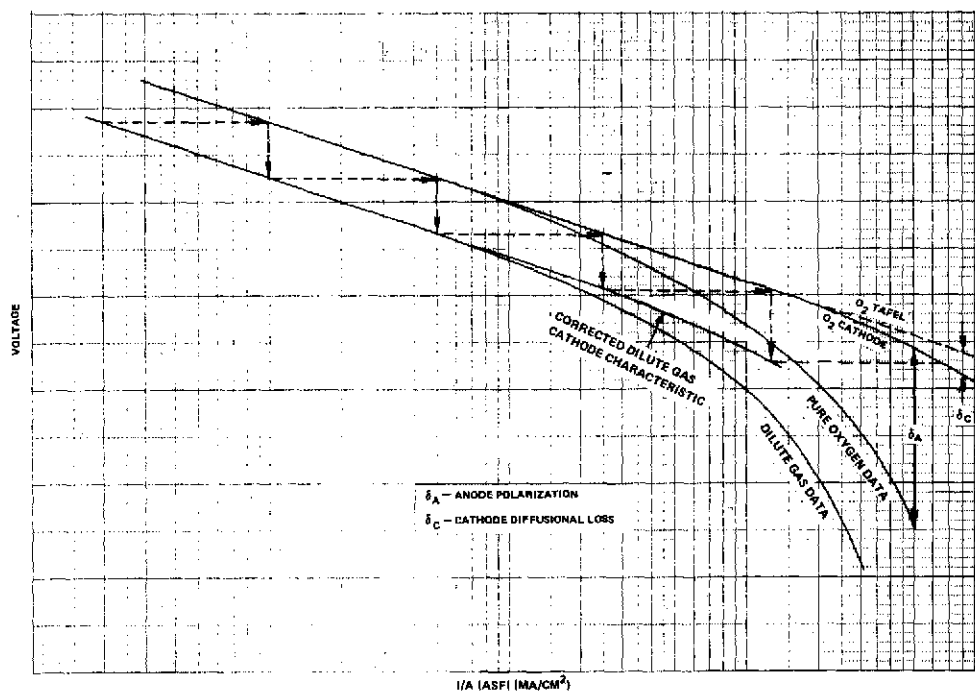


Figure 34 — Dilute Gas Diagnostic Method

A point in the activation region is selected on the dilute gas (20% O_2) data curve and the current is multiplied by 5, the ratio of oxygen partial pressures. The corrected point is plotted and compared to the O_2 data curve; if the point falls on the O_2 curve no anode polarization has occurred. When a deviation occurs between the corrected point and the actual O_2 curve, the deviation is attributed to anode polarization. A correction is then made up to the 20 percent O_2 curve corresponding to this amount of anode polarization and the

procedure is repeated. When the true O_2 polarization curve is obtained, the difference between this curve and the generated O_2 data is anode loss. The deviation of the corrected cathode performance curve from the O_2 Tafel line is normally attributed to diffusional loss.

This approach does not separate anode losses into such categories as poisoning, flooding, concentration polarization and undescribed resistance but it does clearly show which electrode has the major effect on cell performance.

Off-Design Tolerance: If a cell is improperly filled, or if the contact between the ERP and cell is inadequate, the off-design tolerance characteristics of the cell will depart from the theoretical value. Off-design tolerance data can be generated in various ways. In the passive water removal cells, the most convenient and most severe method is to vary product water vacuum. Since the vacuum is changed almost instantaneously, the cell is subjected to a very rapid transient, taxing the transport properties of the ERP much more severely than off-design tolerance conditions imposed by slowly changing dew points on saturated gases.

Post-Test Analysis: All cells are subjected to post-test analysis. This includes visual (and microscopic) examination of components for observable changes in physical properties, structural defects or peculiar deposits. Because of the importance of low corrosion rates, all of the single cells in this program were carefully analyzed for carbonate conversion. Selected cells were also sectioned for laboratory tests, including floating half-cell tests of individual electrodes and measurement of catalyst activity and platinum migration.

5.3 Summary of Single Cells Tested

Two types of testing were performed in the Single Cell Program. Research and Technology (R&T) tests were one type, comprising the first level of testing. This test is performed on any items which are beyond the present state-of-the-art. This is a relatively informal level of testing in order to maximize the flow of technical information. Reviews of the progress of this testing are held regularly with the NASA Project Manager. When any item, in his judgment, is sufficiently demonstrated, the next level of testing is begun.

Verification and Endurance (V&E) tests were the second type, comprising the second and third levels of testing. All cell tests in Phase II were of this type. The Verification test is a short duration test, consisting of two weekly test cycles, interrupted by a shutdown. The objective of a Verification test is to demonstrate the ability of the article under test to perform at the conditions in question. The Endurance test is of longer duration; the weekly duty cycle is used for some tests, continuous operation for others. Both Verification and Endurance tests are of more formal nature. They require written notification to the NASA Project Manager with pertinent description of the test article. Three designs were submitted for NASA approval and were tested in Phase I of the program. In carrying out this type of test, the NASA Project Manager reviews the results of the Verification test and decides which items shall undergo Endurance testing.

The load profile used for V&E testing was designed to be a working approximation of the proposed duty cycle with times chosen to maximize diagnostic data with minimal operator

coverage. Major features are steady-state operation at the nominal system design point (100 to 200 ASF) (107.6 or 215.2 ma/cm^2), weekly calibrations to the peak power point 460 ASF (495 ma/cm^2), periodic IR and off-design tolerance excursions as needed, and a weekly shutdown on inert gases simulating a holding period of indefinite duration.

A statistical summary of the single cell testing during Phase I and Phase II of the program is given in Table XIX.

TABLE XIX
FULL SIZE SINGLE CELL OPERATION

Number of cells tested	26
Number of configurations tested	7
Total cell test time	45,977 hours
Longest cell run (100 ASF) (107.6 ma/cm^2)	5400 hours
Longest cell run (200 ASF) (215.2 ma/cm^2)	6680 hours
Reasons for shutdown:	
Stand Failure	1*
Cell Failure	1*
Investigation of Decay	22
Continuing on Test	2

*During Phase I

A summary breakdown of the cells tested in Phase II into design configuration and types of tests is presented in Table XX.

TABLE XX
FULL SIZE SINGLE CELL TEST CATEGORIES

<u>Design No.</u>	<u>Description of Unitization</u>	<u>Verification and Endurance Test Cells</u>
3	Hypon Impreg. Matrix	16, 17, 18*, 19
4	Laminated TFE/Polypropylene	21, 22
5	Hypon Impreg. Matrix	23, 24
6	Hypon Impreg. Matrix	25, 26*, 27, 29*
7	Laminated Polysulfone	28, 30

*Cells 18, 19, 26, and 29 delivered to NASA.

Details for each cell are given in Table XXI. These include the small differences in construction of the unitized electrode assemblies, passive water removal assemblies and flow fields; and initial, peak and final voltages, initial IR, load level, operating times, and comments.

5.4 Single Cell Test Results

This section reviews the results of the cells tested during Phase II. Overall performance levels ranged from satisfactory to excellent and can be summarized as follows.

	<u>Performance mV at 100 ASF (107.6 ma/cm²)</u>
EMS Performance Model	890
Typical Cells	880 - 910
Best Cells	> 910
Worst Cells	< 880

The results of each test are discussed in following text. Performance levels, IR, off-design tolerance, electrolyte retention, and performance stability are discussed as appropriate to each test.

TABLE XXI
CELL TEST HISTORY

Cell No.	Design No.	UEA Description	PWR Description	O ₂ Field	H ₂ Field	Load Time (Hrs.)	Performance ^① Volts at 100 ASF			IR at 100 ASF ^①	Comments
							Initial	Peak	Final		
15	3	Hypon Matrix Unit Construction PPF Electrodes 22 Mil Sinter	Hypon Matrix 11 Mil Sinter Goretex Membrane	Field Machined in End Plate 0.030"	Polypropylene Screen 0.024"	3132	0.890	0.892	0.880	13	Refilled at 80 hours. Refurbished at 3010 hours. Test Completed in Phase I.
16	3	Same as 15	Same as 15	Machined insert 0.015"	Polypropylene Screen 0.024"	1544	0.895	0.895	0.840	9	Refurbished at 310 hours.
17	3	Same as 15	Same as 15	Machined insert 0.015"	Polypropylene Screen 0.024"	6680	0.875	0.892	0.806	6	Performance quoted at 200 ASF ^② Refurbished at 352 hours, 4000 hours and 6132 hours.
18	3	Same as 15	Same as 15	Machined insert 0.015"	Polypropylene Screen 0.023"						Delivered to NASA
19	3	Same as 15	Same as 15	Machined insert 0.015"	Polypropylene Screen 0.023"						Delivered to NASA
20		Hypon Matrix Integral UEA/PWR		Machined insert 0.015"	Polypropylene Screen 0.022"	646	0.880	0.890	0.870	11	Cell shorted in assembly - Internal TC
21	4	Polypropylene Film on TFE Asbestos PPF Eldes 22 Mil Ni ERP	Hypon Matrix 11 Mil Sinter Goretex Membrane	Machined insert 0.015"	Polypropylene Screen 0.018"	2598	0.867	0.890	0.865	12	Performance quoted at 200 ASF. ^②
22	4	Same as 21	Same as 21	Same as 21	Polypropylene Screen 0.022"	3320	0.890	0.907	0.864	11	Refurbished at 324 hrs.
23	5	Hypon Matrix Unit Construction 22 Mil ERP, Au-Pt Cath.	Same as 21	Same as 21	Polypropylene Screen 0.028"	5010	0.900	0.908	0.820	13	Refurbished at 332 and 4670 hrs.
24	5	Same as 23	Same as 21	Same as 21	Polypropylene Screen 0.022"	2349	0.785	0.785	0.700	12	Performance quoted at 500 ASF ^③ Refurbished at 1651 hrs.
25	6	Epon Matrix Unit Construction PPF Eldes Polysulfone ERP 0.031"	Same as 21	Same as 21	Polypropylene Screen 0.023"	5400	0.913	0.913		9	Refurbished at 5400 hrs.
26	6	Hypon Matrix Unit Construction Ni ERP .022 Mil Au-Pt Cathode	Same as 21	Same as 21	Polypropylene Screen 0.029"	19	0.930	0.930	0.930	5	Delivered to NASA
27	6	Hypon Matrix Unit Construction PPF Eldes Polysulfone ERP 0.031"	Same as 21	Same as 21	Polypropylene Screen 0.022"	2061	0.870	0.870	0.818	9	Performance quoted at 200 ASF. ^② Ran 1530 hrs. at 200 ASF. ^② Daily Tolerance Excursions from 1450 hrs to 1980 hrs.
28	7	Polysulfone Frame PPF Eldes Ni ERP, 0.022"	Same as 21	Same as 21	Polypropylene Screen 0.015"	2115	0.875	0.888	0.863	14	Run as corrosion rig before running as fuel cell.
29	6	Same as 26	Same as 21	Same as 21	Polypropylene Screen 0.030"	9	0.908	0.908	0.908	8	Delivered to NASA
30	7	Polysulfone Frame PPF Anode, Au-Pt Cathode Ni ERP, 0.022"	Same as 21	Same as 21	Polypropylene Screen 0.018"	2113	0.933	0.939	---	8	Refurbished at 311 hrs.

① 107.6 ma/cm²② 215.2 ma/cm²③ 538 ma/cm²

Cell Nos. 16 and 17

Single Cell Nos. 16 and 17 were fabricated and placed on test during Phase I. Testing continued into and was completed in Phase II. These cells represented the "state-of-the-art" at the completion of Phase I. They are of similar construction and were approved by the NASA Program Manager as Single Cell Verification Design No. 3. Both cells were fabricated of Hypon using the impregnated matrix/integral frame technique. The primary test objective was determination of the compatibility of Hypon frames, and also, in Cell No. 17, to evaluate the electrode endurance at 200 ASF (215.2 ma/cm^2).

Both cells completed the scheduled two-week Verification Test Program, consisting of weekly load cycle profiles of 6-1/2 days on load and one-half day off load. Cell No. 16 operated at 100 ASF (107.6 ma/cm^2) for the bulk of its test period while No. 17 operated primarily at 200 ASF (215.2 ma/cm^2).

Electrolyte carbonation data was obtained on both cells after the two week Verification Test Program. This data is shown on Figure 35, together with all carbonation results to date for comparison. These pure Hypon cells (initially after verification) showed relative electrolyte conversion levels much lower than the earlier composite Arylon/Hypon cells. The effect was greater than would be expected from the carbonation test rig data, but was consistent with their improved performance stability.

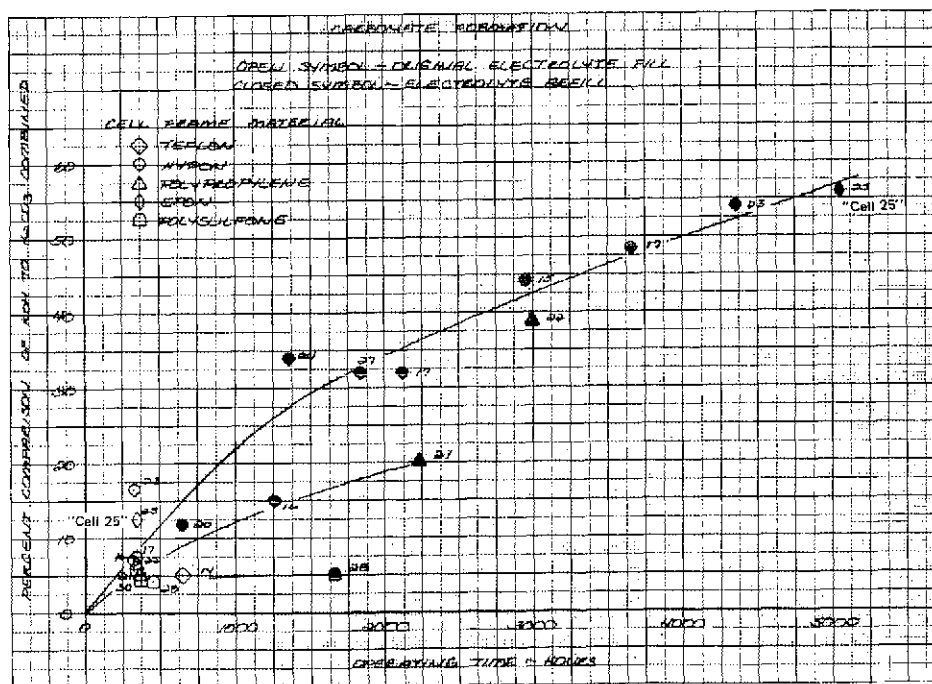


Figure 35 — Electrolyte Carbonation Data

Although the construction of both cells is identical and the electrolyte carbonation data equivalent, the early performance stability of the two cells is different. Initial performance at higher current densities also differed significantly. See Figures 36 and 37. Diagnostic data show a progressive reduction in the performance of Cell No. 16 at current densities above approximately 50 ASF (53.8 ma/cm²) indicating increased diffusional type losses. The electrodes of Cell Nos. 16 and 17 came from different manufacturing lots. Review of electrode fabrication data indicates that while the electrodes used in Cell No. 16 had adequate performance, they did display lower performance at higher current densities. These data suggested an inadequate cathode structure in Cell No. 16, which was traced to over-compression of the electrodes during the fabrication process.

Cell No. 16 accumulated 1544 load hours operating to a weekly 6-1/2 days on load and one-half day off load 100 ASF (107.6 ma/cm²) profile. As shown in Figure 36, because of its relatively high degradation rate, it was shut down at 1544 hours for post-test carbonate analysis.

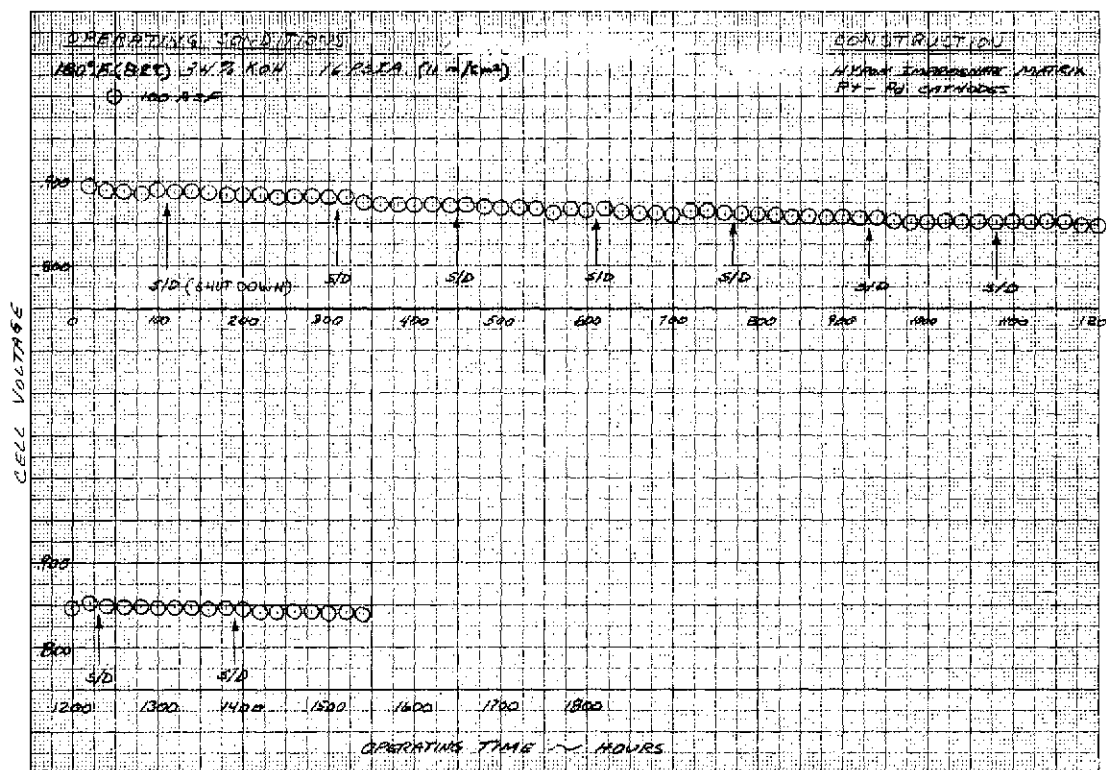


Figure 36 — Performance History of Cell No. 16

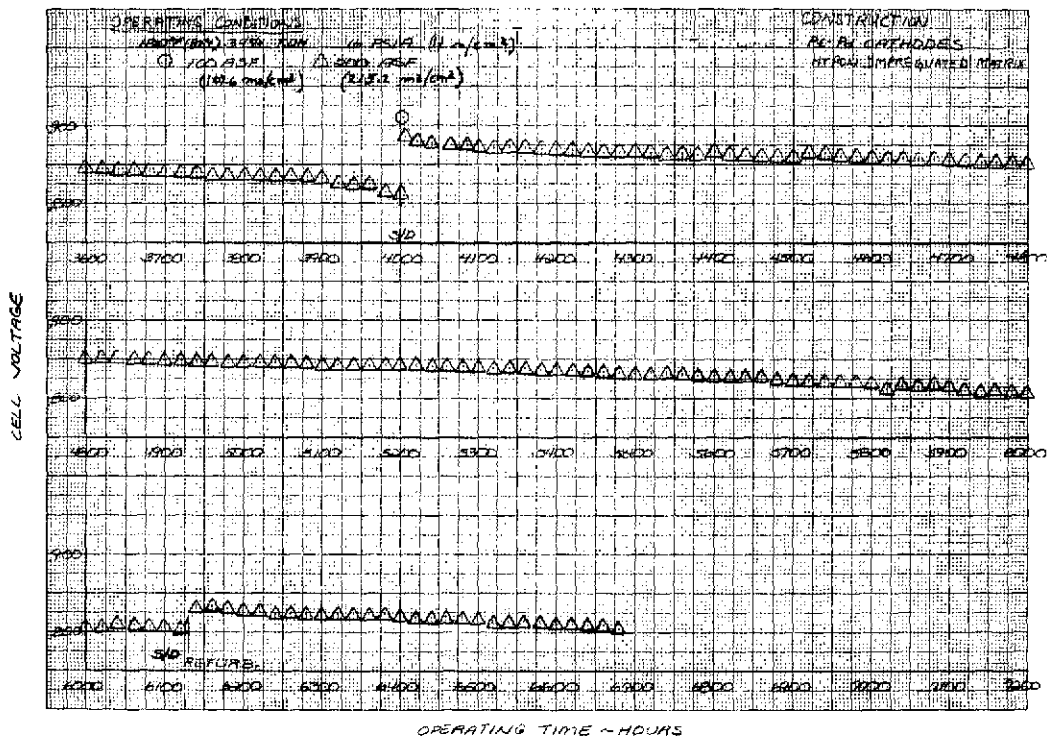
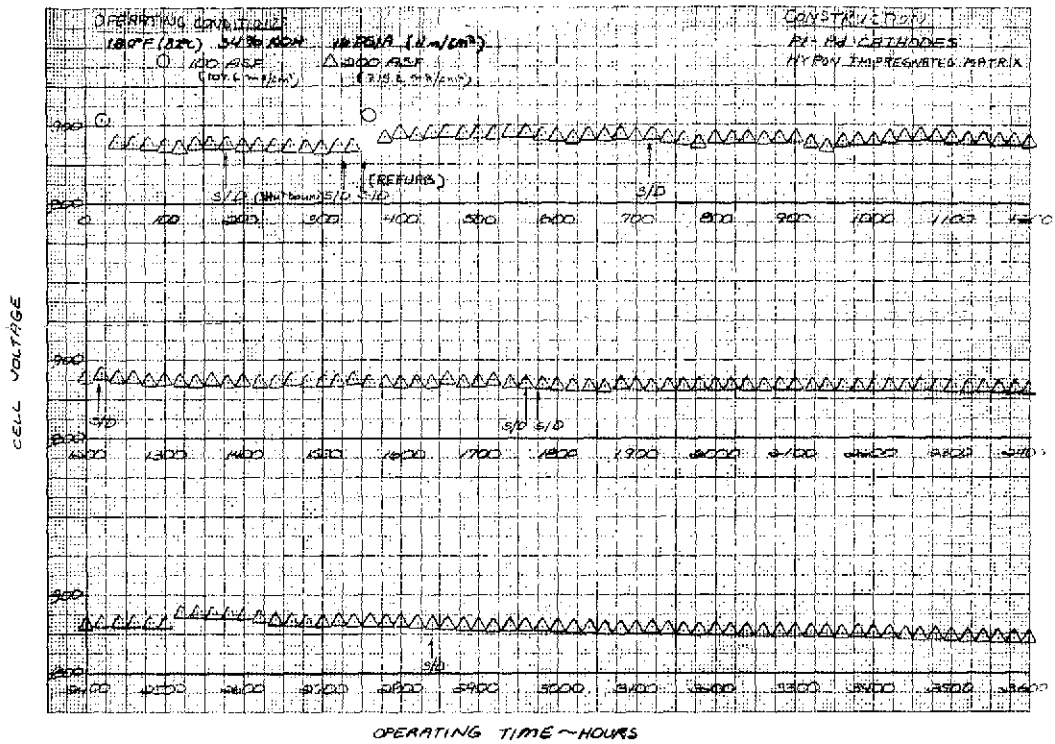


Figure 37 — Performance History of Cell No. 17

The test of Cell No. 16 (and also Cell No. 20) provided the first long-term carbonation data on cells of Hypon construction. Close inspection of both cells also indicated some discoloration and softening of the frame material in the oxygen inlet and exit plenum areas of the UEA. An analysis performed on samples from these frame areas produced the following results:

- The "softness" of the frame was due to a loss of resin (up to 10%).
- The discoloration (purple) was due to loss of nitrile groups from the Hycar additive in the Hypon resin, probably by formation of a purple, heterocyclic organic dye.
- High potassium levels were found in areas where discoloration and resin loss occurred.
- There was no evidence that the desired Hycar rubber precipitation occurred during fabrication.

It was recommended that Hycar be eliminated from the resin formation, unless the Hycar could be precipitated during fabrication of the epoxy/asbestos composite. A UEA was then fabricated with Epon/asbestos, without Hycar. This material is presently being evaluated in Cell No. 25.

Cell No. 17, with PPF electrodes, accumulated 6680 hours at 200 ASF (215.2 ma/cm^2). The test objectives were to determine the compatibility of Hypon frames and evaluate electrode endurance at 200 ASF (215.2 ma/cm^2). Cell refurbishment occurred following the initial Verification Test Program at 350 hours, and again at 4000 hours and 6131 hours. As shown in the carbonation summary, Figure 35, the Hypon frame results in carbonation rates too high to satisfy long term operating objectives. The initial carbonate conversion of KOH to K_2CO_3 was 7.5 percent at 350 hours. This level, however, was an improvement over earlier Hypon-Arylon cells.

A carbonate analysis at 4000 hours indicated 48.5 percent conversion of KOH to K_2CO_3 . About three-quarters of this is attributed to frame corrosion, the remainder to reactants, fill, and component background. The carbonation results at 6131 hours, an additional 32 percent conversion of KOH to K_2CO_3 were consistent with earlier refurbishment at 4000 hours.

Cell No. 17 represents the state-of-the-art of lightweight strip cells at the end of Phase I. Compared to earlier cells, the performance level of Cell No. 17 was superior, 892 mv @ 200 ASF (215.2 ma/cm^2). It also increased significantly after refurbishment. This increase is typical for unleached electrodes.

Figure 38 presents the performance of Cell No. 17 as a function of current density. The performance is high and relatively flat. Throughout the endurance testing periodic Tafel diagnostics were conducted; see Figure 39. They provided insight into activation and diffusion losses with time. This figure also illustrates the effect of refurbishment on performance losses.

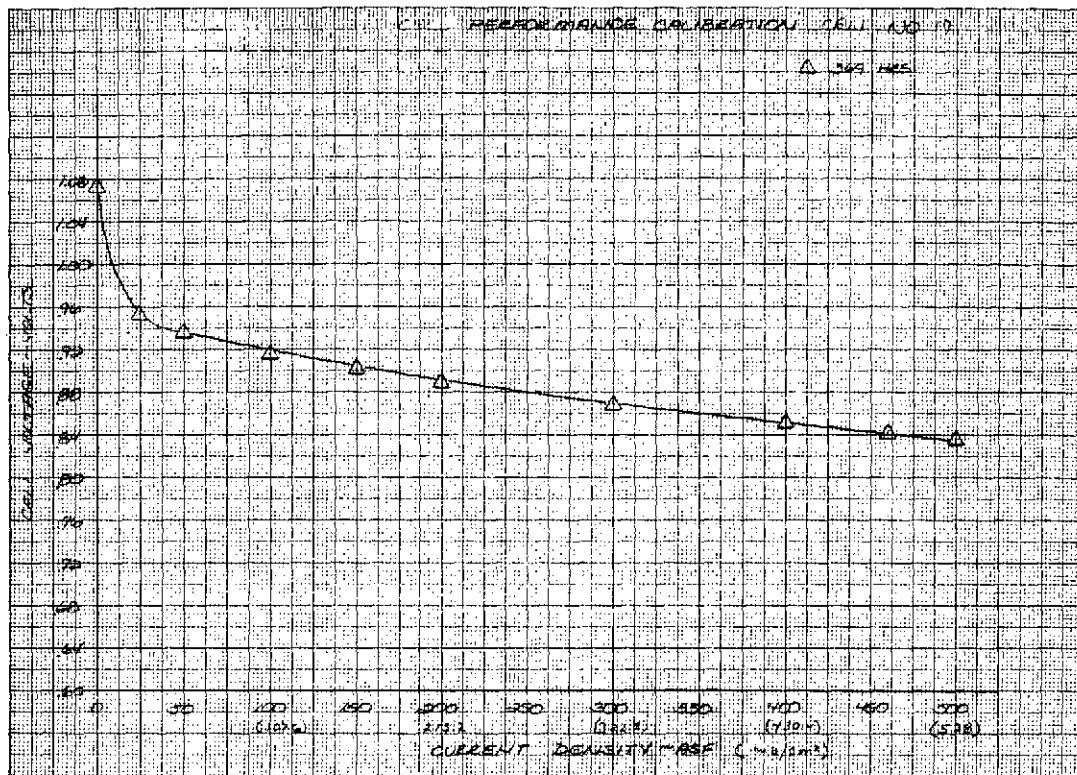


Figure 38 — Performance Calibration Cell No. 17

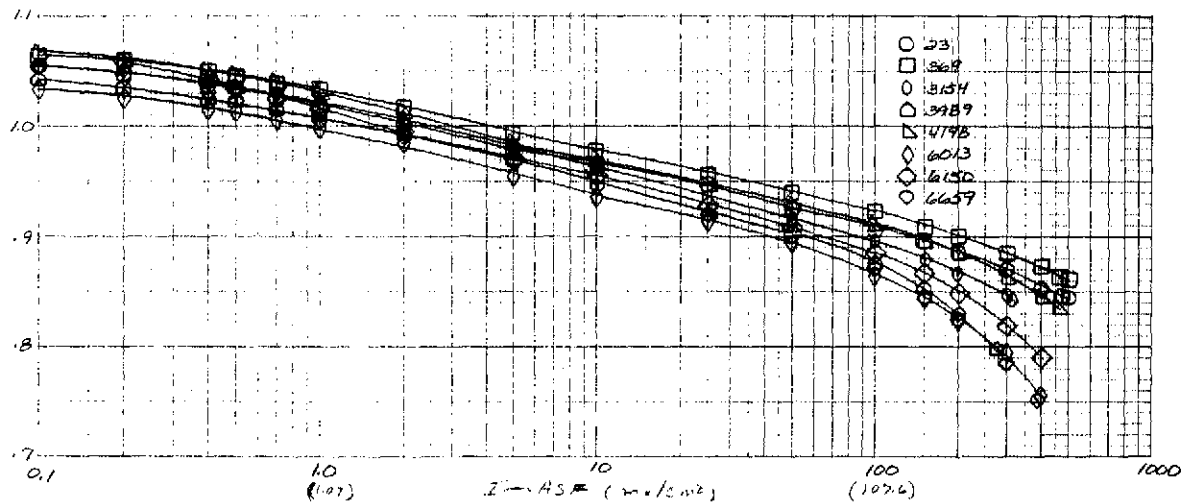


Figure 39 — Cell No. 17 Tafel Data

After restart at 4000 hours, cell performance was higher than expected, 885 mv @ 200 ASF (215.2 ma/cm²). This represents a recovery of some 73 mv of the total 78 mv decay at 200 ASF (215.2 ma/cm²). Of this total, about 53 mv was attributable to carbonation and, hence, recoverable, and the remainder (25 mv) was a result of platinum migration, and, hence, not recoverable. The higher restart level was, therefore, considered to be caused by a temporary activation of the cathode during restart. This hypothesis appears to have been confirmed by the relatively rapid decay of the cell after restart, as shown in Figure 37. Figure 37 shows that the refurbishment at 4000 and 6000 hours also accounted for some recovery of activation losses. Recent laboratory cell evaluations have shown a correlation between carbonate level and performance loss in the activation region.

Following the second refurbishment, diagnostics indicated that the bulk of the performance loss was activation loss and hence not recoverable. Consequently, Cell No. 17 was shut down

at 6880 hours. Cell No. 17 accumulated 1.33 million $\frac{\text{amp-Hr}}{\text{ft}^2}$, the largest $\frac{\text{amp-Hr}}{\text{ft}^2}$ product of any base cell to date. A summary of Cell No. 17's performance losses is presented in Table XXII.

Teardown inspection showed the cell to be in good condition with no apparent signs of shorting or crossover.

TABLE XXII

PERFORMANCE LOSSES OF CELL NO. 17

VOLTAGE LOSS BREAKDOWN (200 ASF)LOAD TIME PERIODS (HRS)

	<u>0-4000</u>	<u>4000-6130</u>	<u>6130-6680</u>
TOTAL DECAY (mV)	80	88	86
ACTIVATION LOSS	32	40	40
ATTRIBUTABLE TO CARBONATES	56	33	10
OTHER LOSSES (ASSUMED TO BE ANODE DIFFUSION)	+8	15	36

DECAY RATE SUMMARY (200 ASF)OPERATING TIME (HOURS)DECAY RATE FROM INITIAL

1,000	-2.0 $\mu\text{V/hr}$
2,000	5.5
3,000	6.7
4,000	16.5
4,300 (REFURBISHED AT 4000 HOURS)	3.0
5,000	6.6
6,000	11.9
6,680 (REFURBISHED AT 6130 HOURS)	11.9

Cell Nos. 18 and 19

These two cells were of the same design and construction as Cell Nos. 16 and 17. They were delivered to the NASA LeRC for testing and evaluation.

Cell No. 20

Cell No. 20 is the first cell in which the unitized electrode assembly and the passive water removal assembly were bonded into one piece. Bonding these two components into one unit eliminates the gasket used between them in the usual single cell test arrangement. This is the bonded configuration incorporated in the EMS. The end result is an assembly of greater integrity and reliability. Cell No. 20 was fabricated in this manner to demonstrate the feasibility of fully bonded construction. The value of this technique is more beneficial when applied to multi-cell stacks than single cells since it minimizes the number of subassemblies which must be handled and sealed.

The performance of Cell No. 20 remained stable throughout the test, as shown in Figure 40. The pH of the product water also remained good, indicating no problem with the passive water removal subsystem. However, an internal short did exist. The short was traced to a thermocouple placed in the anode cavity. After accumulating 646 load hours, testing was voluntarily terminated to provide room for the next Verification Test.

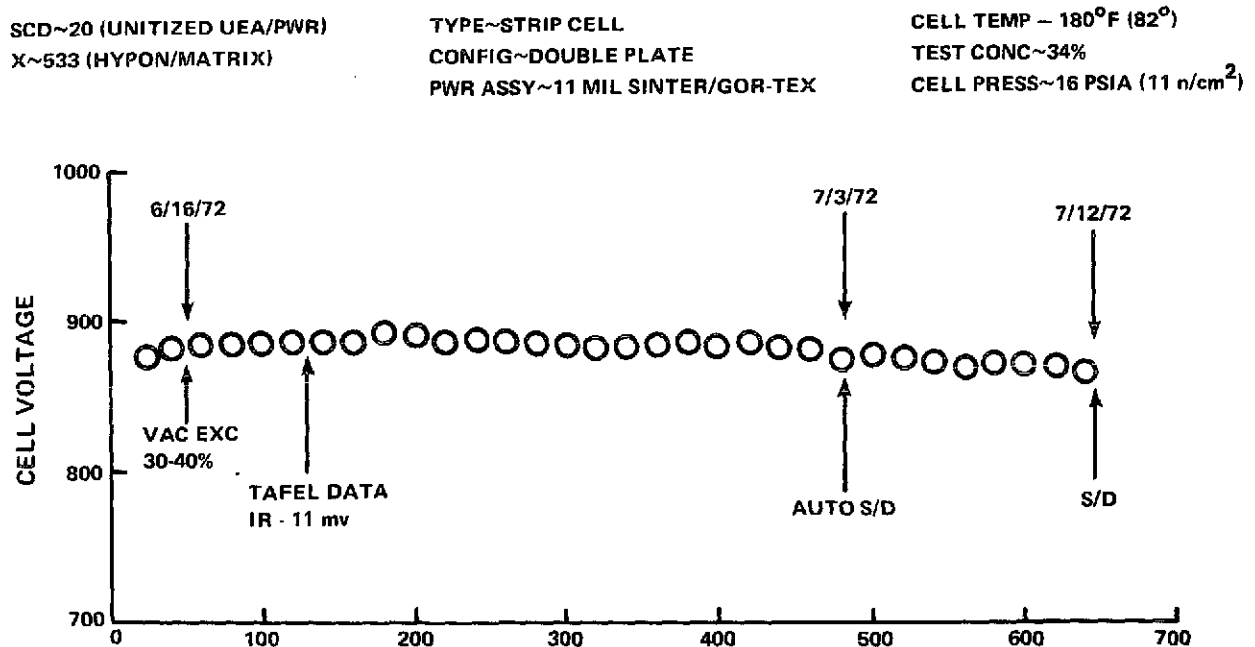


Figure 40 — Performance History of Cell No. 20

Cell Nos. 21 and 22

These cells had unitized electrode assemblies laminated of 30 percent asbestos-filled Teflon and polypropylene film. They were approved by the NASA Program Manager as Single Cell Verification Design No. 4. Both cells had passive water removal (PWR) assemblies of the standard Hypon construction and incorporated alcohol leached electrodes. After refurbishment each cell showed a significant performance increase similar to that exhibited by unleached electrodes.

The test objective of these cells was to evaluate the compatibility of polypropylene frames with the fuel cell environment. Preliminary testing of this frame material produced encouraging carbonate formation results. The conversion of KOH to K_2CO_3 in Cell Nos. 21 and 22 are shown in Figure 35. The results from the test of Cell No. 21 were not as good as the Teflon results, and the results of the test of Cell No. 22 were comparable to the Hypon experience to date. The higher-than-expected carbonate formation has been attributed to additives used by the film fabricator in the processing of the polypropylene film.

Cell No. 21 accumulated 2600 hours at 200 ASF (215.2 ma/cm²). Its performance history is shown in Figure 41. The somewhat erratic performance behavior experienced on this cell was traced to a blocked hydrogen port caused by a misaligned gasket. Final performance was 886 mv @ 200 ASF (215.2 ma/cm²) for a decay of only 24 mv from peak performance.

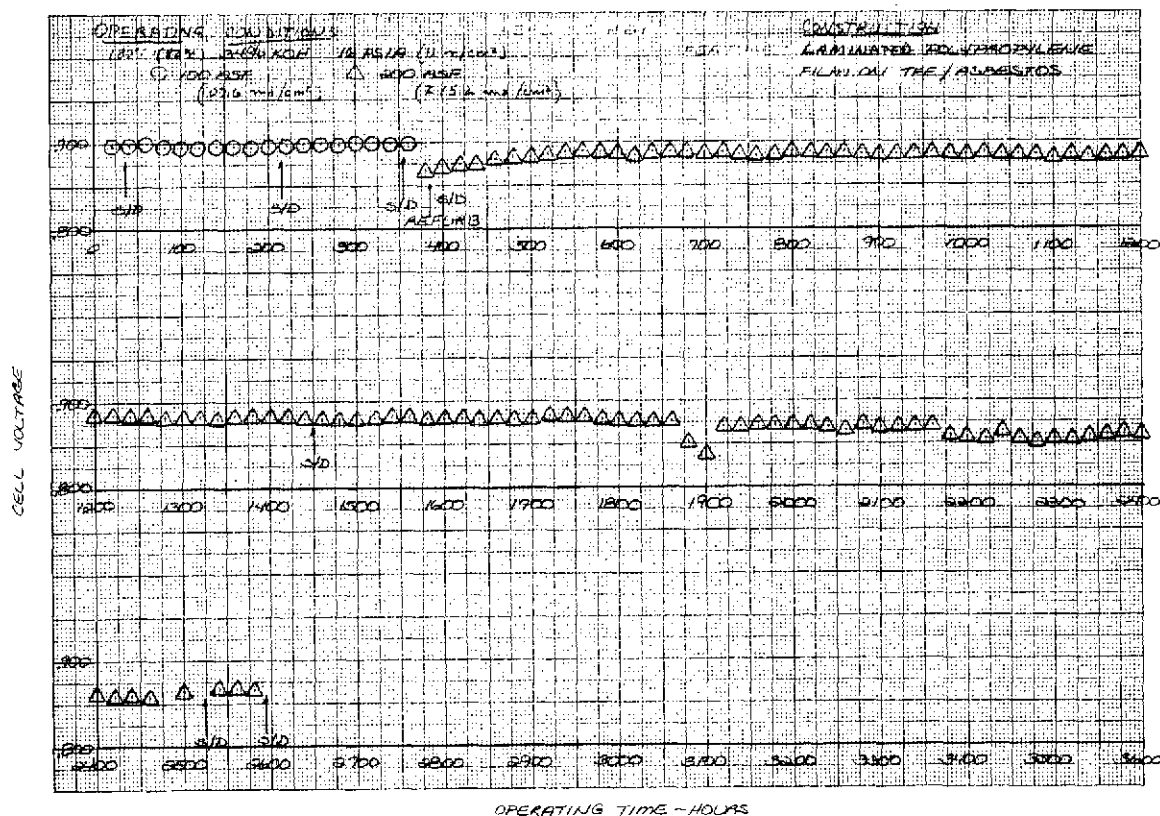


Figure 41 — Performance History of Cell No. 21

Cell No. 22 accumulated 3320 hours at 100 ASF (107.6 ma/cm^2). The test was terminated because of crossover. Performance stability on this cell was good until just prior to shutdown, as shown in Figure 42. Periodic Tafel diagnostics throughout the endurance operation indicated that internal shorting existed in both Cell Nos. 21 and 22, which became aggravated with time. Figure 43 shows the increase with time in shorting current obtained from periodic Tafel diagnostics. The tendency for internal shorting and potential for crossover may be a result of the poorer dimensional control obtained with laminated construction.

Cell Nos. 23 and 24

Cell Nos. 23 and 24 were the first strip cells to incorporate gold/platinum cathodes. They were Verification and Endurance tested as NASA-approved Design No. 5. The objective of these tests was to obtain endurance experience with Au-Pt cathodes in full size cells.

The performance history of Cell No. 23 is shown in Figure 44. The cell was first operated to the NASA two-week verification schedule. At the end of this period, it was refurbished and placed on steady-state endurance at 100 ASF (107.6 ma/cm^2) load. The initial performance was slightly better than comparable PPF cathode cells, but somewhat lower than laboratory cell experience. The initial performance rise common in PPF cells was seen to a lesser extent in this cell. This difference is apparently attributable to the wetting characteristics of the catalysts.

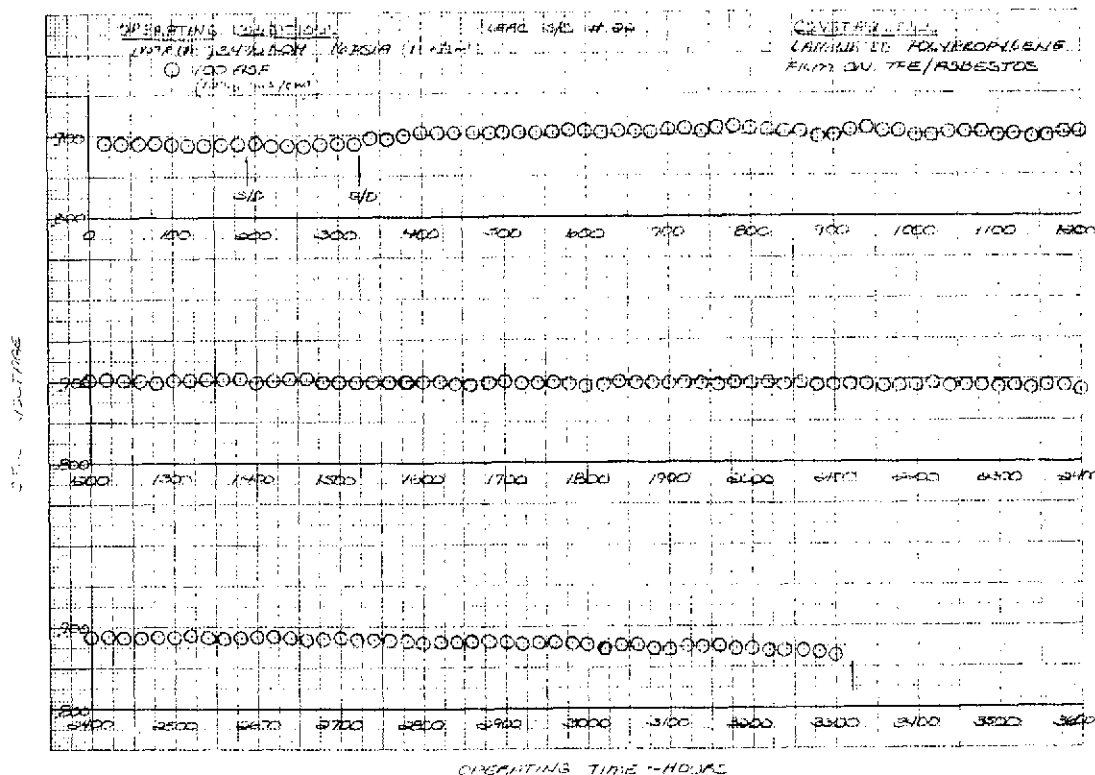


Figure 42 — Performance History of Cell No. 22

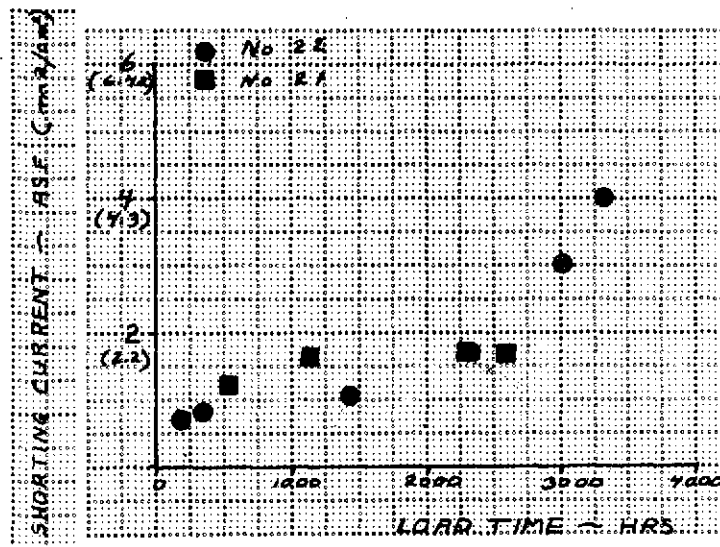


Figure 43 — Cell Shorting Implied from Tafel Data

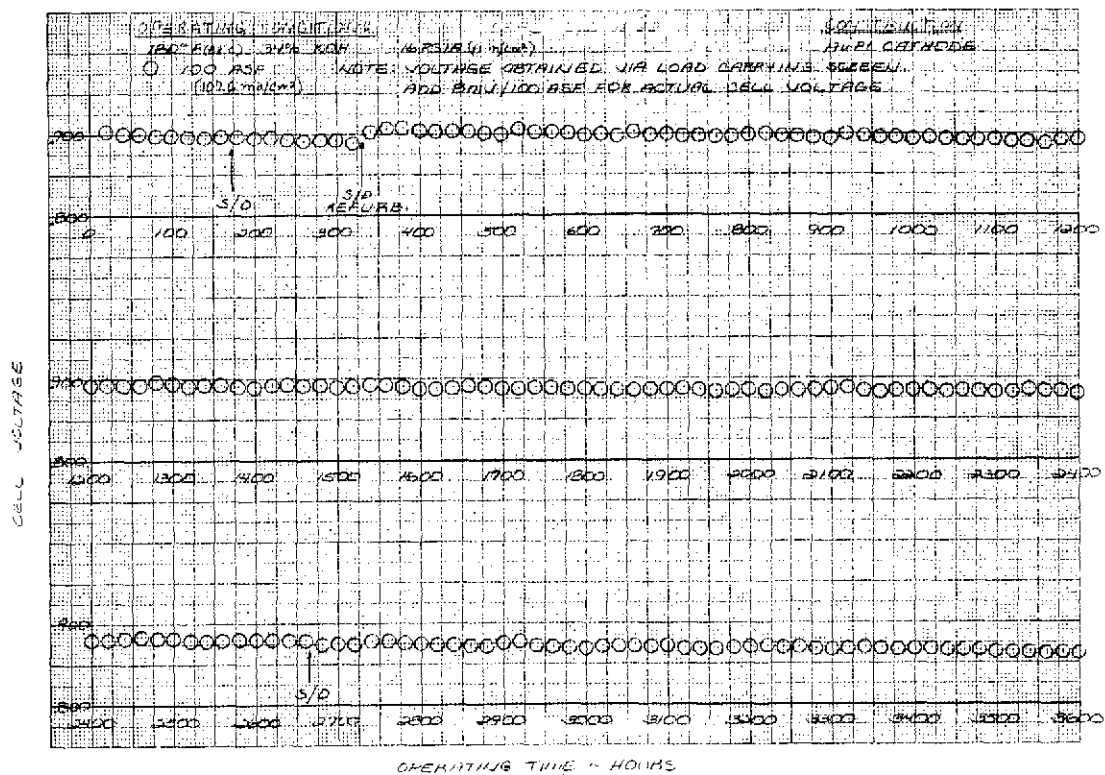


Figure 44 — Performance History of Cell No. 23

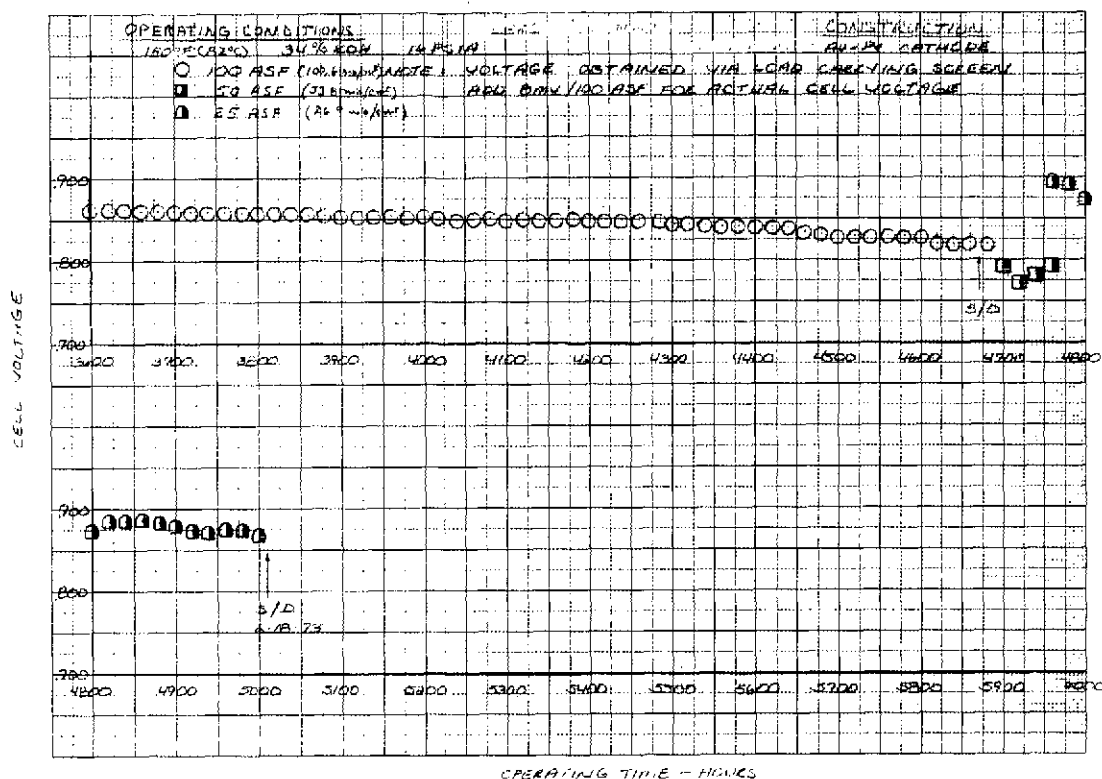


Figure 44 — Performance History of Cell No. 23 (Continued)

Refurbishment after the verification test resulted in recovery of all the performance decay due to carbonate formation. Throughout the first 4000 hours of the endurance portion of the test, the cell exhibited stable performance characteristics with a decay rate of about 18 $\mu\text{V/hr}$. The Tafel data, shown in Figure 45, indicate a loss of 15 mv in the activation region. At 4267 hours, the running concentration was adjusted to 30 percent KOH to compensate for an estimated 50 percent carbonate conversion resulting from corrosion of the Hypon frame. At 4624 hours, a further adjustment to 28 percent KOH was made. The cell was shut down for refurbishment at 4690 hours. Refurbishment was not effective in restoring performance although a gain of 20 mv was achieved in the activation region. A dilute gas diagnostic test showed that the majority of the diffusion losses were due to the anode. The test was continued at a reduced load until 5000 hours to obtain cathode life data.

Post-test laboratory analysis confirmed that anode flooding was responsible for the lack of performance recovery after refurbishment. Resintering of a sample of the anode restored all of the lost performance. The condition of the gold-platinum cathode was satisfactory. The loss of activation was 15 mv, which is comparable to PPF cells.

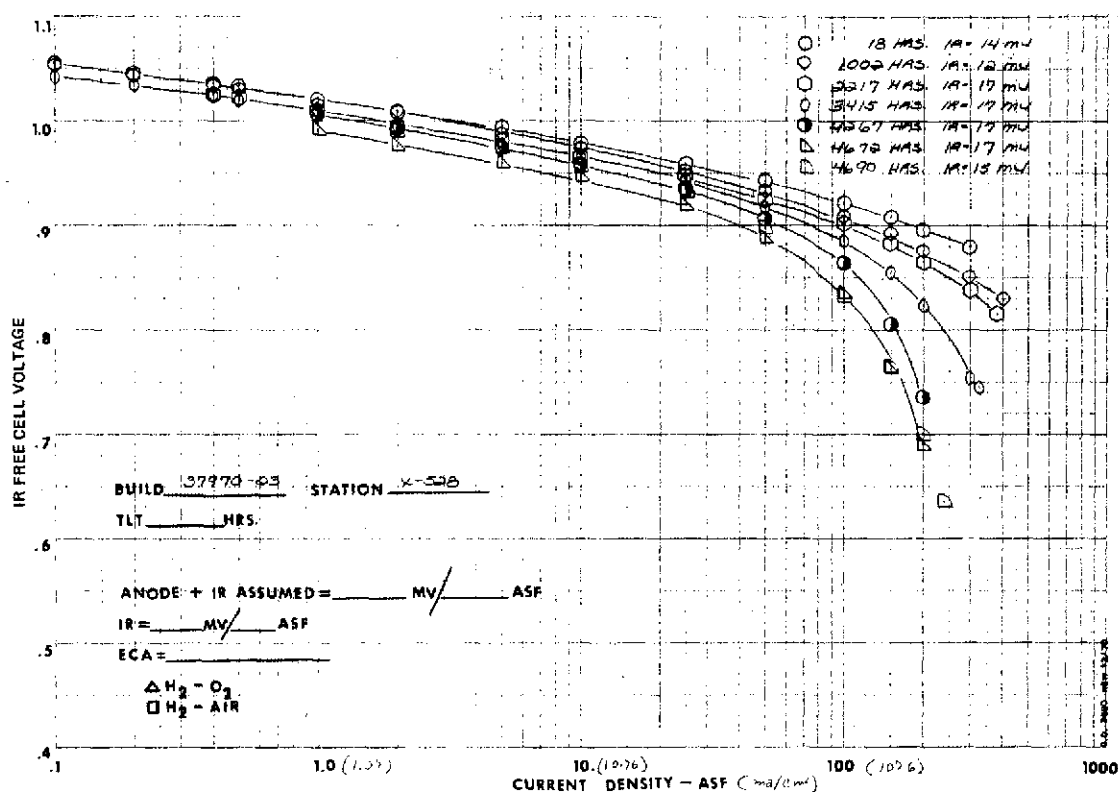


Figure 45 — Tafel Data Cell No. 23

Cell No. 24 was identical to No. 23. It was also used for a Verification and Endurance test of Design No. 5. The objective of the test was to demonstrate the high current density capability of gold-platinum cathode cells. Accordingly, after a two-week verification test and refurbishment, the cell was set on endurance at 500 ASF (538 ma/cm²) as shown in Figure 46.

At 1465 hours, a problem with the test stand vacuum system necessitated a return to 100 ASF (107.6 ma/cm²), and resulted in an automatic shutdown. Following restart, diagnostics were conducted which showed a loss of dry-side tolerance because of carbonate formation. The unit was shut down for refurbishment at 1652 hours. Refurbishment resulted in the recovery of 13 mv of activation loss and a total of 32 mv at 100 ASF (107.6 ma/cm²) and 40 mv at 500 ASF (538 ma/cm²). The 500 ASF (538 ma/cm²) endurance was continued until 2348 hours at which time the cell was shut down for analysis. Prior to shutdown, a dilute gas diagnostic test was conducted which showed cathode losses in the diffusion range to be the main reason for the cell decay; see Figure 47. A comparison of 500 and 100 ASF (538 and 107.6 ma/cm²) operation (Figure 48) shows that while decay at 500 ASF (538 ma/cm²) was significantly greater, the operation at 100 ASF (107.6 ma/cm²) was not affected. This may be due to increased diffusional losses having a greater effect at higher current densities and also to an apparent decrease in dry side tolerance occurring at high current densities. The decrease in dry side tolerance, shown in Figure 49, can possibly be

explained by higher electrode temperatures that may occur during high current density operation. At 500 ASF (538 ma/cm^2) the waste heat generation increases and the thermal gradient from the electrodes to the endplate increases to maintain thermal equilibrium. Consequently the endplate temperature, which is used with the passive water removal system vacuum level as the basis of estimating electrolyte concentration, may be a good measure of electrode temperature at low current density but not at high current density. This is not an inherent cell problem but rather a problem with a specific test fixture. If a considerable amount of testing at high current density were to be conducted, the fixture would require an improved method for determining electrode temperature.

Half-cell tests of the cathode from cell No. 24, conducted as part of the post-test analysis, showed an activation loss of 10 - 12 mv. In summary the Au-Pt cathode data of Cells No. 23 and 24 indicate:

- (1) Initial performance of the Au-Pt cathodes is slightly better than that of PPF cathodes,
- (2) Au-Pt cathode activation losses are comparable to PPF cathodes, and
- (3) Diffusional losses of Au-Pt cathodes may be slightly higher than PPF electrodes.

However additional evaluation is required before these results can be assumed characteristic of Au-Pt electrodes.

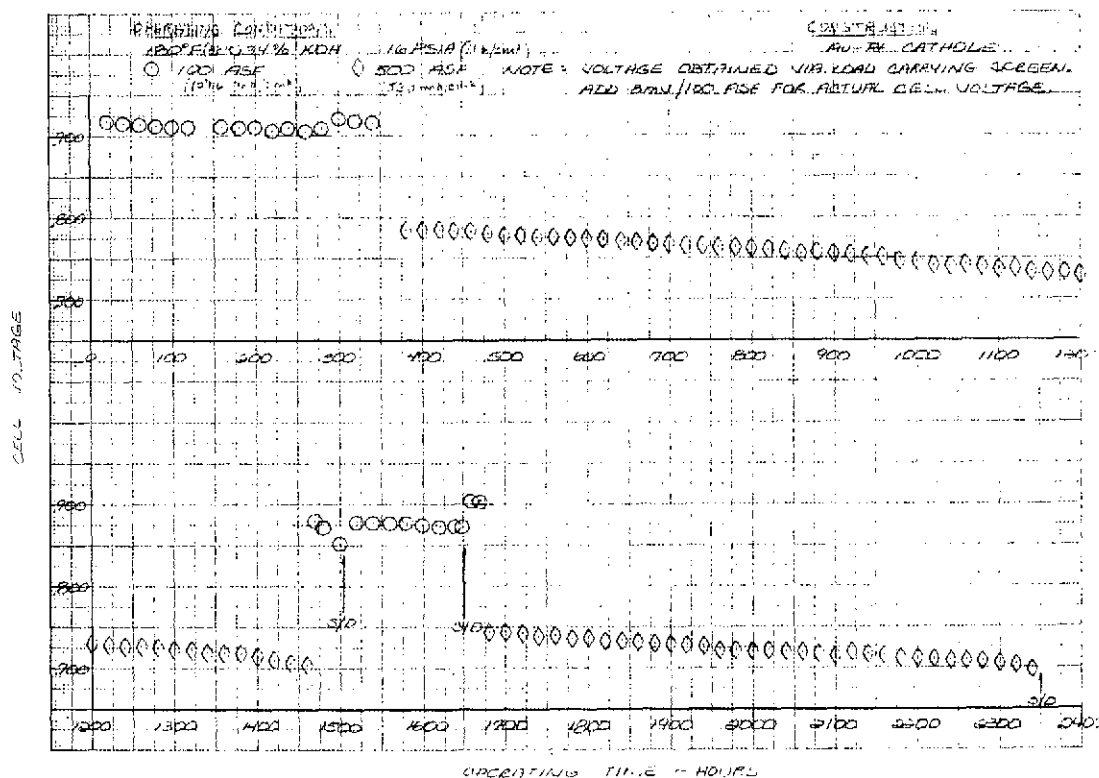


Figure 46 — Performance History of Cell No. 24

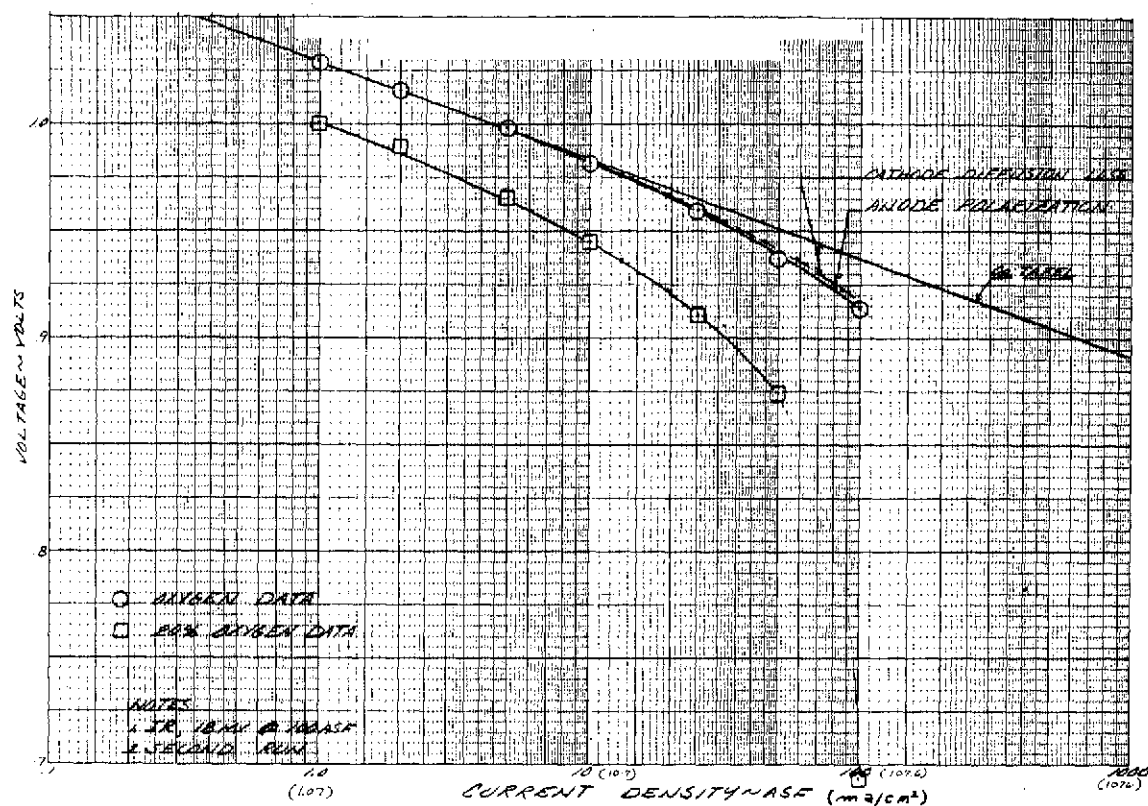
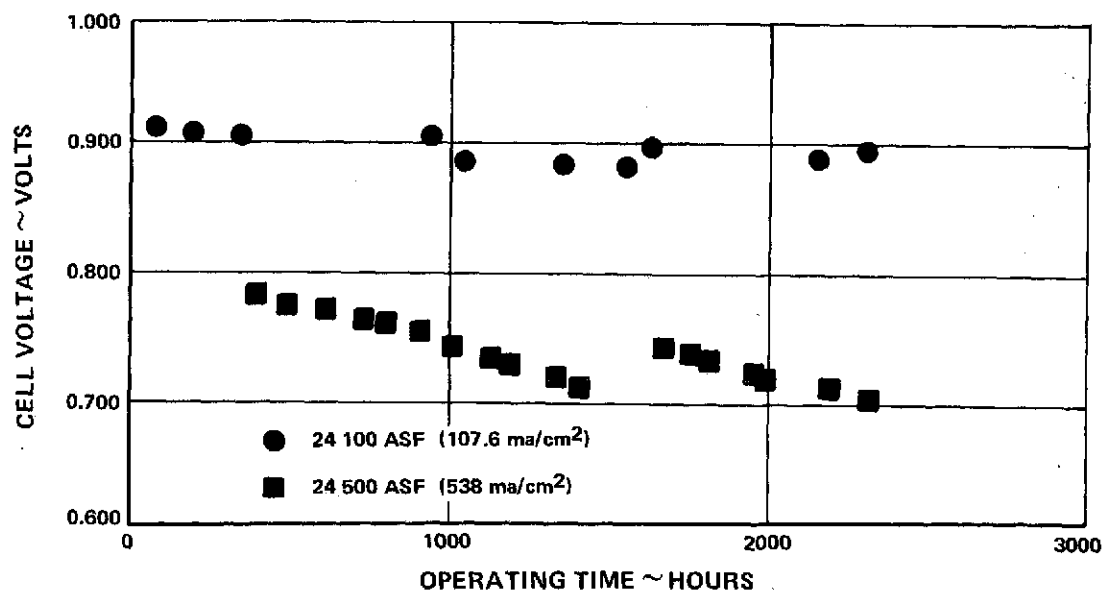


Figure 47 – Dilute Oxygen Diagnostic Test Data of Cell No. 24

Figure 48 – Comparison of 500 and 100 ASF (538 and 107.6 ma/cm^2) Operation on Cell No. 24

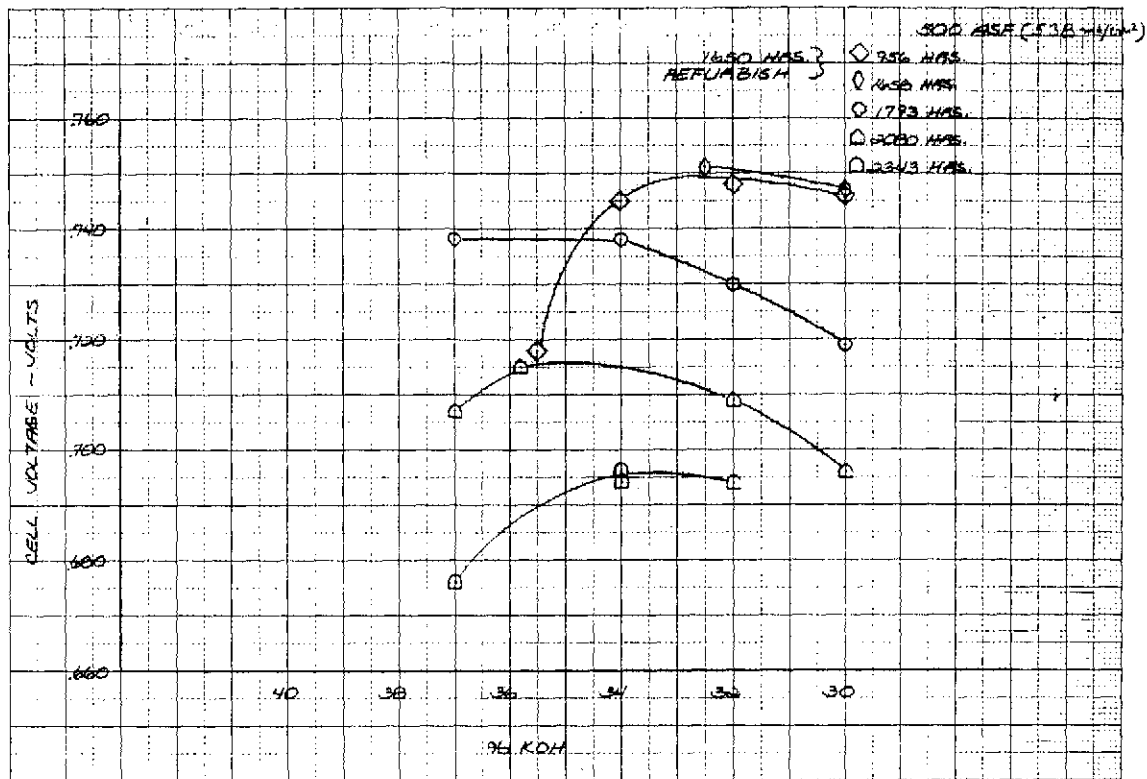


Figure 49 — Tolerance Excursion Data from Cell No. 24

Cell Nos. 25 and 27

Cells Nos. 25 and 27 were both constructed using the impregnated matrix method. Cell No. 25 was fabricated using Epon 828 and incorporated a PPF anode and cathode. Cell No. 27 was fabricated using Hypon and incorporated a PPF anode and Au-Pt cathode. Both cells include the first nickel plated-porous polysulfone ERP's. This configuration was approved by NASA to be Verification Design No. 6. The primary test objective was to evaluate the new lightweight ERP.

Cell No. 25 has accumulated 5400 hours of operation at 100 ASF (107.6 ma/cm^2); see Figure 50. Performance and off-design tolerance were both stable. Early in the test after initial refurbishment at 426 hours the cell showed a loss in wet side tolerance, see Figure 51. However after continued operation it stabilized and returned to normal. The poor wet side tolerance probably was the result of incompletely draining the cell of electrolyte after refurbishment. Off-design tolerance was checked again at 5034 hours, revealing a loss in "dry-side" tolerance; see Figure 51. Operating concentration was changed from 34 percent KOH to 30 percent KOH to allow more endurance time on the non-metallic ERP. A dilute oxygen (20 percent oxygen) diagnostic was conducted at 5375 hours. The results indicated that losses in the diffusion region were attributable to the anode and the carbonate level was

building up. Consequently the cell was shut down for refurbishment at 5400 hours. The carbonate level after shutdown was 56 percent conversion to K_2CO_3 . Figure 35 shows that the carbonate level of Cell No. 25 was consistent with the Hypon data. The cell was disassembled for visual inspection. No apparent physical deterioration of the non-metallic ERP was found. The cell will be refurbished for further endurance and diagnostic testing during the next phase of the program. The primary conclusion of this test is the lightweight porous polysulfone ERP is as good as the nickel ERP.

This was the first cell fabricated without the addition of Hycar to the impregnation material. The resulting frame was considerably more brittle than the Hycar-Epon mixture. Consequently Hycar will be added to the impregnate used in future cells.

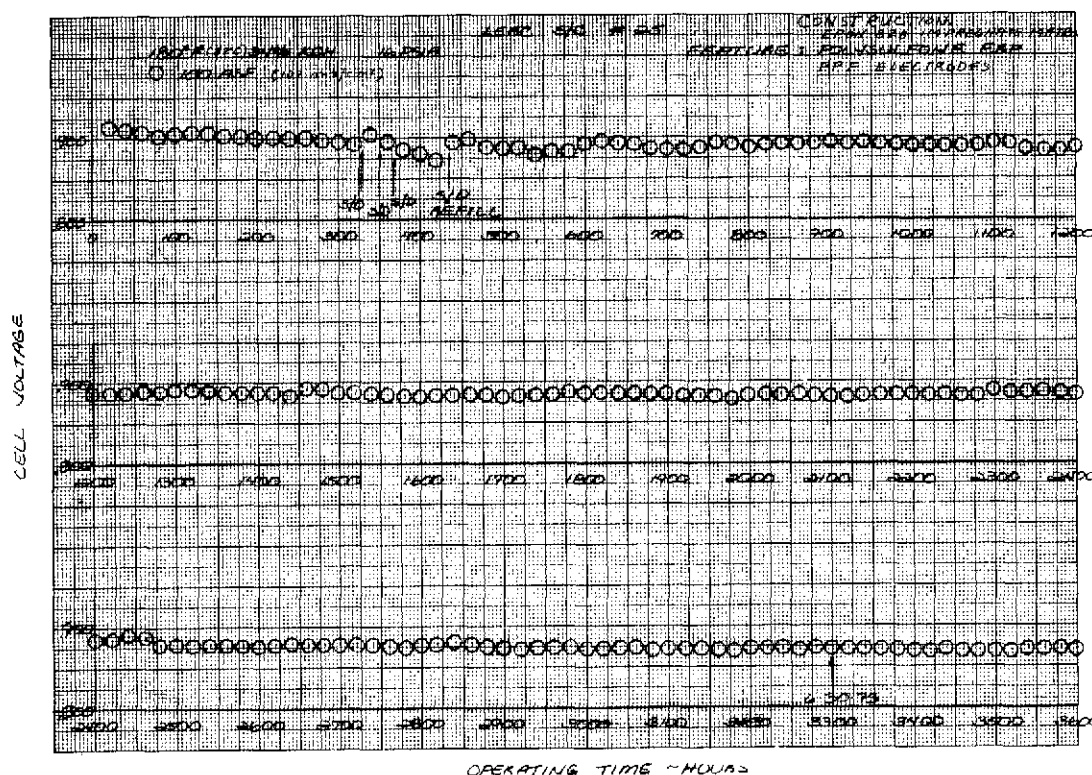


Figure 50 — Performance History of Cell No. 25

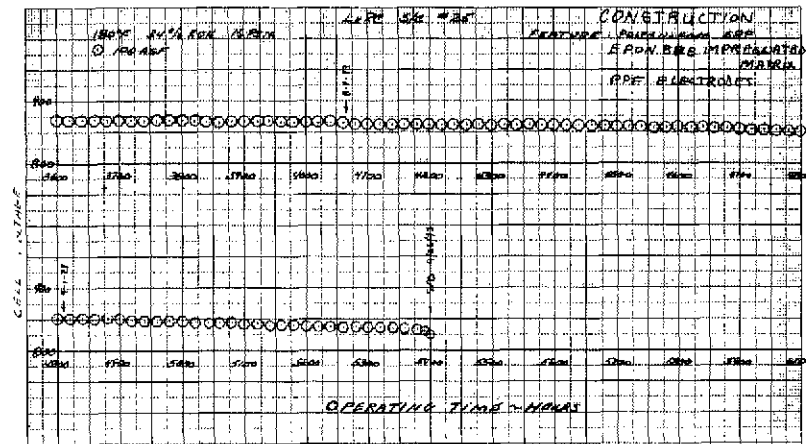


Figure 50 — Performance History of Cell No. 25 (Continued)

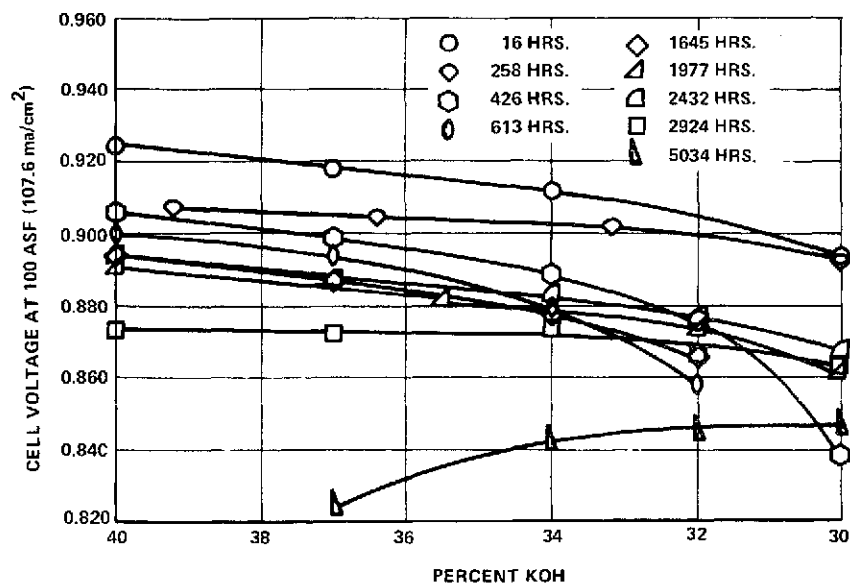


Figure 51 — Tolerance Excursion Data Cell No. 25

Cell No. 27 accumulated a total of 2061 hours of operation. The cell's performance history is shown in Figure 52. A total of 1530 hours were accumulated at an operating current density of 200 ASF (215.2 ma/cm²). The off-design tolerance response remained good through 1328 hours. A loss in performance on the "dry" side occurred on subsequent tolerance excursions, both at 200 ASF (215.2 ma/cm²) and 100 ASF (107.6 ma/cm²), as shown in Figures 53 and 54. This loss in dry side tolerance is typically associated with increasing carbonate level within the cell, but appears to be premature in cell No. 27.

An accelerated schedule of tolerance cycles was conducted on Cell No. 27 at the suggestion of NASA Program Manager. Daily tolerance excursions were conducted from 1450 hours through 1980 hours. The cell decay increased during this period, however, it was not clear whether the tolerance excursions or carbonate buildup was the primary cause.

Tafel and dilute oxygen diagnostics were conducted at 2000 hours in an attempt to determine which electrode was responsible for the high decay. The Tafel slope had increased because of apparent diffusional losses in the activation region (1-10 ASF) (1.076 - 10.76 ma/cm²). The change in Tafel slope prevented an accurate interpretation of the dilute oxygen data. Consequently the cell was shut down for analysis.

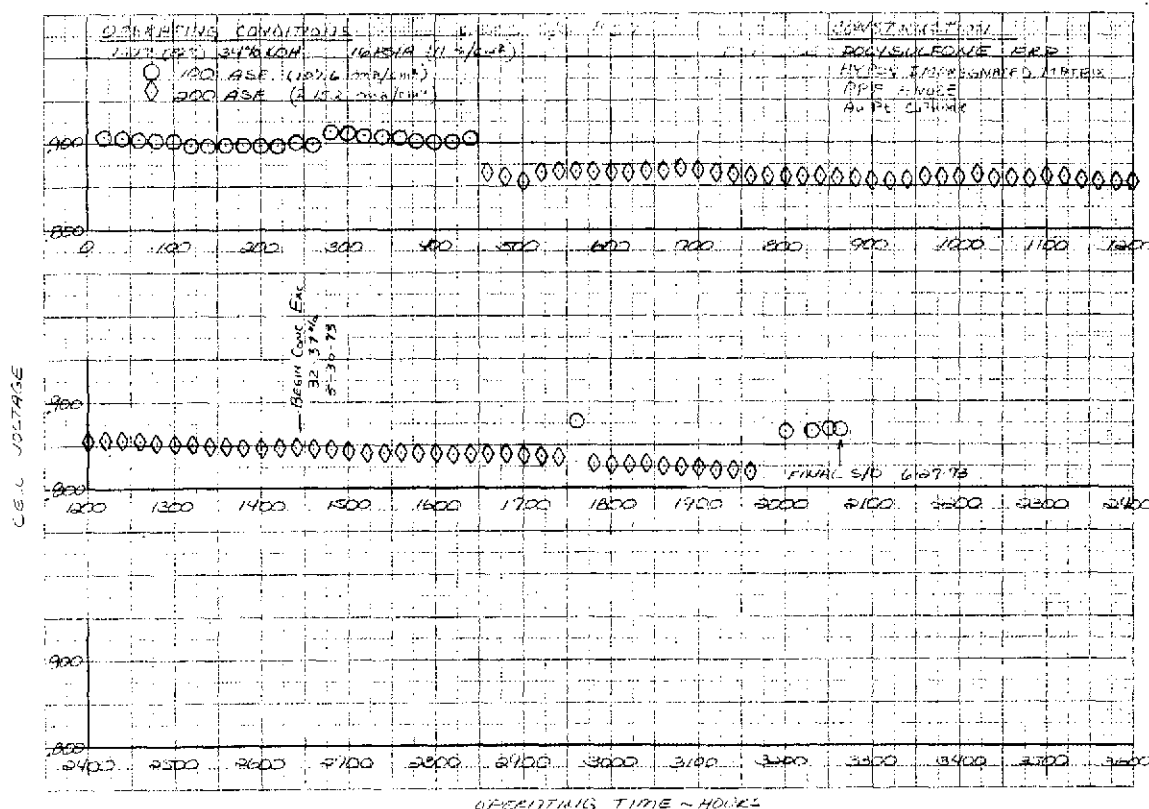


Figure 52 -- Performance History of Cell No. 27

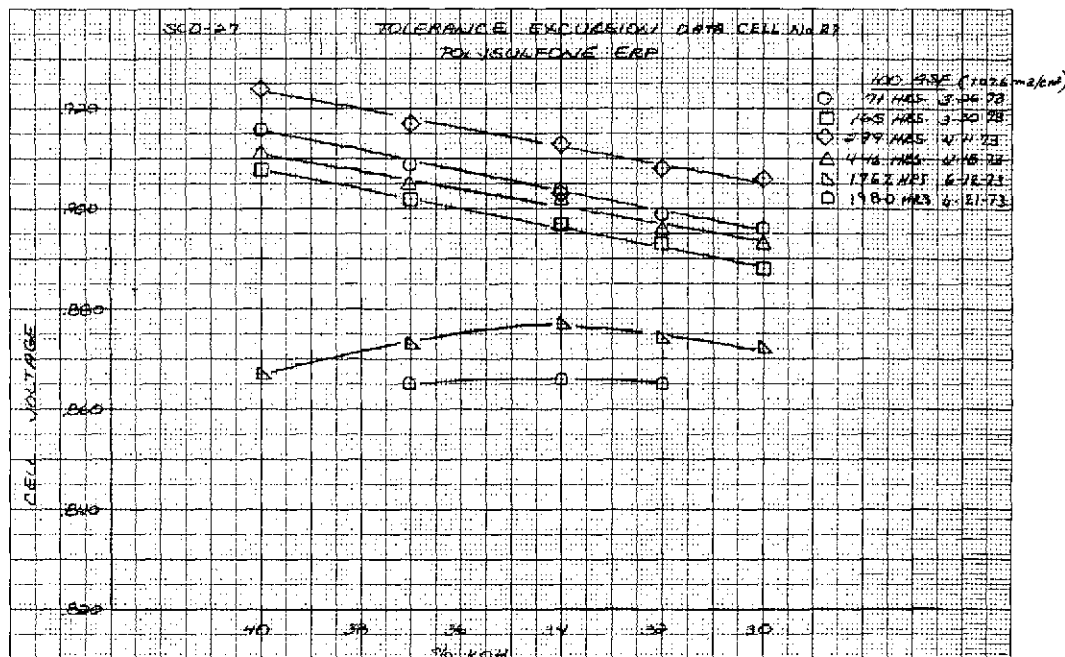


Figure 53 – Tolerance Excursion Data Cell No. 27 (Polysulfone ERP)

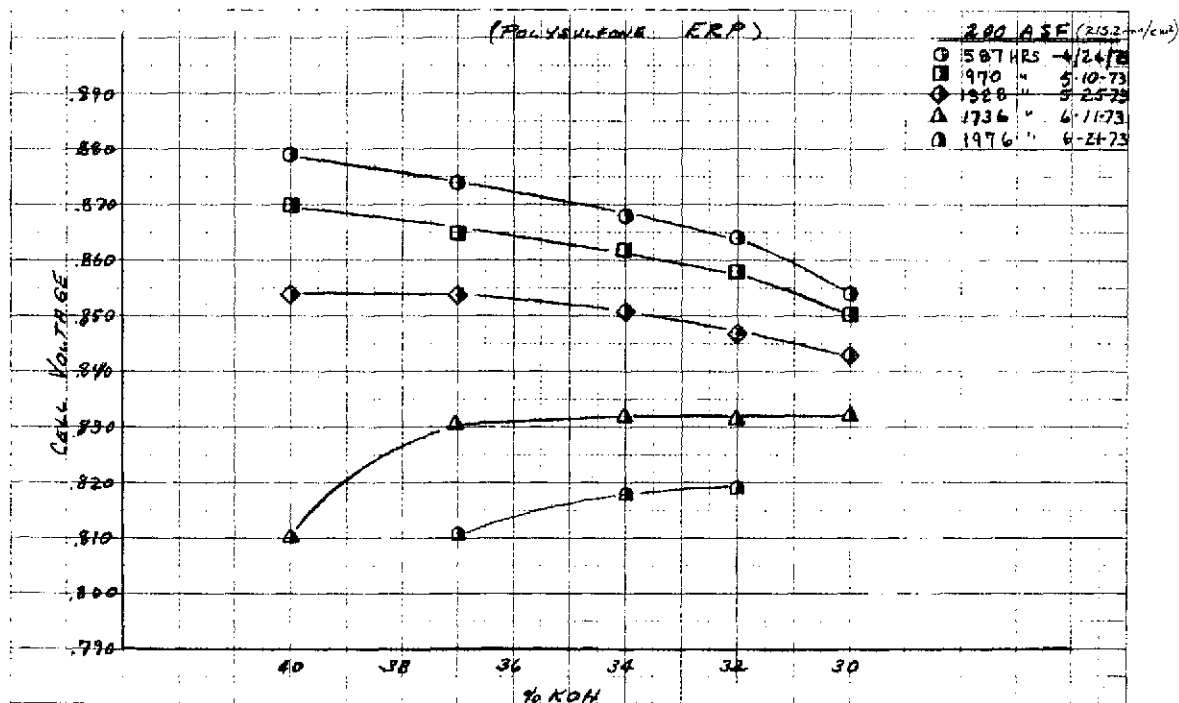


Figure 54 – Tolerance Excursion Data Cell No. 27 (Polysulfone ERP)

The post-test evaluation showed the carbonate level after shutdown was equivalent to a 32 percent conversion of electrolyte. Figure 35 shows that the level of carbonate in Cell No. 27 was consistent with previous Hypon data. This cell is to be refurbished for additional testing. Diagnostics will be conducted to determine a cause for the poor performance. No indication of the lightweight ERP being the cause of the problem was found. The results of a P&WA study of half-cells to evaluate the effect of potassium carbonate on electrode performance are shown in Figures 55 and 56. These data show the effect of increasing carbonate formation on half-cell performance for PPF anodes and Au-Pt cathodes.

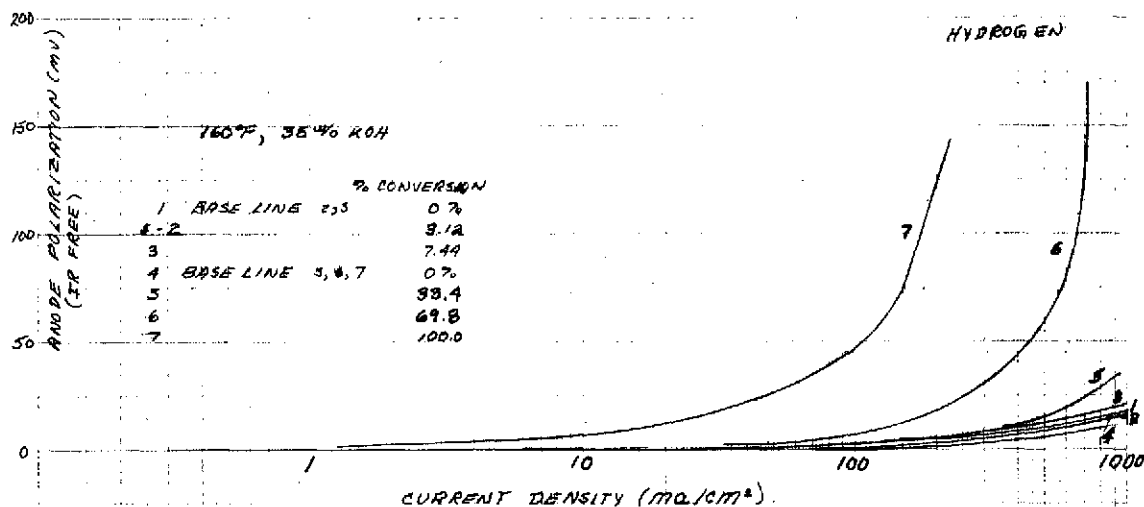


Figure 55 — Effect of Carbonates on PPF Anode Polarization

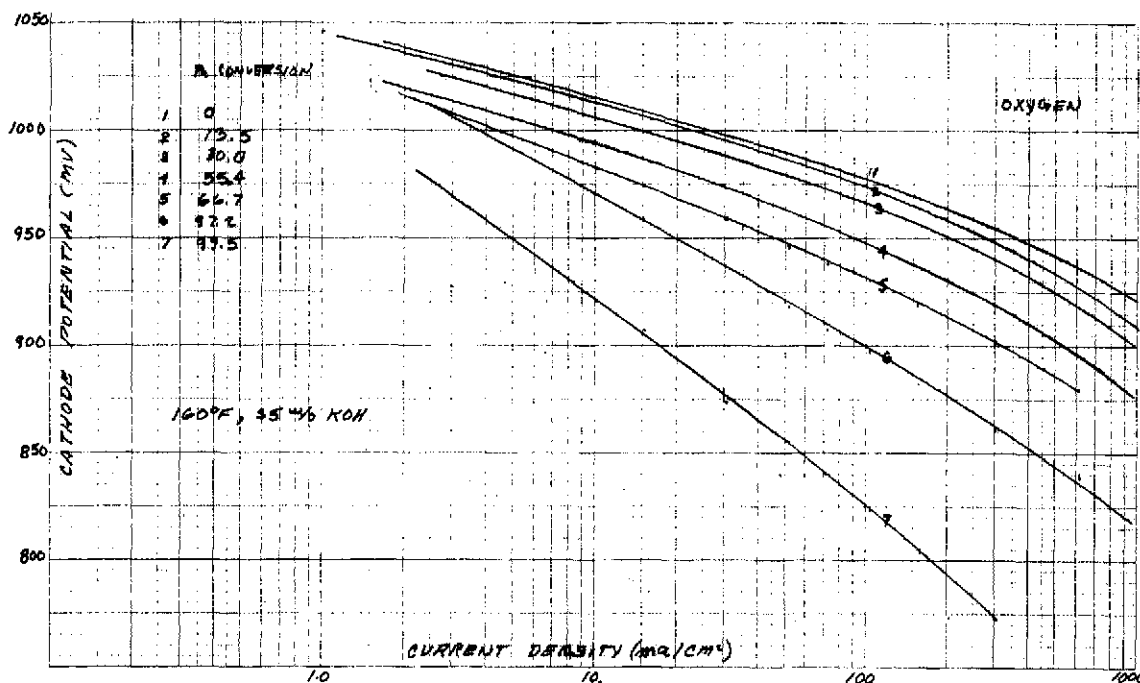


Figure 56 — Effect of Carbonates on Au-Pt Cathode Performance

Cell Nos. 26 and 29

Cell Nos. 26 and 29 were both delivered to the NASA-LeRC for evaluation. They were both built to the Verification Design No. 6 configuration.

Cell Nos. 28 and 30

These cells were of the configuration approved by the NASA Program Manager as Verification Design No. 7. These cells were of laminated polysulfone film construction.

Cell No. 28 was fabricated with PPF electrodes and accumulated 2115 hours of operation. Its operating history is presented in Figure 57. Carbonate conversion determinations were made at the completion of its Verification Test and after shutdown at 2115 hours. The first test showed low levels of carbonate formation equivalent to the low carbonate conversion associated with Teflon cells. The test after shutdown showed the lowest level of carbonation, 5 percent conversion of electrolyte, achieved to date. Both of these data are shown on Figure 35. Wrinkling and distortion of the electrodes of this cell occurred during fabrication. This problem results from the film unitization process and additional work is required to eliminate it. It is the result of polymer shrinkage caused by high temperature bond and differential thermal expansion of the polymer and electrode substrate.

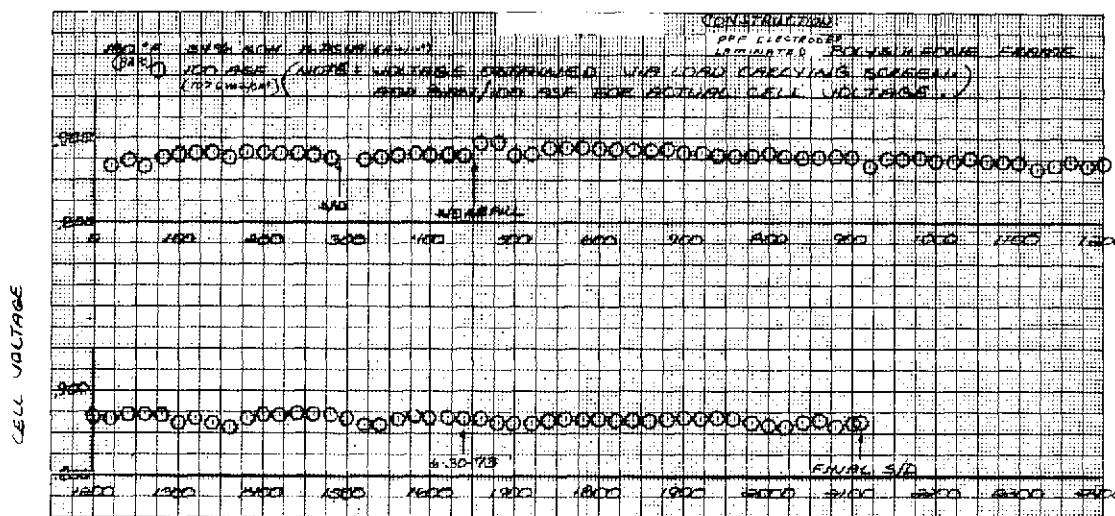


Figure 57 – Performance History of Cell No. 28

Attempts to fabricate a passive water removal (PWR) assembly using polysulfone film were unsuccessful. Sufficient bubble pressures could not be obtained to satisfy the 12 psi (8.27 n/cm^2) minimum differential pressure requirement. For this reason, Cell No. 28 was assembled with a Hypon PWR.

Performance was stable but relatively low compared to other PPF cells. The low performance may have been due to poor condition of the electrodes. In addition to the wrinkling caused by polysulfone UEA fabrication, the conditions imposed upon this UEA during corrosion testing may have had some detrimental effect on catalyst structure.

Cell No. 30 was fabricated with a PPF anode and a Au-Pt cathode. However, like Cell No. 28 it has a Hypon PWR. The objectives of this cell's test program were to obtain:

- (1) Endurance experience with Au-Pt cathodes, and
- (2) Carbonate data for polysulfone frames.

Based on the encouraging carbonate levels in Cell No. 28, this material and Cell No. 30 have the potential for 10,000 hours of operation without refurbishment. By the end of the contract period Cell 30 had accumulated 2113 hours. Figure 58 shows the performance history of this cell, to date.

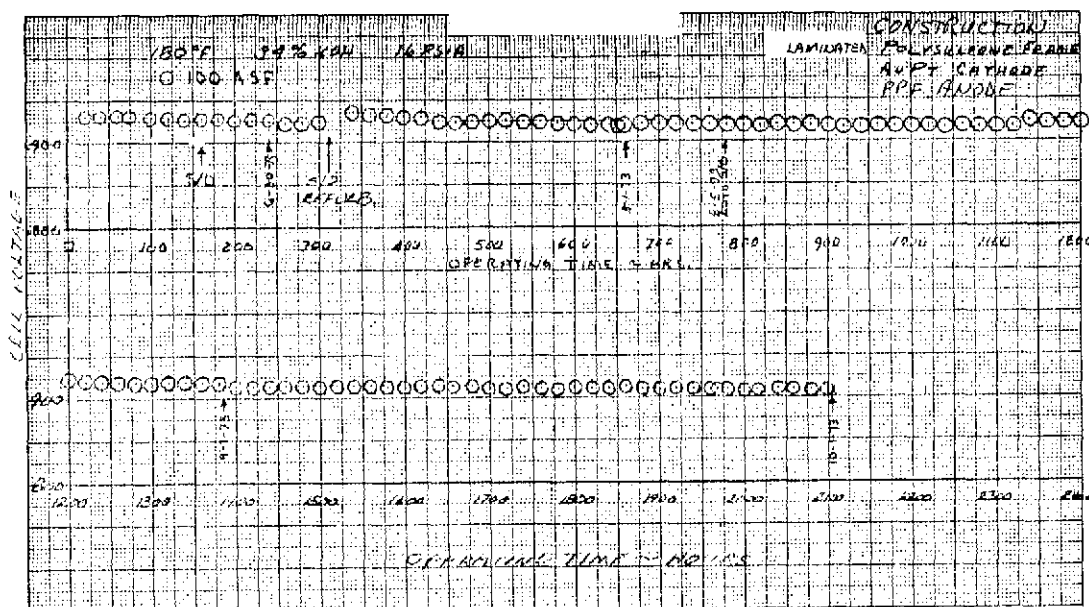


Figure 58 — Performance History of Cell No. 30

The initial performance of 933 mv at 100 ASF (107.6 ma/cm^2) is the highest level demonstrated on any full size operating cell. During the two week verification cycle, the performance decreased to 925 mv followed by a step change increase to a peak of 939 mv after refurbishment at 450 hours. A review of the early performance history of previous Au-Pt cells (Cell Nos. 23 and 24) indicated that Cell No. 30's performance is consistent with the previous data. The results of a dilute oxygen diagnostic, shown in Figure 59, indicate that performance losses are mostly cathode polarization. No similar dilute oxygen data exists for comparison (i.e. a full size operating cell at 1100 hours). This diagnostic tool will be used to monitor anode and cathode performance throughout the endurance evaluation.

The result of carbonate analysis from the initial refurbishment at 450 hours was 4.5 percent conversion, consistent with the results obtained on Cell No. 28; see Figure 35.

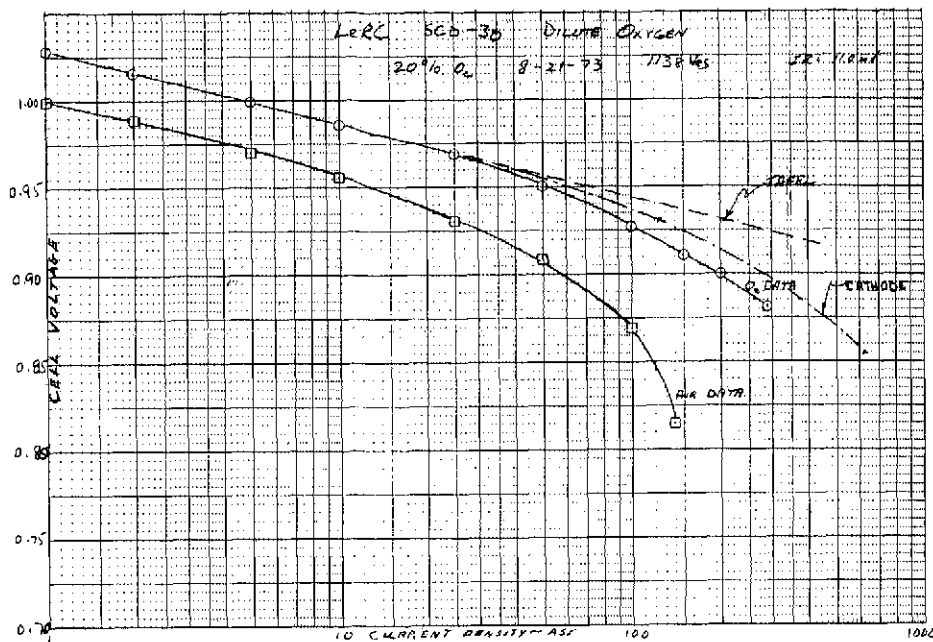


Figure 59 — Dilute Oxygen Data - Cell No. 30

B. Evaporative Cooler Development

1.0 Requirements and Operation

The EMS requirements for uniform temperature over the entire cell area under all operating conditions and power levels and at minimum weight can be achieved with intercell cooling by evaporation of water.

Servicing two adjacent strip cell plaques, these intercell coolers maintain cell temperature by heat conduction from the cell plaques to an internal water reservoir. See Figure 60. Waste heat generated by the fuel cell is conducted through the oxygen/water plates to the water passages. The evaporation temperature at the membrane interface is controlled by the pressure maintained in the steam chamber. Water pressures higher than the steam chamber pressure ensure that the water passages are always supplied with cooling water. Steam from the membranes flows parallel to the membranes in the steam flow field which connects to a manifold for removal of steam from the stack.

The low weight goals of the EMS required several novel features in this cooling system. Porous polymer membranes were required for water-steam separators, the water and steam flow passages were dimensionally small and yet were required to have low pressure and temperature drops, and structural components were to be made from lightweight polymer materials.

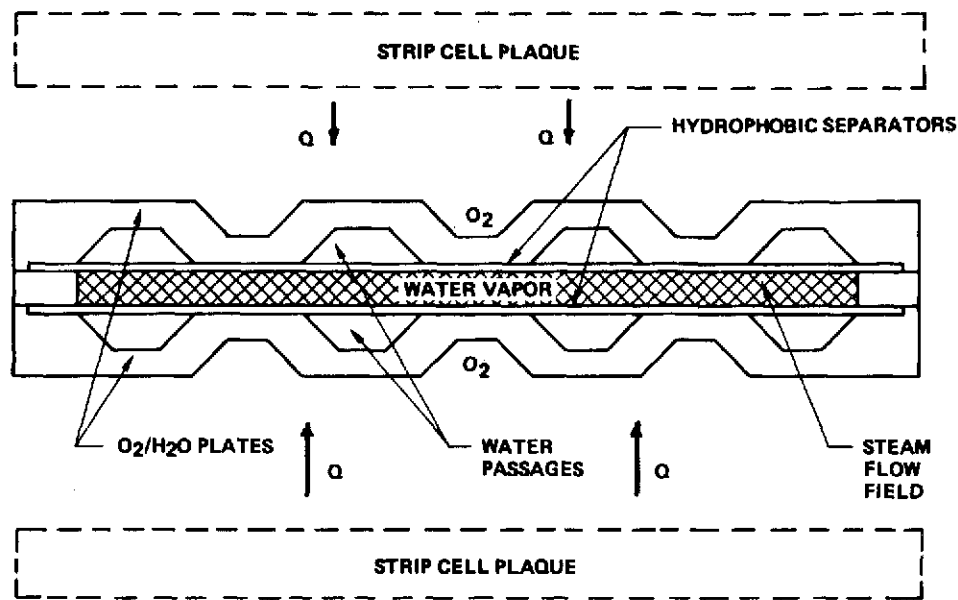


Figure 60 — Evaporative Cooler Schematic

The ideal evaporative cooler has the following characteristics:

- No cell-to-steam temperature gradient exist
- Cell temperature is set by the pressure maintained in the steam chamber, which sets a saturation temperature at the water-membrane interface
- Cell temperature is independent of waste heat flux
- Feedwater consumption is a function only of waste heat flux
- Cell temperature and feedwater consumption is independent of water overpressure

Ideal evaporative cooler performance is illustrated in Figure 61. The curve for the ideal case shows that the steam temperature is on the saturation temperature line for water and that no steam-to-water temperature gradient exists. In an actual cooler, the pressure loss in the steam field results in an increase in the absolute pressure at the water-membrane interface with the resulting increase in the saturation temperature.

In addition, the temperature differential which exists in the water field causes a second deviation from the ideal case. Heat flow from the cell to the membrane is through the parallel conduction paths in the oxygen/water plate and the water. A high thermal conductivity oxygen/water plate minimizes the water reservoir differential temperature. The deviation from the ideal cooler performance caused by the water field temperature rise is also illustrated in Figure 61.

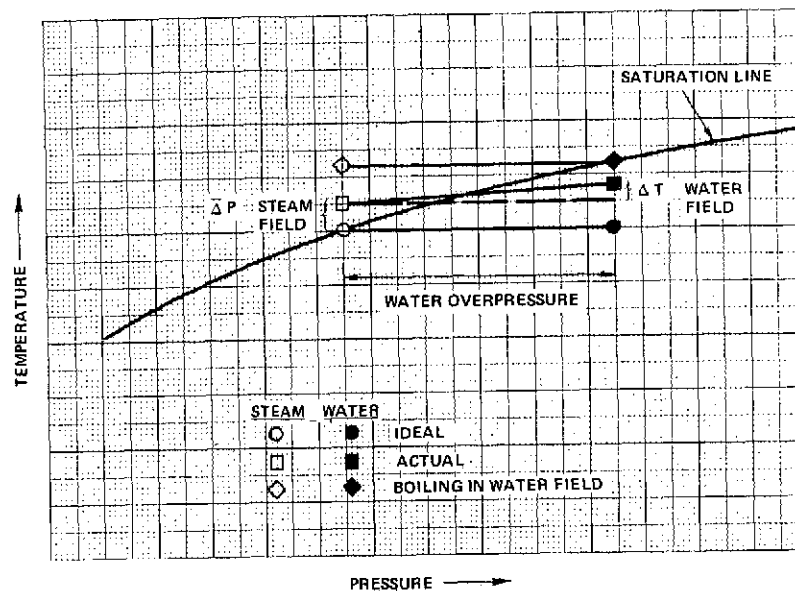


Figure 61 — Ideal Evaporative Cooler Performance

The additive effect of these two deviations from the ideal case sets a minimum cell-to-steam temperature gradient. Although this gradient can be corrected for by maintaining a lower steam pressure and, thus, maintaining the desired cell temperature, the two losses result in a minimum water overpressure constraint on the cooler. Water overpressures, whose saturation temperatures are above the minimum cell-to-steam temperature rise, must be set to prevent boiling in the water reservoir. When boiling occurs in the cooler, temperature control is maintained by the water pressure as shown in Figure 61. Although boiling is not necessarily a failure mode, it does result in higher pressure losses in the water field and increased temperature.

The above operational characteristics and low weight goals impose the following conflicting requirements on evaporative cooler components:

Separator Membrane:

- The water-steam separator membrane should be thin, be highly porous, and have a large mean pore size to provide sufficient steam permeability, while having a sufficiently high water entry pressure which implies a thick, dense and small-mean-pore-size structure.

Steam Field:

- The requirement for a light-weight structure which has a low in-field pressure drop suggests an open, widely-spaced structure while the requirement for sufficient membrane support dictates a closely spaced, dense structure.

Water Field:

- The requirement for an even temperature profile across the water field is best met with a shallow metallic field. The low weight requirement calls for a shallow plastic field which has good thermal conductivity and low in-plane resistance to water flow.

During Phase I an evaporative cooler was designed and tested in subscale units. The fundamental feasibility of this cooling approach was demonstrated, design concepts were verified and materials of construction were identified. As a result the primary objective of the Phase II evaporative cooler was to develop and test a full scale evaporative cooler that could be tested with a pair of six-cell plaques.

2.0 Design and Fabrication

The design of the full scale evaporative cooler was based on the results of the subscale cooler design and tests of the Phase I program. Based on this work, Arylon and filled and unfilled polysulfone were considered for cooler component construction. However filled polysulfone sheets were unavailable in the sizes required. Although unfilled polysulfone was available previous experience had indicated it had potential crazing and stress cracking problems, especially after machining. Using a tape-machining program developed in Phase I, a sheet of polysulfone was machined with a cooler pattern. Subsequent stress cracking did occur during heat treatment in an attempt to relieve stresses, as well as in heat cycling to simulate fuel cell operation. This material probably can be used if special stress relieving techniques are developed.

Because of the uncertainties of polysulfone, Arylon was selected for use in evaporative cooler components. Although not optimum from an oxidation standpoint, Arylon is easily machineable and does not stress crack. This was a major consideration because the Phase II cooler field pattern was tighter than that used in the Phase I oxygen plate. This pattern could result in greater stresses after machining. Details of the oxygen/water plate are shown in Figure 62. The oxygen field depth is 15 mils ($38.1 \times 10^{-5}\text{m}$), water field depth is 10 mils ($25.4 \times 10^{-5}\text{m}$) and the web thickness is 10 mils ($25.4 \times 10^{-5}\text{m}$). The pin pattern on the water side is such that all pins are aligned with oxygen-side pins and bars to give optimum structural integrity. Pin coverage on the water side is 25 percent; oxygen secondary manifold bar pattern results in 37.5 percent coverage; and the primary field bar pattern results in a 50 percent coverage area.

Pressure drop and thermal analyses were conducted for this configuration. The results for the 21 KW design condition are as follows:

	<u>Flow</u>	<u>ΔP</u>	<u>ΔT</u>
Cooling Water	0.49 gph (0.222 kg/hr)/side	0.02 psi (0.014 n/cm ²)	
Steam	0.98 gph (0.445 kg/hr)	1.07 psi (0.74 n/cm ²)	
O ₂ /H ₂ O Plate			22° F (12° C)

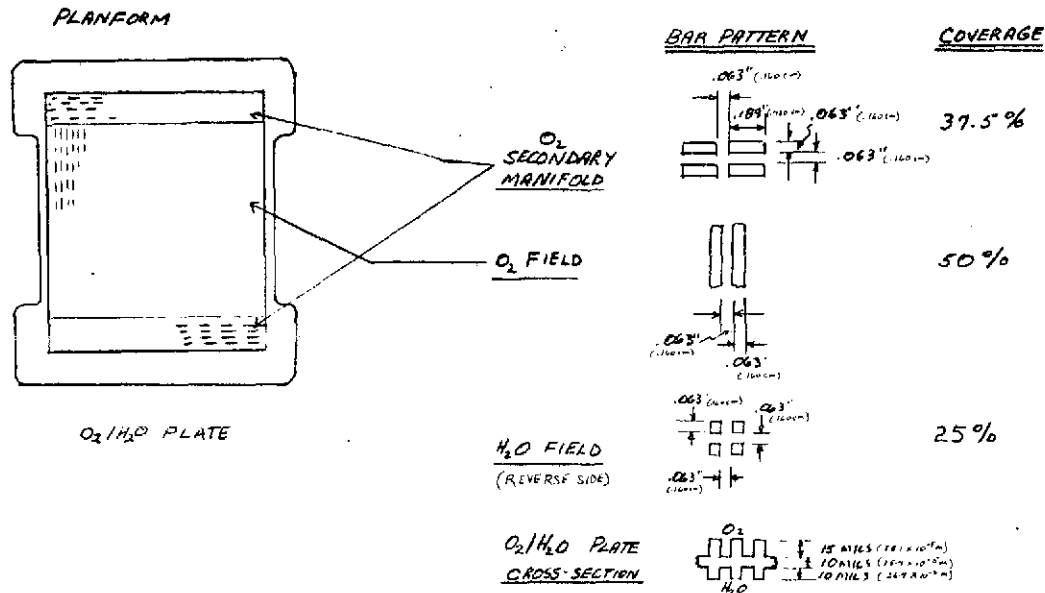


Figure 62 — Details of Phase II Oxygen/Water Separator Plate

From a structural viewpoint, analysis showed a requirement for 2-mil (5.08×10^{-5} m) web thickness to support a pressure differential of 5.2 psi (3.58 n/cm^2) across the oxygen/water plate. The 10-mil (25.4×10^{-5} m) web thickness selected is more than adequate to support this pressure differential.

3.0 Evaporative Cooler Assembly

The complete evaporative cooler assembly was built up as shown in Figure 63. It consists of two separator plates, a steam cavity frame with a tri-layer-screen steam spacer and two porous Teflon membranes. The assembly was made by bonding a porous Teflon membrane to the water side of each separator plate. Two thermocouples were positioned in one of the water fields and two in the oxygen field. Hypon adhesive was used to make all bonded joints in the assembly. Adhesive was kept from entering the 10 mil (25.4×10^{-5} m) water ports by inserting Teflon plugs into the ports during the bonding operation. These plugs were not removed until the assembly was completed. After bonding of the porous Teflon membrane to the water side of the separator plate, the tri-layer screen assembly was tacked to the separator plate. Then the final bond of the separator plates to the separator frame was made. To verify that water entry ports were open and that the internal cavities were clear the unit was flow tested. A water flow rate of 16 lb/hour-psi ($10.5 \text{ kg-cm}^2/\text{n-hr}$) was measured. This was consistent with analytical predictions for a properly assembled unit.

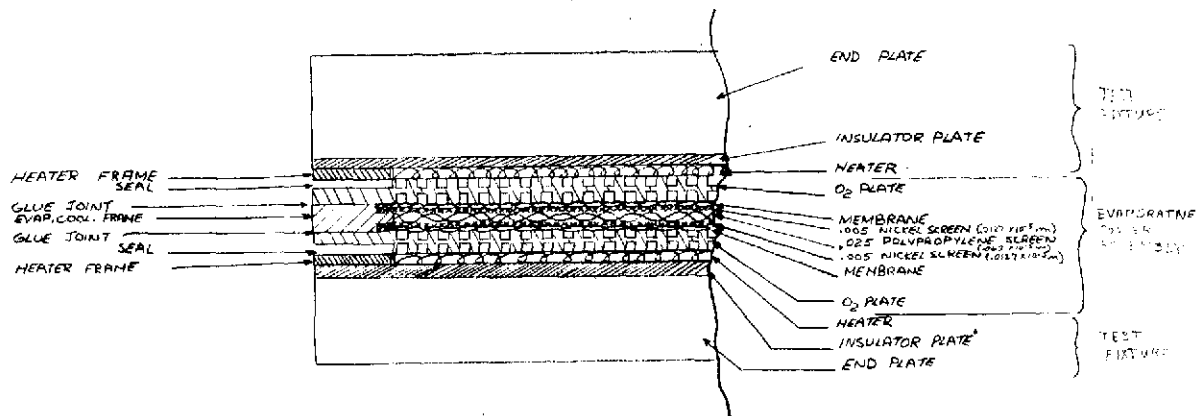


Figure 63 – Evaporative Cooler Assembly and Test Fixture

4.0 Evaporative Cooler Test Results

The ultimate test of the cooler was to be in conjunction with a partial stack. But before it was released for stack testing, it was tested as a component to verify its cooling capability at simulated fuel cell heat loads. Insulator plates were placed between each end plate and the unit to minimize the amount of heat loss. Two 500-watt heaters, one on either side of the evaporative cooler were used to simulate heat generation by each of the six-cell plaques. Metal heat dispersion plates were placed between heaters and cooler to distribute heat uniformly as it would be generated by a plaque. Water and steam sealing was accomplished by the use of flat Butyl gaskets. Initial testing was conducted to insure against malfunctioning of the test unit or test facilities. Subsequently, a one week verification test was conducted simulating the fuel cell load profile shown in Figure 64. The electrical heaters supplied heat loads equivalent to current densities of 100, 140, and 460 ASF (107.6, 150.6, and 495 ma/cm²). The results of the one week verification test are shown in Figure 65. The water and oxygen plate temperature and the amount of condensate collected as a function of time are shown. The temperature differential of 17°F (9.5°C) across the cooler plate and the steam pressure drop of 1.3 psi (0.89 n/cm²) at the peak power design point of 460 ASF (495 ma/cm²) compared favorably with the predicted values of 22°F (12°C) and 1.1 psi (0.76 n/cm²) respectively. On the basis of this test, the evaporative cooler was released for use in partial stack testing.

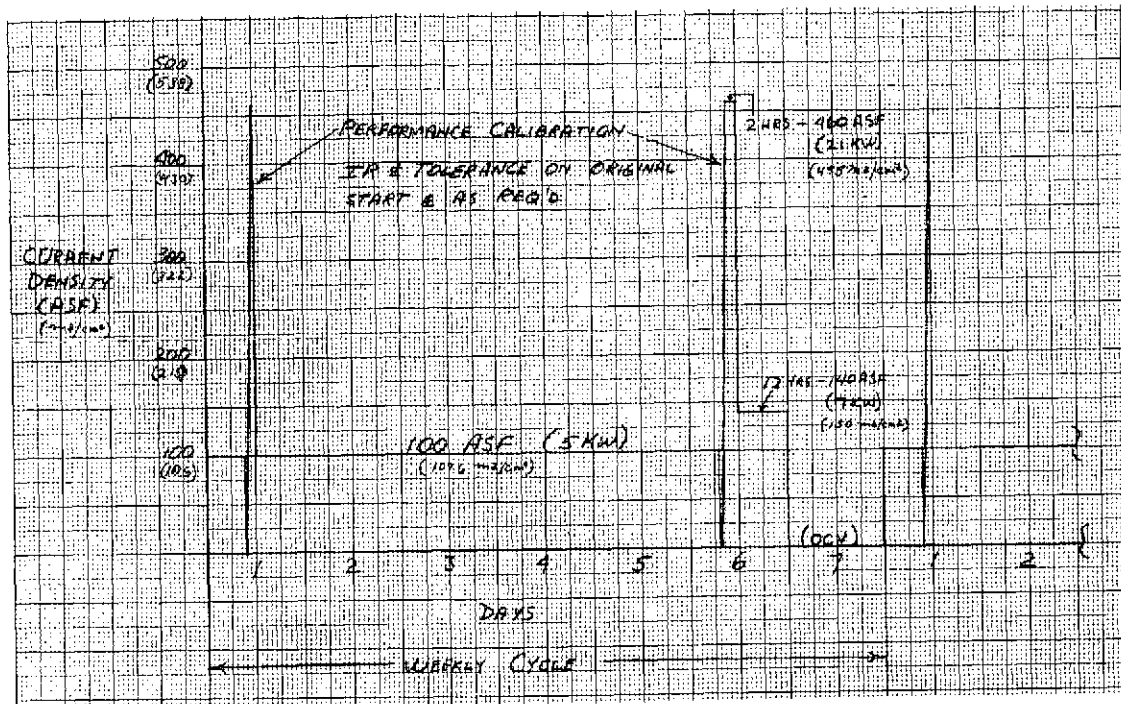


Figure 64 — Typical Fuel Cell Load Profile

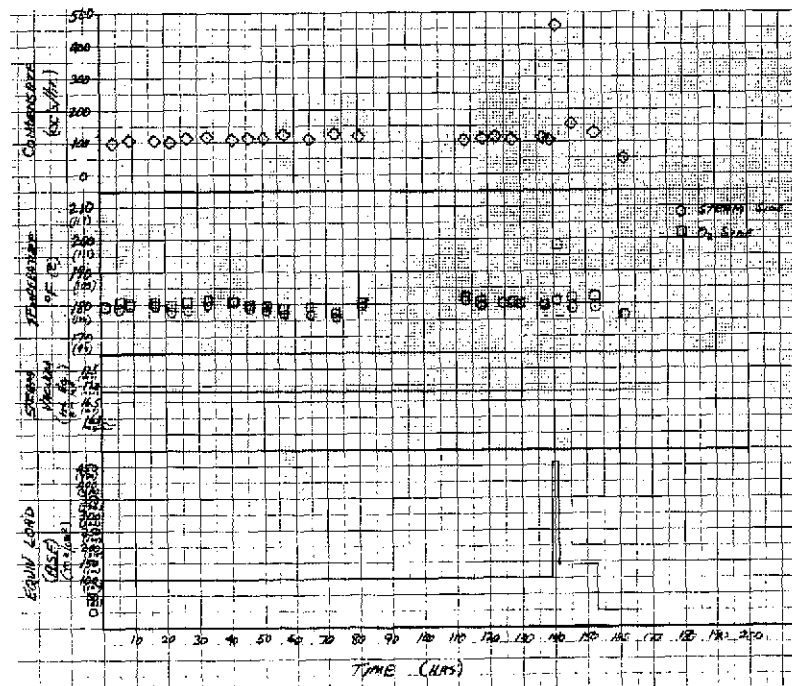


Figure 65 — Evaporative Cooler Verification Test

C. Plaque and Partial Stack Development

1.0 Introduction

A plaque is a multi-cell planar stack. The plaque concept offers weight advantages which are of particular benefit to high power, high voltage systems such as the Engineering Model System. In such systems, a large number of series connected cells is required. The plaque, by packaging a group of series-connected cells into one thin plate, allows the system's power section to be assembled from fewer components. By having a number of cells share common reactant plates, coolant plates, and fluid manifolds, fewer components and sealing planes are required. The plaque concept is illustrated in Figure 66.

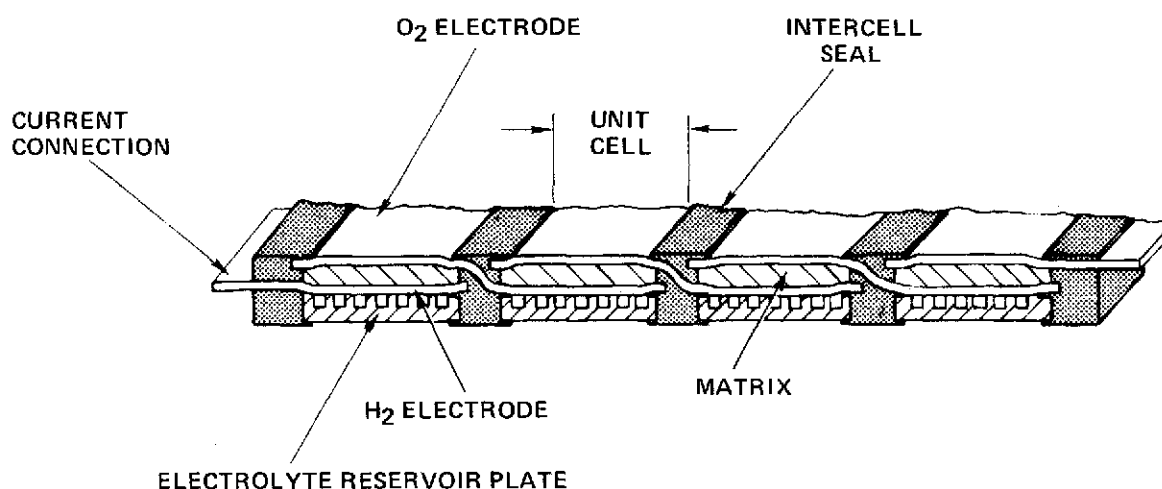


Figure 66 — Plaque Concept Showing Intercell Seal

At the beginning of Phase I there were two major problems envisioned with successful development of a plaque. One is unique to the plaque, the other is common to all fuel cells:

- **Intercell Seal** — Series connection of cells in a common plane means the anode of one cell must be electrically connected to the cathode of an adjacent cell. Thus a current carrying member must pass from the hydrogen side to the oxygen side of the plaque without allowing any possibility of gas leakage.
- **Large Total Cell Area** — By grouping a number of cells into one planar sheet, the total cell area of the plaque is large. The problems associated with achieving proper reactant flow distribution and dimensional tolerances is the same as that for large area cells.

Although it was not without its problems, this test demonstrated the fundamental feasibility of the plaque concept. Its problems were primarily associated with materials (corrosion resistance), and fabricability (dimensional tolerances).

2.0 Plaque Fabrication

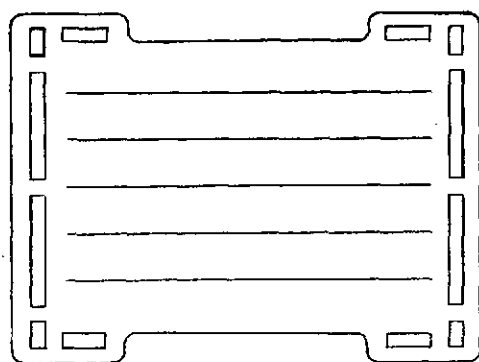
Plaque fabrication efforts were focused on three objectives during Phase II:

- (1) Improve dimensional tolerance of parts
- (2) Reduce intercell seal width from 0.5 inch (1.27 cm) to 0.375 inch (0.95 cm)
- (3) Use materials for construction of improved corrosion resistance

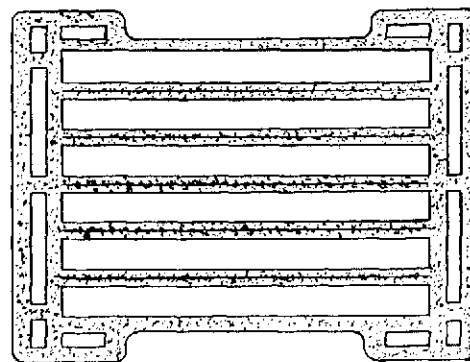
Three new operable plaques were fabricated during Phase II and a fourth was assembled from components of the first two. Two trial plques were also fabricated at the outset of the program phase. These parts were fabricated using the basic method developed in Phase I. In this method a plaque-sized piece of matrix material is impregnated with epoxy in the frame and intercell seal area and allowed to semi-cure. Slots are cut in the center of the intercell seals to be the length of the active area. The electrode screens are then threaded through the slots and the screens positioned in the epoxy-impregnated asbestos matrix. The layup is then press-cured between platens with the epoxy flowing around the electrode screens to create a gas seal; see Figure 67. Electrolyte reservoir plates are bonded in place on the anode side using a 3 to 4-mil (7.62 to 10.16×10^{-5} m) epoxy-impregnated matrix "tape" between the cells. The epoxy-impregnated tape is mated with adjacent electrolyte reservoir plates and press-cured forcing a small amount of epoxy-impregnated asbestos from this bond. Finally, a 3 to 4-mil (7.62 to 10.16×10^{-5} m) epoxy-impregnated asbestos frame is press-cured in place to give added rigidity to the frame and to bond each of the end sinters in place. A cross section of the assembly fabricated in this manner is shown in Figure 68. Figures 69 and 70 show hardware fabricated during this program.

The two trial plaques and the first full-size operable plaque were fabricated as described above using Epon 828 rather than the Hypon epoxy used in Phase I. Epon was substituted for Hypon because of the relatively high levels of carbonation found in Hypon cells tested earlier. These units showed good dimensional control and showed no cross leakage or cell-to-cell shorting. These plaques, however, were very fragile and difficult to handle during component checkout and assembly. Consequently, the decision was made to revert to Hypon as the impregnate despite the fact that single cell and non-operating cell results indicated that Hypon was relatively poor as a corrosion resistant frame material. This step was taken to allow continuation of partial stack evaluation and testing while an improved epoxy program was initiated in search of a superior corrosion resistant material.

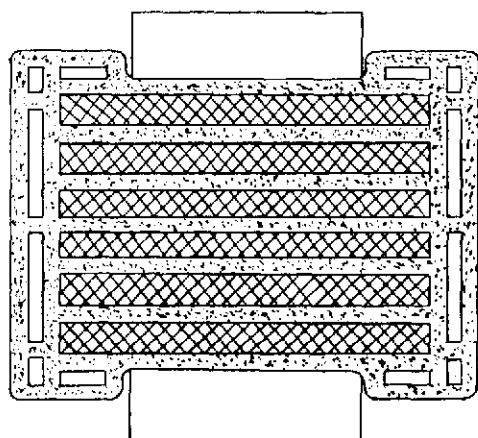
The second and third plaques were fabricated with Hypon. The electrodes used in the first and second plaques were of the PPF type. The third plaque was assembled with PPF anodes and Au-Pt cathodes.



ASBESTOS WITH PORTING AND
INTERCELL SLITS



FRAME AND INTERCELL STRIPS
IMPREGNATED WITH EPOXY



ELECTRODES POSITIONED, PRESSED & CURED

Figure 67 —
Plaque Impregnated Unitization Method

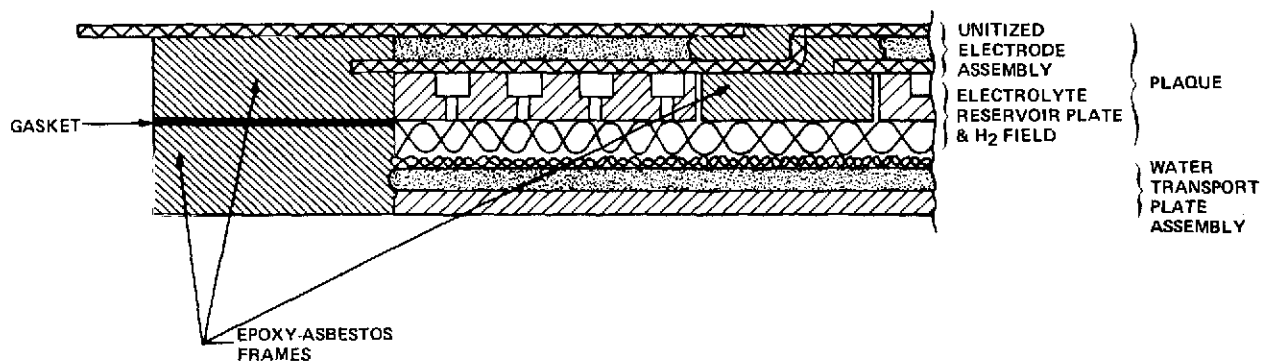


Figure 68 — Plaque Cross Section Showing Electrolyte Reservoir Plate and Hydrogen Field

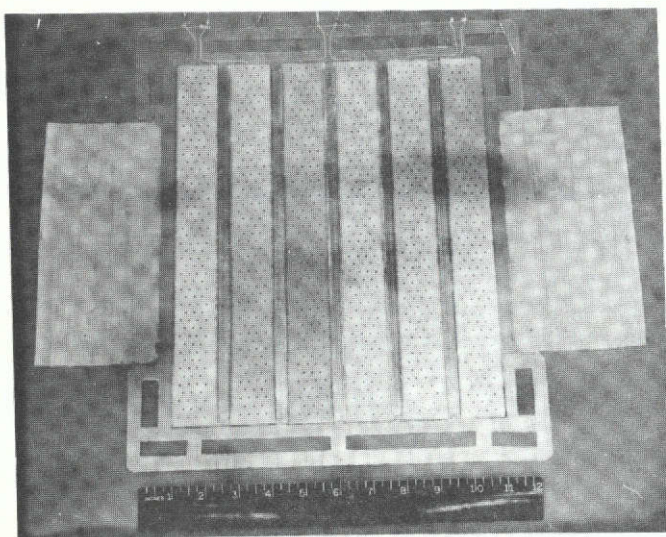


Figure 69 —
Six-Cell Plaque - Anode Side

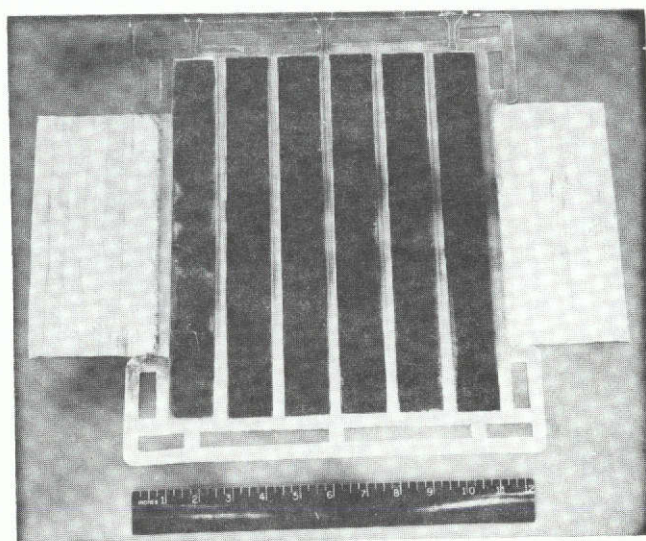


Figure 70 —
Six-Cell Plaque — Cathode Side

3.0 Test Fixtures and Assembly

One of the most important functions of the plaque test fixture is to provide uniform cell compression over the total cell area. During Phase I, one-inch (2.54-cm) thick stainless steel end plates were fabricated. Seal testing indicated that seal loads higher than had been anticipated were required. To this end, one and one-half inch (3.81 cm) thick stainless steel end plates were designed and fabricated to limit deflections. Butyl rubber gaskets were again used sealing component parts and end plates. Stack cell compression was again set by selection of the proper combination of gasket and screen thicknesses.

A complete assembly layup of the partial stack is shown in Figure 71. Six butyl gaskets are required for sealing at the various component interfaces. In initial assemblies, difficulty was encountered in keeping gaskets positioned before torque loading. In the last assemblies, seals were bonded to components, considerably simplifying the assembly. Screens of proper thickness were cut to fit in hydrogen and water transport plate cavities and spot glued in place to prevent shifting during assembly.

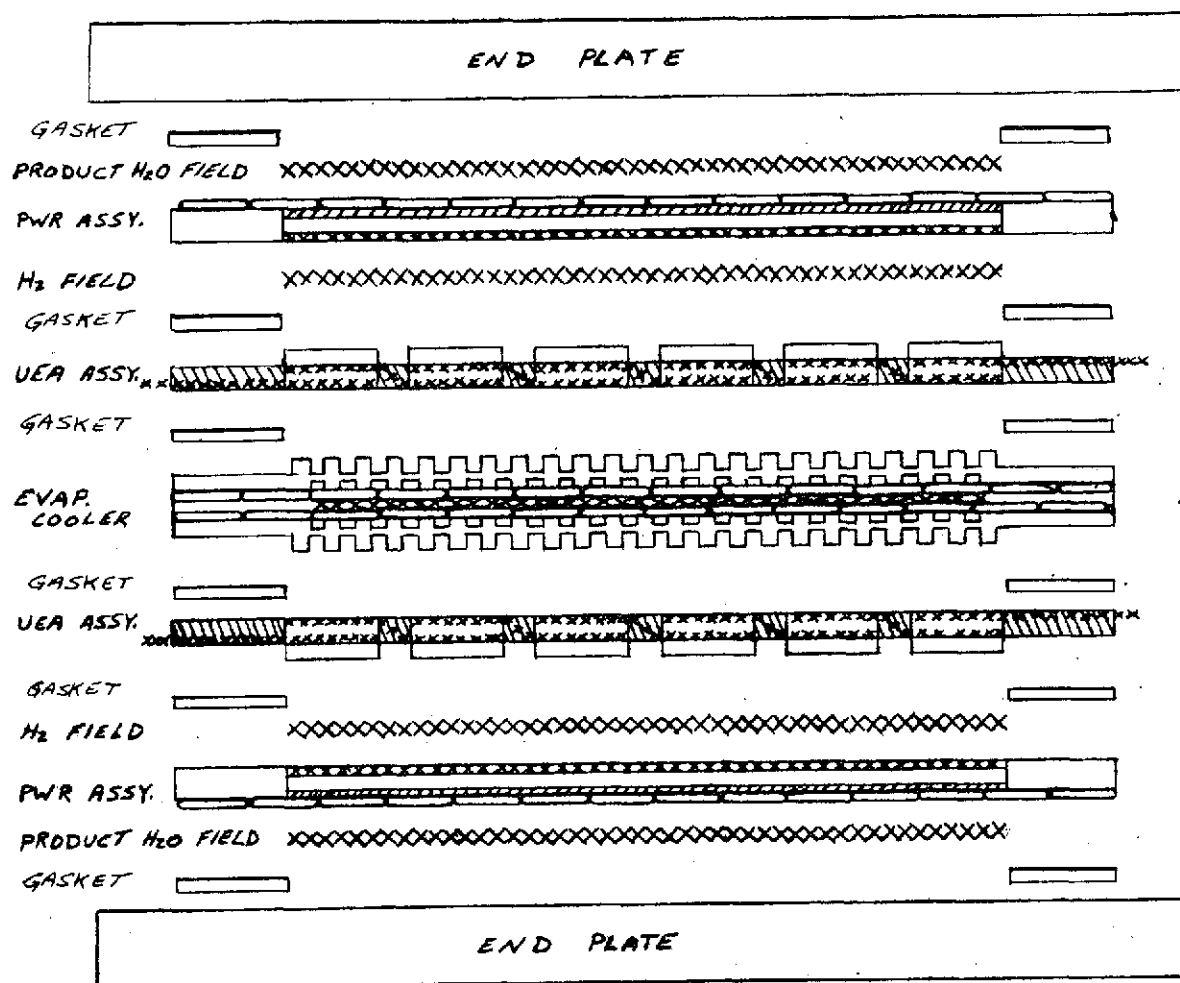


Figure 71 — Partial Stack Assembly

4.0 Partial Stack Test Results

During the Phase II contract period, four partial stacks were assembled and tested. The plaques and passive water removal assemblies used in these units were all fabricated using the Hypon-impregnated matrix method. Three of the partial stacks used PPF anode and cathodes (Designated Design No. 1) while the fourth had PPF anodes and 90 Au-10Pt cathodes (Designated Design No. 2). A total operating time of 296 hours was accumulated.

The first partial stack was tested successfully in February. It consisted of two 6-cell plaques with passive water removal assemblies, mounted on each side of an evaporative cooler assembly. The plaques were connected electrically in series to produce a 12-cell repeating section.

Fifty-two hours of testing were accumulated on this partial stack. During this period, two performance calibrations to the peak power design point of 460 ASF (495 ma/cm²) and a tolerance sweep between 30 and 40 percent KOH were taken. Verification that the evaporative cooler was functioning properly was obtained from the observed change of only 1°F (0.6°C) in water field temperature over the full load range during both performance sweeps. Initial performance of the partial stack was excellent, as shown in Figure 72.

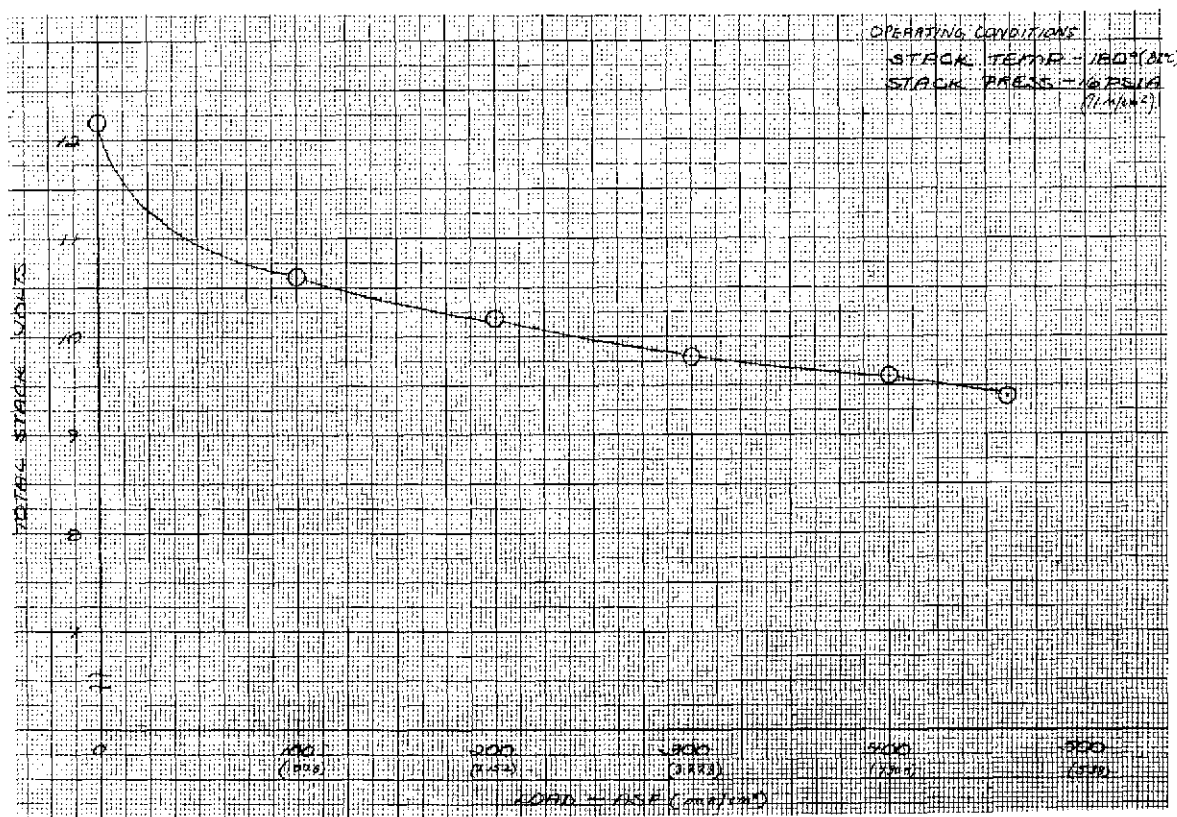


Figure 72 — Partial Stack No. 1 Performance

Individual cell voltages and internal resistances are shown in Figure 73. Cell Nos. 1 and 7 had additional in-plane conductive losses because the external and interplaque connections had not been optimized for maximum conductivity. This is reflected in the lower voltage of these two cells. With the possible exception of Cell No. 6, all of the other cells had excellent performance.

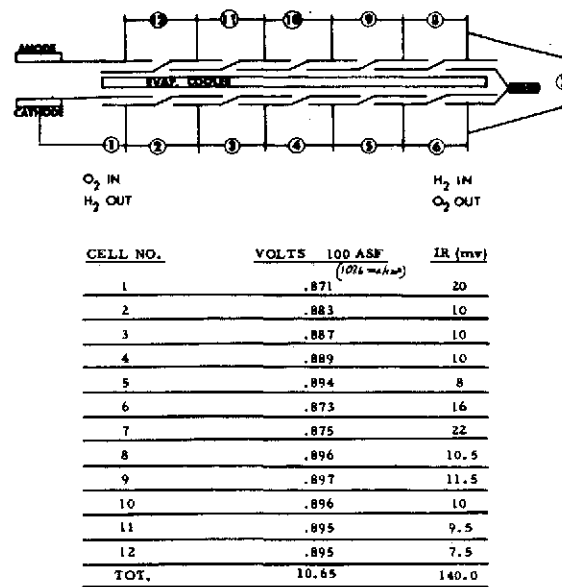


Figure 73 — Partial Stack No. 1 Individual Cell Voltages and Internal Resistances (IR)

Performance of the partial stack was stable during the first 28 hours of operation. At this time, a tolerance excursion was taken. Overall tolerance of the partial stack was good, as shown in Figure 74. Individual tolerance responses of all cells were also good, except that of Cell No. 7, which exhibited a somewhat flatter response.

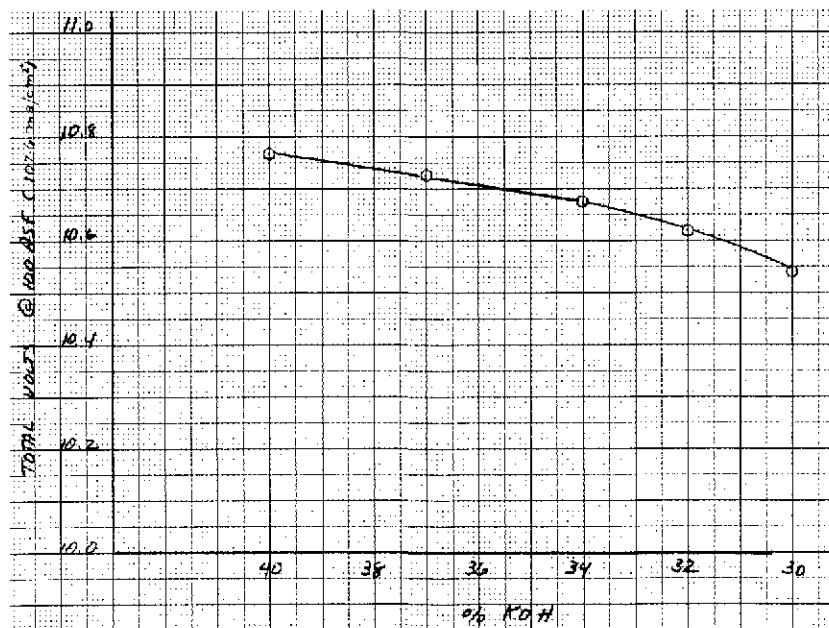


Figure 74 — Partial Stack No. 1 Tolerance Excursion

During the tolerance excursion, the performance level of Cell No. 12 decreased and did not recover. After a weekend shutdown and restart, the voltage of Cell No. 12 was still low. Hydrogen inlet and exit lines were reversed, but no beneficial effect was observed on Cell No. 12. The hydrogen reversal adversely affected Cell No. 1, however, and the test was terminated, with indications of internal heating.

Teardown inspection indicated the internal heating was caused by hydrogen-to-oxygen leakage, most probably at the hydrogen manifold because of insufficient seal pressure. The polypropylene screen extensions from the hydrogen fields into the port areas apparently relaxed considerably during the test, resulting in seal unloading. A trace leak may have been present from the start of the test. The leak would have been aggravated when the hydrogen inlet and exit lines were reversed because of the slightly greater hydrogen pressure at the new inlet. Cell No. 1 ERP was damaged, but all other parts of the stack were in excellent condition.

In summary, the test of Partial Stack No. 1 demonstrated the basic capability of the design of this repeating section. Cell performance, tolerance, and initial stability were good, and the evaporative cooler functioned properly.

Because of the seal problems experienced with the Partial Stack No. 1 running, steps were taken in the succeeding partial stacks to correct the problem. Polypropylene screen extensions into the gas and product water port areas were eliminated and replaced with machined Arylon port inserts of the proper thickness. The machined inserts were not subjected to being compressed at the anticipated loads and, therefore, resulted in maintaining local butyl gasket seal loads. This change was made in both hydrogen and product water porting schemes as shown in Figure 75. It was not changed in the steam porting of the evaporative cooler because the cooler assembly is a bonded assembly which prevents the polypropylene screen extension from being readily replaced. The oxygen ports are directly machined into the oxygen plate.

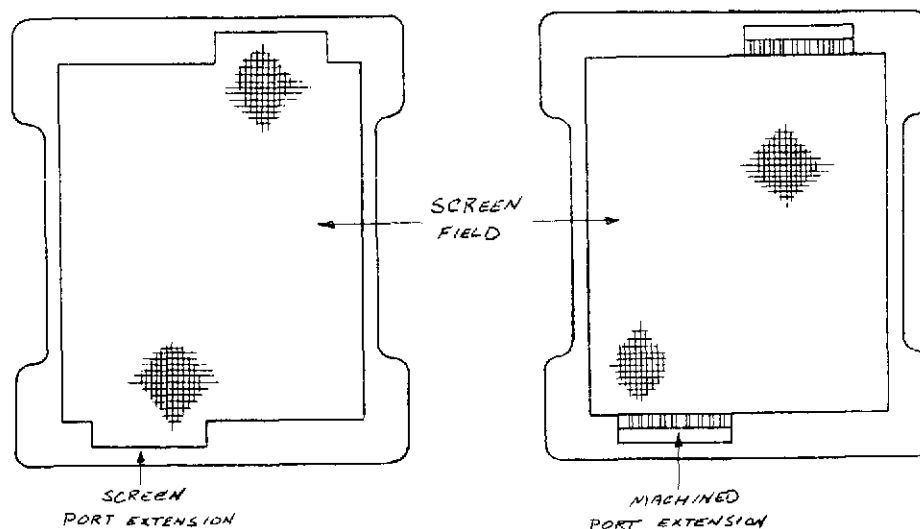


Figure 75 — Port Modifications

The second partial stack was successfully tested in March. Initial performance of Partial Stack No. 2 was good - comparable to, or slightly higher than on Partial Stack No. 1. A log of the individual cell voltages is given in Figure 76. The evaporative cooler functioned properly. Seventy-six hours of testing were accumulated on Partial Stack No. 2.

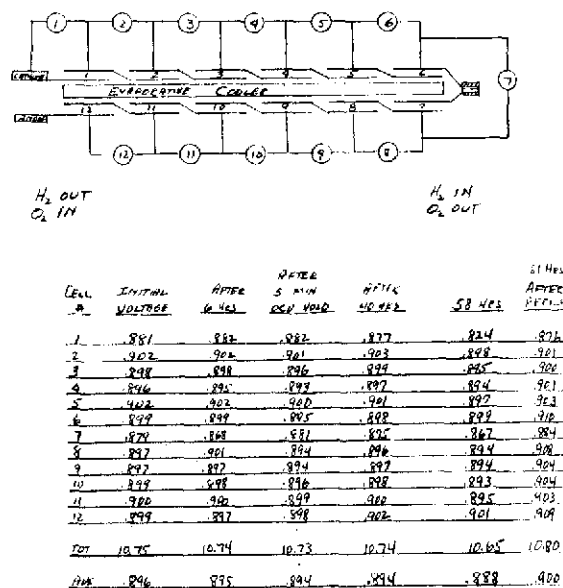


Figure 76 — Partial Stack No. 2 Individual Cell Data

During this time, all of the cells were stable, except for Cells Nos. 1 and 7 (see Figure 76). Both showed signs of decay on the first fill. Cell No. 7 started to decay very early, but could be recovered by going to open circuit for short periods of time. Cell No. 1 was stable for the first 35 hours, but then started to decay. A tolerance excursion indicated that Cells Nos. 1 and 7 had insufficient electrolyte.

A refill of Partial Stack No. 2, at 60 hours load time, resulted in almost complete performance recovery of Cell Nos. 1 and 7, which were also stable for the remainder of the test. Endurance plots for the four end cells are shown in Figure 77. In the case of Partial Stack No. 2, Cell Nos. 6 and 12 were as stable as the interior cells.

During heatup after the refill, a hydrogen to steam field leak developed. The stack was therefore run without the evaporative cooler for 15 hours. Heat removal was accomplished by setting a lower oven temperature. Finally, hydrogen-to-product-water chamber leakage developed, forcing the rig to be shut down.

Teardown inspection revealed that the hydrogen field gasket had slipped into the steam manifold, along the long, interior side of this manifold. This was the only portion of the stack where polypropylene screens were still used in the port areas. The screens are believed

to have relaxed, allowing the hydrogen field gasket to slip. With the slippage of this seal, all seals in the steam manifold plane became unloaded, allowing hydrogen leakage into the steam manifold, and eventually into the product water chamber. No other damage was observed on any of the components.

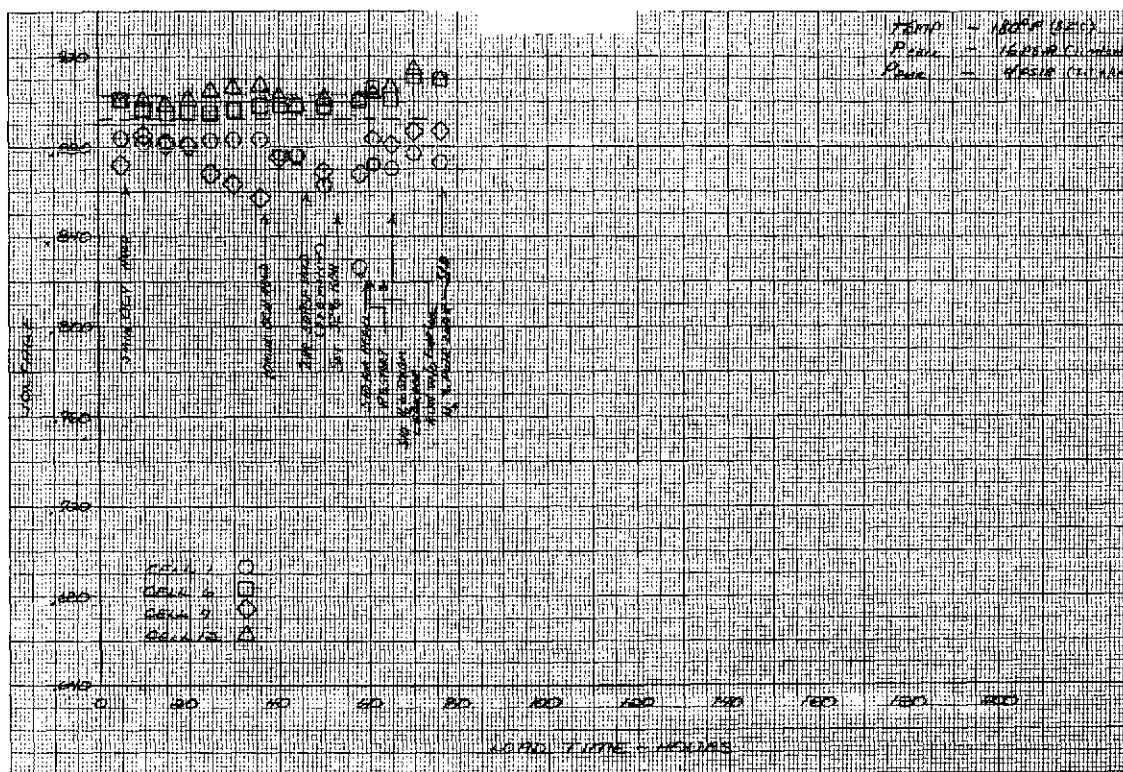
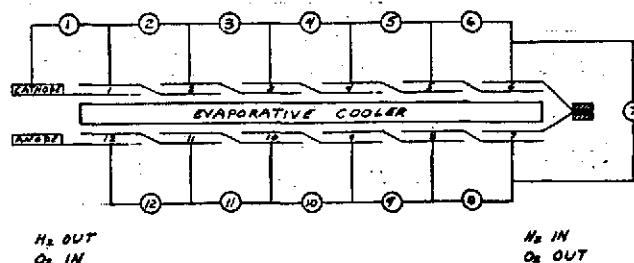


Figure 77 — Performance History - Four End Cells in Partial Stack No. 2

To prevent gasket slippage, it was decided that gaskets in the partial stack tested were to be glued in place. A third stack was assembled of the better components from the first two stacks. The test objectives for this unit were to evaluate glued-in seals for future stacks and continue the investigation of possible decay problems associated with end cells.

Partial Stack No. 3 was operated successfully for 30 hours before shutting down for the weekend. Performance of all cells at the 100 ASF (107.6 ma/cm^2) endurance condition were stable during this time. Cell voltages before the weekend shutdown are shown in Figure 78. As in previous partial stacks, Cell Nos. 1 and 7 were low because of the added screen IR to load take-off points where voltages were read. Cell No. 1, however, was considerably lower than expected. This is attributable to cell damage when failure occurred in Partial Stack No. 1. Performance of both Cell Nos. 1 and 7 were stable during this portion of the test.



CELL #	VOLTAGE @ 100 ASF (107.6 ma/cm ²)
1	0.865
2	0.906
3	0.908
4	0.911
5	0.922
6	0.916
7	0.884
8	0.908
9	0.912
10	0.912
11	0.919
12	0.922
TOT	10.88
AVG	0.901

Figure 78 — Partial Stack No. 3 Performance Data

A performance calibration was conducted before the weekend shutdown. As shown in Figure 79, performance response was good. During the performance calibration, signs of evaporative cooler problems appeared when cooler temperatures rose significantly at high current densities. Cooler temperatures as high as 197°F (92°C) were observed during the calibration. Normal evaporative cooler operation was observed after returning to the 100 ASF (107.6 ma/cm²) endurance condition. Six hours were accumulated at the 100 ASF (107.6 ma/cm²) endurance point after the weekend shutdown, but evaporative cooler problems finally forced shutdown of the rig. Teardown inspection revealed plugged evaporative cooler water ports, apparently from excess glue used to bond the butyl gaskets to the frames. No signs of seal slippage were observed. Thus, the use of glued-in gaskets is an effective method of insuring positive sealing in this partial stack design, although additional care must be taken during assembly to insure that the very small (10 mil) (25.4 x 10⁻⁵m) water ports are not blocked.

The final partial stack built and tested during Phase II included all of the improvements developed during the initial three stack tests. These included the use of: (1) glued in seals, (2) machined Arylon port inserts, including evaporative cooler steam port inserts, and (3) 90 Au-10Pt cathodes and PPF anodes.

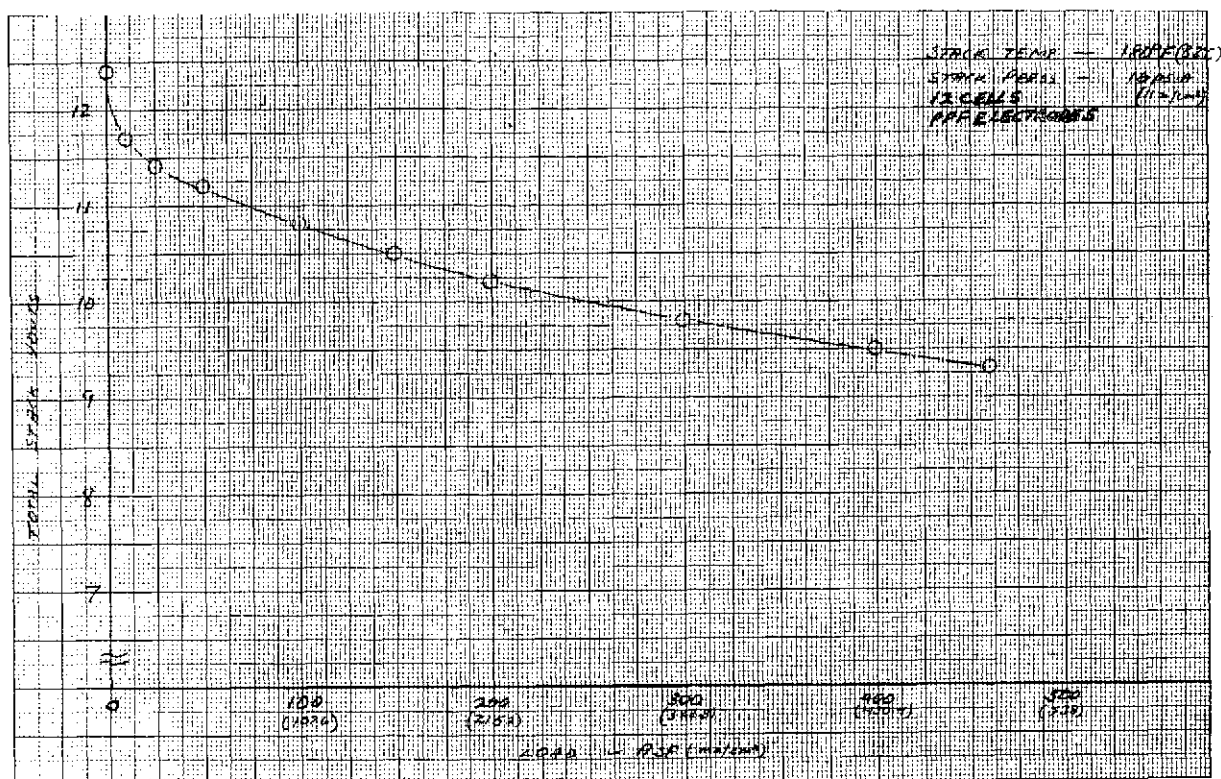


Figure 79 — Partial Stack No. 3 Performance Calibration

Partial Stack No. 4 was tested for about 35 hours with excellent performance, as shown in Figure 80. Cell Nos. 1 and 7, as described previously, showed reduced performance levels because of the additional screen resistance losses in this experimental configuration. The average performance levels of the other cells was better than the full size strip cells, and comparable to the better laboratory cells with Au-10Pt cathodes.

At 35 hours, however, the performance level of both Cell Nos. 1 and 7 began to decay as seen in Figure 81. After 50 hours, it was evident that these particular cells favored wet side conditions, indicating that KOH had been lost to the point where the ERP was no longer able to supply the required KOH to the cell. The following data confirmed this loss of KOH:

KOH Concentration-%	Volts at 100 ASF (107.6 ma/cm ²)		IR at 100 ASF (mv) (107.6 ma/cm ²)	
	Cell No. 1	Cell No. 2	Cell No. 1	Cell No. 7
34	0.865	0.872	40	42
32	0.875	0.892	38	33

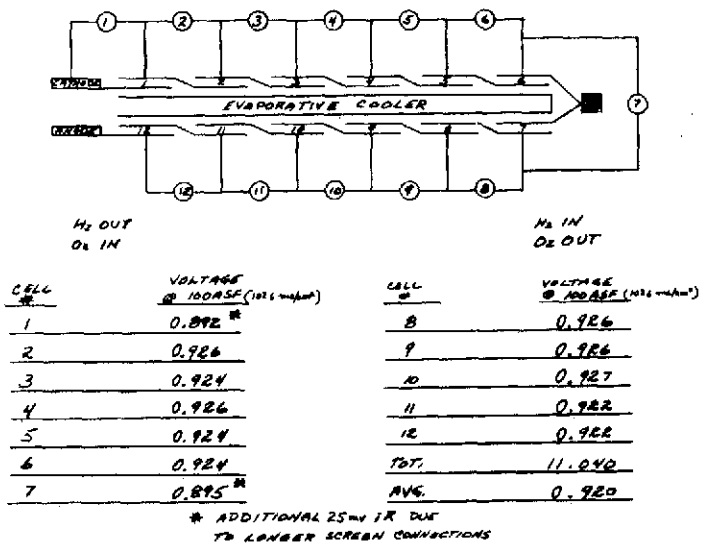


Figure 80 --
Partial Stack No. 4
Performance Data

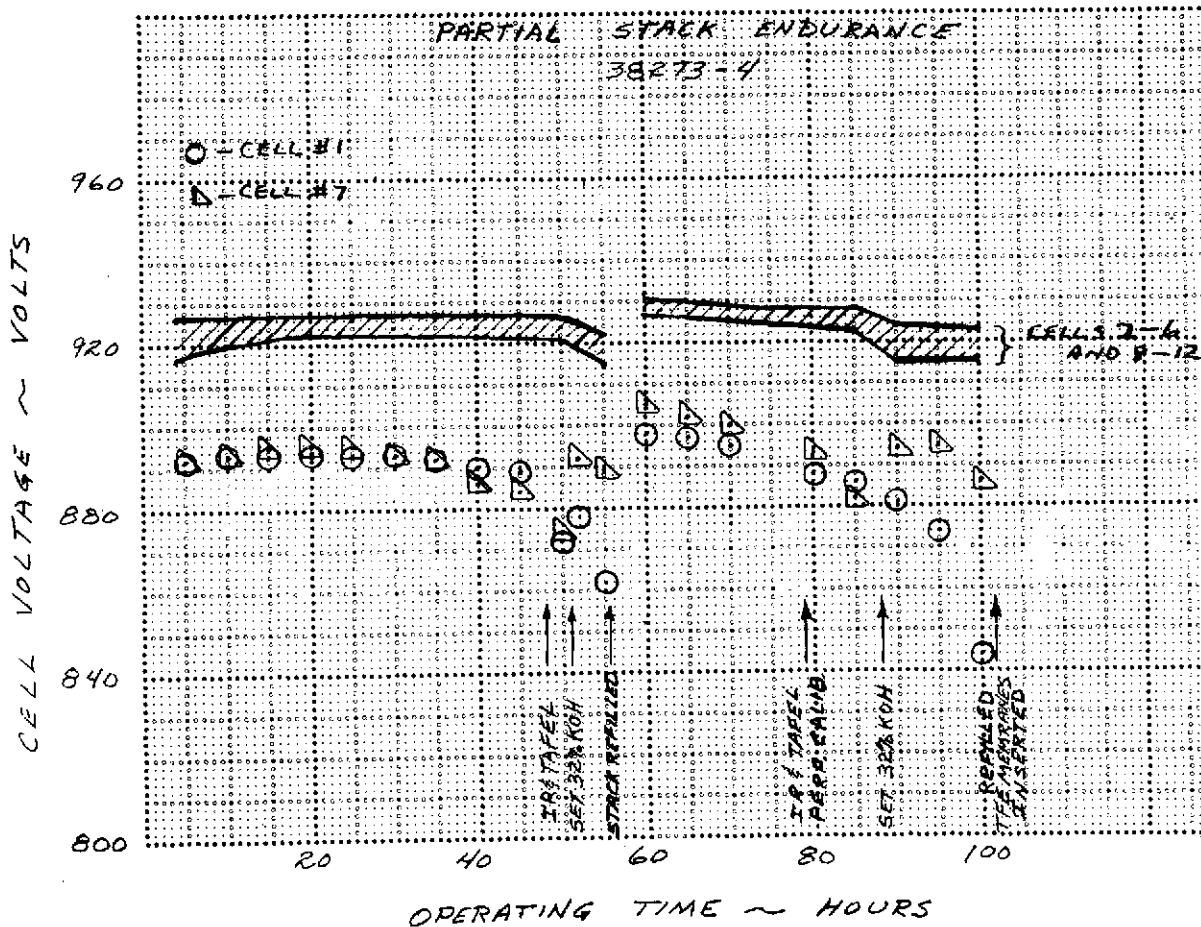


Figure 81 -- Partial Stack No. 4 Endurance Data

A decrease in cell IR's at 32 percent KOH indicates that increased volume, from wetting up to 32 percent KOH, results in wetting of dry areas in the active cell components.

As seen in Figure 81, the good cells also decayed slightly around 50 hours, when the operating conditions were shifted strongly to the wet side in an attempt to stabilize Cell Nos. 1 and 7. After 56 hours, the stack was shut down because of the decreasing voltage of Cell No. 1.

Partial Stack No. 4 was the first partial stack with enough mechanical integrity to permit accurate evaluation of performance trends. When end-cell decay was noted in previous plaques, particularly Plaque No. 5 from Phase I, it was assumed that KOH was lost from the end cells because of a pumping/expulsion mechanism. Although it seemed unlikely that good PPF cathodes, and especially Au-Pt cathodes, would pump, two tests were undertaken to evaluate the pumping/expulsion hypothesis. Since the current and voltage gradients resulting from the cut-back electrode screens could enhance any pumping tendency, a single cell was assembled with similar screens. This cell was operated with oxygen flow set at 12 times consumption to simulate the current collection operation of a plaque end-cell. This cell did not pump even at 1000 ASF (1076.0 ma/cm^2).

As a result of these tests, the pumping/expulsion theory was considered not applicable, and a second hypothesis proposed. If the reactant chambers were not adequately drained, the presence of electrolyte film or droplets could provide a path for ionic conduction, from individual cells to the common water transport plate, or across intercell seals from cell-to-cell. Such a path would give rise to shunt currents, whose magnitude would depend on the position of the cell and the resistance of the ionic path. Since a maximum voltage of 6 volts can exist for each half of the stack (between Cell Nos. 1 and 6 or 7 and 12), this is more than sufficient to cause reactions to occur at each with resultant current flow and concentration changes.

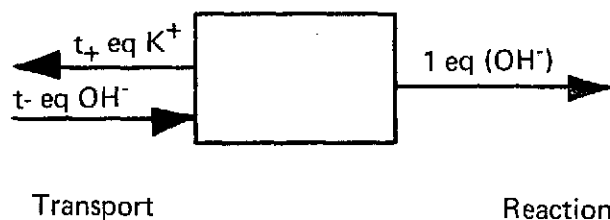
At the high potential end of the stack (Cell Nos. 1 and 7) the following anodic reactions may occur:

- 1) $2 \text{ OH}^- \rightarrow \text{O}_2 + \text{H}_2\text{O} + 2\text{e}^-$
- 2) $\text{H}_2 + 2 \text{ OH}^- \rightarrow 2 \text{ H}_2\text{O} + 2\text{e}^-$
- 3) $\text{M} + n \text{ OH}^- \rightarrow \text{M} (\text{OH})_n + n\text{e}^-$ M = Metal Components

At the other end of the plaque (Cell No. 6 or Cell No. 12) the possible reactions are:

- 4) $2\text{e}^- + \frac{1}{2} \text{ O}_2 + \text{H}_2\text{O} \rightarrow 2 \text{ OH}^-$
- 5) $2 \text{ H}_2\text{O} + 2\text{e}^- \rightarrow 2 \text{ OH}^- + \text{H}_2$

Whichever pair of reactions occur, the result is the same as far as changes in cell concentration are concerned. These changes are shown schematically on the next page.



The sum of the reactions is then the loss of t_+ equivalents of KOH from Cell Nos. 1 or 7 for each equivalent of electrode reaction, and the reverse is true for Cell Nos. 6 or 12. The loss of the KOH from Cell No. 1 would cause a resultant loss of water from the cell since the PWR will maintain a constant vapor pressure and cell concentration. Therefore, a loss of volume will occur in the high potential cells, principally Cell Nos. 1 and 7, and a volume increase should be observed in Cell Nos. 6 and 12. This should result in poor dry side tolerance in Cell No. 1 (7) and poor wet side tolerance in Cell No. 6 (12).

As a first evaluation of this hypothesis, Partial Stack No. 4 was refilled and subjected to a more rigorous draining procedure. The drain schedule was extended to 60 hours, with periodic repositioning and nitrogen purges of all compartments.

After this draining procedure, the stack was restarted and run for 45 hours, as shown in Figure 82. Cell Nos. 1 and 7 were initially restored to their original performance levels, but began to decay within 20 hours. Once again, both cells showed signs of KOH loss. Cell No. 12 indicated a gain in KOH, since its performance level dropped substantially during a wet side excursion. These results appeared to confirm the shunt current theory.

Since the rigorous drain procedure had no beneficial effect on the stability of Cell Nos. 1 and 7 (high voltage end of each plaque), the unit was torn down and visually inspected. No obvious electrolyte bridging was evident from visual inspection. However, it was suspected that electrolyte bridging may have occurred between the plaque and the passive water removal plate assembly. To eliminate this possibility, a porous Teflon membrane, similar to that used in the PWR assembly, was placed between the water transport plate and the hydrogen field polypropylene screen, as shown in Figure 83. As the porous Teflon is hydrophobic, this would eliminate any shunt current paths through the water transport plate if they had previously existed. The stack was run for 25 hours before any significant decay of Cell Nos. 1 and 7 was noted. As in previous testing, a tolerance check indicated a loss of KOH from both of these cells. In addition to the decay of Cell Nos. 1 and 7, Cell No. 12 also showed a considerable loss of performance. The tolerance response of this cell indicated an overfilled condition. Figure 82 shows the performance of Cell Nos. 1 and 7 for the entire test program.

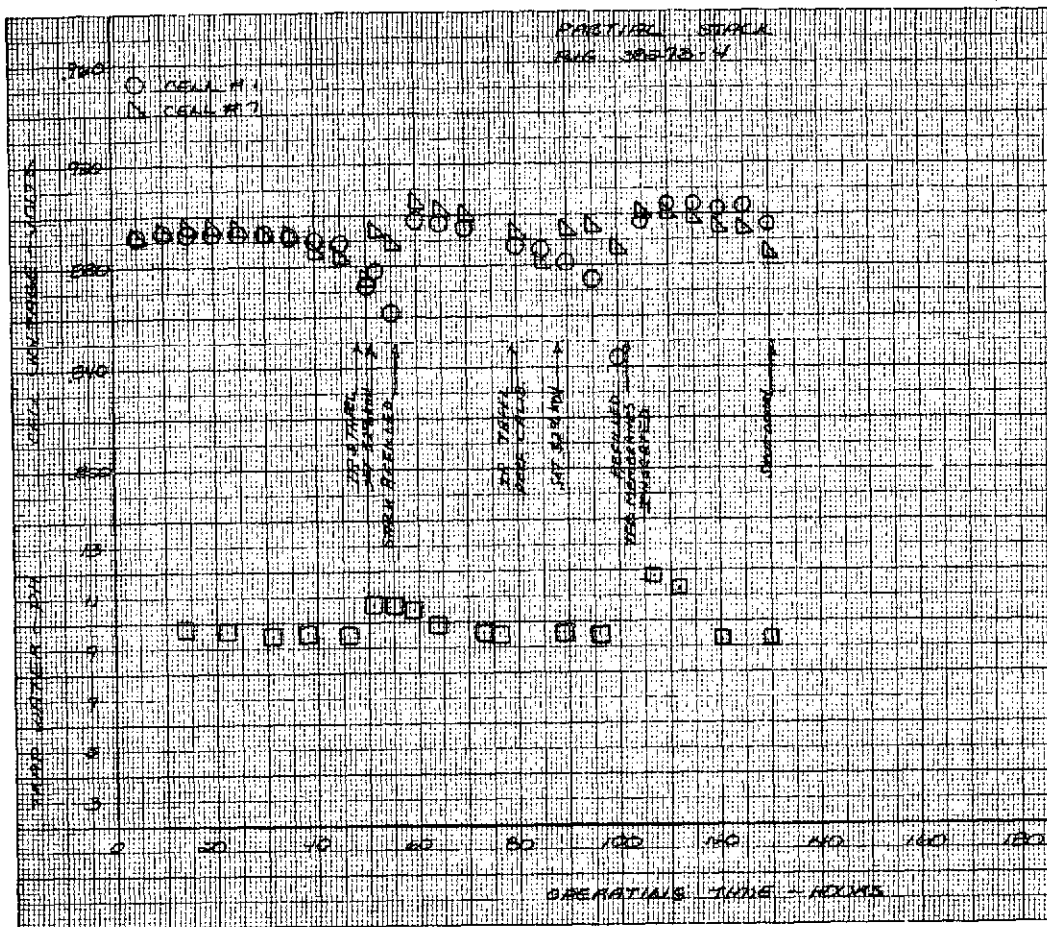


Figure 82 — Performance of Cell Nos. 1 and 7 in Partial Stack No. 4

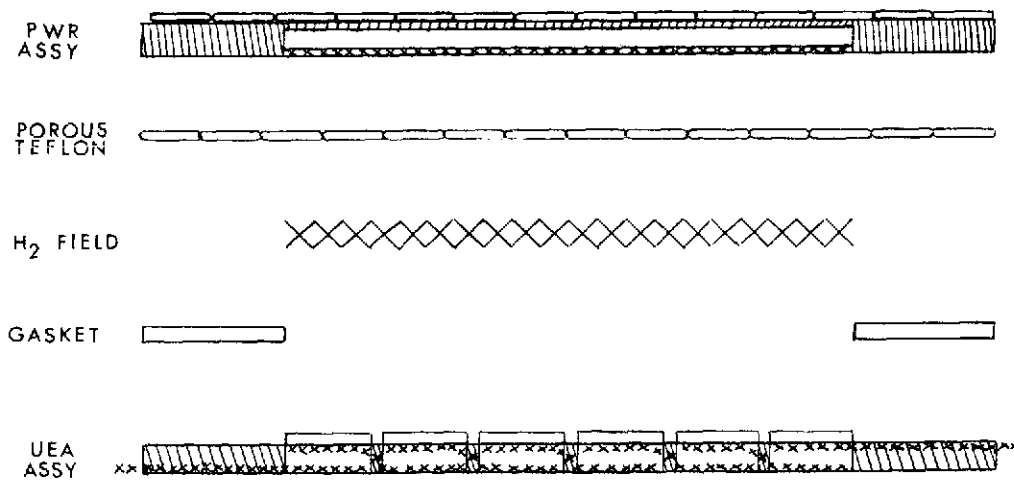


Figure 83 — Porous TFE between PWR and Hydrogen Field Screen

To further explore the problem, it was proposed that shunt currents could be measured by inerting the stack, applying a voltage from an external power supply across the cell plaques, and measuring the resulting current. Current flow occurring prior to the application of 1.2 volts per cell (voltage required for electrolysis) would be attributed to electrolyte shunts. The results of this measurement is shown in Figure 84. The resistance for both plaques was determined to be on the order of 290 ohms. Based on the operating stack voltage, the shunt current should be 30 to 40 ma during operation at normal voltages. Knowing the electrolyte volumes in each cell and its ERP, it was calculated based on the analysis presented above that enough KOH could be lost from the high potential end cells to result in significant cell degradation after about 50 hours at operating current, and that decay could be seen as early as 25 to 30 hours after startup. This quantity of KOH could be sufficiently great to be determined by weighing. As a result a test to determine KOH transfer directly was set up.

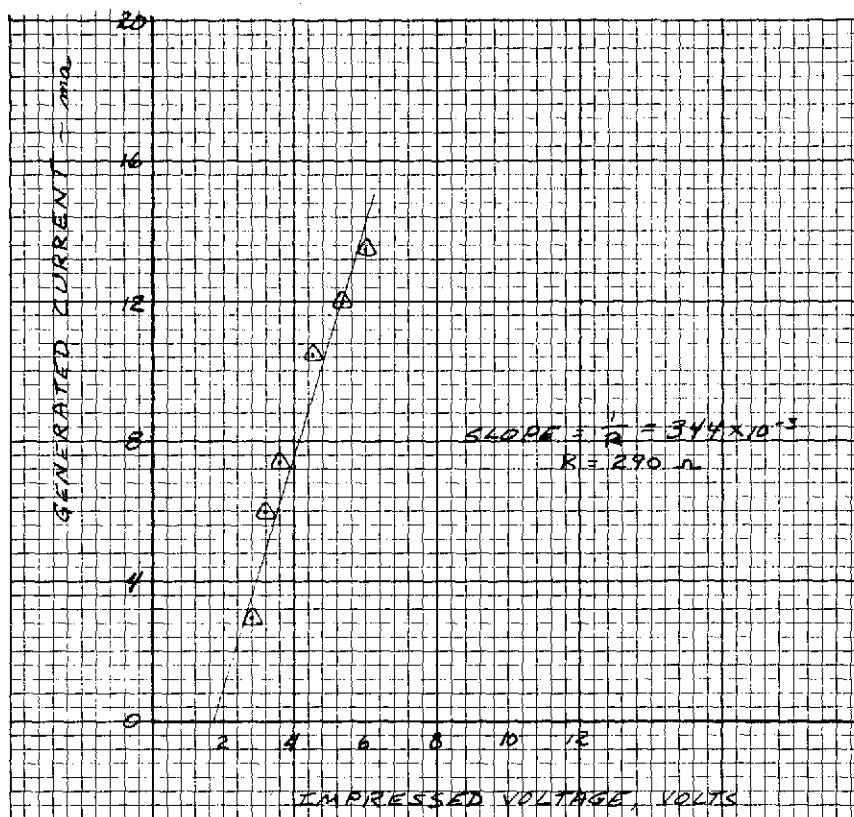


Figure 84 — Impressed Voltage vs. Current for Partial Stack No. 4

A potential of 5 volts was imposed across a six-cell plaque placed in an inert atmosphere. The intent was to weigh the end-cell electrolyte reservoir plates at intervals to determine if electrolyte transfer was occurring. Since the electrolyte reservoir plates were bonded on the anode side and could not readily be weighed, an ERP was placed on each of the end-cell cathodes.

These ERP's were easily weighed and replaced. The end-cell ERP's were partially filled with 3 grams of 27 percent KOH. At 5 volts imposed potential, current drain was about 11 ma, and after 140 hours, 0.4 grams had been lost from the high voltage end ERP and 0.2 grams gained at the low voltage end. These results definitely indicated that electrolyte was transferred from one end of the plaque to the other and most probably through films on the intercell strips or through the intercell strip itself.

Review of the plaque design indicated the problem might be cured by a change in the cell design and the fabrication technique used. The electrolyte reservoir plates are attached to the anode side of the plaque using epoxy impregnated asbestos strips in the intercell strip area. In so doing, the electrode screens are also completely covered, sealing the 3/8 inch (0.15 cm) intercell strip width between the anode screens. However, on the cathode side, no similar strip was used, thus leaving a very small gap between electrode screens as is shown in Figure 85. This gap between screens was as small as 20 to 30 mils (50.8 to 76.2 $\times 10^{-5}$ m) in some areas, providing an area for low resistance electrolyte film bridges to form after filling. One solution would be to add the epoxy impregnated matrix to the intercell strip on the cathode side. Another solution is to add a strip of non-wetting material such as Teflon in the intercell area on each side. The non-wetting material would prevent formation of electrolyte films on the intercell strips preventing shunt currents and transfer of electrolyte.

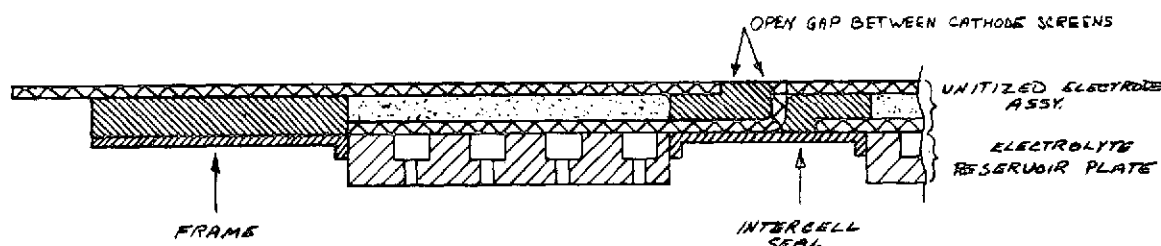


Figure 85 — Plaque Cross Section

To determine whether non-wetting materials would prevent formation of electrolyte films and to ensure no electrolyte was wicking through the frame itself, bench tests of a simulated plaque were conducted. The test setup is shown in Figure 86. The test article is a two cell plaque with a 3/8 inch (0.95 cm) intercell strip (comparable to six-cell plaque intercell strips). Reservoirs of water and electrolyte were provided for each cell in the two-cell test piece. Liquid was allowed to wick up the matrix of each cell, and a voltage comparable to plaque voltage was imposed across the unit. The water side was analyzed for total potassium ion content at varying intervals. With a non-wetted intercell strip, there was no evidence of potassium ion transfer, indicating that electrolyte wicking across the non-wetting strip or through the frame is not a problem at the test conditions. All testing was performed at room temperature in an inert atmosphere. This approach will be a candidate solution to overcome shunt currents in future plaque designs.

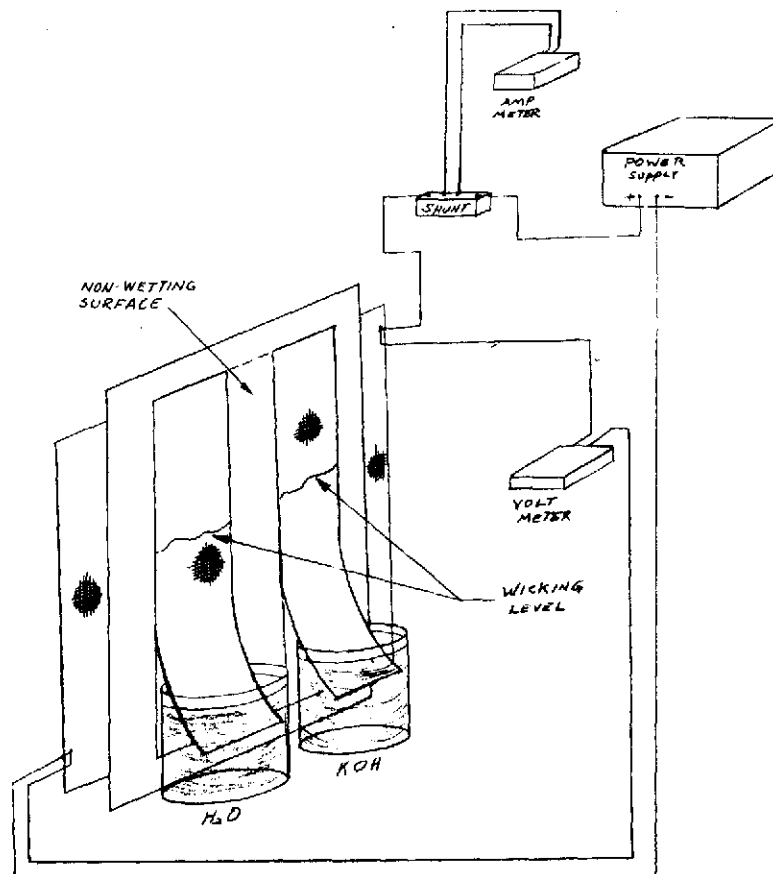


Figure 86 — Shunt Current Test Setup

APPENDIX A
ENGINEERING MODEL SYSTEM

APPENDIX A

Introduction

One of the tasks of Phase I was to perform a System Design to define an Engineering Model System which met NASA's goals for an advanced power-plant. This design was used to establish individual technology goals and to guide the technology tasks. The EMS description in this appendix is the description that was presented in the Phase I Final Report (November 1972).

1.0 Selection of System Concept

The NASA design and performance objectives shown in Table A-1 were the basis of the Engineering Model System design. Several of these objectives significantly influenced the selection of the system concept for the Engineering Model System; these are tabulated and discussed below.

TABLE A-1
Engineering Model Fuel Cell System Design
and Performance Objectives

<u>Life</u>	
Operating Duration	10,000 hours, or longer, with refurbishment
<u>Structural</u>	
Weight	20 lb/kw (9.1 Kg/kw), sustained power
Volume	0.5 ft ³ /kw (14,200 cc/kw), sustained power
<u>Reactants</u>	
Fuel and Oxidant	Hydrogen and oxygen, nominal propulsion grade
Specific Consumption	0.7 lb/kw-hr (0.32 Kg/kw-hr)
Source Pressure	35 psia (24.2 n/cm ²) minimum; 1000 psia (690 n/cm ²) maximum
<u>Thermal</u>	
Nominal power heat rejection mode	Spacecraft surface radiators
Peak power heat rejection mode	Other than radiators; open cycle, steam venting water boiling, etc.
Coolant outlet to radiators	Maximum temperature consistent with life and performance goals
<u>Electrical</u>	
Voltage	117 volts with minimum to maximum variation over the operating power range of $\pm 5\%$ from 20% to 100% of sustained power
Power	7 kw sustained. 21 kw (min.) peak, short duration (2 hrs) at a minimum of 100 volts
Ancillary Component Power	Minimized
Degradation	5 μ V/hr/Cell (Maximum), at sustained steady-state loads.
<u>General</u>	
Start-stop cycles	400
Components and controls	Minimum number, high reliability, no rotating parts.
Maintainability	Field maintenance and repair capability.
Check-out Validation	In place (installed) checkout capability
Start-up time	Instantaneous.
90% of Sustained Power	5 minutes
Shutdown Time	Instantaneous
By-Product Water	Discharged water shall meet potability requirements of MSC Specification C-21B. Water discharge parameters shall be conducive to transporting and storage.

Fuel Cell Power Section Weight

System Weight - 20 lbs/kw (9.1 Kg/kw) of sustained power

Power Output - 1.4 kw minimum, 7 kw sustained, 21 kw peak
(2 Hours)

Voltage Band - 117 plus 5 percent, minus 14.5 percent over the
full power range

These requirements call for a power system weighing less than 140 lbs (63.5 Kg). Based on the 2 hour peak power rating, the system specific weight is 6.7 lbs (2.99 Kg) per kw. To achieve the voltage regulation band requires a large total cell area in the fuel cell power system. For the EMS, approximately 60 ft² (5.57 m²) of total cell area is required. Achieving the system weight goals with a full cell power section of this total cell area requires that the power section weight be reduced by a factor of 3 compared to the current state-of-the-art. This requires that the thickness of all power section components be significantly reduced and that low density, polymer-type materials be used.

Waste Heat and Product Water Removal Subsystems

Peak power heat rejection - Other than radiators: open cycle.

Components and controls - Minimum number, high reliability, no rotating parts.

The open cycle operating requirement of 21 kw for two hours led to the selection of direct evaporation cooling of the cells and the use of passive water removal for both the closed and open cycle modes of operation. Combining the product water removal and waste heat removal subsystems into a common loop resulted in a considerable simplification of the controls required for a powerplant capable of both open and closed cycle modes of operation. The objective of no rotating components and minimizing parasite power was met by using the pressure energy of the reactants to drive the fluid circulators.

Cell Operating Conditions

Reactant pressure - 35 psia (24.2 n/cm²) minimum

Operating life - 10,000 hours

Specific reactant consumption - 0.7 lbs/kw-hr (0.32 Kg/kw).

A low cell operating pressure was dictated by the minimum reactant, supply pressure specified. Allowing for component pressure losses, particularly the reactant driven coolant pump, resulted in the selection of a cell operating pressure of 16 psia (11.04 n/cm²). Life considerations, balanced by the guidelines calling maximum coolant temperature to the spacecraft radiator, resulted in the selection of an operating temperature of 180° F (82.2° C). These operating conditions, particularly the low reactant pressure, result in unavoidable performance penalties. For example, a cell operating at a reactant pressure of 16 psia (11.04 n/cm²) has a voltage output approximately 40 milli-volts less than if it were operated at 60 psia (41.4 n/cm²) - the reactant pressure commonly used in other systems. This results in a specific reactant consumption for the 16 psia (11.0 n/cm²) cell of 0.83 lb/kw-hr (0.376 Kg/kw-hr) vs. 0.80 lb/kw-hr (0.363 Kg/kw-hr) for the 60 psia (41.4 n/cm²) case. Thus the low operating pressure is in conflict with the ambitious specific reactant consumption objective.

Cell Packaging

Voltage - 117 nominal

This voltage level requires that approximately 130 cells be connected in series electrically. To meet other requirements discussed above, the selected power section design includes plastic structural components and passive water removal assemblies as a part of each cell. These non-conducting components prevent cell-to-cell current transfer directly through the stack (current flow perpendicular to the cell plane) requiring the use of edge current transfer. Edge current transfer coupled with the large number of cells required to provide the output voltage level resulted in selecting a planar multi-cell stack method for packaging the cells. This cell packaging concept results in lower structural weight and offers flexibility in meeting different system voltage and power levels.

2.0 System Operation

The system selected to meet the EMS performance and operational objectives is shown in Figure A-1. Reactants are supplied to the power section by demand type pressure regulator valves. These valves assure that the hydrogen and oxygen pressures in the stack are kept equal and at 16 psia (11.04 n/cm²) over the full range of reactant flows associated with the power being supplied by the power section. Pressure energy in the hydrogen is being used to derive a positive displacement water pump.

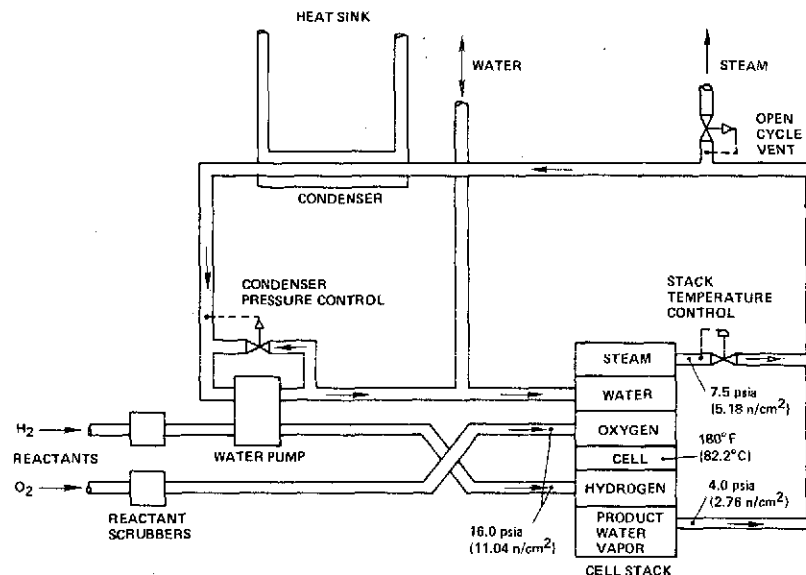


Figure A-1 - Simplified EMS Schematic

Waste heat is removed from the stack by evaporative coolers located next to each cell. By controlling the cooler pressure at 7.5 psia (5.17 n/cm^2), the cell temperature is maintained at the associated water vapor temperature of $180^\circ F$ ($82.2^\circ C$). Product water is removed by the passive water removal method. Product water from the cell diffuses through a gas-tight water transport plate and evaporates into a 4 psia (2.76 n/cm^2) cavity. Control of this pressure maintains the proper water balance in the cells over the full EMS operating range.

The combined water vapor streams from the evaporative coolers and the product water vapor cavities flow in a common line to the condenser where the latent heat of evaporation is transferred to the spacecraft coolant. The condensate flows to the water pump. A bypass valve on this pump modulates flow to maintain the condenser pressure, and hence, the pressure in the product water vapor cavities. A portion of the pump discharge water returns to the power section for cooling. Excess water is removed from the loop and supplied to the spacecraft potable water storage system. Whenever the vapor loop heat load is greater than the spacecraft cooling loop capacity, the pressure in the vapor loop rises. This opens the vapor loop vent valve which automatically transfers the system from closed cycle to open cycle operation. During open cycle operation, water for cooling is drawn from the spacecraft water storage system.

3.0 Power Section Components Description

The basic components of the Engineering Model System Power Section are the cell, the passive water removal water transport plate, and the evaporative cooler. The schematic diagram of the evaporative cooler is shown in Figure A-2. The cooling water side is located adjacent to the cell oxygen passages. The water cavity is separated from the steam cavity by a porous hydrophobic membrane. The non-wetting characteristic of this membrane prevents water flow but allows vapor and gases to flow through it. Waste heat from the cells flows through the oxygen water plate causing the water to evaporate. This water vapor passes through the membrane pores and into the vapor cavity. As shown in the system schematic, Figure A-1, make-up water is automatically supplied to the water cavity by a pressure regulator which maintains a constant water to steam overpressure during all operating modes. By controlling the pressure in the steam cavity, the corresponding evaporation temperature is set, maintaining the cells at a constant operating temperature.

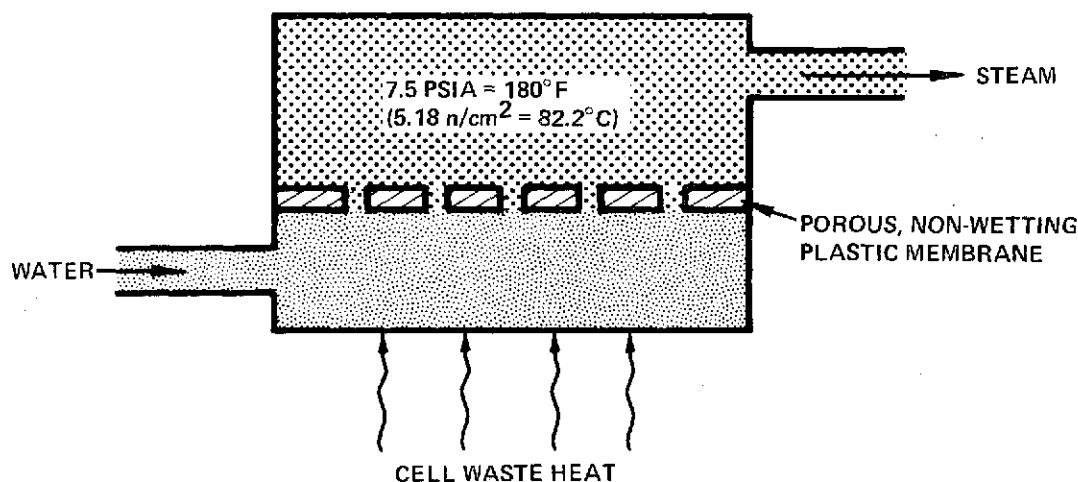


Figure A-5 - Evaporative Cooler

The water transport plate is shown schematically in Figure A-3. Its functions are to : 1) allow diffusion of product water from the cell to the vapor cavity, and 2) seal the 16 psia (11.04 n/cm²) hydrogen from the 4 psia (2.76 n/cm²) water vapor. The water transport plate consists of an electrolyte filled matrix similar to that used in the fuel cell. This fine pore structure provides a gas seal and offers a low resistance path for diffusion of the product water. The electrolyte reservoir for the matrix is provided to accommodate the electrolyte volume changes that occur during different operating conditions assuring that the matrix

is always filled with electrolyte. To prevent electrolyte loss from the water transport plate under transient conditions an electrolyte barrier is provided. This barrier consists of a fine pore hydrophobic membrane similar to that used in the evaporative cooler. It allows vapor to pass through its pores while retaining electrolyte. The 4 psia (2.76 n/cm²) water vapor pressure combined with the 180°F (82.2 °C) cell temperature results in a nominal 34 percent electrolyte concentration in the cell.

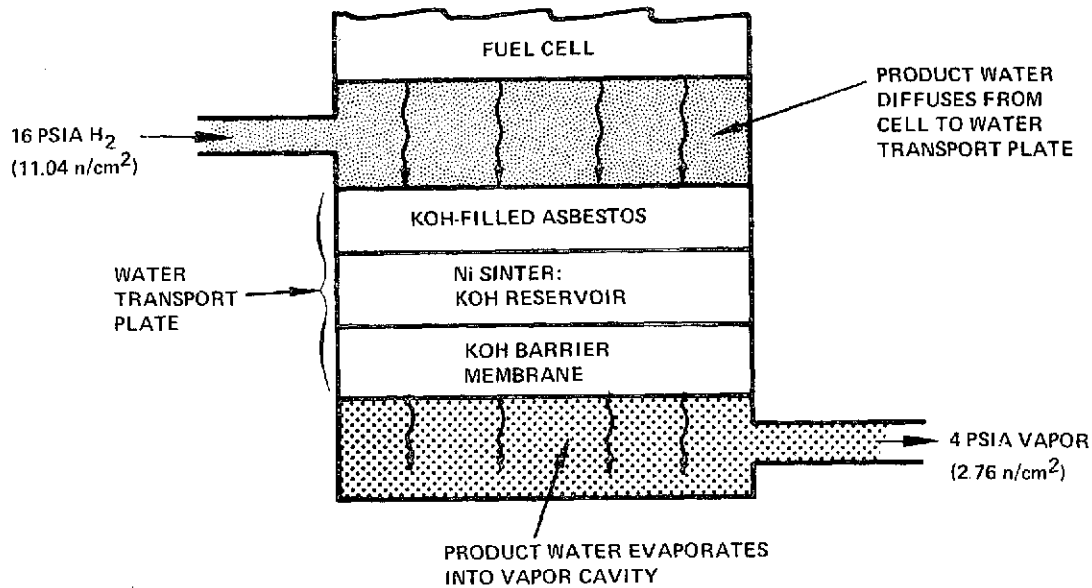


Figure A-3 - Passive Water Removal

4.0 Ancillary Components Description

The components used in the reactant supply and the water vapor loop are the coupled reactant regulator, absolute and differential pressure regulators, the reactant driven water pump and the condenser. Control of the reactant supply to the stack is provided by a coupled hydrogen and oxygen pressure regulator. The coupled reactant regulator maintains the hydrogen and oxygen pressures equally and at the desired level over the full range of system supply pressure. The regulator consists of hydrogen and oxygen regulators coupled by an aneroid bellows sense assembly.

Pressure regulating valves used in the vapor loop are: 1) the evaporative cooler steam pressure regulator, 2) the cooling water to steam differential pressure regulator; 3) the open cycle vapor vent regulator, and 4) the condenser pressure control regulator. Three of these regulators are of the absolute pressure sensing type set to maintain a given pressure within

a small control band. The water supply regulator is similar except that it is referenced to the cooling steam to maintain a set differential pressure.

The reactant driven pump is a diaphragm type using spool valves to control the reactant flow, and check valves to control water flow through the pump. Reactant pressure operating on one side of the diaphragms forces the assembly in one direction; when it comes to the end of its travel a pilot valve reverses the reactant flow direction and the pump travels in the opposite direction. The pump requires no electrical power or controls. The only moving parts are the oscillating diaphragms and spool valves. Prototypes of reactant driven coolant pumps have been tested under other programs.

The condenser which converts the product water vapor and the steam from the evaporative coolers to liquid water is a plate-fin type heat exchanger cooled by the spacecraft coolant system.

5.0 Power Section Sizing

The basic cell voltage-current density characteristic is used to size the power section. The engineering model system cell performance model is based on high power density cell test data generated over wide ranges of pressure, temperature and current densities: pressures of 15 to 60 psia (10.3 to 42.4 n/cm²), temperatures of 150 to 250°F (65.5 to 121.1 °C), and current densities to 3000 ASF (3228 ma/cm²). To prepare an EMS cell performance model, these data were corrected to the 16 psia (11.04 n/cm²), 180°F (82.2°C) EMS cell operating conditions. The estimated performance at EMS operating conditions is shown in Figure A-4, along with data from the high power density cells. The figure indicates the high activity and low polarization losses of the high power density cell and shows the lower level of performance which results from the 16 psia (11.04 n/cm²) operating pressure. The EMS performance model used in system studies is shown in Figure A-5. The initial performance line is the same as the cell performance at the 16 psia (11.04 n/cm²), 180°F (82.2°C) temperature shown in Figure A-4 with allowances made for edge current conduction losses. The performance line labeled "minimum" is the result of a 21 mV allowance for performance decay over the 10,000 hour operating duration. These initial and minimum performance models were used in a series of trade studies to select the total cell stack area and the number of series connected cells for the EMS stack.

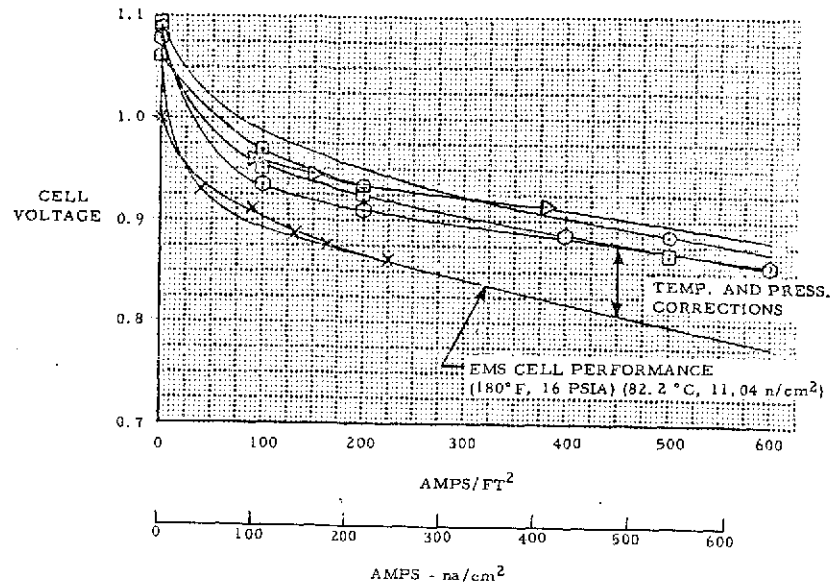


Figure A-4 - High Power Density Cell Performance

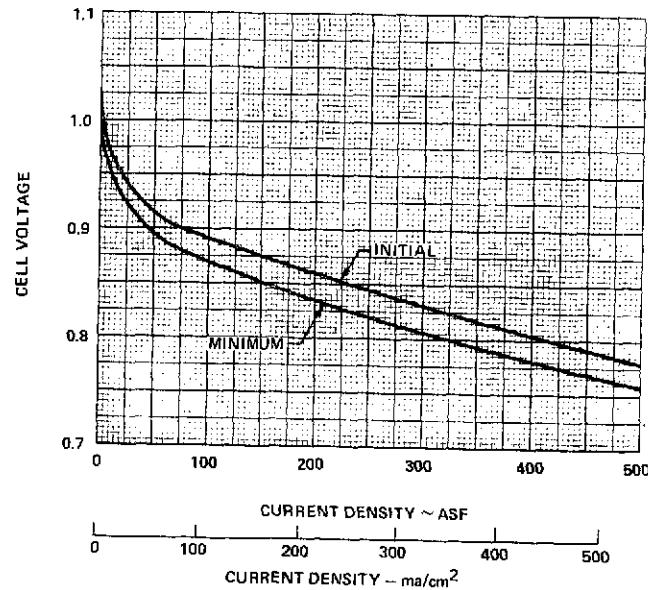


Figure A-5 - EMS Cell Performance Model

The EMS power section contains 60 ft² (5.57 m²) of the total cell area divided into 132 equivalent series connected cells. The selection of this total cell area resulted from studies of reactant consumption, voltage regulation, and powerplant weight. Increased cell area results in lower reactant consumption and improved voltage regulation at the expense of increased powerplant weight. The mechanics of sizing a power

section involve an iterative procedure to select the total cell area and number of series connected cells that satisfies; a) minimum voltage requirement at maximum power output and maximum cell performance, and b) maximum voltage requirement at minimum power output and maximum cell performance. EMS sizing required that an additional condition be satisfied since minimum powerplant voltages are specified at two power levels (100 volts at 21 kw and 117 minus 5 percent volts at 7 kw).

The selected stack size of 60 ft^2 (5.57 m^2) of total cell area with 132 equivalent cells in series was selected based on the following:

- . It satisfies minimum voltage requirements at both 21 and 7 kw with margin.
- . Although it does not meet the maximum voltage requirements, a voltage limiter can be used at low power. Additional studies showed this to be the most weight-effective solution to meeting this type of voltage regulation specification.
- . The resulting voltage vs power characteristics are considered adequate since actual Space Shuttle voltage requirements are not fully defined and the primary purpose of the preliminary design EMS is to provide guidelines for the technology advancement tasks of this program.
- . 132 equivalent cells in series provides greater flexibility in cell and plaque arrangement, i.e., the number of cells per plaque and the series-parallel electrical arrangement of plaques within the stack.

6.0 Power Section Description

Introduction

The EMS stack components are the cells, arranged in plaques, the passive water removal water transport plates and the evaporative coolers. To meet weight goals, plastic structural components were selected. The use of non-electrically conducting stack components - the water transport plate, the evaporative cooler, and the non-metallic reactant and the coolant flow distribution plates - requires the use of edge current flow to connect the cells in series electrically. Edge current transfer requires different approaches for minimizing resistance losses than those used in stacks where current flows through the stack,

perpendicular to the cell plane. Both electrical connection arrangements have resistance losses associated with transferring current from cell to cell. Losses in the through stack arrangement are due to the resistance of the metal plates used to form the reactant and coolant flow cavities and the contact resistance between adjacent plates and the cell. In the edge current transfer arrangement, the losses are due to the resistance of electrode substrate. They are minimized by selecting low-width cells i.e. - rectangular cells of high aspect ratio.

There is significant flexibility in selecting cell geometry for edge current transfer stacks. This is illustrated by the results of a parametric weight study. Figure A-6 shows the trade-off which can be made between minimizing cell frame weight and the weight of the cell current conductor. The square cell geometry minimizes the amount of perimeter per unit area thus keeping the weight of the frames to a minimum. Because of the longer path for current flow, the cross sectional area of the current carrying cell member, the electrode screen, must be increased to keep resistance losses low. A high aspect ratio cell geometry reduces conductor weight at the expense of higher frame weight. Figure A-7 shows how an arbitrarily selected area of $0.25 \text{ ft}^2 (232 \text{ cm}^2)$ - could be packaged into 4 different geometry cells varying from square ($6 \times 6 \text{ inches}$) ($15.2 \times 15.2 \text{ cm}$) to a high aspect ratio rectangle ($2 \times 18 \text{ inches}$) ($5.1 \times 45.6 \text{ cm}$). In each design, the fluid manifold area was kept the same as was the IR loss from tab to tab. The latter was accomplished by changing the wire diameter of the current transfer screens which are a part of each electrode.

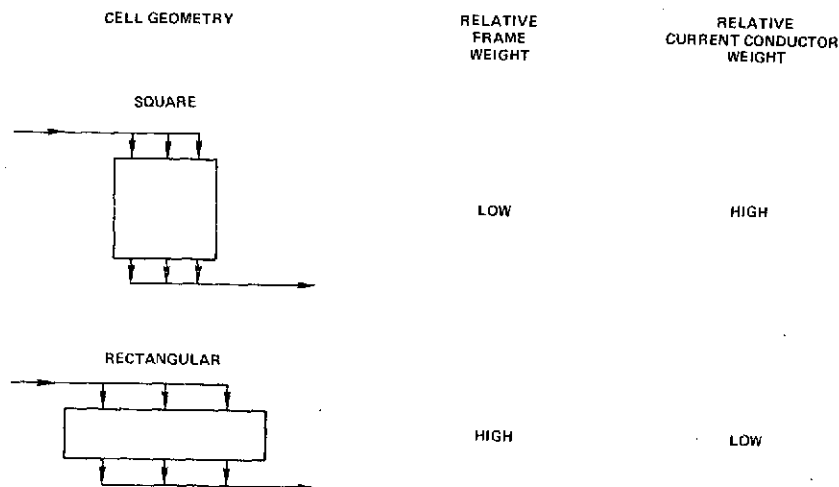


Figure A-6 - Design Options for Edge Current Transfer Cells

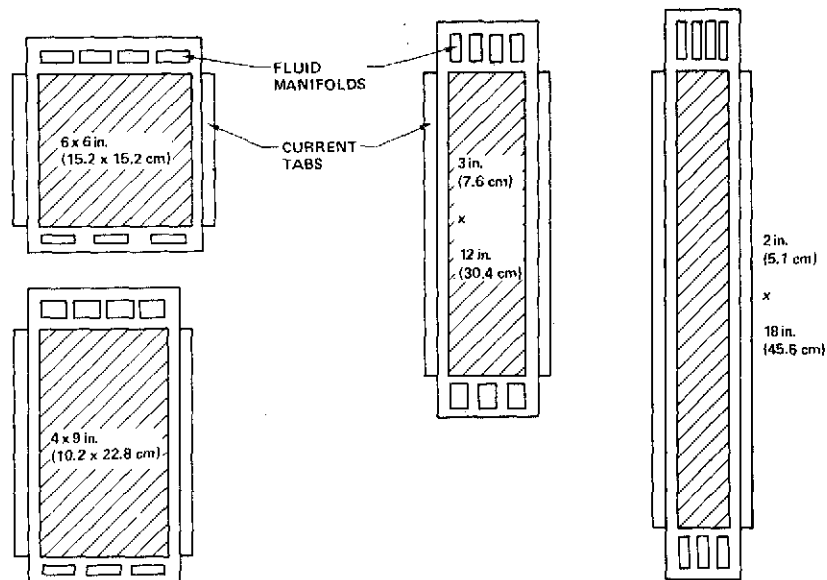


Figure A-7 - Various Cell Geometries for Edge Current Transfer Cells
36 in²(232 cm²) Active Area

The relatively poor frame weight per unit area of the rectangular cells can be improved by grouping cells into a plaque. A plaque is defined as an edge current transfer cell assembly with the number of cells per plaque ranging from one to as many as desired. The improved packaging efficiency available with the plaque is illustrated in Figure A-8. This figure shows that as additional cells are arranged in plaque form, the overall assembly approaches a square format. Economics of scale also result since the perimeter to area ratio for large total cell area is less than for small areas. Both effects result in a lower frame weight per unit of active area for plaques which contain several cells.

The results of this parametric weight study are shown in Figure A-9. Plaque weight per unit cell area is shown as a function of the number of cells of a given geometry packaged into a plaque. The weight is made up of the cell elements, the edge frame and the intercell seals. The cell elements included are the electrodes with their current conducting screens, the matrices, and the non-metallic electrolyte reservoir plate. Other power section components which are a constant weight per unit area are not included. The figure shows the narrower cells result in significant weight savings. Further weight reduction results from grouping a number of cells together in a plaque. It is seen that considerable latitude is available to select cell geometry and a number of cells per plaque to achieve a balance between minimum weight and practical package size.

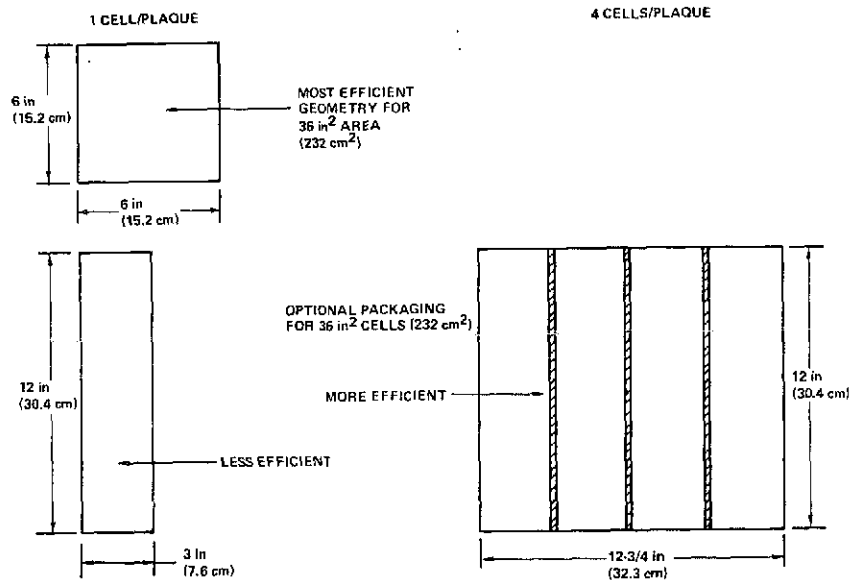


Figure A-8 - Effect of Geometry on Frame Weight

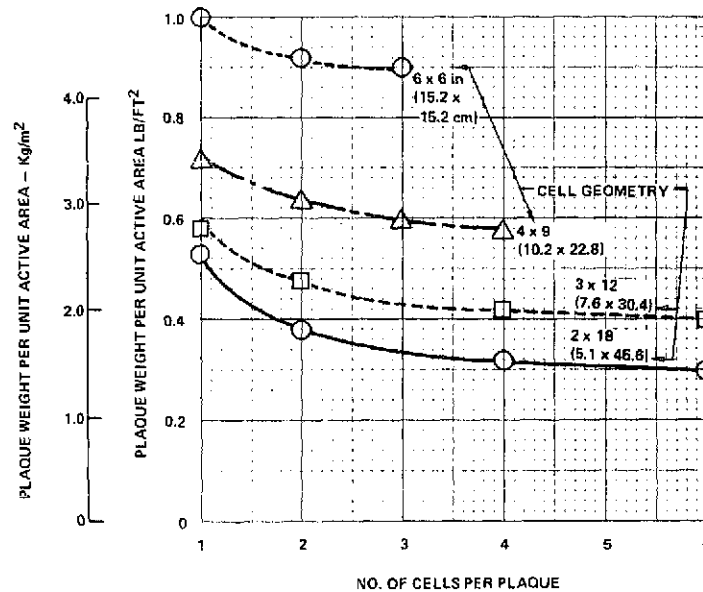


Figure A-9 - Effect of Cell Geometry and No. of Cells per Plaque on Plaque Weight

With lightweight cell construction, which the plaque concept makes possible, it is feasible to use a number of smaller cells rather than a single large one. This can improve reliability of a power system by allowing arrangement of the total cell stack area into a group of electrically parallel sub-stacks. For example, if a powerplant requires a total cell area of 30 ft²

(2.79 m²) and 30 series connected cells to meet system voltage-power requirements, the power section could consist of either one stack of 1.0 ft²(929 cm²) cells, two parallel connected stacks each using 0.5 ft²(464 cm²) cells, or four parallel connected stacks containing 0.25 ft²(232 cm²) cells.

EMS Cell/Plaque Arrangement

The approach described above was taken in packaging the 60 ft²(5.57 m²) of total cell area and the 132 series connected cells required for the EMS power section. The total cell area was arranged so the total powerplant current flows in four parallel paths. A malfunction which could cause a loss in performance in any one path would result in the cells in the other three paths picking up more of the load thus minimizing the net effect on the system.

The series - parallel electrical arrangement of the EMS power section is based on the use of six cells per plaque. Four plaques are connected in parallel to form a substack; thus each plaque carries one-fourth of the total system current. 22 substacks are connected in series to form the complete stack of 132 series connected cells.

The plaques with their water transport plates, the evaporative coolers and product water vapor spacers are grouped together as shown in Figure A-10 to form the complete power section. The power section contains 88 plaques 44 evaporative coolers and 45 product water vapor spacers, housed between end plates.

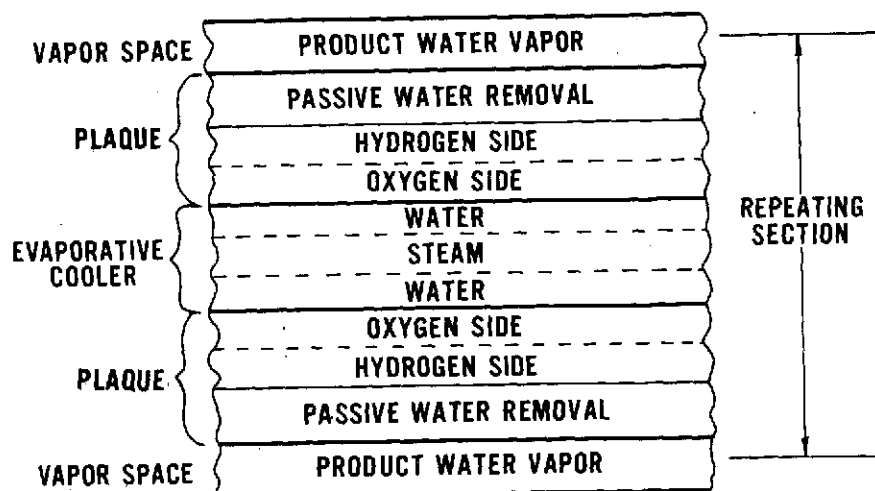


Figure A-10 - EMS Stack Concept

Plaque Description

The EMS baseline plaque is an integral assembly containing six cells, intercell seals, and manifolds molded into a plastic edge frame. A plan view of the plaque is shown in Figure A-11. Each cell is 12 inches (30.4 cm) long and 1.37 inches (3.48 cm) wide (16.4 in² (106 cm²) active area). Total active area per plaque is 0.68 ft² (630 ft²). The six cells are electrically connected in series by connecting the anode of one cell to the cathode of the adjacent cell through the intercell seal. These seals are 0.25 inches (0.64 cm) wide and insulate adjacent cells from each other, physically support the various cell elements, and isolate the reactant gases from each other at the cell edges. The 0.50 inch (1.27 cm) wide edge frame assembly is molded around the cells and fluid manifolds to provide a unitized plaque assembly.

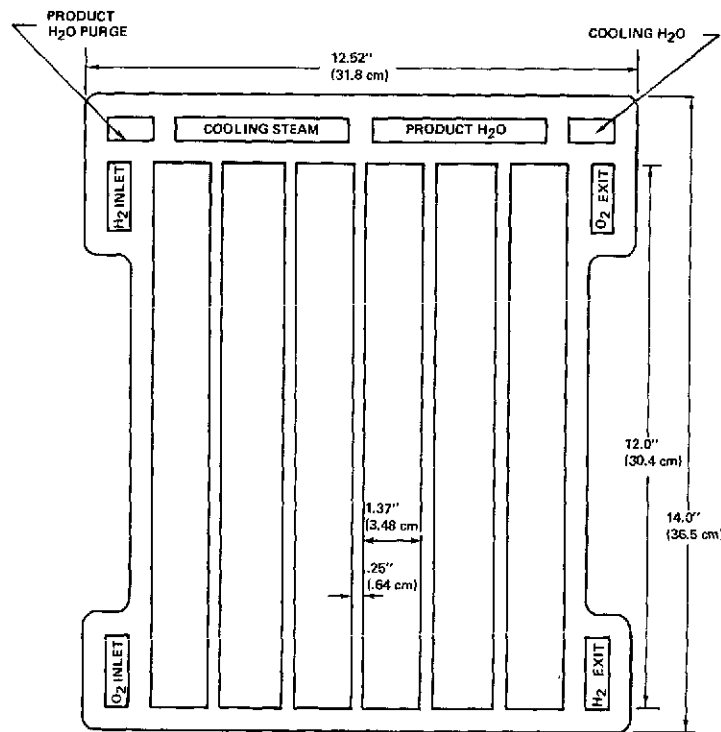


Figure A-11 - EMS Baseline Plaque Plan Form

Fluid distribution is handled in two steps: manifolds and ports. Manifolds are fluid flow passages perpendicular to the plaque plane; they provide flow to or from the ports. They are formed when the openings in the edge frames of adjacent stack components are aligned during final stack assembly. As shown by the plaque plan form, there are eight manifolds within the EMS stack; two for reactant gas inlet, two for reactant gas

purge, one for cooling water inlet, one for cooling water vapor exit, one for product water vapor exit, and one for product water vapor purge.

Ports are fluid flow passages parallel to the plaque plane. They provide the flow path between the manifolds and cells. Manifolds and ports are sized to provide low pressure drops consistent with uniform plaque-to-plaque flow distribution.

The reactant purge manifolds are larger than required by flow considerations and were chosen to make the plaque plan form symmetrical. A cross-sectional view of the plaque and the associated water transport plate is shown in Figure A-12. The figure shows the relationship of the component ports, their thicknesses and materials. The total thickness of the cell is 44 mils(1.12 mm) and the water transport plate 24 mils(0.61 mm). A 10 mil(0.25 mm) hydrogen flow spacer is used resulting in a total passive water removal fuel cell assembly thickness of 78 mils(2.01 mm).

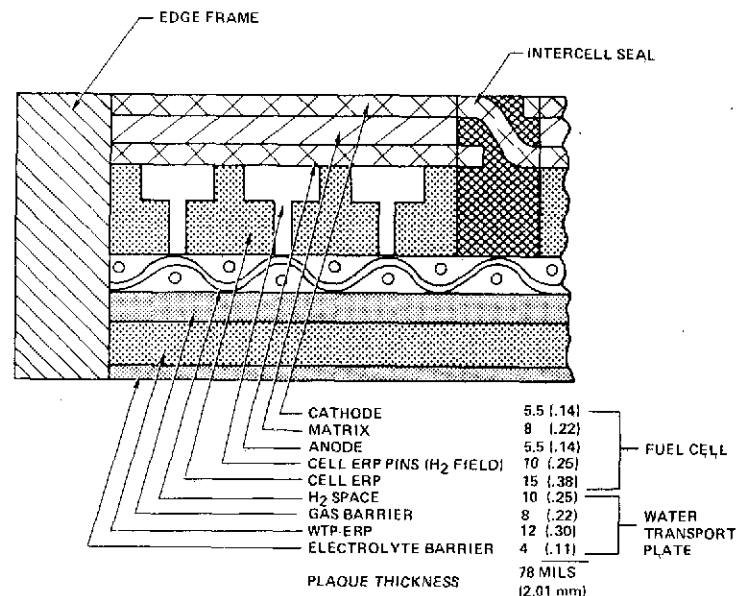


Figure A-12 - Cross Sectional View of Plaque

Evaporative Cooler Description

Waste heat is removed by the evaporation of water in cooler assemblies positioned between the cathodes of adjacent plaques. Total thickness of the cooler assembly is 98 mils(2.5 mm) and the planform size is the same as the plaques. Evaporative stack cooling has two distinct advantages: 1) it maintains an isothermal plaque, which in combination

with passive product water removal maintains uniform cell electrolyte concentration; and 2) vapor is easily vented overboard for open cycle heat removal if the spacecraft radiator is inoperative or is reduced in capacity.

Figure A-13 shows the cooler cross section. It contains a water vapor spacer between the supported hydrophobic separators enclosed by two coolant plates. With this design, a liquid water reservoir is maintained adjacent to the plaque on either side of the cooler assuring good thermal control of both plaques. One vapor chamber accommodates the steam emanating from both separators. The supported hydrophobic separators, the vapor spacer and the coolant plates are bonded together at their edges to form a unitized assembly. These edge frames, as with the plaque edge frames, contain the sealing surface area, manifolds and ports.

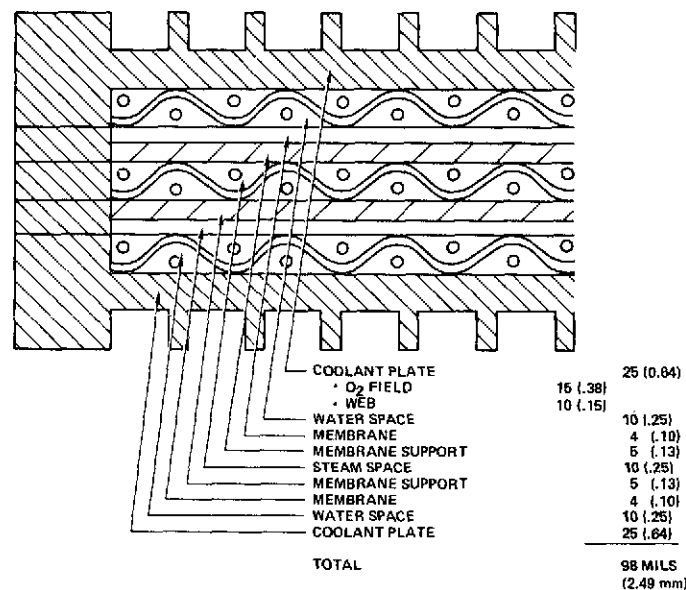


Figure A-13 - Cooler Cross Section

The coolant plates are unfilled plastic and serve three basic functions: 1) they form oxygen and liquid cooling water flow fields, 2) they provide the heat conduction path from the cells to the cooling water, and 3) they provide the desired electrical insulation between adjacent back-to-back plaques. A pin and bar pattern on one side of the plate covers 50 percent of the plaque area and forms the 0.015 inch(0.38 mm) deep oxygen flow field while the other side contains space for a 0.010 inch(0.25 mm) thick plastic mesh to form the water flow field. Waste heat is conducted from the cells through the pin and bars of the oxygen flow field and the plate

web to the cooling water. Hydrophobic separators are 4 mil(0.10 mm) porous sheets of TFE with the structural integrity to withstand approximately 5 psi(3.45 n/cm²) pressure differential. They are porous to allow the passage of steam from the liquid surface to the lower pressure vapor chamber. The hydrophobic properties of the separator also allow the passage of any non-condensable gases that might be present in the water reservoir. A plastic cloth, considerably more porous than the separator but of a finer weave than the steam and water flow field mesh, is bonded to the separator for mechanical support.

The vapor chamber spacer is a 10 mil(0.15 mm) thick plastic mesh which separates and supports the hydrophobic separators and forms the steam flow channel. It is configured to allow vapor parallel to the plane of the hydrophobic separators.

All flow passages are sized to provide proper distribution and low pressure drops as discussed in a later section. All elements within the cooler assembly are designed to transmit a lateral compressive load sufficient to ensure good thermal contact between the cooler and adjacent plaques.

Power Section Size and Weight

Envelope dimensions of the EMS baseline stack are 13.5 x 14 x 11.6 inches (34.3 x 35.5 x 29.5 cm). The estimated total weight is 60.1 lbs (27.2 Kg). Details of this total weight are shown in Table A-II.

TABLE A-II

EMS Power Section Weight

<u>Assembly</u>	<u>Weight, lb(Kg)</u>
Fuel Cell	30.6(13.9)
Water Transport Plate	13.8(6.2)
Evaporative Cooler	<u>15.7(7.1)</u>
TOTAL	60.1(27.2)

The EMS section weight estimates are based on the cell, water transport plate and evaporative cooler configuration defined above.

These configurations differ from those of the passive water removal cells and plaques and evaporative coolers tested during the program in only the heights of certain flow fields. The thickness dimensions of the fuel cell, water transport plate and oxygen/water coolant plate configurations tested were equal to or less than those of the baseline design as a review of Section IV will show. Flow field spacers larger than baseline dimensions were used where procurement lead time and cost did not permit their use in the first phase of this program. Commercially available screens were used for the hydrogen, product water vapor and cooling steam flow fields. Analysis indicates that flow fields with better pressure drop-flow characteristics would allow reduced thicknesses for these ports.

7.0 Flow Studies

Plaque and stack fluid flow studies were conducted to define flow passage configurations which have proper flow distribution and pressure drop characteristics. The flow passages for hydrogen, oxygen, cooling steam and product water vapor were studied. The criteria used for design of the reactant gas flow passages were: 1) the gases cannot back-flow during purge, and 2) the system must be able to purge to atmospheric pressure.

Flow trade-off studies were conducted to define manifold, port and field configurations. The basic field flow configuration selected was that of sweep flow along the cell/plaque length with the hydrogen and oxygen flowing in opposite directions. Counterflow of reactant gas minimizes the possibility of inlet drying and the development of concentration gradients along the cell length.

A computer analysis was used to predict plaque and stack pressure drops and to predict the degree of flow maldistribution caused by manufacturing tolerances on flow passage dimensions. A plus or minus 2 mil(0.05 mm) manufacturing variation on all critical dimensions was assumed. Table A-III presents the flow study results which show adequate purging from cell-to-cell within a plaque and from plaque-to-plaque within the stack.

The oxygen flow study summarized here was completed before it was determined that the oxygen recycle loop would be a part of the EMS. The additional plaque exit flow and the increased oxygen flow field height, of 0.015 inches(0.38 mm), will result in improved oxygen flow distribution.

TABLE A-III
Flow Study Results

	<u>Hydrogen</u>	<u>Oxygen</u>
Flow through exit manifold during purge, % of consumption flow	25	50
Stack inlet flow - lb/hr (Kg/hr)	2.96(1.46)	28.2(13.9)
<u>Minimum cell channel purge</u> - %	53	34
<u>Average cell channel purge</u>		
Pressure drop of field and secondary - psi (n/cm ²) manifolds	0.15 (0.10)	0.26 (0.18)
<u>Minimum plaque purge</u> - %	41	9
<u>Average plaque purge</u>		
Stack pressure drop - psi(n/cm ²)	0.29(0.20)	0.48(0.33)

Computerized finite difference analyses were conducted to predict the pressure drops for the cooling steam and product water vapor manifolds, ports, and fields. These pressure drops are particularly important since they are factors that must be considered in determining cell electrolyte concentration. Steam and product water vapor pressure drops vary with flow (power output) and are one of the causes of cell electrolyte concentration variations. To minimize this concentration variation, cooling steam flow and product water vapor flow paths are parallel to each other. Temperature-water vapor pressure-concentration characteristics of potassium hydroxide electrolyte are such that concentration variations are minimized if water pressure variations (cell product water vapor pressure) are accompanied by corresponding temperature variations (cell cooling steam pressure).

Ports for the two flow fields are extensions of the field so that the mesh fills the area between the fields and the manifolds. The flow passage model used for the cooling steam and product water vapor is the same as that used for the reactants except for the port configuration. At the time these studies were conducted, design data for flow in the plane

of meshes (as occurs in the steam and product water vapor fields) were unavailable, nor was mesh of the desired size available for design information testing. Therefore, flow through the meshes were approximated as flow in small channels through successive expansions and contractions.

8.0 Electrolyte Reservoir Plate Requirements

For effective operation, certain elements within the cell (anode, matrix, and cathode) and the water transport plate (gas barrier) must always be full of electrolyte. Electrolyte reservoir plates (ERP's) are included in the plaque assembly to accommodate changes in electrolyte volume during system operation. The actual required thickness of the ERP's is a function of; a) the range of electrolyte concentration variations, b) the useable capacity of the ERP, and c) the volume of electrolyte contained within the plaque elements that must remain full.

Electrolyte concentration variations during system operation results primarily from; a) cell temperature and water vapor pressure variations caused by droop and hysteresis characteristics of the system pressure regulators, b) variations in the temperature gradient from the cell to the evaporative cooler, and c) temperature and water vapor pressure variations caused by variations in pressure drops of cooling steam and product water vapor through flow fields, manifolds, and ports. The net result is that cell temperature and water vapor pressure, therefore electrolyte concentration, varies with power output, from plaque-to-plaque within the stack, and with location in each plaque. The magnitude of cell temperature and pressure variations due to each of the above causes has been discussed above. The electrolyte concentration variation was estimated for the end and exit of the 1st and 88th plaques to establish the maximum variation. The largest electrolyte concentration variation due to all the above affects was found to be 28 to 42 weight/percent KOH. This results in a maximum-to-minimum electrolyte volume ratio of 1.7 during normal EMS operation.

Fill and expulsion data of sintered nickel plates used as ERP's in high power density cells along with a plate porosity of 70 percent were used in determining the thickness of the ERP's. Calculations based on these considerations were conducted to determine that the ERP web thicknesses required for normal EMS operation are 11.4 mils (0.29 mm) for the cell and 9.0 mils (0.23 mm) for the water transport plate.

Two other effects require consideration in the selection of ERP thickness; electrolyte carbonation and bootstrap startup. Since one of the goals of the technology advancement program is the development of highly compatible

cell structures, no allowance for structure produced carbonation is provided. In addition, it is envisioned that the EMS will incorporate reactant purifiers to limit the CO_2 content of the incoming reactants to 0.25 ppm. With this CO_2 ingestion rate, the conversion of KOH to K_2CO_3 will be less than 5 percent² over the 10,000 hour EMS life. This low level of carbonate formation has a negligible effect on ERP thickness.

During a bootstrap start, the water removal system remains inoperative until the cell stack has attained a temperature approaching normal operation levels. The product water formed during this interval remains in the cell as a liquid. ERP thickness, in addition to that necessary for the concentration variations during normal operation discussed above, must be provided to store the startup product water. The amount of startup product water (therefore required startup ERP thickness) depends primarily on the stack heat capacity and whether or not the EMS energy output is returned to the stack via electric heaters. Total ERP thickness for bootstrap startup was estimated to be 3 to 7 mils (0.08 to 0.18 mm) depending on the amount of EMS energy output being returned to the stack. As a result, a 5 mil (0.13 mm) bootstrap startup allowance was proportioned between the cell and WTP ERP's. The resulting total ERP web thickness for the cell is 15 mils (0.38 mm) and 12 mils (0.30 mm) for the water transport plate.

9.0 System Controls

EMS stack operating conditions are maintained by monitoring and controlling two parameters - stack temperature and product water vapor pressure. In the preliminary design EMS, each of these parameters is measured and controlled independent of the other. As explained earlier, stack temperature is indirectly controlled by a pressure regulator at the cooling steam exit. Product water vapor pressure is controlled during closed cycle operation by a pressure regulator that varies the condensate pump bypass flow rate. During open cycle operation, it is controlled by varying steam flow to space through the vent regulator.

Two alternates to this concept have been identified and can reduce the electrolyte volume variation caused by control valve tolerance and cell-to-cooler temperature gradient. These would, therefore, reduce the required ERP thicknesses as discussed earlier, resulting in reduced stack weight. The alternates are; a) direct control of stack temperature and b) coupling of the two controls. Direct stack temperature control eliminates the cell temperature variation caused by cell-cooler temperature gradients (up to 20°F (11.1°C) at peak point for the preliminary design EMS). With coupled controls, variations in one parameter (caused

by control tolerance, indirect sensing, etc.) is accompanied by a corresponding change in the other parameter. In this way, cell electrolyte concentration can be maintained within a narrower range even though cell temperature and water vapor pressure change.

To study the effects of these alternate control concepts, only electrolyte volume variations caused by control tolerances and cell-to-cell temperature gradients were considered. Figure A-14 summarizes the results of this study and shows that a significant reduction in electrolyte volume ratio is realized if either or both alternates are used. The figure shows the relationship between electrolyte volume ratio and temperature variation (tolerance of the cell temperature control due to droop and hysteresis) for both the independent and coupled controls. Curves are included for direct and indirect cell temperature sensing (0 and 20°F (0 and 11.1°C) cell-to-cooler temperature gradient). A ± 0.2 psia (0.14 n/cm²) tolerance on product water vapor pressure control is included. To illustrate the effects, consider a 3°F (1.7°C) temperature variation (this is consistent with cooling steam pressure variation of about 0.5 psia (0.35 n/cm²) as included in the preliminary design EMS). The figure shows that electrolyte volume variation can be decreased from 1.73 to 1.11 if both alternates are included. Considering the alternates individually, the reduction is to 1.52 for direct cell temperatures sensing only and to 1.27 for coupled controls only.

Based on this study it is clear that these two alternates should be considered further in future phases of the program. The benefits can be utilized in either of two ways; a) to reduce stack weight since a lower electrolyte volume ratio means ERP thickness is required, or b) to relax tolerance requirements on control components with minimum impact on stack weight.

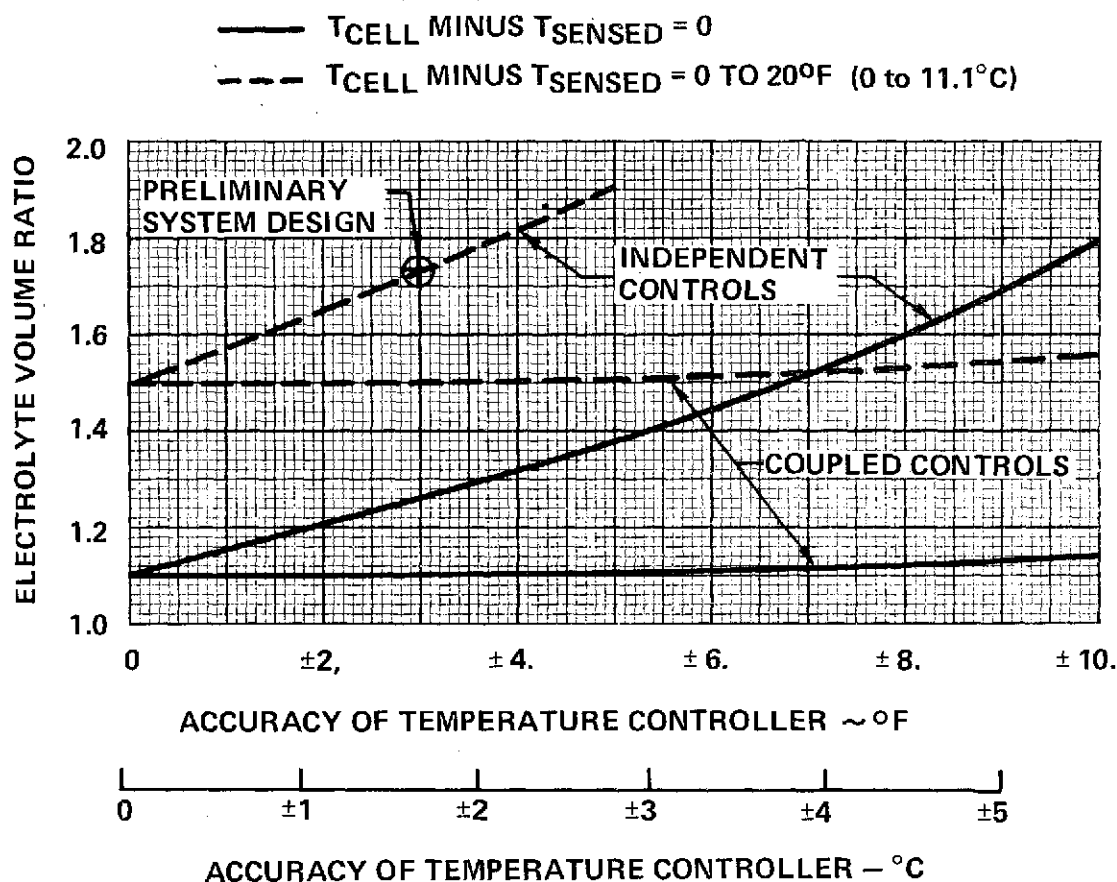


Figure A-14 - Results of Alternate Control Concepts Study

10.0 System Characteristics

System Operation

A complete schematic of the EMS is shown in Figure A-15. The functions of the additional components, not shown in the simplified schematic of Figure A-1, are described below:

Oxygen Recycle - An ejector and recycle line are provided to accomplish:

- 1) Better distribution of inerts to increase time between purges and
- 2) Humidification of the oxygen to preclude any possibility of inlet drying.

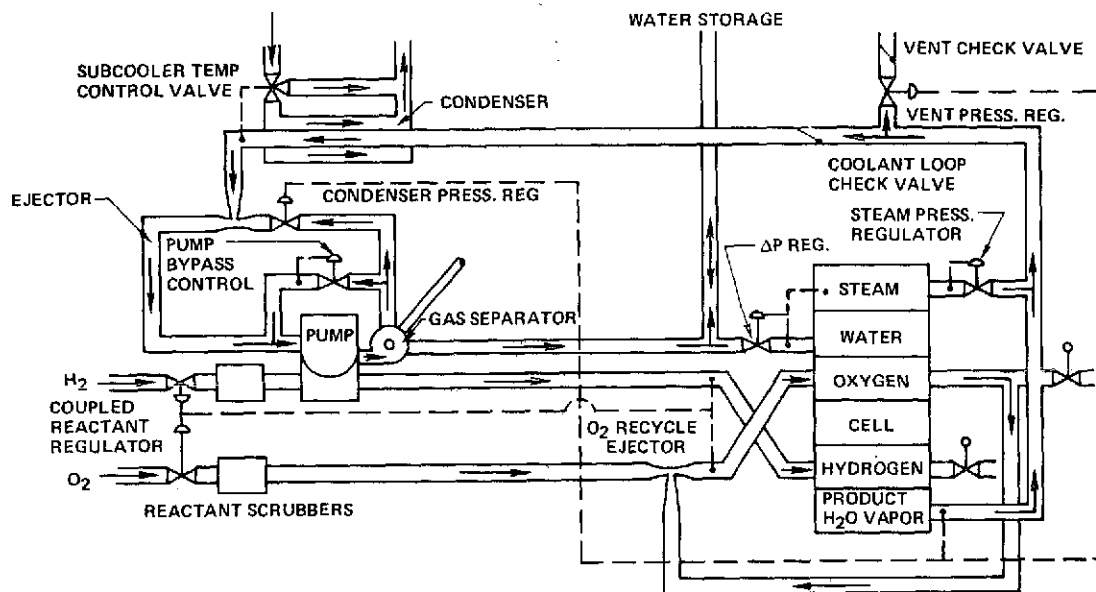


Figure A-15 - EMS System Schematic

Condenser Discharge Ejector and Pressure Regulator - This loop controls the product water vapor pressure by varying the primary flow of the high pressure water to the ejector. Should the product water vapor pressure be too high, the valve opens to increase flow to the ejector lowering the pressure in the condenser. The ejector also pressurizes the condensate flow allowing the pump to handle condensate with less sub-cooling and/or with a greater fraction of non-condensable gases.

Pump Bypass Control - The excess water flow not required by the ejector is bypassed by this line.

Gas Separator - The separator removes non-condensable gases from the water loop. The pump discharge pressure is approximately 15 psia (10.3 n/cm^2) allowing direct venting of non-condensables to atmosphere.

Cooling Loop Check Valve - During open cycle operation with the condenser inoperative, this valve prevents cooling water from back-flowing into the vapor line.

Purge Valves - Valves for periodic purging of inerts in the hydrogen and oxygen are provided. Additional valves are provided for purging the water cavities and vapor lines before and after storage.

The EMS is capable of operating over its full power range with or without the spacecraft heat sink in operation. The condenser is sized to condense all cooling steam and product water vapor at a power level of 7 kw. The condensed product water vapor is removed from the loop and transferred to the spacecraft potable water storage system. As power increases above 7 kw, the condenser cannot maintain the desired pressure in the product water vapor line and the open cycle vent valve opens. Since the condenser is still operating, the vent flow removes only the excess vapor which the condenser cannot handle. At power levels between 7 and approximately 10.5 kw, there is sufficient product water being condensed to provide the cooling water required, therefore, excess water continues to be transferred to the spacecraft. Above 10.5 kw additional cooling water is required and the water flow direction is from the spacecraft to the EMS.

If the spacecraft heat sink is completely inoperative, water from the spacecraft is supplied for cooling over the full power range. The water flow to and from the spacecraft as a function of output power is shown in Figure A-16. The upper solid and dotted lines is the amount of product water produced in the cells. The upper solid line shows the flow of water to and from the spacecraft if the radiator remains operative. The lower solid line defines the product water flow from the spacecraft if the condenser heat sink is not available.

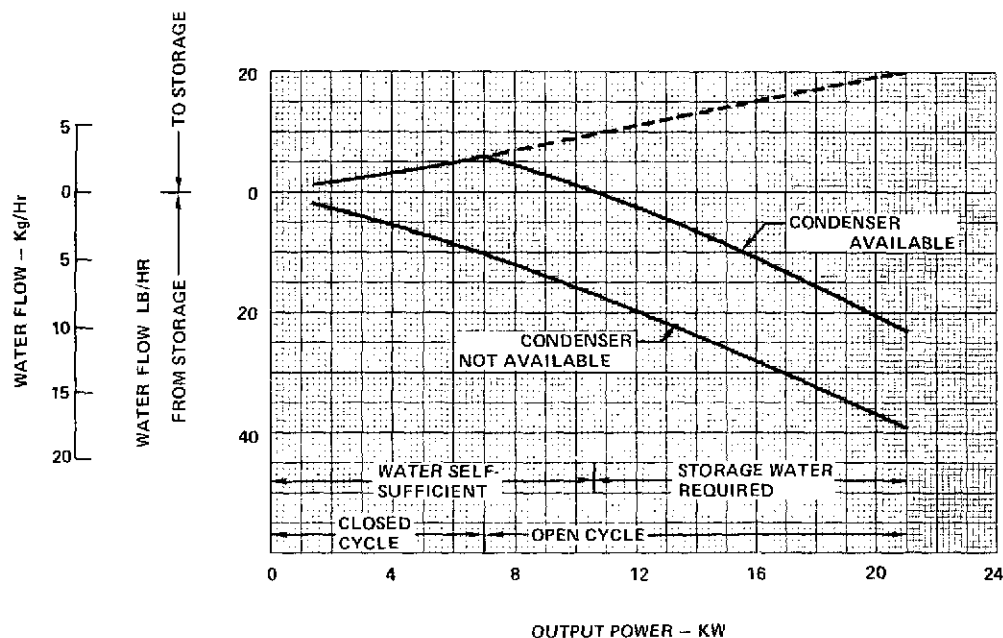


Figure A-16 - Water Flow to and from Spacecraft

System Performance

The specific reactant consumption of the EMS as a function of output power is shown in Figure A-17.

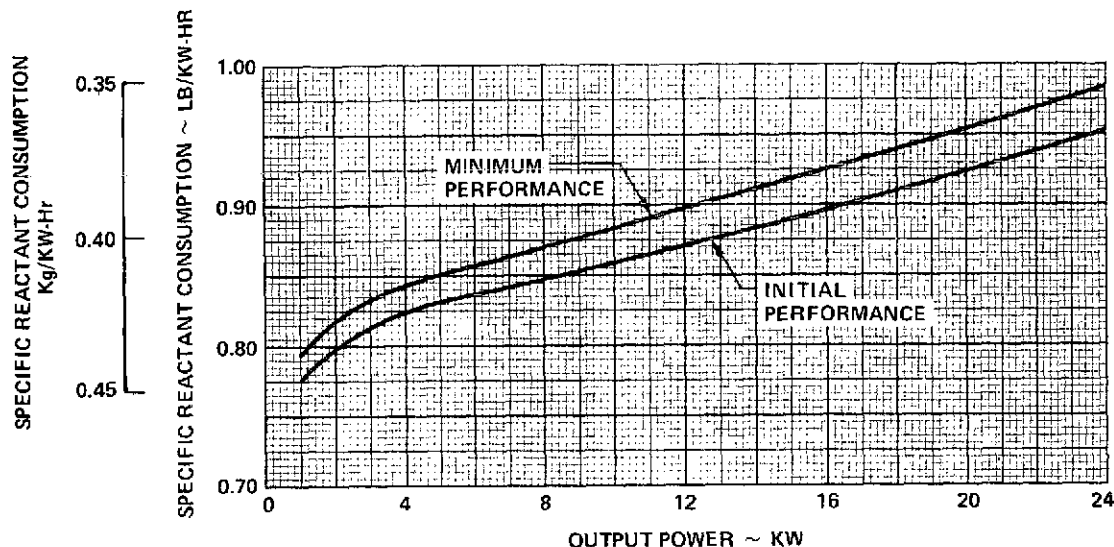


Figure A-17 - EMS Specific Reactant Consumption

System voltage versus output power is shown in Figure A-18. The EMS meets all system voltage regulation requirements with substantial margins at the 7 kw sustained power and 21 maximum power levels. The use of a voltage limiter to hold system voltage below the maximum allowable level at the 1.4 kw minimum power point was judged to be most weight effective. A voltage limiter allows a system to operate down to zero net power within specified voltage regulation.

The current density at 21 kw is 460 ASF(495 ma/cm²). At the 7 kw sustained power level, the cells are operating at a current density of 136 ASF(146 ma/cm²). Based on a NASA provided load profile, the average EMS output during a typical Space Shuttle mission would be approximately 5 kw. Thus, the average current at which the EMS would operate for a Shuttle type application would be approximately 90 ASF (97 ma/cm²).

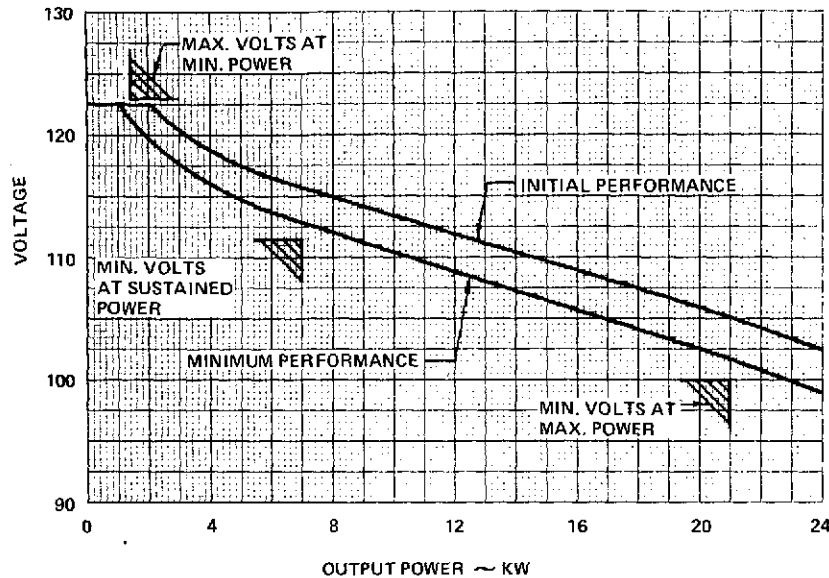


Figure A-18 - System Voltage vs. Output Power

Weight and Size

The emphasis during the first phase of this program was on the fuel cell power section and its components. No resources were devoted to system packaging studies beyond those performed in the precontractual time period. Estimates of system weight and size prepared during Phase 1 were therefore based on precontractual estimates of ancillary components characteristics and the detailed studies made of the base-line EMS power section.

System weight and volume characteristics based on these results are summarized in Table A-IV. The estimated EMS weight of 105 lbs(47.6 Kg) is well under the objective of 140 lbs(63.5 Kg). Estimated specific weight is 14.8 lb/kw(6.7 Kg/kw) of sustained power compared to the goal of 20 lb/kw(9.1 Kg/kw). Estimated specific volume per kilowatt of sustained power is 0.33 ft³/kw(9.4 x 10³ cm³/kw) also well under the objective of 0.5 ft³/kw(14.2 x 10³ cm³/kw).

TABLE A-IV

Estimated Weight of Engineering Model System

Power Section	60.1 (27.2)
End Plates	6.0 (2.7)
Ancillary Components and Structure	<u>38.6 (17.5)</u>
TOTAL	104.7 lbs. (47.4 Kg)

United Aircraft Research Laboratories



Report M210390-1

Improvement of Epoxy-Based Structures
for Fuel Cell Unitized Electrode
Assemblies (UEA)

REPORTED BY

R. A. Pike
R. A. Pike

APPROVED BY

M. A. DeCrescente
M. A. DeCrescente, Chief
High Temperature Materials

DATE April 1973

Report M210390-1

Improvement of Epoxy-Based Structures for Fuel Cell

Unitized Electrode Assemblies (UEA)

SUMMARY

This report presents the results to date of an investigation undertaken in support of SWEF, whose objective is to establish an optimum epoxy resin formulation and reinforcing system for producing composites to be used as frame assemblies in alkaline electrolyte cell UEAs. The work covers the period from January 8 to April 13, 1973.

A summary of accomplishments to date in this investigation are listed below.

1. The level of carbon dioxide and carbon monoxide formation which occurs on oxidation of an epoxy resin casting at 250°F has been correlated with epoxy resin structure, type of amine hardner, cure accelerator, and resin cross-link density.

2. Based on these correlations three new epoxy resin systems have been formulated which show a marked improvement in stability as measured by CO₂ formation over the currently used epoxy resins. The best formulation consists of Ciba-Geigy ERE-1359 cured with diaminodiphenylsulfone using a BF₃ accelerator.

INTRODUCTION

Epoxy based frames are used for all current alkaline electrolyte cell UEAs. Corrosion of the resin matrix in the cell environment produces carbon dioxide which converts the electrolyte from KOH to K_2CO_3 thus decreasing cell life and efficiency. Although there are materials available which have shown greater KOH resistance in cell environments than epoxy, fabrication difficulties and cost considerations negate their use for UEA frame construction at the present time.

The approach for the current investigation, related to improvement in KOH compatibility of epoxy resins, includes the following factors:

1. Evaluate the effect of
 - epoxy resin type (structure)
 - hardener type (structure)
 - advantage or disadvantage of accelerators
 - cross-link density of cured resin.
2. Evaluate the effect of glass or asbestos reinforcement in the optimized epoxy resin matrix.
3. Delineate the mechanism of KOH corrosion.

Two epoxy resin systems are currently being used for UEA frame construction. These are U. S. Polymeric E-755 glass/epoxy prepreg and B. F. Goodrich Hypon resin (standard epoxy containing Hycar polymer - carboxylic acid terminated polyacrylonitrile) with asbestos reinforcement. The E-755 system is superior to the Hypon in terms of carbon dioxide formation.

The following specifications have been set for UEA frame materials:

- environment - 25-45 percent KOH; oxygen to several atmospheres partial pressure
- temperature - 250°F (300°F for future operation)
- compressive creep (stress relaxation) less than 5 percent at 1000 psi/250°F for 1500 hrs.

This report covers the results which have been obtained in part 1 (above) of the overall program.

RESULTS AND DISCUSSION

Material Compatibility Tests

All analytical tests to determine oxidative and KOH corrosion resistance of the specified epoxy systems have been carried out at SWEF under the direction of Mr. Henry Cote. Initially the following three tests were to be carried out:

1. Oxidation resistance - Differential Scanning Calorimeter (DSC);
NASA-LeRC Oxidation Test with gas chromatography analysis
2. KOH corrosion pot test.

Analytical results obtained to date have been mainly from the NASA-LeRC test together with limited DSC data.

The NASA-LeRC test conditions are as follows: an epoxy resin test sample having a 150 sq cm surface area is heated 100 hrs at 250°F in a sealed helium/oxygen (70/30) atmosphere (500 cc total gas volume) at 35 psia. An aliquot sample is analyzed by gas chromatography and the methane, carbon monoxide and carbon dioxide concentrations in ppm are determined. SWEF has shown good correlation between NASA-LeRC test results and those from the KOH corrosion pot test. Thus, low CO₂ formation in the oxidation test normally means high KOH corrosion resistance.

Epoxy Resin Casting Preparation

Each casting was made by curing the specified epoxy and hardener in an aluminum cup to give a 2.25 in. diameter disk 0.2 to 0.3 in. thick. The resulting disks were cut (SWEF) to provide the required surface area. Usually two disks of each resin were sufficient. With the 3M Co. and Hexel resins the vendor supplies only glass prepreg. The disks were made by removing the resin from the glass filament with solvent, evaporating the solvent under vacuum and curing the resulting resin. Cure schedules were those specified by the resin vendor or as determined by UARL personnel where in-house formulations were used.

Control samples, for comparison purposes, of Hypon and E-755 resins with and without reinforcement were prepared by SWEF.

Epoxy Resin/Hardener Formulations - Initial Screening

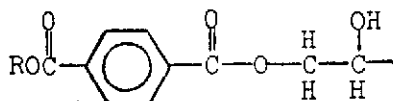
There is no definitive literature data on the effect of concentrated alkaline solutions on epoxy resins, particularly under the conditions encountered in fuel cell applications. It was therefore necessary in the initial phase of the investigation to select resins of widely varying structure cured with a variety of catalysts (hardeners) to obtain a comprehensive evaluation of structure vs stability. The type of epoxy resin and catalysts selected for the initial evaluation are listed in Table I together with the NASA-LeRC oxidation test results for each system. Structures of each type of resin used are shown in the Appendix.

Theoretical Analysis of Test Results

Based on the results of the initial screening tests, the following tentative correlations between stability and structure were delineated and used as a basis for selecting additional resins for testing:

1. Anhydride cured epoxy resins are inferior to aromatic amine cured systems in terms of CO_2 formation.

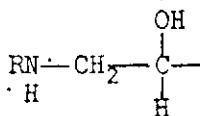
This would be primarily associated with the ease of saponification by KOH of the ester groups formed during the reaction of anhydrides with epoxy groups.



2. Aromatic amines such as diaminodiphenylsulfone (DADS) are more effective in retarding CO_2 formation than phenylene diamines (0820, Furane 9245), cycloaliphatic amines (MBCA) or methylene dianiline.

This may be due, in part, to the lower base strength of the amino groups in DADS because of the electron withdrawing effect of the sulfone group. The base strength of these amines in decreasing order is: alicyclic amines > phenylene diamines > methylene dianiline > diaminodiphenylsulfone.

The lower base strength of the amine linkage in the cured epoxy should result in increased reactivity toward attack by base, particularly at the hydroxy substituted positions which would be more acidic.



This could ultimately lead to chain cleavage with formation of CO_2 and CO. However, since this does not appear to be the case it suggests that oxidative degradation of an epoxy resin may not involve the hydroxyl centers in the molecule.

3. Use of BF_3 as an accelerator which results in formation of ether linkages (less free hydroxyl) appears to give improved resistance to CO_2 formation. The elimination of the acidic OH group by ether formation $2-\text{C}-\text{OH} \rightarrow \text{C}-\text{O}-\text{C}$ results in a lower activity toward base attack.

It is interesting to note that when using DADS as a resin hardener, BF_3 amine complexes are normally used as accelerators because of the low base strength of the amine. This allows much shorter cure schedules than are otherwise possible with the sulfone amine alone.

4. Epoxy novalac and resorcinol epoxy resins are superior to standard bisphenol A or cycloaliphatic epoxy resins.

This is a very tentative conclusion based on the oxidative test results since it is difficult to separate the effect of resin structure and cross-link density. The cycloaliphatic resins however (Union Carbide 2256) are clearly inferior to the other systems. The brominated epoxy system, Shell EXR-67, shows promise but the presence of bromine in the resin may on long term aging result in formation of KBr.

5. The greater the cross-link density of a given system, the greater is the resistance of CO_2 formation.

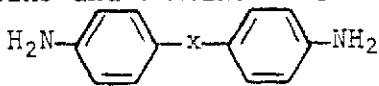
Besides the functionality of the resin, it is necessary to know how far apart the functional groups are spaced, since this determines the cross-link density. Cross-linking density may be defined as the number of effective cross-links per unit volume. In the DGEBA standard epoxy, for example when $n = 0$, the epoxy groups are separated by seven units, the aromatic ring being counted as one unit. Commercial DGEBA resins such as Epon 828 have an average n number somewhat greater than 0. Actually the cycloaliphatic type epoxy resins (Union Carbide 2256) theoretically provide the shortest distance between epoxy groups. However, as noted 2256 contains DGEBA resin which will provide more distance between cross-links. In this case the presence of a high percentage of methylene groups which apparently lead to instability negate the effect of higher cross-link densities. The epoxy novalacs also have a higher cross-link density when fully cured than the standard epoxy resins due primarily to the presence of the methylene groups connecting the phenolic rings in the novalac portion of the resin. The presence of these methylene groups, however, may reduce the stability of the resin to some extent but not to the degree found in the cycloaliphatic systems.

In addition, it is difficult to take advantage of all the potential cross-link sites in an epoxy novalac since if completely cross-linked a very brittle system results which tends to crack. Normally somewhat less than the theoretical amount of amine is employed to cure such resins to avoid this problem.

The resorcinol based resins theoretically should provide the highest and most uniform cross-link formation of the resins tested. For example, in ERE-1359 the epoxy groups are separated by 5 units. With the correct type of amine hardener, decreased CO₂ formation should result without formation of a highly brittle system.

Although the limited scope of the initial screening study does not allow an exact definition of each of the effects discussed above the tentative hypotheses were used to formulate a second series of resins. These are described in the following section.

Epoxy Resins Systems Having Improved Stability

The following series of resins were designed to show the effect on CO₂ formation of (a) epoxy novalac vs resorcinol based resins and combinations of the two, and (b) variation of amine base strength of type H₂N--NH₂ where

x = sulfone (SO₂), oxygen (O), and phenylene (no group between the benzene rings). In addition, the brominated ERX-67 resin was reformulated to further examine the effect of ring substituted halogen. The epoxy substituted methylenedianiline, Araldite X8183/137 was also retested using the benzidine hardener. The formulations are listed in Table II.

The test results of the NASA-LeRC oxidation test as carried out at SWEF are listed in Table III.

These results clearly show that the resorcinol based epoxy system Ciba-Geigy ERE-1359 with the diaminodiphenylsulfone hardener and BF₃ accelerator (E3) provides increased resistance to CO₂ formation over the U. S. Polymeric E-755 resin control.

The epoxy novalac modified ERE-1359 resins E⁴ and E⁵ with either DADS or benzidine hardener also show decreased CO₂ formation compared to the currently used resin system. These results are very encouraging and indicated that the previously discussed correlations of resin structure, catalyst and cross-link density have some degree of merit. The Ciba-Geigy resin ERE-1359 used in UARL-E3 and -E⁴ formulations was cured with ninety percent of the stoichiometric amount of DADS. The castings were prepared by dissolving the solid amine in the epoxy resin at 100-110°C, the BF₃ · MEA was then added and the casting cured at 125°C for 2 hrs followed by 2 hrs at 200°C. The resulting casting was clear orange-red color of excellent integrity. Typical properties of the Ciba ERE-1359 resorcinol diglycidyl ether are listed in Table IV.

It is expected that further optimization of the UARL-E3 and -E4 formulations will lead to additional improvements in resin stabilization. UARL-E5 will not be considered further since the benzidine hardener is a known carcinogen and on large scale use would present health and safety handling problems.

These results, it should be noted, were obtained on epoxy resin castings. Since the primary use is as a laminating resin with either glass or asbestos reinforcement additional formulation variations may be necessary to achieve suitable handleability for this purpose.

RECOMMENDATIONS FOR FURTHER WORK

The following recommendations are for optimization of the UARL-E3 and -E4 epoxy resins as a laminating resin.

1. Determine best ratio of epoxy/amine hardener as indicated by NASA-LeRC oxidation and KOH pot tests.
2. Optimize cure schedule.
3. Determine suitable solvent system for use in preparing prepreg tapes or for asbestos mat impregnation.
4. Determine molding parameters of optimized resin/reinforcement system.
5. Characterize resulting laminates as to mechanical, physical and KOH corrosion resistant properties.

In addition other epoxy resins which on a theoretical basis would result in improved stabilization should be screened as castings using the NASA-LeRC oxidation test.

ACKNOWLEDGEMENT

Some of the castings in the initial series of resins were supplied by Dr. D. A. Scola of UARL. The cooperation of both Dr. Scola and SWEF personnel, Mr. Henry Cote and Mr. Ray Gelting is gratefully acknowledged.

Table I

NASA-LeRC Oxidation Test Results of Various
Epoxy Resin-Hardener Formulations^a

Class	Resin/Hardener	Oxidation Products, ppm		
		CH ₄	CO	CO ₂
1. Diglycidyl ether of bis-phenol A (DGEBA) "Standard Epoxy"	Epon 828/DMP-30	15	120	3700
	(Hypon) Shell Epon 828/DMP-30 ^b /Hycar	44	2300	8300
	Hypon/asbestos - high cure	20	200	4000
	- low cure	50	400	5000
2. Cycloaliphatic (containing 37% DGEBA)	Union Carbide ERL 2256/MBCA ^c	25	160	13,000
	2256/0820	16	3730	11,650
3. Epoxy novalac	3M 1009-26/amine (contains 33 w/o DGEBA)	55	2600	5900
	3M 1009-36/anhydride	150	3300	5600
	Hexel F-161	101	1514	2928
	Ferro 293/anhydride	-	1816	2800
	U.S. Polymeric E-755/ DADS ^d -BF ₃	23	563	976
	with asbestos reinforcement	20	800	1000
	with glass reinforcement	10	570	1350
4. Brominated epoxy	Shell EXR-67/MDA ^e	10	950	1300
	Shell EXR-67/Furane 9245	5	9	1415
5. Resorcinol based epoxy	Ciba ERE-1359/MBCA	88	1747	1037
	Ciba ERE-1359/MDA	23	101	1771
	Shell X-801/MDA	71	2323	5661
6. Amine Based Epoxy	Ciba TGMD-8183/137-Furane 9245	11	3058	7085

^aNASA-LeRC oxidation tests run at SWEF^bTris(dimethylaminomethyl) phenol^cMethylene bis-cyclohexylamine^d4,4'-diaminodiphenylsulfone^eMethylenedianiline

Table II

Epoxy Resin Formulations for Improved Oxidative
and KOH Resistance

<u>Formulation No.</u>	<u>Epoxy Resin</u>	<u>Curing Catalyst</u>	<u>Accelerator</u>
UARL-E1	36 w/o ERX-67 ^a 64 w/o Epon 828	BF ₃ · MEA ^b	-
UARL-E2	64 w/o ERX-67 36 w/o DEN-438 ^c	DADS ^d	BF ₃ · MEA
UARL-E3	ERE-1359 ^e	DADS	BF ₃ · MEA
UARL-E4	64 w/o ERE-1359 36 w/o DEN-438	DADS	BF ₃ · MEA
UARL-E5	64 w/o ERE-1359 36 w/o DEN-438	Benzidine	-
UARL-E6	Araldite X8183/137 ^f	Benzidine	-
UARL-E7	64 w/o ERE-1359 36 w/o DEN-438	DADPE ^h	-
UARL-E8	64 w/o Epon X-801 ^g	Benzidine	-

^aTribromo-N,N-diglycidylaniline^bBoron trifluoride-monoethylamine^cDow Chemical epoxy novalac^dDiaminodiphenyl sulfone^eResorcinol diglycidyl ether^fTetra glydicylmethylenedianiline^g2,6-diglycidyl-1-glycidoxyphenol^hdiaminodiphenyl ether

Table III

NASA-LeRC Oxidation Test to Determine CO₂ Formation on
UARL Formulated Epoxy Resin Castings

<u>Epoxy Resin</u>	Oxidation Products, ppm		
	<u>CH₄</u>	<u>CO</u>	<u>CO₂</u>
UARL-E1	40	1100	1300
-E2	4	260	930
-E3	11	110	330
-E4	40	360	440
-E5	7	760	650
-E6	22	890	1000
-E7	11	1650	5700
-E8	11	2600	1950
U.S. Polymeric E-755 ^a	23	567	976

^aResin system currently used (see Table I)

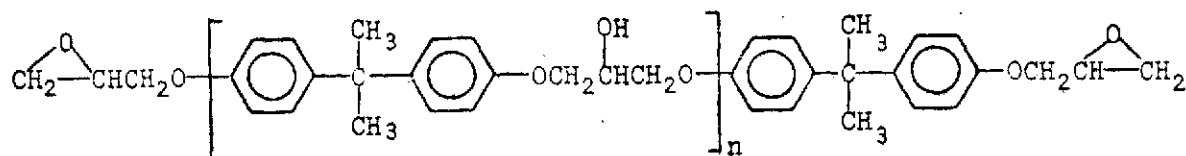
Table IV

Properties of Ciba ERE-1359

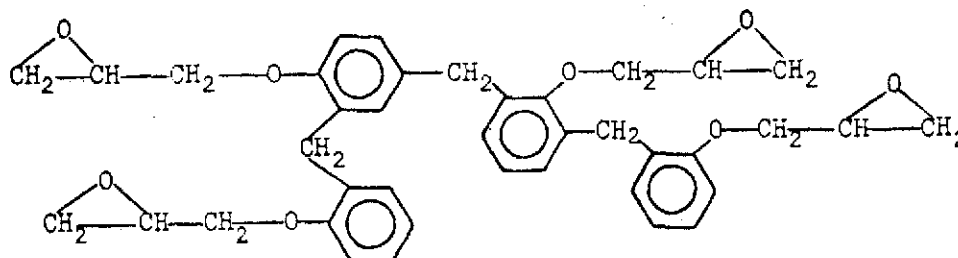
Viscosity, cps (25°C) (77°F)	300-500
Epoxy value, eq./100 gm	0.79
Weight per epoxide (WPE)	127
Color, Gardner 1933	6 max.
Lbs/gal (25°C) (77°F)	10.1
Flash point, open cup	300°F
Molecular weight	222.2

APPENDIX

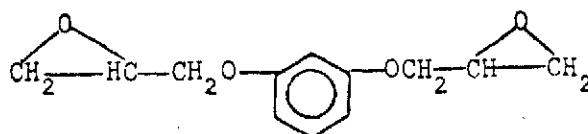
A. Epoxy Resin Structures



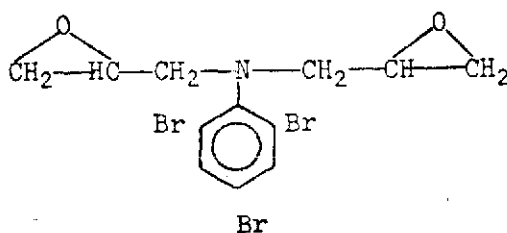
Diglycidyl ether from epichlorohydrin and bisphenol A
"Standard Epoxy"



Epoxy Novalac

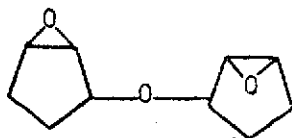


ERE-1359, Resorcinol diglycidyl ether

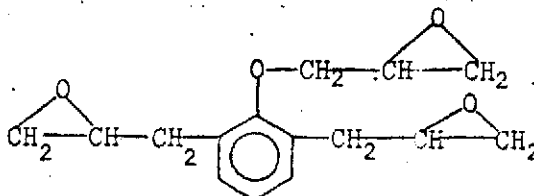


Brominated Epoxy, Shell EXR-67

APPENDIX (Cont'd)

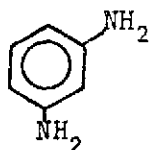


Cycloaliphatic Epoxy

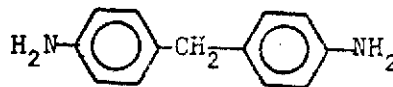


Phenolic Substituted Epoxy, Shell Epon X-801

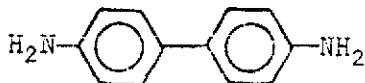
B. Amine Hardeners



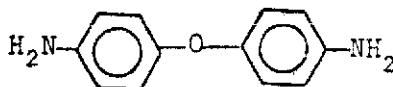
Metaphenylenediamine (MPA)



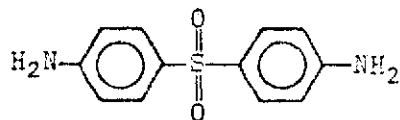
Methylene dianiline (MDA)



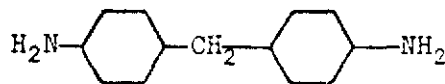
Benzidine



diaminodiphenyl ether



diamino diphenylsulfone (DADS)



methylene-bis-cyclohexylamine (MBCA)